CHAPTER 1

INTRODUCTION

1.1 Background

In this modern age of rapid industrialization, the world has been facing a serious environmental problem associated with these industrial processes. One of the major environmental problems in the regard is water pollution [1]. Water discharged from chemical process industries as wastewater is associated with various contaminant *e.g.* heavy metal ions, dyes, pesticide residues *etc*. depending on the chemical processes involved. The water ultimately gets mixed with the main water bodies and if it is not properly treated, creates serious problem of contamination of soils and water [2]. In this context, heavy metal ions such as cadmium, zinc, copper, lead, nickel, *etc.* are considered to be hazardous to the environment as they are toxic and non-biodegradable even at low concentrations [2, 3]. Among these heavy metals, cadmium contamination is a serious problem for its toxicity and mobility in soil. The permissible limit of cadmium metal ion in waste water is 2 mg/L [4]. Although zinc is considered as an essential element for life and acts as a micronutrient when present in trace amounts [5], however as recommended by WHO, beyond the permissible limit of 5.0 mg/L in drinking water, Zn^{2+} also imparts toxicity [6, 7].

Cadmium (Cd^{2+}) is released in the water bodies from industries like electroplating, cadmium-nickel batteries, phosphate fertilizers, pesticides, mining, pigments, alloys and also from sewage sludge [3, 7, 8]**.** Zinc (Zn^{2+}) are released from metals, chemicals, pulp and paper manufacturing processes, steel works with galvanizing lines, zinc and brass metal works, viscous rayon yarn and fibre production, *etc.* [5].

Various treatment processes such as chemical oxidation, reduction, precipitation, solidification, electrolytic recovery, solvent extraction, membrane separation, ion exchange and adsorption on activated carbon are used for the removal of metal ions from waste water [3**,** 9]. However, specific application of such methods however is sometimes restricted because of technical or economical constraints.

Recently, researchers have been using various surfactants in water treatment for the separation of metal ions and other toxic substances [10-16]. The surfactants have the ability to get dispersed on the surface of target molecules in aqueous solution thereby imparting opposite charges on the surface. These adsorbed surfactants result electrostatic repulsion between molecules stabilizing the structure of the colloid [10, 17].

Dyes are extensively used in production of textile, rubber, paper, plastic, cosmetic, *etc*. Textiles are the maximum consumers of dyes for coloration of fibers [18]. As dyes impart toxicity to the aquatic life and damage the environment, severe problems emerge from the discharge of dye-bearing wastewater into natural streams and rivers. Synthetic dyes are common water pollutants and often can be found in trace quantities in industrial wastewater due to their high solubility in water. As dyes are recalcitrant organic molecules, they are resistant to aerobic digestion and stable to light, heat and many oxidizing agents. Therefore treatment of dye containing wastewater is quite difficult [19, 20].

Currently, malachite green has been identified for its toxicity and carcinogenicity by the Food and Drug Administration [20]. Malachite green is toxic to human cells and might cause liver tumor formation and classified as a Class II Health Hazard. This chemical can be easily manufactured economically; it is still being used in certain countries with less preventive laws for non-aquaculture purposes [21].

Dyes in waste water are usually treated with either by expensive physical or chemical processes. But these processes are not quite effective in treating the wide range of dye containing waste [22]. The conventional wastewater treatment has low

removal efficiency for reactive and other anionic soluble dye as it relies on aerobic biodegradation and the dyes have poor biodegradability [23].

Recent years, adsorption techniques have been widely used for the removal of effluents from water. The techniques are economically feasible for bulk separation process [24, 25]. This technique also can be used for the removal of different types of dyes and other organic pollutants [26, 27]. It is also widely used for the removal of metal ions from waste water [28]. Among many type of adsorbents, activated carbon is the most widely used one, in a variety of applications for its excellent adsorption capacity [24, 25, 29]. However, it has got some limitations associated with its relatively higher production cost. In order to reduce the cost of waste water treatment, efforts have been undertaken by the researchers to develop low-cost alternative adsorbents from various agricultural, industrial, natural/biological waste materials [23]. The enhanced adsorption of industrial wastes on the surfaces of agro/bio-wastes can enhance the efficiency and economy of the process. It is essential to understand adsorption characteristics, i.e., mechanisms and kinetics of adsorption for designing suitable adsorption column for large scale industrial application [30].

In this work, the adsorption potential of locally available low-cost PSH has been investigated for the removal of heavy metal ions and dye from their aqueous solution. Role of different parameters *e.g.*, the influence of solution pH, temperature, particle size of the adsorbent, solution-solid ratio and initial metal ions concentration on the metal ion adsorption characteristics of PSH using batch kinetic and equilibrium adsorption experiments has been studied. Moreover, the effects of anionic surfactant, such Aerosol 22 on the adsorption processes were also studied to improve the metal ions adsorption. The performance of PSH as adsorbent was compared with granular activated carbon (GAC). The results of the adsorption kinetic have been analyzed using different kinetics models. The isotherm equilibrium results were also fitted in Langmuir, Freundlich and D-R isotherms respectively [31-36].

1.2 Problem statement

Pollution by heavy metals ions and dyes has become a serious matter of concern due to potential hazardous effect of these materials in the environment and human being. Normally, heavy metal ions are present in soil and water as trace minerals. However, the rapid industrialization without any significant concern about the environment results in the huge accumulation of these toxic and hazardous metal ions in natural water resources such as, river, lake, soil, *etc*. Similarly presence of dyes in waste water discharged from synthetic dye making industries is also another problem to the environment. In this regards, adsorption is a common method for the removal of metal ions from waste water. Researchers have been going on for the development of nonconventional adsorbent as a substitute of activated carbon and ion exchange resin due to their prohibitive regeneration cost. At present, activated carbon is a common adsorbent agent used in industries for the treatment of waste water. The consequences of high operating costs and problems with regeneration of the spent activated carbon impede its major application [37]. PSH is a naturally available material and it is much cheaper than activated carbon. Moreover it can have very high adsorption capacity for metal ions and dye residues from waste water. Significant amount of PSH is available in the form of biowaste from plant oil industry.

1.3 Objective

The objectives of this study are:

1- To characterize the PSH as adsorbent for dye and heavy metal ion removal.

2- To investigate the effectiveness of PSH for the removal of dyes and heavy metals using kinetic and equilibrium study.

3- To compare the adsorption capacity of PSH with commercial activated carbon by experimentation and other reported adsorbents from literature

4- To analyze the influence of the anionic surfactant on metal ions removal using PSH, in terms of adsorption rate (adsorption kinetic) and capacity (adsorption isotherm).

1.4 Scope of the study

The PSH samples was collected, prepared and characterized thoroughly by the measurement of particle size, surface area, porosity, zeta potential, chemical composition and also by SEM and FTIR studies. The batch adsorption isotherm and kinetics studies has been utilized for dye and metal ions adsorption onto PSH in aqueous solution with respect to initial metal ion concentration, pH, adsorbent dosage, particle size and temperature. Some analysis has been done using Aerosol 22 to study the effect of anionic surfactant on metal ions adsorption by PSH and also by GAC for the comparison of adsorption behavior. The kinetic experimental data has been analyzed using pseudo-first-order, pseudo-second-order and intraparticle diffusion model. Studies on the batch adsorption process were made and equilibrium isotherm data has been analyzed using Langmuir, Freudlinch and Dubinin-Radushkevich isotherm equations.

1.5 Conclusion

The main purpose of this chapter is to provide a brief description of the research topic which will be conducted through this thesis. The problem statement has been mentioned. The objectives of this research and the scope of work have been discussed as well.

CHAPTER 2

LITERATURE REVIEW

2.1 Adsorption on solid/ liquid interface

The word “adsorption” refers to taking up of gaseous or liquid components from mixtures onto the internal and/or external surfaces of porous solids. In chemical engineering field, adsorption is a type of heterogeneous separation process, where specific components of gaseous or liquid mixtures are transferred onto the porous surfaces of solids, which is generally known as adsorbent [38]. Adsorption takes place only at the interface, compared to “*absorption*” which occurs when the components (adsorbate) travel into great lengths between the atoms, ions, or molecules of the adsorbent. This characteristic differentiates adsorption from “*absorption*” [39].

Ragnarsdottir [40] defined adsorption as a process in which the dissolved constituents in groundwater are attracted to the surfaces of minerals with the pores through which the water flows. The dissolved constituents can be of natural source, *e.g.* originated from minerals during dissolution by the coexisting water or anthropogenic derivation which is introduced into the environment by a range of industrial processes.

Dissolved mineral constituents commonly present in the water are charged ions with a positive charge (such as Pb^{2+}) or a negative charge (*e.g.* arsenate, AsO_4^{2-}). The mineral surfaces have an electric charge as the metal ions (Me) forming the structure of the minerals are not completely coordinated with oxygen at the surface of the mineral (>Me-O^-). The surface is afterward neutralized by a H^+ ion from the acidic water (>Me–OH) and the acidity (pH) of the groundwater afterward affects this

mineral surface charge. Generally, water with high acidity generates minerals with a positive charge and waters with a low acidity generates mineral with a negative charge. In neutral water (intermediate pH), the mineral surface commonly has a zero charge. As an example, the surface of the mineral feldspar which becomes like $>MeOH_2^+$ at low pH and as $>Me\text{-}O^-$ at high pH (> denotes the mineral surface). As a consequences, positively charged metal cations (*e.g.* Pb^{2+}) adsorb to feldspar at higher pH ($>Me\text{-}OPb^+$) and that negatively charged ions (anions), such as arsenate, adsorb to feldspars at lower pH ($>Me\text{-}OH_2AsO_4^-$). The ion bonding is either strong direct bonds with the surface (inner sphere complex, *e.g.* Pb^{2+}) or weak electrostatic bonds (*e.g.* Na^+). Na^+ gets firmly coordinated with four water molecules ($Na(H_2O)_4^+$) and act as a 'shield' to prevent direct bonding, categorized as weaker electrostatic bonding [40].

The interaction of gas, liquid, or solid on the surface of a solid or liquid in adsorption process depends on the nature of adsorbent and adsorbate. Adsorptions are of two types, namely, physisorption and chemisorption. Adsorbed molecules are seized on the adsorbent by the weaker van der Waals' forces in physisorption. In chemisorption a single layer of molecules, atoms, or ions is attached to the adsorbent surface by chemical bonds. Table 2.1 shows a comparison between physical and chemical adsorption. Adsorption has a significant influence in surface science and engineering, such as corrosion, heterogeneous catalysis, chromatography *etc.* [41].

Table 2.1: Comparison between physisorption and chemisorption [39]

	Physisorption	Chemisorption
Characteristics of bonding	Reversible and non-dissociative.	Could be irreversible and usually dissociative.
Saturation level	Multilayer	Monolayer
Adsorption kinetics	Fast (Due to its nature of being a non-activated process)	Depends on the reaction rate (It is usually an activated process, the kinetics could be variable)
Adsorption enthalpy	Commonly 5-40 kJ/mol. (*i.e.* heat of liquefaction). It relies on properties such as molecular mass and polarity.	Commonly 40 – 800 kJ/mol. It relies on chemical bond strengths, which allow the wide range of the adsorption enthalpy.
Temperature range of adsorption.	Near or less than the condensation point of the gas. (*e.g.* CO_2 < 200 K)	Practically unlimited. But, the temperature range may be narrow for a molecule to be effectively adsorbed.

2.2 Environmental applications

Many environmental applications employ adsorption as an effective separation technology. Organic contaminants such as phenol and aniline, which exist in industrial waste water and marine, can be removed employing adsorbents such as activated carbons, clays, coal, vermiculite *etc*. [42, 43]. On the other side, adsorption can be considered as a cost effective and feasible method for dye removal from wastewater [44]. The other application of these adsorbents are for removal of organics materials from water, organic solvents dehydration, mercury removal from chlor-alkali-cell gas effluent, separation and recovery of nutrients (e.g nitrogen and

phosphorus) from waste water, capture of volatile compounds from gas streams and ground water, waste water odor treatment, capture and recovery of solvent vapor, removal of radon, hydrogen sulfide, and other sulfur compounds from gas streams, removal of heavy metal *etc.* [45, 46].

The advantages of adsorption includes easy installation and maintenance, can be fully automated, high removal efficiency, efficient separation of toxic organic and/or refractory compounds, availability of many types of adsorbents [39].

The disadvantages of adsorption includes the gradual deterioration of adsorption capacity, problems caused by particulates in the feed, bed fires risk in the abatement of volatile organic compounds *etc.* The removal efficiency might be decreased by the high content of macromolecular compounds, which possibly block active sites in an irreversible way. Therefore used adsorbent needs to be regenerated (high energy consumption) or disposed (causing waste) and sometimes it makes the process less economic [39].

2.3 Application background

2.3.1 Adsorption materials

A few elemental rules for adsorption are;

- Non-polar molecules are able to adsorb more effectively compared to polar molecules
- Larger molecules are able to adsorb more effectively compared to smaller molecules
- Non-soluble/slightly soluble molecules are able to adsorb more effectively compared to highly soluble molecules
- pH can affect the amount of adsorption (based on the polarity / solubility)

- An increase in temperature may negatively affect adsorption capacity, although higher temperature does increase the rate of diffusion to adsorption sites. This is due to the fact that adsorption is an exothermic process. However, for water-treatment applications and ambient vapor-phase applications, the temperature effect is insignificant [39].

There are a few cost-effective adsorbents for treating wastewater, particularly for the purpose of heavy metals removal, like the following [47];

- Fly ash – a type of industrial solid waste, a by-product of thermal power plants. It can coagulate easily after adsorbing heavy metals.
- Peat moss – a form of complex soil material, made up of largely lignin and cellulose. Its surface area is large (>200 m^2/g) [47].
- Iron(III) hydroxide waste – Iron(III) hydroxide waste as well as waste slurry from the fertilizer industry, rice husk, xanthate, coconut shell and carbon have been considered as attractive alternatives for removing heavy metals from wastewater.
- Chitosan – In terms of the molecular structure, it resembles the cellulose. Chitosan is generated from chitin, an easily available material found in the exoskeleton of shellfish and crustaceans. After cellulose, chitin is the second most abundant natural biopolymer. It is an effective adsorbent for most heavy metal [47].

2.3.2 Kinetics

Adsorption kinetics is the time dependence of adsorption on solid surfaces of adsorbent. The adsorption dynamic involves the time evolution of the adsorption processes. Lagergren Pseudo-first-order kinetic model and Pseudo-second-order kinetic models are popularly used to describe the adsorption process, particularly liquid-phase adsorption and biosorption. The rate-controlling mechanism or rate-limiting step can be found from the Weber and Moris intraparticle diffusion model [39, 46].

The Lagergren pseudo-first-order model is typically used to describe physisorption mechanism and it is expressed by Eq. 3.3. The adsorption data are also analyzed in terms of pseudo-second-order model to explain the mechanism of chemisorption and it is expressed by Eq. 3.4. The intra-particular diffusion was characterized using the relationship between specific sorption (q_t) and the square root of time ($t^{1/2}$) as expressed by Eq. 3.7. If the intra-particle diffusion is involved in the adsorption process, a plot of the amount of adsorbate adsorbed per unit mass of adsorbent (q^t) against square root of time ($t^{1/2}$) will give a straight line and the particle diffusion would be the controlling step if this line passed through the origin [48].

Intraparticle diffusion involves the pore and solid diffusion mechanism. Pore diffusion is also known as macroporous diffusion, while microporous diffusion is solid diffusion. Pore diffusion occurs when solutes diffuse into the pores. The pores are so large to the extent that, the solutes are able to escape from the force field of the adsorbent surface [49]. On the other side, solid diffusion occurs when solutes diffuse into the adsorbent surface. This is possible when the pores are very small and the solutes cannot escape from the force field of the adsorbent surface. In this case, solute molecules can be transported through activated pores, which include transfer between active sites [49]. When both pore and solid diffusion occur simultaneously, the faster process dominates the transfer mode.

The following stages of diffusional mechanism have been described the best employing adsorption kinetic;

1. The rapid external diffusion which involve the diffusion of molecules from bulk phase towards the interface space.
2. Internal diffusion which involves the diffusion of molecules inside the pores.
3. Surface diffusion which involve the diffusional of molecules in the surface phase.
4. Adsorption / desorption elementary processes or flat plateau phase where the diffusion is blocked due to the non-availability of sites for the molecules to get attached [36, 46].

2.3.3 Thermodynamics

Thermodynamic calculation of adsorption equilibrium constant, Ka is described by Eq. 3.14. Dependence of the thermodynamic equilibrium constant, Ka on temperature is estimated by applying Van't Hoff equation as Eq. 3.15. The negative value for the Gibbs free energy indicated that the adsorption process is spontaneous and with the increase in temperature the degree of spontaneity of the reaction is increased. The positive value of ÄH indicates the overall adsorption process as endothermic, while negative value shows exothermic. The positive value of ÄS will describe the redistribution of energy between the adsorbate and adsorbent or an increase in randomness during the adsorption process [50].

2.3.4 Equilibrium

Equilibrium isotherm is usually implemented to characterize the equilibrium of adsorption and ion-exchange systems. The equilibrium isotherm shows how the adsorbed material is being distributed between the adsorbed phase and the solution phase at equilibrium conditions. A certain isotherm can be considered specific for a given system at a specified temperature range [39]. For adsorption, only one isotherm is possible at a specified temperature range, while for ion-exchange, more than one isotherm can exist for different concentration, which takes place as a result of the concentration-valence effect [51]. Among the adsorption isotherms are Langmuir, Freundlich and Dubinin-Radushkevich isotherms are most frequently used by the researchers.

2.3.5 Langmuir isotherm

A significant assumption for the Langmuir isotherm is that the adsorbents possess fixed individual sites, where each one of them adsorbs only one molecule, resulting in the formation of a monolayer. A monolayer is a layer with the thickness of a molecule [49].

2.3.6 Freundlich isotherm

For the Freundlich isotherm to be made applicable, the most important assumption is that the adsorbents possess a heterogeneous surface made up of sites with varying adsorption potentials, and every site is assumed to be able to adsorb molecules.

The empirical constants K_f and *1/n* (Eq. 3.8) are obtained experimentally from the laboratory, and they correspond to the particular system under investigation [52]. As a rule of thumb, an isotherm is favorable if its shape is convex upward. On the flip side, when its shape is concave upward, it is said to be unfavorable. The characteristic isotherm shapes are shown in Fig. 2.1 [39]. The parameter *La*, also known as the "separation factor", serves to describe the equilibrium regions in a quantitative manner; [39].

- $La = 0$ for irreversible adsorption
- $La < 1$ for favorable adsorption
- $La = 1$ for linear adsorption
- $La > 1$ for unfavorable adsorption

The same goes for the parameter *1/n* in the Freundlich isotherm.

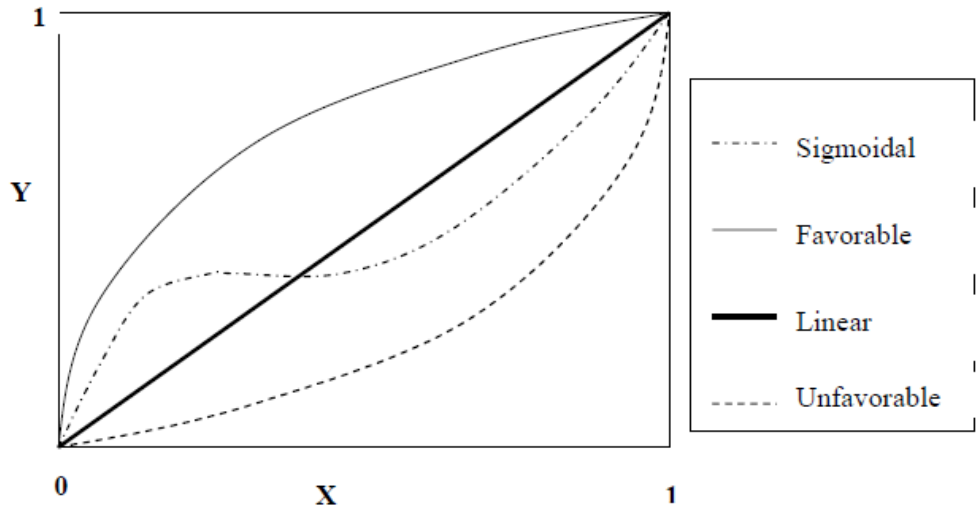

Fig. 2.1: Characteristic isotherm shapes [39].

2.3.7 Dubinin-Radushkevich isotherm

Dubinin-Radushkevish postulated The Micropore Volume Filling Theory (TMVF) for the adsorption of gas phase based on the Polany's potential theory of the adsorption [52]. D-R theory is applied to adsorption data to find out its mechanism and the theory provides the adsorption capacity and adsorption energy. The isotherm can be used to describe adsorption on both homogenous and heterogeneous surfaces. The linearized form of the equation can be expressed by Eq. 3.11 [53-55]. ε is the Polanyi potential which is related to the equilibrium concentration as Eq. 3.12. The mean free energy E (kJ mol^{-1}) of sorption can be estimated by using β values as expressed by Eq. 3.13. If the E value is between 8 and 16kJ/mol, the adsorption process follows by chemical ion-exchange; if E < 8 kJ/mol, the adsorption process is of a physical nature and if E value is higher than 16kJ mol^{-1}, the adsorption process follows by particle diffusion [51, 56-60].

2.4 Particle analysis

The particle analysis is pertinent with adsorbent properties such as surface area, particle shape, size distribution, and mechanical strength which is of particular importance when dealing with heterogeneous operations, *i.e.*, adsorption, ion exchange and catalysis [39].

2.4.1 Surface area

The solid surface consists of both the geometrical area (as determined from the shape) and the internal surface (the porous structure area) as well. The surface area is given as specific surface area, with the unit of m^2/g. For porous solid, the internal surface contributes the most to the percentage of the total surface, so high values of the

specific surface area may be attained. It is possible for the specific area of an activated carbon to reach up to 1500 m^2/g [39].

2.4.2 Particle shape

Sphericity is defined as how close a particle resembles a sphere.

$$\Phi_S = \frac{\text{Surface area of sphere having the same volume as the particle}}{\text{actual surface area of the particle}}$$

Typical values of sphericity for granular particles range between 0.6 and 0.95. The sphericity of most crushed materials usually ranges between 0.6 and 0.8 [38, 47, 49].

2.4.3 Particle size

Mass transfer properties and effectiveness of adsorption (also true for the case of reaction on a catalyst) are affected by the particle size (expressed are average diameter) and the shape of solid particles. The frequently used sizes are; [39]

- 20 – 100 μm diameter spheres in the case of fluidized-bed reactors
- 0.3 – 0.7 cm diameter spheres in the case of fixed-bed reactors

For particle with irregular shape, the particle diameter is calculated assuming it as sphere with the same volume as the particle. Usually, it is difficult to calculate the volume of particle with irregular shape and thus this value is taken as equal value from mean nominal diameter by sieve analysis (average sieve diameter) [39].

2.4.4 Particle density

It is defined as the mass of particles divide by its hydrodynamic volume (the volume of all open and closed pores). Practically, a hydrodynamic volume is identified without considering the closed pores and somehow it is defined as “apparent” or

“envelope” density. The term “skeletal density” also has been used for particle density which is defined as the mass of particles divide by the volume of solid material making up the particle and it includes the closed pores. Bulk density or packing density is the density which includes all the pores and voids (interparticle spaces). The values depend on the particle form whether it is powder, tablets or extrudates and also depends on the packing procedure. It is extensively used in reactor designing [39].

2.4.5 Pore structure

Pore structure is the most important property of adsorbent materials and it dictates the usage of the adsorbents. The adsorption capacity and even the dynamic adsorption rate are related to the total number of pores, pore shapes and pore sizes. Pores are generally differentiated as macro-, meso- and micropores [39]. Porosity is a characteristic of solids that shapes their structures, and it is exhibited by the presence of void spaces between internal supermolecular structures [61]. Porosity can be caused by the aggregation of particles and the detachment of a part of the mass of the solid as well. For the latter process, the pores produced are comparable in size and shape with the particles detached [39].

2.4.6 Pore shape and pore size distribution

The shape of adsorbent pores is mainly unidentified, but it is normally approximately identified as

a) Cylindrical: pores having a circular cross section,
b) Ink bottle: pores having a narrow neck and wide body, or
c) Slit-shaped: pores between parallel plates [62, 63]

Pore size can be divided into (1) micropores (diameter < 20 Å, or diameter < 2 nm width) (2) mesopores (diameter 20-500 Å, or diameter 2 nm-50 nm width), and (3) macropores (diameter > 500 Å, or >50 nm width) as defined by the International Union of Pure and Applied Chemistry (IUPAC) [64]. Micropores can be further

subdivided into primary (diameter < 8 Å, or < 0.8 width) and secondary micropores (diameter 8-20 Å, or 0.8-2 nm width). The macropores correspond to the entrance to the internal adsorbent pore structure, the mesopores aid the diffusive transport of adsorbate to adsorption sites and the micropores correspond to the region where the majority of trace elements are adsorbed. It is difficult to obtain the pore size distribution of the micropore region [65-68], but it is usually very useful for verifying the adsorption capacity of a given adsorbent at the particular adsorbate size.

Adsorptive molecules diffuse through macropores, mesopores, and finally into micropores. Micropores are typically the largest portion of the internal surface, and they are the main contributor to the total pore volume. In addition, most of the adsorption of gaseous molecules occurs within the micropores. This is due to the fact that in the particular region, the pressures are relatively low and the attractive forces are stronger. Apart from the surface area and pore volume, the distribution of the pore radii of a solid is also equally important. Solids used in catalysis, adsorption and ion exchange are usually porous and exhibiting large surface areas [39].

Physical adsorption mainly occurs due to van der Waals forces and electrostatic forces between adsorbate molecules and the atoms which make up the adsorbent surface. Therefore, adsorbents are characterized first by surface properties such as surface area and polarity. A large specific surface area is preferable for providing large adsorption capacity, but the creation of a large internal surface area in a limited volume inevitably allows large numbers of small sized pores to form between adsorption surfaces. Macropores and micropores result from granulation of fine powders or fine crystals into pellets, or it may originate the texture of raw materials. Macropores serve as diffusion paths for adsorbate molecules from outside the granule to the micropores in fine powders and crystals [69]. The total porous structure of an activated carbon is formed by a wide range of pore sizes. The macropores act as “tunnels” which allow molecules to reach the smaller pores in the interior where they are adsorbed or tied to the adsorbent surface. Macropores do not significantly contribute to the overall adsorptive process since they have a relatively low surface area but they affect the rate admission of the molecules to the meso- and micropores.

Mesopores, which branch from the macropores, serve as ways by which molecules get to the smaller micropores. Mesopores may trap molecules, but their overall contribution is small given their relatively low surface area. Most of the adsorption process takes place in the micropores which constitute the largest part of the internal surface area of the adsorbent [70]. The micropore size dictates the accessibility of adsorbate molecules to the adsorption surface, so the pore size distribution of micropore is another essential property for characterizing adsorptivity of adsorbents [69].

Table 2.2: Pore size distributions

Type	Pore size (Å)
macropore	≥500
mesopore	20-500
micropore	< 20

Surface polarity corresponds to affinity to polar substances such as water which is known as hydrophilicity. The examples are zeolites, porous alumina, silica gel, or alumina silicate. Beside that, non-polar adsorbents are generally “hydrophobic”. Typical non-polar adsorbents are carbonaceous adsorbents, polymer adsorbents and silicalite. These adsorbents have more affinity to oil compared to water [69]

Adsorbate having large molecule could not be adsorbed on small pore size adsorbent. On the other hand, adsorbent having large pores might not be able to adsorb small adsorbate. The electric charge of the surface groups may also enhance the adsorption process of the target molecules. The adsorbate which has the same electrostatic charge as of the adsorbent surface would result in repulsion. Repulsion by like charges would inhibit the process of adsorption. However, if the adsorbent surface and the adsorbate carry opposite charges, the adsorption of such molecules would be enhanced [70].

2.4.7 Effects of adsorbent pore structure on adsorption process

The adsorbent pores size affects the adsorption of contaminants in two ways; first, adsorption strength increases with decreasing pore size because of:
a. The increases in contact area between the adsorbate and the adsorbent surface [64].
b. Once the micropore width is less than about twice the adsorbate diameter, the adsorption potentials between opposing pore walls begin to overlap [65].

Second, size exclusion limits the adsorption of contaminants of a particular size and shape if pores are too small. In aqueous systems, when the pore width is smaller than about 1.7 times the second largest dimension of the adsorbate, the size exclusion will be observed [66].

The requirements for an effective adsorbent for the removal of micro pollutants are a large volume of micropores with widths that are about 1.5 times larger than the kinetic diameter of the target adsorbate. It is required to prevent pore blockage and to develop a hydrophobic pore surface chemistry which, when expressed as the sum of the oxygen and nitrogen contents, should not exceed 2 to 3 mmol/g [62].

2.4.8 Adsorbent surface groups

The adsorption capacity of an adsorbent is determined by its porosity and surface area, but it is also strongly influenced by the presence of functional groups at the adsorbent surface. Heteroatoms such as oxygen, hydrogen, chlorine and sulfur are either derived from the starting material and become a part of the chemical structure as a result of imperfect carbonization, or chemically bonded to the carbon during activation or during subsequent additional treatments, such as oxidation. The heteroatoms are bound to the edges of carbon layers and form surface groups that greatly affect the adsorption behavior of the adsorbent. The surface characteristic is strongly influenced by the carbon-oxygen surface structure [67, 68].

2.4.9 Adsorbent surface chemistry

The presence of heteroatoms such as oxygen, nitrogen, hydrogen and phosphorus had relation with some adsorbent characteristics by a certain measure of surface chemical heterogeneity. The content of these elements varies, depending on the nature of an organic precursor and the method of activation. The heteroatoms are important in determining the acidity/basicity of adsorbent surfaces in aqueous dispersion [62]. The acidic character of adsorbent surfaces is related to the surface oxygen contents. Oxygen-containing functionalities such as carboxylic acid or carboxylic anhydride, lactone or lactol, and phenolic hydroxy, work as the sources of surface acidity [68, 69]. Fabish and Schleifer [71] advanced the opinion that no surface oxides are responsible for basic sites in aqueous solution. Leon, *et al.* [72] studied the surface basicity of two series of carbons and provided direct proof that oxygen-free carbon sites (Cπ) can adsorb protons from solution.

Adsorbents should be hydrophilic so that they are wetted by water to be useful for water treatment applications [73]. A suitable adsorbent should be mechanically stable with a relatively large surface area, and chemically unreactive towards the solute as well as the solvent [74].

2.5 Physic seed nut (*Jatropha curcas L.)*

Physic nut (*Jatropha curcas L.*) is a multipurpose shrub or small tree which mainly grows in the wild and has many attributes and numerous uses. It has an economic importance in producing oil. The crops belong to the family of Euphorbiaceae which comprises approximately 8000 species, belonging to 321 genera [75]. Recently, it is also being planted as a commercial crop, due to gradually increased interest for biodiesel [76]. It has been stated that the centre of origin of the physic nut probably was in Mexico (and Central America) because they only found in cultivated form in Africa and Asia. However, the “true” centre of origin is still has to be investigated

[75]. The plant is cultivated in Central and South America, Southeast Asia, India and Africa [77-79].

In Malaysia, wild *Jatropha curcas L.* plant is known as *jarak pagar* mainly in Peninsular Malaysia area. The plant has a low moisture demands, low fertility requirements and tolerance to high temperatures which make it well growing under such climatic [80]. It is also known as the drought resistant shrub or tree [77-79]. Katwal and Soni [81] described that the tree has the ability to flourish in many climatic zones with rainfall 250–1200mm. Besides that, it can be also cultivate on moderately sodic and saline, degraded and eroded soil. The ideal plant density is 2500 stand/ha, which is raised from seeds or cuttings and the rainy season is the best period to plant stem cuttings. It accomplishes its maximum productivity within five years and can fulfill for 50 years.

2.5.1 Botanical description

The plants can reach a height of up to 5m and shows articulated growth, with morphological gaps at every augmentation. Five to seven shallow lobed leaves with a length and width of 6 to 15cm is alternately arranged. On branches, the inflorescences are terminally formed and appeared to be complex, possessing co-florescences with paracladia. Botanically, it can be described as a cyme. The plant is monoecious and flowers are unisexual; irregularly hermaphrodite flowers emerge. The fluctuations in rainfall and temperature/light will induce dormancy. The seedlings normally form five roots, one central and four peripheral [75, 82, 83].

Dehgan and Webster [82] observed that the plant is pollinated by moths because of it is sweet, heavy perfume at night, greenish white flowers, versatile anthers and protruding sexual organs, copious nectar, and absence of visible nectar guides. It was proved by the seed set does not occur without hand-pollination, when insects are excluded from the greenhouse [82]. The infrequent hermaphrodite flowers can be self-pollinating. Throughout field trials, Heller [84] investigated pollination occurred after

a while with a variance of insects to visit to the flowers. This mechanism promotes cross-pollination, relatively. After pollination, a trilocular ellipsoidal fruit is formed. The exocarp remains fleshy until the seeds are mature. The seeds are black, 2 cm long and 1 cm thick with a small caruncle. Gupta [85] investigated that the physic nut is a diploid species with $2n = 22$ chromosomes.

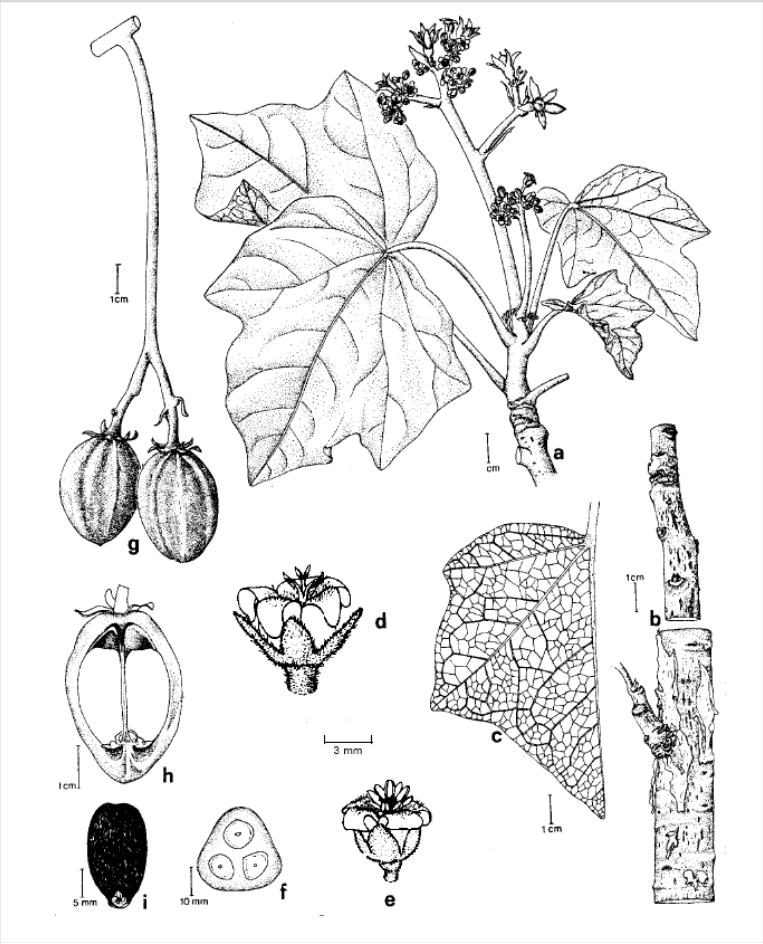

Fig. 2.2: Sketches of some essential parts of the physic nut: a. flowering branch, b. bark, c. leaf veinature, d. pistillate flower, e. staminate flower, f. cross-cut of immature fruit, g. fruits, h. longitudinal cut of fruits, i. seed [75]

2.5.2 Properties

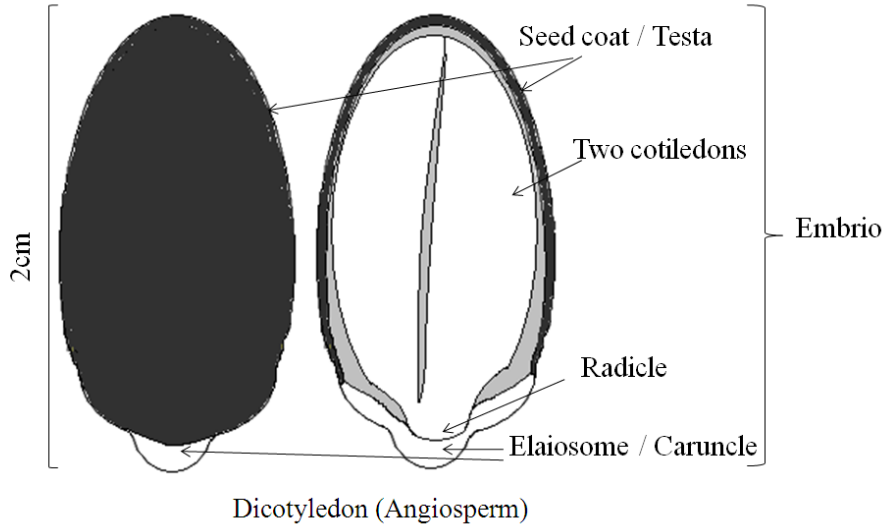

Fig. 2.3: A middle cleavage of physic nut seed.

The hull is the wall of the physic seed or known as a seed coat or testa and the true seed lies within the kernel with a very thin layer of endosperm. The physic seed hull has a hard and blackish hull with a similarity with sunflower seed hull but different in size, shape and without white stripes. The seed is comprised of a hull, a thin layer of endosperm and an embryo within the two fleshy halves (cotyledons) of a physic seed. The cotyledons supply carbohydrates and protein for the developing embryo until it grows up into a seedling with photosynthetic leaves and functional roots.

The sphericity values for the seed and kernel are 0.64 and 0.6 respectively, both shapes are close to an ellipsoid and the fruit (0.95) is close to a sphere. Hulls of the fruit contain tannin which are combustible and can be utilized as green manure and in biogas production [81]. Tannins have the ability to form chelates with iron and other metal ions because of the vicinity of hydroxyl groups on the aromatic rings [86]. Table 2.3 shows chemical compositions of physic nut's kernel, shell and meal.

Table 2.3: Chemical compositions of physic nut's kernel, shell and meal

	Kernel	Shell	Meal
Dry matter (%)	94.2-96.9	89.8-90.4	100
Constituents (*% in DM*)			
Crude protein	22.2-27.2	4.3-4.5	56.4-63.8
Lipid	56.8-58.4	0.5-1.4	1.0-1.5
Ash	3.6-4.3	2.8-6.1	9.6-10.4
Neutral detergent fiber	3.5-3.8	83.9-89.4	8.1-9.1
Acid detergent fiber	2.4-3.0	74.6-78.3	5.7-7.0
Acid detergent lignin	0.0-0.2	45.1-47.5	0.1-0.4
Gross energy (MJ kg^{-1})	30.5-31.1	19.3-19.5	18.0-18.3

* Trabi (1998) [87]

Table 2.4 shows the average moisture content of physic fruit and different parts of the fruit. The hull of the fruit contained very high moisture content compared to nut shell and kernel [81].

Table 2.4: The moisture content of different parts of the physic nut's fruit

Part of fruit	N	Average moisture content, %w.b.
Hull	3	88.95$\pm$0.54
Kernel	3	34.09$\pm$0.95

Shell	3	51.87±1.10
Whole fruit	3	77.03±0.70

*N is the number of samples. Each sample was from 200g of fruits. Data are mean values + standards deviation [81]

2.5.3 Toxicology

The toxicity of the seeds is mainly due to a toxic protein (curcin) and diterpene esters present in the seeds component. Curcin which is similar to ricin is the poisonous protein that can be found in the castor bean (*Ricinus communis*). The pure substance is lethal when administered in quantities of micrograms and these are the strongest toxins in the plant kingdom. Prof. Wink of the University of Heidelberg carried out the study on these substances and discovered that it promoted skin tumors in a mouse cocarcinogenesis experiment [88]. He discovered that the seed cake still contained about 11% oil, in which the thermo stable toxic diterpenes were bound. Heating it up to 100^{o}C for 30 minutes did not deactivate the lectins in whole seeds and dry seed cake; the lectins could be deactivated by 5 minutes cooking of ground seeds or seed cake and the oil had no mutagenic properties especially when handled with care and there was no risk for workers [88].

2.5.4 Uses

The physic nut is extensively cultivated in the tropics as a living fence infields and settlements and it is a drought-resistant species. Many parts of the plants are used in traditional medicine. However, the seeds are poisonous to humans and many animals. In many countries, physic nut was planted in arid areas for soil erosion control or prevention, fire wood, as hedge plant, for plant protection and reclaim land [75, 76, 81]. Fig. 2.4 shows the diagram of the different uses of *Jatropha curcas L.*

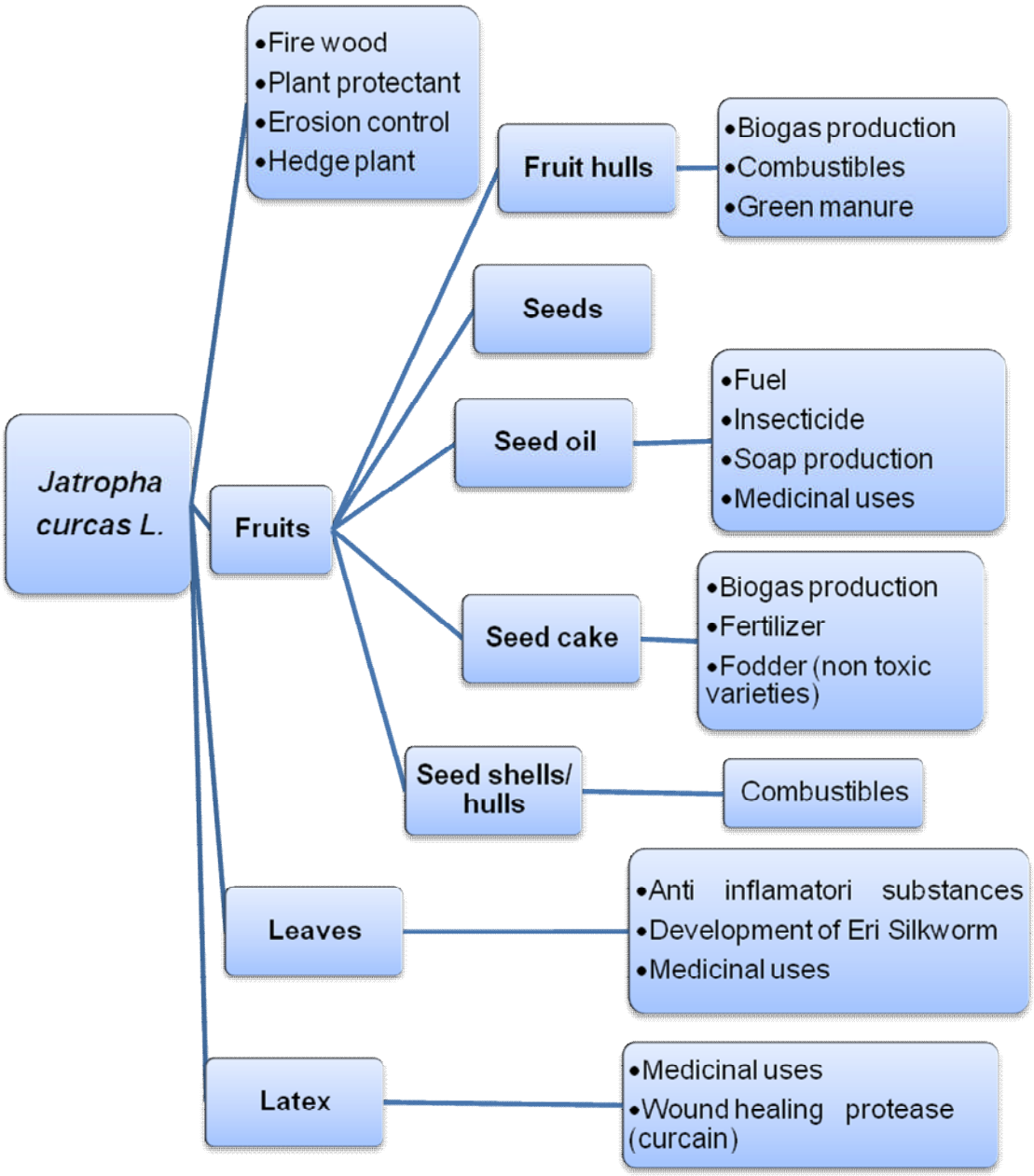

Fig. 2.4: The uses of *Jatropha curcas L.* [89]

Before the oil extraction process, a few procedures have to be conducted like the followings; first, dehulling which is separating the hull from their fruits; secondly, nut

shelling which separating nut shell/ hull from kernel; thirdly; drying and finally; the oil extraction [81].

The physic nut can produce diesel fuel for energy and also the nut oil is a raw material for soap production. In medicinal purposes**,** all parts of the plant are used in traditional medicine and for veterinary purposes. The oil is extensively used for skin diseases and to relieve pain such as that caused by rheumatism and has a strong purgative action. The seed oil can also be utilized as a fuel, lubricant, insecticide and when mixed with iron oxide, they can be used in varnish. A decoction of leaves is used as an antiseptic after birth of child and against cough. Besides that, leaves can be utilized for rearing of silkworm, in dyeing in medicines, and as an anti-inflammatory substance [75, 81].

Some components of the jatropha plant can be utilized in medical and cosmetic purposes. This “bitter, damp, cool, toxic, antipruritic and styptic” plant has been mentioned in the Great Compendium of Chinese Materia Medica and the Chinese Dictionary of Medicinal Plants, 2003 [90, 91]. However, it was not mentioned in ancient materia medica and the Chinese Pharmacopoeia [92]. The latex of the brances and leaves has medicinal, pesticidal and mollusk control properties. It has been used for wound healing, which demonstrated the coagulating effects on blood plasma to arrest bleeding of wounds and to defeat skin diseases by its antimicrobial properties against certain bacteria, especially in Yunnan, Panzhihua and Hainan [75, 81]. As a plant protectant and molluscicide, the extracts from all parts of the physic nut has insecticide properties. The oil extract from the seed were widely used to control various pests [75].

The seed cake is generated in large quantities after oil extraction as its commercial exploitation is vital for the economic viability of the physic nut system. It also has high energy value and can be pressed into briquettes and burned as fuel. High quality protein concentrate could also be produced from seed cake after detoxification [93, 94]. This detoxified seed cake has been used in the diets of farm animals and

aquaculture species. Instead of that, the seed cake and parts of physic plant could also be utilized to produce biogas and fertilizer [81, 95].

The fruit hulls which are also tannin containing combustible can be used as green manure, and in biogas production. Finally, the yellow oil from the roots has strong antihelminthic properties [81].

2.5.5 Economy view

The alternative resources of energy meet a wide importance as a result of the rigorous energy crisis and increase of petroleum prices. Many countries, like India have been starting to give attention extensively on the concept of alternating biodiesel produced from plantations of Jatropha on eroded soils for conventional diesel fuel. Recently, the plant is being grown in various parts across the world. The oil extraction from jatropha seeds produces a significant amount of hulls waste [96]. About 350L oil and 2.40 tonne hulls are produced from one tonne of jatropha seeds. Hence, the disposal of Jatropha hulls will create problem in the future if Jatropha is being commercialize for the production of biodiesel [96].

2.6 Lignocellulosic material

Lignocellulosic resources are extremely widespread and abundant. Forests contain about 80% of the world's biomass. Cellulosic or lignocellulosic materials are composed of mixture of carbohydrate polymers (cellulose and hemicelluloses) and a cementing material, lignin. The carbohydrate polymers are firmly bound to lignin mainly by hydrogen bonds and also by some covalent bonds. Cellulose is the most abundant global source of biomass and has been mostly unutilized. 90% of plant biomass is composed of lignocelluloses. Examples of cellulosic materials are paper, cardboard, wood, and other fibrous plant material [97-98].

2.6.1 Lignocellulosic waste as biosorbents

Current expensive conventional methods for pollutants removal, such as, heavy metals ions, dyes, ammonia and nitrates from the environment can be replaced by adsorbents obtained from plant wastes which are more feasible. This approach is very useful because of high adsorption properties of lignocellulosic wastes, as a consequence to their ion-exchange capabilities. The adsorbent which is made from agricultural waste will reduce the cost of waste disposal, add value to the waste material and offer a potentially economical alternative to replace commercial activated carbons [99, 100].

Numerous researches have been reported using chemically modified plant wastes as an adsorbent. For example, rice husks/rice hulls, spent grain, sugarcane bagasse/fly ash, sawdust, wheat bran, corncobs, wheat and soybean straws, corn stalks, weeds, fruit/vegetable wastes, cassava waste fibers, tree barks, azolla (water fern), alfalfa biomass, coirpith carbon, cotton seed hulls, citrus waste and soybean hulls show good adsorption capacities for Cd, Cu, Pb, Zn and Ni [101-107]. Habitually, the plant waste were modified with formaldehyde in acidic medium, NaOH, KOH/K_2CO_3 and CO_2, or acid solution or just washed with warm water [99, 105, 107].

Lignocellulosic wastes have shown the ability to adsorb dyes from aqueous solutions; such as, the adsorption of reactive dyes by sawdust char and activated carbon [108]; ethylene blue by *Rosa canina* sp. seeds waste [109]; anionic dyes by hexadecyl trimethyl ammonium modified coir pith [110]; and methylene red by acid-hydrolysed beech sawdust [111]. Besides that, the adsorption of ammonia and nitrate removal by using agricultural waste materials has also been studied [112, 113]. The adsorption properties of the original lignocellulosic material could be enhanced by prehydrolysis. This is due to the removal of hemicelluloses during sulphuric acid

treatment, which open the lignocelluloses matrix's structure and increased the surface area. Then, the activation of the material's surface results in the rising of the number of dye binding sites [99, 111].

The structure of lignocelluloses which is resistant to degradation because of the crosslinking between the polysaccharides (cellulose and hemicellulose) and the lignin via ester and ether linkages is the barrier for the production and recovery of valuable materials from lignocellulosic waste [99, 114, 115].

2.6.2 Lignocellulosic material as a composite sorbents

A lignocellulosic composite is a reconstituted product. It is prepared by a mixture of one or more substances using some sort of a bonding agent to grasp the components together. Plywood, particleboard, fiberboard, and laminated lumber are some of the examples of lignocellulosic composites [116]. At present, researches have been going on to utilize agro-based sorbents for the removal of heavy metals, pesticides, and oil from rain water run off in several cities in the United States [117].

Composites prepared from agro-based resources change dimensions with the changes in moisture content. This is due to the attraction of moisture through hydrogen bonding to the cell wall polymers, which contain hydroxyl and other oxygen-containing groups. The hemicelluloses, as well as accessible cellulose; non-crystalline cellulose, lignin, and surface of crystalline cellulose are essentially responsible for moisture sorption. The cell wall swells by the moisture, and expands the fiber until the cell wall is saturated with water. After the cell wall becomes saturated, moisture remains present as free water in the void structures and no further expansion will take place. This is a reversible process and with the losses of moisture the fiber shrinks in dimension [117].

The agro-based composites are degraded naturally because of organisms that distinguish the carbohydrate polymers, generally on the bars of hemicelluloses in the cell wall. The organisms have the capability to hydrolyze these polymers into

digestible units using their particular enzyme systems. The fiber cell wall gets weakened due to the biodegradation of the high molecular weight cellulose because crystalline cellulose is primarily responsible for the strength of the cell wall. The fiber cell wall become weaker as the cellulose polymer undergoes degradation through oxidation, hydrolyses, and dehydration reactions. The similar types of reactions occur in the presence of acids and bases [117].

Exposure the agro-based composites to outdoors, allows it to undergo a U-V induced photochemical degradation. The lignin component is responsible for the characteristic color changes and as a primary place, the degradation takes part. The lignin acts as a bonding agent in the cell walls which held the cellulose fibers together. As the lignin degrades, the surface becomes more abundant with cellulose. Compared to lignin, cellulose is more prone to ultraviolet light degradation. Once the lignin has been degraded, the poorly bonded carbohydrate-rich fiber simply erodes from the surface, and then exposes new lignin to further degradative reactions. Ultimately, this “weathering” process is the reason for the surface of the composite to become rough and explains for a significant loss in surface fibers [117]. The cell wall polymers go through pyrolysis reactions with increasing temperature to impart volatile and flammable gases. The hemicelluloses and cellulose polymers are degraded by heat much prior to the lignin is. The lignin component contributes to char formation, and the charred layer helps as a shield to the composite from further thermal degradation [117].

Li, [118] found that the modification of sunflower and sawdust biomass by NaOH increased the metal ion binding capacities by the methyl esters present in the biomass. It was observed that carboxyl groups in these materials had the ability to bind metal ion. However, lignin did not contribute for the binding site due to the absence of carboxyl group. Only the cellulose molecule contained hemicelluloses which could bind metal ions with its carboxyl groups.

2.7 Different inorganic adsorbents

Silica gel, activated alumina, and activated carbon are some of the traditional microporous adsorbents. Recently developed microporous adsorbent is crystallin aluminosilicates or zeolites. The choice of adsorbent for practical separation processes is limited to the microporous adsorbents with a range of pore diameter from a few Angstroms to a few tens of Angstroms which is required by adequate adsorptive capacity. Classes of adsorbent depend on the difference in the adsorptive properties such as micropore size and structure. As an instance, properties of zeolitic adsorbent are controlled by its crystal structure and there is virtually no distribution of pore size.

2.7.1 Active carbon

Many adsorption studies have been done using commercial activated carbon to remove heavy metals from wastewater, such as Cd, Ni, Cr, Cu, Cr [119-123]. Yet, active carbon remains the one of expensive adsorbent materials. In recent years, development of surface modified activated carbon has been generated a variety of activated carbons with far superior adsorption capacity to improve the economy of adsorption [123].

2.7.2 Granular activated carbon

Without activation, most porous carbonaceous materials have a natural internal surface area of around $10m^2/g$ and the activation process expands the internal surface structure to approximately 1000 m^2/g. Granular activated carbon (GAC) is the most often used adsorbent for the elimination of organic and inorganic pollutants. The

carbon activation processes consist of carbonization phase, which involves heating the carbon source to a temperature of 600^{o}C in the absence of air and than the carbonized char is activated by steam at 1000^{o}C or by chemical treatments with acid or acid salts. The process develops porosity as well as increases the surface area [124]. Granular activated carbon has some disadvantages also. For example, the price of activated carbon is costly, the activated carbon loading into the containment vessels using water-carbon slurries increase the complexity of the system and cost [125], activated carbon is also easily smashed into useless fines under high crash and overload stresses [126], the operating costs for regeneration or disposal of spent activated carbon is prohibitive *etc*. [125].

2.7.3 Biosorbent

Bailey *et al*. [127] gave the detailed description of the variety of sorbents such as bark/tannin-rich materials, lignin, chitin/chitosan, dead biomass, seaweed/algae/alginate, Xanthate, zeolite, clay, fly ash, peat moss, bone, gelatin, beads, leaf, mould, moss, iron-oxide-coated sand, modified wool and modified cotton. Some of the reported adsorption capacities reported for cadmium, chromium, lead and mercury are like the following: 1587 mg Pb/g lignin, 796 mg Pb/g chitosan, 1123 mg Hg/g chitosan, 1000 mg Hg/ g CPEI cotton, 92 mg Cr(III)/g chitosan, 76 mg Cr(III)/g peat, 558 mg Cd/g chitosan, and 215 mg Cd/g seaweed [127].

The capability of lowering transition metal-ion concentration to parts per billion concentrations makes the natural biopolymers seems industrially attractive. Certain waste from agricultural operations or natural materials that are available in huge quantities may have potential to be used as low cost adsorbents, as they are unused resources of widely availability and also are environmentally friendly [128]. The biomass adsorbent-based biosorptive processes are more cost-effective than activated carbon because the natural adsorbents are renewable resources [126, 129]. For regeneration, the spent biosorbent substrate which adsorb an inorganic species can be diluted in nitric acid to strip the metal ion and after that once in solution again, the pH

will be changed to precipitate the metal ion from solution that were concentrated on the adsorbent material [130]. In the case of adsorption of organic compounds, composting the spent biosorbent will degrade the adsorbent medium as well as the adsorbate [126].

2.8 Heavy metal

2.8.1 Environmental and heavy metal ion

Heavy metals are a group of toxic elements, with specific gravities of usually greater than 5 (although there are major exceptions), but there is no rigorous scientific basis or chemical definition for this group. Heavy metals that are of significant environmental concern are included in the United States Environmental Protection Agency's (USEPA's) list of priority pollutants. The common ones are, for example, Cr (7.19), Co (8.90), Ni (8.90), Cu (8.96), Zn (7.13), Ag (10.5), Cd (8.65), Hg (13.6), Ti (11.9) and Pb (11.4). The number in parenthesis represents the specific gravity of each element [131].

Nevertheless, heavy metals are also required micronutrients, *i.e.*, essential ingredients for living cells, with the exceptions of cadmium, mercury and lead. Thus, toxicity effects of these elements are largely a function of concentration. As show in Fig. 2.5, these elements are beneficial and have nutritional values lower than some critical dosages, but become inhibitory to toxic with an increase in concentration. The threshold toxic concentrations differ for each heavy metal, and are governed primarily by the chemistry of each heavy metal in question and associated physiological effects. On the other hand, nonessential heavy metal elements are inhibitor to growth at all concentrations [131].

Pollution with heavy metal is a matter of global concern due to the potentially hazardous effect of these materials to the environment. The adsorption of metal by

solid surfaces is a significant process that controls trace metal concentrations in the aqueous system [132]. Heavy metal ions such as cadmium, zinc, copper, lead, nickel etc are considered to be hazardous to both human life and the environment [132]. About 20 metals are categorized as toxic and half of these are released into the environment in quantities which are hazardous to human health [133]. This is due to their acute toxicity and non-biodegradability even when the heavy metals are present at low concentration [2].

Most of the heavy metals are not biodegradable substances and accumulate in the environment. The concentration of the metal ions has to be reduced in the environment to enhance the environmental quality standards particularly in water pollution control [127]. Zinc and cadmium metal ions are often present in industrial wastewater. They are hazardous to the aquatic ecosystem and pose possible human health risk by accumulation throughout the food chain and may affect human beings. Due to several industrial activities the concentration of zinc ions in waste water is often higher than the tolerance limit [134].

The harmful effects of cadmium on biosphere are well documented [11]. Toxic effects of cadmium on humans include both chronic and acute disorders like testicular atrophy, hypertension, damage to kidneys and bones, etc [135]. Because of high toxicity and mobility in soil, cadmium is creates lot of environmental problem [4].

The common techniques for the removal of metal ions from wastewater include precipitation with lime, ion exchange, ultra filtration, reverse osmosis *etc.* But these processes are either relatively expensive or inadequate when the permissible concentration of the metal ion is low. Besides, these techniques often generate huge amount of metal-bearing sludge causing difficulties in disposal. Lately, much attention has been paid on the removal of metal ions through biosorption technique, which does not generate toxic sludge. Further, metal ions can be recovered from the loaded adsorbent for reuse. Although activated carbon is the best choice in this regard and is being used for the treatment of municipal and industrial wastewater for many years, the high cost of activated carbon restricted its use in many countries. This leads

to the search for efficient, cost-effective and non-conventional adsorbents using various agricultural, industrial, natural/biological waste materials [136]. Therefore, it is essential to understand adsorption characteristics such as mechanism and kinetics of adsorption with such bio adsorbent because the studies of adsorption kinetics are ultimately a prerequisite for designing an adsorption column [30].

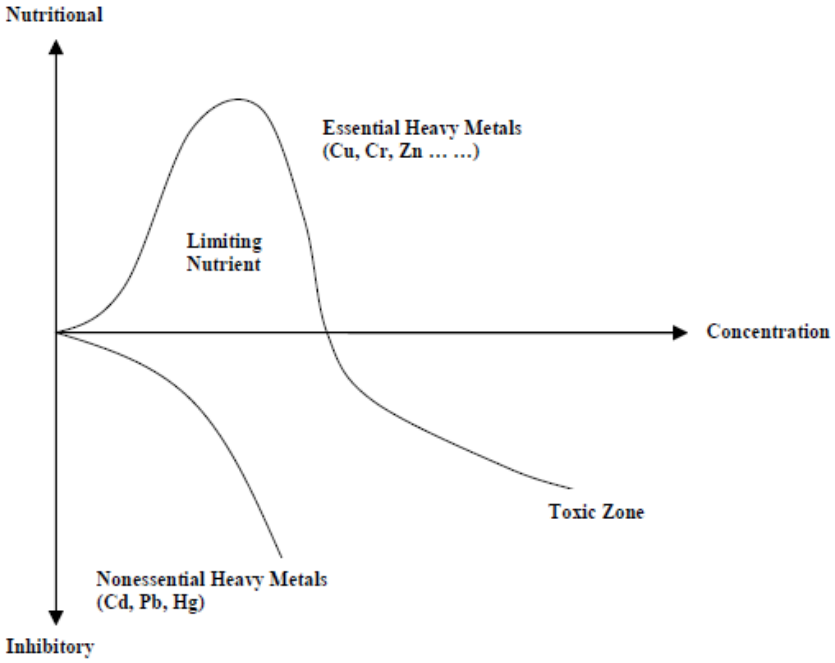

Fig. 2.5: Nutritional and inhibitory effects of heavy metal concentrations on living cells / microorganisms [131]

Human activity and industrial development during the last fifty years have greatly modified metal cycles on regional and global scales. While mining, metallurgical, electroplating industries, *etc.*, have resoundingly boosted the production and usage of heavy metals in our life cycles, the lowering of pH in rain and surface waters as well as the increased use of surfactants have further enhanced the mobility of heavy metals in the environment. Understandably, the presence of heavy metals in aquatic, terrestrial and atmospheric environment is of high concern. Such heavy metals may

exist as cations, anions, non-ionized species and complex macromolecules in the aqueous phase. With the glaring exception of elemental mercury, most of the heavy metals and their compounds are practically absent in the atmosphere under ambient conditions, as their boiling points are extremely high [131].

2.8.2 Electronic structure of Zn^{2+} and Cd^{2+}

Electronic structures of the heavy metals are able to govern their speciation and fate in the natural environment, as well as their separation and/or control by engineered processes. Besides that, the biochemical actions of metals as nutrients or toxicants are also dictated by the electronic structures [131]. For instance, the electronic configurations of metal cations such as cadmium (Cd^{2+}) and zinc (Zn^{2+}) are:

$$Cd^{2+}: 1s^2 2s^2 2p^6 3s^2 3p^6\ 3d^{10}\ 4s^2\ 4p^6 5s^2\ 4d^8$$
$$Zn^{2+}: 1s^2 2s^2 2p^6 3s^2 3p^6 3d^{10}$$

The transition metal cation, Zn^{2+} and Cd^{2+} has d-orbital and surrounds electron clouds which are more readily deformable by electric fields of other species. Generally, these ions are fairly strong Lewis acids and be liable to form inner sphere complexes with ligands in the aqueous phase. Cd^{2+} is also a strong electron acceptor and a relatively “soft” cation, while Zn^{2+} is a “borderline” cation. Most of the toxic heavy metals are fall under “borderline” and “soft”. Usually, the toxicity of metals increases as one moves from hard cations to borderline, and then to soft. Relative affinities of these metal ions to form complexes with O-, N-, and S-containing ligands, vary extensively. Borderline and soft cations display higher affinities towards nitrogenous and sulfurous species, while hard cations prefer oxygen-donating ligands (Lewis bases). Thus, the soft cations bind strongly with sulfhydryl groups in proteins of the cells. Due to the fact that sulfhydryl groups do form active sites on proteins, their blockages through heavy metal binding result in severe toxic effects [137].

Table 2.5: Characteristic of cadmium and zinc

Charateristic	Cadmium	Zinc	Ref.
Physical properties	soft, malleable and ductile	brittle at normal temperatures and malleable at 100^{o}C to 150^{o}C	138, 139
Colour	silver-white or silver gray	bluish-white, shiny metal	139
Origin	rare ores like sphalerite and greenockite, as a derivative from the process of producing zinc, copper, and lead, mining, smelting, oil and coal combustion, waste incineration, preparation of fungicides and fertilizers, spent nuclear fuel and radioactive wastes from operating nuclear reactors and fuel reprocessing plants.	mine ores, zinc manufacture facilities, iron and steel production, corrosion of galvanized structures, coal and fuel combustion, waste disposal and ignition, and the application of zinc-containing fertilizers and pesticides	139, 140, 141
Usage	industry of nickel-cadmium batteries, anticorrosive coating for steel and cast iron, as a component of certain specialty alloys, as a semiconductors, such as cadmium selenide and telluride; dyes and pigments; stabilizers in plastics, such as polyvinyl chloride; and neutron absorbers in nuclear reactor, such as control rods	protective coating of other metals, such as iron and steel, alloyed with other metals to strengthen the metal, dry cell batteries, white paints, ceramics, rubber, wood preservatives, dyes, fertilizers and as ingredient in ordinary products like sun blocks, diaper rash ointments, deodorants, athlete's foot preparations, acne and	139, 142,

	and shields.	poison ivy preparations, and anti-dandruff shampoos	
Toxic effect	cytotoxic, embryotoxic, headache, chest pains, respiratory system like bronchial and pulmonary irritation, muscular weakness, pulmonary edema, cause renal dysfunction, bone degeneration, liver damage, blood damage, death.	stomach cramps, nausea, vomiting, anemia, damage of the pancreas, and lowering the levels of high-density lipoprotein cholesterol	139, 143

Table 2.6: Salient properties of Zn^{2+} and Cd^{2+} [131]

Name of Cations	Type	Salient Properties
Zinc, Zn^{2+}	Borderline Cations	• Spherically non symmetric • Electronic configurations do not conform to inert gases • Form inner-sphere complexes with O- and N-atom-containing ligands • Toxic
Cadmium, Cd^{2+}	Soft Cations	• Spherically non symmetric • Electronic configurations do not conform to inert gases • Exceptionally high affinity towards S-atom-containing ligands • Toxic from a physiological viewpoint

Considering the processes for heavy metals removal, equipment configurations and physical arrangement often vary widely. However, with a few minor exceptions, Lewis acid-base interaction aided by precipitation, sorption, sieving, *etc.*, constitutes the primary mechanism for heavy metals separation. Naturally occurring humus, dead bacterial and fungus cells, seaweeds, as well as many other biorenewable materials, do contain surface functional groups (carboxylate, carbonyl, phenolic) with moderate to high affinity towards heavy metals. Significant progress has been made in the recent past in modifying such materials into chemically stable, mechanically strong and durable sorbents [144, 145]. As emphasis is laid on sustainable development, these sorbent materials are likely to be economically competitive, and large-scale commercial production is anticipated to follow [131].

2.8.3 Separation Strategies

Table 2.6: Size of a heavy metal cation (Me^{2+}) in water in different physiochemical states [131]

State Dissolved	**Speciation**	**Approximate Diameter (Nanometer)**
Water	H_2O	0.2
Hydrated free metal ion	$[Me(H_2O)_n]^{2+}$	Around 0.5
Inorganic complexes	$[Me(NH_3)_n]^{2+}$ $[MeOH]^{+}$ $[Me(OH)_2]^{0}$ $[MeC0_3]_2^{2-}$	Less than 1.5
Organic complexes	$[Me(COO)_2]^{0}$ $[Me(NH_3)_n]^{2+}$ $[Me(EDTA)]^{2-}$	1 - 5
Macromolecules / colloids	Me – Humate Complex Me – Fulvate Complex Me – NOM-coated silica	10 - 500
Surface binding onto microparticles	$\begin{vmatrix} FeO^- \\ FeO^- \end{vmatrix}$ (Me^{2+})	100 – 10,000
Precipitates	$Me(OH)_{2(s)}$ $MeCO_{3(s)}$	> 500

To achieve efficient and effective separation of heavy metals from the aqueous phase and other complex systems, Lewis acidity / basicity, ionic charges, sorption

affinity onto particulates containing surface functional groups, redox state, aqueous-phase solubility, physical sizes of the metal-ligand complexes, *etc.*, can be manipulated. Speciation of heavy metals in the dissolved states varies, and so do the sizes of these species. Table 2.6 shows the estimated sizes of divalent heavy metal cations, Me(II), in different physiochemical forms. The relative sizes of the heavy metals also influence their fate and transport behaviors in a natural environment [131].

2.8.4 Selectivity for the removal of heavy metal ions

Usually, removal of heavy metal cations from water and wastewater streams involves a situation where only a trace concentration of the heavy metal ion (usually in the range of ppm) needs to be selectively removed in the presence of other competing non-toxic, non-regulated ions (*e.g.,* Ca^{2+}, Ma^{2+}, Na^{2+}, *etc.*). The selectivity of ions is a tough and also a challenging proposition; removing only the trace contaminant constitutes an efficient and economic solution. The current treatment processes that remove all the ions – heavy metals and non-toxic (*e.g.,* solidification/stabilization, membrane filtration, precipitation, *etc.)* invariably face difficulties in justifying the associated costs. An additional problem associated with the handling the abundant quantities of sludge produced, and again disposal is an environmental and economic concern [146].

Generally, the most important factors that influence the selectivity behavior of cations in solution are valence and ionic radius [147]. The ionic potentials (Z^2/r) of the metals estimated based upon the charge (Z^2) and radius of the ion (r) follows the order: Zn>Cd. Ion of higher ionic potential should have adsorbed more strongly if the metal adsorption on the adsorbent were completely electrostatic [147]. Many researchers explained selectivity by examining the metals and clays hard–soft acid base (HSAB) behavior [148].The HSAB principle states that hard Lewis acids prefer to complex or react with hard Lewis bases and soft acids prefer to complex or react with soft bases. Hard ion have high electronegativity, low polarizability, a small ionic

radius, and a lack of an unshared pair of electrons in their valence shell, while the opposite is true for soft ion [149].

Misono *et al.* [150] observed that the softness decreased in the order Cd>Zn and the metal selectivity followed the same sequence according to the HSAB principle. However, some literature showed that there are inconsistencies in the application of HSAB principle, mainly with respect to the trace metal cations [151]. McBride [152] reported that harder transition metals tend to be preferred over softer transition metals, but softer nontransition metal (e.g., Pb^{2+}) are preferred over harder nontransition metals (e.g., Cd^{2+}). A high ionic potential of Zn^{2+} causes it to be adsorbed as strongly as Pb^{2+}. In the lower pH range (up to pH 5), the metals especially Cd^{2+} and Zn^{2+} are mostly adsorbed on the permanent charge sites of adsorbent as well as the complexes. At pH 5, a predominant involvement of adsorbent surfaces on the complexes such as edge surfaces of adsorbent and broken edges of the adsorbent in the adsorption of the metals is assumed [147].

2.8.5 Potential of different treatment processes

Chemical precipitations using hydroxide, carbonate or sulfide, or some combination of these chemicals are the standard treatment methods for the removal of heavy metals from wastewater. The most regular technique is the hydroxide precipitation process, due to its simplicity, ease of operability and economical characteristics if lime is utilized. The theoretical minimum solubility values of metal hydroxide are low; however, these levels sometimes are effectives in practice because of poor solid or liquid separation, slow reaction rates, fluctuation of pH, and the presence of other cations as well as complexing agents in the wastewater [153].

Existing literature data [154-158] show that the concentrations of heavy metals, such as copper, lead and zinc, in the treated effluent can be decreased to about 0.5 mg/L by the hydroxide precipitation process with proper control of pH, clarification and filtration. An effective alternative to hydroxide precipitation for removal of heavy

metals from wastewater, regardless of whether a solution of sodium sulfide, hydrosulfide, or slightly soluble ferrous sulfide slurry is used as the reagent has been demonstrated by sulfide precipitation [159-162].

Bhattacharyya et al. [163] found that sulfide precipitation is an effective process for the removal of cadmium, copper, lead, zinc, arsenic and selenium. The results of their research revealed that this process is capable of decreasing the concentrations of heavy metals to less than 0.1 mg/L. However, filtration may be required following clarification for effective removal of metal ions because of the relatively small particle sizes. The potential for hydrogen sulfide gas evolution, sulfide toxicity, and odor makes the inorganic sulfide precipitation less attractive. By using organic sulfide compounds, such as Trimercapto-S-Triazine (TMT), some of these problems with the inorganic sulfide precipitation can be eliminated but the high cost of TMT makes the process economically unfeasible [153].

Ion exchange is principally a volume reduction process. During the process the ions are removed from the wastewater and concentrated on the exchange resin. Next, through regeneration step, the ions are released from the resin and are dissolved in the regenerant solution. Ion exchange is capable of reducing the concentrations of heavy metals to non-detectable levels. However, it requires relatively high capital and operating costs which makes this process impracticable for economic utilization, unless the treated effluent is recycled and reused [153].

2.8.6 Factors affecting Metal Removal by Adsorbent

Solution pH, metal type and concentration, surface loading, presence of complexing ligands and competing adsorbates, ionic strength, temperature, as well as type of adsorbent are several factors that affects heavy metal ion removal from aqueous solution [164].

2.8.6.1 Solution pH

It was first observed by Sigworth and Smith, [165] that metal removal by activated carbon was inversely proportional to the solubility of the metal. Metal removal increases with the increasing pH for uncomplexed cationic heavy metals. The metal removal versus pH curve is referred to in the literature as a "pH – adsorption edge" [164]. In particular, pH affects the condition of the outer hydration sheaths of the metal ion, aqueous metal speciation, complexation and solubility, as well as the electrochemical behavior of the carbon surface. Netzer and Hughes [166] reported that the starting of cationic metal adsorption corresponded with the loss of the outer hydration sheath of the metal ions. At a pH slightly lower than the pH at which $Me(OH)^-_{(aq)}$ forms would remove the outer hydration sheath [164].

2.8.6.2 Metal type and concentration

Usually, the metal removal will be enhanced at the lower pH at which the cationic metals formed aqueous hydroxide complexes $[Me^x(OH)_n^{(x-n)}]$ and solids $[Me(OH)_{2(s)}]$. The formation of the first metal hydroxide species can be represented by the following chemical reaction:

$$Me^{2+} + H_2O \xleftrightarrow{K_1} Me(OH)^+ + H^+;$$

Pb, Cu, Zn and Ni form hydroxide complexes in the following order based on increasing pH: (value of K_1 is given in parenthesis)

Pb (6.45) > Cu (7.73) > Zn (8.96) > Ni (10.0)

Values of K_1 are taken from Smith and Martell [167]. For a variety of commercial activated carbons the initiation of metal – pH adsorption edges followed this type of trend [168]. For anionic and select cationic metals, the removal phenomenon is more complex. For example, Huang and Blankenship [169] reported that Hg(II) is adsorbed

by activated carbon and is reduced to Hg^0 and the mercury volatilized once in the Hg^0 form.

The removal mechanism is affected strongly by the concentration of the metal ion. The surface precipitation can occur if the concentration of the cationic metal is large enough such that $Me(OH)_{2(s)}$ forms. If the metal concentration is lower than the metal's solubility, then the primary removal mechanisms are supportive in nature (physical / chemical adsorption, ion exchange). The denominator of the surface concentration expression approaches zero, while the removal approaches 100% can cause the metal surface concentrations under these conditions to increase rapidly [164].

2.8.6.3 Surface loading

As with organic adsorbates, the increase in the adsorbates' aqueous and surface phase concentrations occur with the increase in the adsorbate surface loading (initial mass of metal per gram of carbon) [164].

2.8.6.4 Complexing ligands, competing adsorbates, ionic strength and temperature

The metal ion removal in the metal-only system can be modified by the presence of complexing ligands and competiting adsorbates. To find out the ligand's effects on metal adsorption informations, like type and concentration of ligand and metal, carbon type and solution pH are required. In systems with more than one adsorbate, competition may occur between the adsorbates for the surface sites. The level of competition is dependent on the type and concentration of the competing ions, number of surface sites, and the affinity of the surface for adsorbate. Altering aqueous metal chemistry and the structure of the electric double layer which surrounded the carbon surface may results in some modification in the ionic strength. It can affect the metal ion adsorption. Again the temperature of adsorption also influences the degree of both aqueous and solid-phase reactions occur [164].

2.9 Dyes

2.9.1 Malachite green

The current estimated numbers of different commercial dyes and pigments are around 10,000 and the annual productions are over 7 x 10^5 tones globally. Dyes are extensively used in productions of textile, rubber, paper, plastic, cosmetic *etc.* Textile ranks first in the usage of dyes for the coloration of fiber [22]. Synthetic dyes are common water pollutants and often can be found in trace quantities in industrial wastewater due to their solubility. However, as dyes impart toxicity to aquatic life and damage the aesthetic nature of the environment; severe problems emerge from the discharge of dye-bearing wastewater into natural streams and rivers. Furthermore, it is very difficult to treat wastewater containing dyes since the dyes are recalcitrant organic molecules and are resistant to aerobic digestion, stable to light, heat and oxidizing agents. It is probably associated with by their structure and molecular size [170]. Photosynthetic activity in aquatic life is also significantly affected by the presence of dyes as they reduce the light penetration and may also be toxic to some aquatic life due to the presence of aromatics, metals, chlorides, *etc.* [171].

Amongst all other dyes of its category, malachite green is the most extensively used for coloring purposes [172]. Malachite green is extremely toxic. It possesses carcinogenic properties to human beings and it affects the immune and reproductive systems [173]. Moreover, it can irritate the respiratory tract if inhaled can cause

irritation to the gastrointestinal tract upon ingestion, can irritate the skin with the redness and pain if contact with the skin. It will lead to permanent injury of human eyes and laboratory animals if contacted with eye [174].

The discharge of Malachite green into the streams affects the aquatic life and causes detrimental effects in liver, gill, kidney, intestine, gonads and pituitary gonadotrophic cells [175]. Lack of carcinogenicity information and the exposure to worker and consumer, is the main reason for the selection of malachite green chloride by the National Institutes of Environmental Health Sciences for carcinogenicity testing in National Toxicology Program (NTP). At present, it is nominated for toxicity and carcinogenicity testing by the Food and Drug Administration [20].

Malachite green is also known as aniline green, basic green 4, diamond green B, or victoria green B. It's IUPAC name: 4-[(4-dimethylaminophenyl)-phenyl-methyl]-N,N-dimethyl-aniline.It is a toxic substance frequently used as a dye industry [21]. In solution form, it can also be utilized as a topical antiseptic or to treat parasites, fungal, protozoan and bacterial infections and some other diseases caused by helminthes on a wide variety of fish and other aquatic organisms; and also as bacteriological stain [175, 176].

Historically, malachite green is one of the simplest forms of arylcarbonium ion colorants. It is the earliest group of synthetic dyes which was developed for textile applications. Malachite green as arylcarbonium ion colorants are still being used these days, mostly as a basic (cationic) dye for the colorant for acrylic fibers and paper, and as pigments. Their structure and properties are quite similar to the polymethine dyes, especially cyanine [177]. Fig. 2.7 showed that the molar extinction coefficient of Malachite Green dissolved in water is of 148,900 $M^{-1}cm^{-1}$ at 616.5 nm [178].

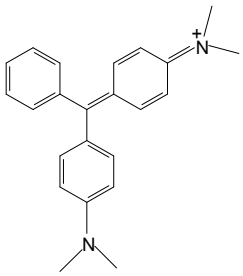

Fig. 2.6: Structure of Malachite Green 125 [177]

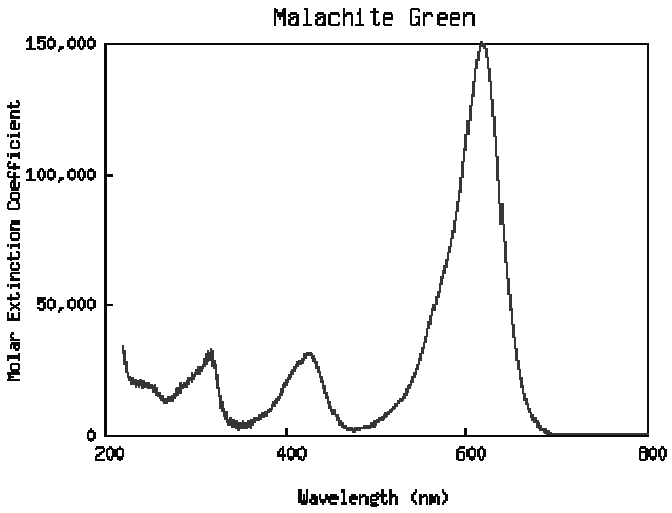

Fig. 2.7 : Molar extinction coefficient of Malachite green [179]

There is a major health risk to humans who eat fish contaminated with malachite green as detected in Canada in the year 1992. Malachite green was found to be toxic to human cells and might cause liver tumor formation, and it has been classified a Class II Health Hazard. As this chemical is ease to manufacture at low-cost, it is still in use in certain countries with less preventive laws for non-aquaculture purposes. In 2005, at Hong Kong, this chemical was traced in eels and fish imported from China and Taiwan. Also, in 2006, it was detected by the United States Food and Drug Administration (FDA) in seafood imported into that country for human consumption by China, where the chemical is also banned for use in aquaculture. Due to continued

malachite green contamination, FDA blocked the importation of several varieties of seafood in June 2007 [21].

The convectional wastewater treatment has low removal efficiency for reactive and other anionic soluble dye as it relies on aerobic biodegradation. Further more; the low biodegradation of dyes is another reason for non-effectiveness of the conventional biological treatment process in treating dyes present in wastewater. Dyes are usually treated with some expensive physical or chemical processes which are also not quite effective in threatening wide range of dyes waste [22]. Recent years, adsorption techniques have gained favor due to their proven efficiency in the removal of pollutants from effluents. The efficiency of adsorption for dye removal from wastewaters has made it an ultimate alternative to other expensive treatment methods. The processes are economically feasible with a high quality product [23- 25].

A number of non-conventional sorbents has been studied in literature to remove Malachite green dye from aqueous solution. Akmil-Basar *et al.* utilized activated carbon prepared from pine sawdust and PET for the purpose, Tahir and Rauf have studied the removal of a cationic dye (malachite green) from aqueous solutions by adsorption onto bentonite clay, Guo *et al.* used micro- and mesoporous rice husk-based active carbon, Garg *et al.* utilized treated sawdust for the adsorption of dyes, Hameed and El-Khaiary investigated the potential of rice straw-derived char for the removal of dye from aqueous solution, Mall *et al.* studied the potential of bagasse fly ash and activated carbon for the removal of organic and coloring matter from aqueous solution [22, 180-184].

2.10 Surfactants

Structurally a surfactant molecule consists of a long chain hydrocarbon tail, and a short ionizable or polar group. The hydrophobic tail causes the molecule to be virtually insoluble, with slight solubility imparted by the ionizable or polar group. Normally, a surfactant has only one hydrocarbon tail, however sometimes two tails

join to the same polar group surfactant molecules and it is common in biological membranes [185]. Surfactant is amphiphilic because it contains a hydrophobic part and a hydrophilic part, the polar hydrophilic group is used for its classification. The surfactant is considered to be anionic if on ionization in water, the surface-active portion containing the hydrophobic chain has a negative charge. An example is the alkyl sodium sulfonate, $R\text{-}SO_3Na$, which splits into $R\text{-}SO_3^-$ and Na^+ [185].

The surfactant adsorbed onto a solid surface modifies the surface properties of that solid. When the surfactants added in controlled concentrations, it will change the surface properties of the solid particles from hydrophobic to uncharged hydrophilic entities or vice versa. Surfactants have been used to facilitate the transportation or immobilization of the toxic heavy metal ions and dyes on the adsorbent surface [186]. The used of surfactants also results in the formation of highly ordered aggregates (micelles) that solubilize the dye molecules and prevent their sorption [187].

Myers [188] showed that micellar activity may be improved in the surfactant solutions below the “normal” CMC in the presence of small amounts of solubilized additives (additive-induced micellization). Surface active molecules or surfactants, such as soaps, detergents, lipids, *etc.*, can self-coagulate to form multi-molecular aggregates of colloidal size, and exhibit the effects of colloidal forces in addition to their individual phase behavior [189].

The benefits of using the colloidal synthetic route can be related to the excellent heat and mass transfer, as well as simple handling of the product. The product can be efficiently pumped out of the reactor and into storage tanks. Here, an understanding of how the surfactants adsorb onto different organic phases and operate at different pH is of utmost importance [189].

The attachment and detachment of particles to and from the surfaces needs an understanding of the different interparticle forces and how to control them by manipulating the chemical environment of surfactant type. Again the ability to manipulate interparticle forces is very pertinent when the aggregation is controlled

either by inorganic ions, such as phosphates or organic polyelectrolyte. High surfactant concentration can solubilize grease and re-suspend particulate material [189]. Generally, surfactant is necessary to overcome some of a colloidal problem with the objectives like, particle size control, separation and drying of particles, wetting of dry powders, adsorption of surfactants, stabilization of particles in dispersion, control of flow properties, wetting of surfaces, sintering of fine particles *etc.* [189].

An important property of surfactants is at very low concentrations, dissolved surfactants exist as individual molecules, as with most other solutes. But, at a particle concentration, a situation might arise which favor the surfactant molecules to form aggregates called micelles. This is a consequence of the reluctance of water to incorporate hydrocarbon chains. As shown in Fig. 2.8, the polar groups are all in contact with water, while the hydrocarbon chains form the interior of the micelle. For typical water-soluble surfactants such as sodium laurate, the micelles contain perhaps a hundred molecules which forming spherical shapes [185].

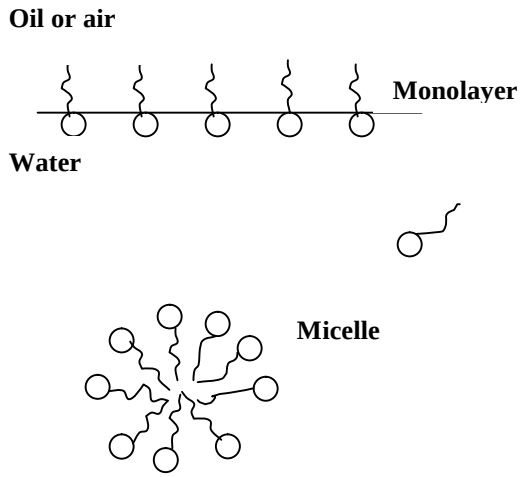

Fig. 2.8: Idealized diagram showing surfactant behavior [185].

2.10.1 Anionic Surfactants

Anionic surfactants are by far the most commonly found surfactants among the various types. Meanwhile, cationic surfactants are usually soluble in acid solutions. The primary amine R-NH_2, for example, gives rise to the R-NH_3^+ ion in the acid solutions. In some cases, quaternary ammonium compounds, which are less sensitive to pH changes, are used, *e.g.*, R-$N(CH_3)_3^+Br^-$ (or Cl^-). As the name implies, non-ionic surfactants contain only electrically neutral polar groups, notably the ethoxy group –OCH_2CH_2-. An example is the ethoxylated fatty alcohol $R(OCH_2CH_2)_nOH$. Other classes do exist as well. Cationic surfactants are usually not considered separately from anionic surfactants, due to their similarity in behavior [185].

Surface tension is a function of surfactant concentration. For example, in the case of potassium laurate, as the concentration is increased, its surface tension will be lowered. However, beyond a certain concentration, the surface tension will not change anymore. It is found that at or in the vicinity of that particular concentration, a host of properties of the bulk solution do change, *e.g.*, density, solubility, osmotic pressure, electrical resistance, light scattering properties, detergency, *etc* [185].

CHAPTER 3

METHODOLOGY

3.1 Introduction

This research focuses on the applicability of physic seed hull, PSH, an agrowaste from plant oil industries for the adsorption of heavy metal ions and dye from aqueous solution. The study focuses attention on the through characterization of the PSH adsorbent and investigations of the adsorption processes from adsorption kinetics and adsorption isotherms. For the kinetic model, Lagergren pseudo first order model, pseudo second order model and intraparticle diffusion model of the adsorption process was studied. Langmuir model, Freundlich model and D-R model were studied to get an idea of the adsorption isotherm process. Effect of anionic surfactant on the improvement on the adsorption properties of PSH was further investigated. A comparison studies also has been conducted to evaluate the PSH capacity by using commercial granular activated carbon, GAC. The capacity has also been compared with data available for other adsorbents from literatures.

In this section details of all the materials *e.g.* adsorbent, adsorbate, chemicals, apparatus and equipment; methods involved during the experimental processes; mathematical models *e.g.* equations and calculations involved during the data analysis process and analytical procedures which provide basic information about the procedure on handling the analytical equipments have been provided.

The entire experimental part of the work can be divided in the following part; first, thorough characterization of PSH; second, batch kinetic and equilibrium adsorption studies of metal ions on PSH; third, batch kinetic and equilibrium adsorption studies of metal ions adsorption with the effect of anionic surfactant using PSH; fourth, batch kinetic and equilibrium adsorption studies of Malachite green dye, MG on PSH; fifth, batch kinetic and equilibrium adsorption studies of metal ions and MG dye using GAC as comparison study.

All the equations and calculations utilized during the data analysis process have been presented in mathematical model section. This section provide the basic equation for measuring the adsorption capacity, isotherm models *e.g.* Langmuir and Freundlich, kinetic models *e.g.* Lagergren pseudo-first order, pseudo second order and intraparticle diffusion model.

The analytical procedures used in the present investigation include FTIR analysis, zeta potential analysis, BET surface area measurement, SEM-EDX analysis, measurement of concentration by atomic adsorption spectrophotometer and UV-VIS spectrophotometer, and analysis of particle size by particle size analyzer.

3.2 Materials

3.2.1 Adsorbent

The Physic seed hull (*Jatropha curcas*), PSH has been used as an adsorbent in this study. It was obtained from Bota in Perak state of Malaysia. The hulls were soaked in water and thoroughly washed with water to remove adhering dirt and soluble components. The washed hull was then oven-dried at 85 ±10^{o}C until constant weight. The washed and dried material was crushed and sieved using Laboratory Sieve to generate average 0.6 mm size of the adsorbent. Similar procedure was utilized to wood derived commercial granular activated carbon (GAC) (Merck, German). GAC with specific surface area of 589.87 m^2/g and particle size of 0.6mm has been used as for a comparison of the adsorption performance with PSH.

Fig.3.1: Physic seeds

Fig. 3.2: Physic seed hulls size 0.6 mm

Fig. 3.3: Granular activated carbon size 1.18 mm

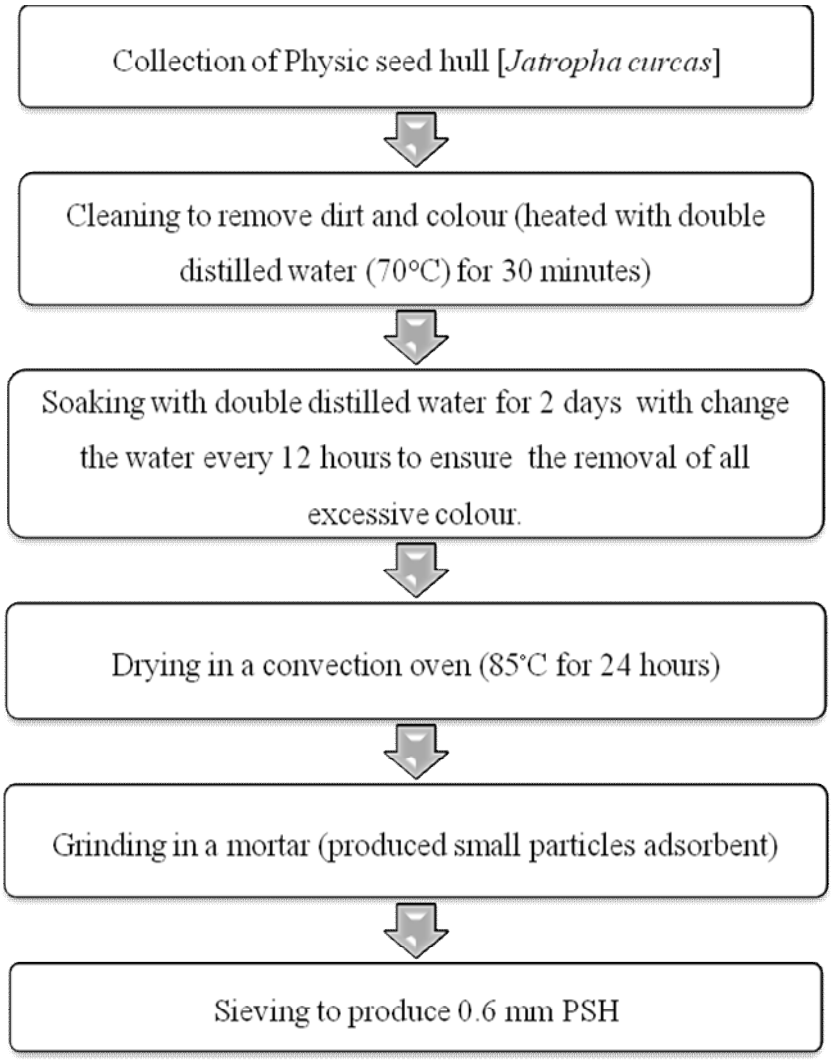

Fig. 3.4: Process of producing PSH adsorbent

3.2.2 Chemicals

Table 3.1

Composition of Universal buffer mixture

0.2M Na_2HPO_4 /mL	0.1M Citric Acid /mL	pH
20.55	79.45	3
38.55	61.45	4
51.50	48.50	5
63.15	36.85	6

The pH of the solution was adjusted using Universal buffer mixture (0.2M NH_2HPO_4/mL and 0.1M Citric acid /mL) to avoid the changes of pH due to the presence of functional groups at the surface of PSH (Table 3.1) [190].

The anionic surfactant Tetra sodium N-(1, 2 dicarboxy ethyl) – N octadecyl sulfosuccinamate (Aerosol 22) was obtained from Cytec. The surfactant used was obtained as analytical grade chemicals and was used without further purification. Stock solutions of surfactants with concentration 1 to 7ppm were prepared by dissolving it in de-ionized water.

$C_{26}H_{43}NNa_4O_{10}S$

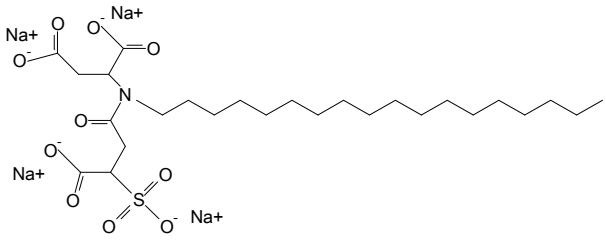

Fig. 3.5: Chemical structure of Aerosol 22

3.2.3 Adsorbates

Cadmium nitrate and zinc nitrate were used as the salts of Cd^{2+} and Zn^{2+} adsorbate. Both the salts were taken in the form an analytical grade (E. Merck). 1000 ppm stock solution of Cd^{2+} and Zn^{2+} has been prepared by dissolving 2.74g of cadmium nitrate ($Cd(NO_3)_2$, $4H_2O$) and 4.55g of zinc nitrate ($Zn(NO_3)_2$, $2H_2O$) in de-ionized water and then diluted to the desired concentration levels ranging from 5 to 50 ppm. The pH was adjusted using Universal buffer solution.

Analytical grade Malachite green dye [C.I. = 42,000, chemical formula $=C_{23}H_{26}N_2Cl$, molecular weight 329.50; λ_{max} = 617 nm (reported)] was obtained from Bendosen Laboratory Chemical, UK without further purification. Stock solutions of dye with concentrations ranging from 10 to 50 ppm were prepared by dissolving the requisite quantity in de-ionized water. The pH was adjusted using Universal buffer solution. The chemical structure of Malachite Green is as shown in Fig. 2.6.

3.2.4 Apparatus and equipments

The mixed solution and the sorbent were agitated in closed polyethylene bottles using a laboratory shaker at 160 rpm (Thermolyne Big Bill Digital Orbital shaker, M73620-26, US).

The concentrations of metal ions were measured using double beam flame Atomic Absorption / Flame Emission Spectrophotometer (AAS) Unit (Model Shimadzu AA-660, Japan). The MG dye concentration was measured using UV-VIS spectrophotometer (HACH UV-VIS Spectrophotometer DR 5000, US).

All plastic sample bottles and glassware were cleaned, then rinsed with de-ionized water and dried at 60 $\pm 10^0$C in a temperature controlled oven. All measurements were conducted at room temperature (25 $\pm$ 2^{o}C). However, for the temperature control experiment, the water bath shaker with temperature control has been used in this study (Poly Science Water bath Dual Action Shaker, US). The pH was measured by Orion pH meter, US.

3.3 Experimental

3.3.1 The characterization of PSH

The PSH was characterized by Fourier transform infra-red (FTIR) Spectroscopy, (Spectrum 2000 Explorer; Perkin Elmer Cetus Instruments, Norwalk, CT) to analyse the organic functional groups present in the adsorbent. The surface morphologies and elemental composition of PSH before and after adsorption of cadmium and zinc were examined with a field emission Scanning Electron Microscope, FESEM-EDX (Leo Supra 50VP, Germany) with gold-coated samples. Elemental composition in terms of C-H-N-S was also measured using CHNS Analyser (CHNS 932, LECO, USA). The surface composition of the sorbent was determined by an energy dispersive X-ray fluorescence (XRF Bruker S4 Pioneer, USA) analysis. The specific surface area and pore size of PSH was measured using BET method by N_2 adsorption isotherm at 77K using a Quantachrome Autosorb Automated Gas Sorption Instrument, UK. BET and BJH methods were used to calculate the surface area and the pore size distribution of PSH. Total volume of pores was calculated at a relative pressure (P/P_0) of 0.99. The zeta potential of PSH was measured using Malvern Zetasizer Nano ZS potentiometer (Malvern Instruments, UK) to assess the surface charge of PSH. The particle size range was measured using Malvern Particle Size Analyser (Model Master Seizer 2000, UK).

3.3.2 Batch and equilibrium studies of metal ions adsorption onto PSH and GAC as comparison

Adsorption isotherm and kinetic experiment was performed to measure the adsorption of Cd^{2+} and Zn^{2+} on PSH from solution using batch adsorption equilibrium study. The studies were carried out by shaking 0.4 g of the adsorbent with 100 mL of the solution containing the desired concentrations of the metal ions solution.

For equilibrium isotherm studies, metal ion solutions of different initial concentrations (5, 10, 20, 30 and 50ppm) were taken in batches of 100mL of metal ion solution and agitated with 0.4g of adsorbent using laboratory shaker at 160rpm at 25 $\pm 2^{o}$C in a series of 200mL plastic bottles for maximum of 7 hours at pH=6. The equilibrium was attained in 7 hours.

For kinetic studies, the samples were collected in different time intervals (2, 5, 10, 15, 20, 30, 40, 50, 60, 120, 180, 240 min) and filtered each time through a 0.45µm Whatman filter membrane with syringe. The experiments were carried out by varying the initial metal ions concentrations, pH, adsorbent dosage, particle size and temperature.

The left out concentrations in the filtrate solution after the adsorption process and the initial solution before the adsorption process were analyzed using flame atomic absorption spectrophotometer with air-acetylene flame. Cadmium and zinc hollow cathode lamp were used. The spectral slit width and the working wavelength were 0.7 and 228.8nm respectively. The quantity of adsorbed metal ions on adsorbent was calculated as the difference between initial concentration and concentration at any time, *t*. Each experiment was duplicated at least under identical conditions. Reproducibility of the measurements was within 10%.

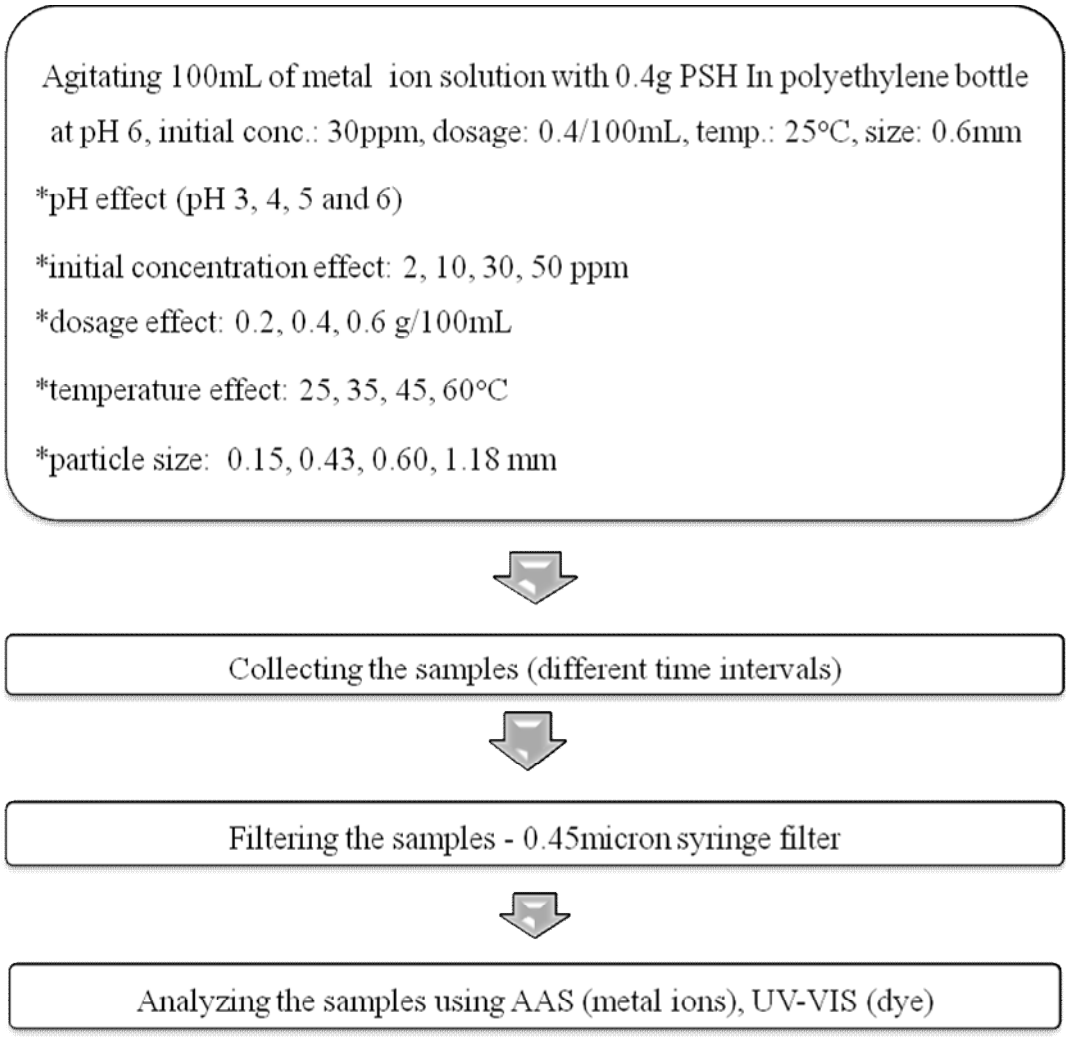

Fig. 3.6: Flow chart for isotherm and kinetic experiment

3.3.2.1 Effect of initial concentration on metal ions adsorption onto PSH

The kinetics of metal ion adsorption was carried out at four different initial metal ion concentrations (2, 5, 10, 30 and 50 ppm). The other parameters maintanined for the study were like the following: pH 6, particle size 0.6 mm, temperature 25 $\pm 2^{o}$C, shaker speed 160 rpm and adsorbent dosage 4g/L. The batch kinetic experiment with time interval was held as per earlier experimental procedure described under section 3.3.2.

3.3.2.2 Effect of initial solution pH on metal ions adsorption onto PSH

The effect of pH on the amount of metal ions removal was analyzed at different pH of 3.0, 4.0, 5.0 and 6.0 respectively. The pH of the solution was adjusted before starting the adsorption experiments using Universal buffer solution. In this study 100 mL of metal ion solution of 10 ppm and 30 ppm were agitated separately with 0.4 g of adsorbent (PSH) of 0.6 mm size, using laboratory shaker at 160 rpm and 25 ±2^{o}C in a series of 200 ml polyethylene bottles. The samples were then collected in different time intervals throughout equilibrium time period following the experimental procedure as described in section 3.3.2.

3.3.2.3 Effect of adsorbent dosage on metal ions adsorption onto PSH

The effect of adsorbent mass on the amount of metal ion adsorbed was obtained by treating 100 mL of metal ion solution of initial concentration of 30 ppm with different weights (*e.g.* 50 mg, 100 mg and 150 mg) of adsorbent (PSH) 0.6 mm size using laboratory shaker at 25 ±2^{o}C for specified time interval at a constant speed of 160 rpm. The experiments were carried out at a pH of 6. After each time intervals, the samples were filtered and the supernatant solution was analyzed following the process as described in section 3.3.2.

3.3.2.4 Effect of temperature on metal ions adsorption onto PSH

Studies on the adsorption of metal ions measurements were carried out by batch experiments. For this purpose, 0.4 g of PSH and 100 ml 30 ppm of the metal ions solution were agitated on a shaker at 160 rpm with varying the temperature in a range of 25, 35, 45, 60 °C at solution pH of 6. The samples were then collected in different time intervals throughout equilibrium time period following the process as described in section 3.3.2.

3.3.2.5 Effect of particle size on metal ions adsorption onto PSH and GAC

The kinetics of metal ion adsorption was carried out at three different particle sizes (0.15, 0.43, 0.60, 1.18 mm). The other parameters maintained for this study were like the following initial concentration 30ppm, pH 6, temperature 25 $\pm 2^{o}$C, shaker speed 160 rpm and adsorbent dosage 4g/L. The batch kinetic experiments with time interval was performed following process as described in section 3.3.2. Similar experiment has also been done for GAC for a comparison of the adsorbents.

3.3.3 Batch and equilibrium studies of metal ions adsorption with the effect of anionic surfactant using PSH

The equilibrium and batch adsorption experiments for the effect of surfactant (Aerosol 22) were carried out by shaking a 0.4g of the sorbent with 100ml of the solution containing the desired concentrations of the metal ions solution (Cd^{2+} and Zn^{2+}) and surfactant. The equilibrium and batch kinetic experiment were performed following process as described in section 3.3.2. However, for batch kinetic experiment, surfactant at the range of 1-7 ppm added for each sample containing 30ppm of metal ions. For equilibrium experiment, 1 ppm of surfactant was added into metal ions solutions ranging in the concentration from 10-65 ppm.

3.3.4 Batch and equilibrium studies of Malachite green dye, MG onto PSH and GAC

The mixed solution and the sorbent were agitated in closed polyethylene bottle for 6 hours using a laboratory shaker with agitation at speed of 160rpm. The freshly prepared solution has been used and the possibility of MG adsorption on the polyethylene bottle was checked at different time intervals. No adsorption of MG was observed on the surface of the bottle. All measurements were conducted at the room temperature (24 $\pm 2^{0}$C) and pH 6. The suspensions were filtered through a 0.45µm

syringe filter. The filtrate was analyzed using UV-VIS spectrophotometer (HACH UV-VIS Spectrophotometer DR 5000, US). The experiments were carried out by varying the initial dye concentrations, pH, particle size, temperature and dosage. Adsorption rates were measured according to predefined procedure with dye concentrations ranging from 10-50ppm. The equilibrium and batch kinetic experiment was carried out following the procedure as described in section 3.3.2.

3.3.5 Batch kinetic and equilibrium studies of metal ions and MG dye using GAC as comparison study

All experiments were conducted as per earlier method (procedure 3.3.2 and 3.3.4) using granular active carbon (GAC) as the adsorbent following the process described in section 3.2.1.

3.4 Mathematical Models

3.4.1 General calculations

3.4.1.1 Adsorption capacity

The concentration retained in the adsorbent phase was calculated according to;

$$q_t = \frac{(C_0 - C_t)V}{m} \tag{3.1}$$

Where C_o (mg/L) and C_t (mg/L) are the concentration in the solution at time $t = 0$ and at time t, V is the volume of solution (L) and m is the amount of adsorbent (g) added.

3.4.1.2 Percentage removal

The percentage removal can be calculated following the equation

$$\%R = \frac{(C_i - C_t)}{C_i} x100 \quad (3.2)$$

Where C_i (mg/L) and C_t (mg/L) are the concentration in the solution at time t = 0 and at time t.

3.4.2 Kinetic models

3.4.2.1 The Lagergren pseudo-first order model

The Lagergren pseudo-first order model in typically expressed in the following way [32];

$$\log (q_e - q_t) = \log q_e - \frac{K_1}{2.303} t \quad (3.3)$$

Where q_t and q_e specifies the amount of metal ion adsorbed (mg/g) at any time t and at equilibrium time respectively and K_1 specifies the adsorption first-order rate constant (min^{-1}). Plot of Log (q_e – q_t) versus t gives a straight line for pseudo first-order adsorption kinetics which allow computation of the rate constant K_1.

3.4.2.2 Pseudo-second-order model

The adsorption data was then analyzed in terms of pseudo-second-order mechanism in the following way [10, 191],

$$\frac{dq}{dt} = K_2 (q_e - q_t)^2 \quad (3.4)$$

where K_2 is the pseudo-second order rates constant (g/mg.min). Integrating and applying boundary conditions $t=0$ to $t=t$ and q=0 to $q=q_t$ gives

$$\frac{t}{q_t} = \frac{1}{K_2 q_e^2} + \frac{1}{q_e} t \quad (3.5)$$

A plot between t/q_t versus t gives the value of the constants K_2 (g/mg h) and q_e (mg/g) can be calculated. The constant K_2 is used to calculate the initial sorption rate h, at $t \rightarrow 0$, as follows

$$h = K_2 q_e^2 \quad (3.6)$$

3.4.2.3 Intraparticle diffusion model

The intraparticle diffusion rate constants are determined from the slope of the linear plot of q_t versus $t^{1/2}$ as described by Weber & Morris [36] and can be represented in the following way:

$$q_t = K_{id} t^{0.5} + C \quad (3.7)$$

where q_t is the amount adsorbed at time t and K_{id} (mg/g.min$^{0.5}$) is the rate constant of intraparticle diffusion. For most adsorption processes, the uptake varies almost proportionately with $t^{1/2}$ rather than with the contact time.

3.4.3 Isotherm Models

3.4.3.1 Freundlich isotherm model

The linearized form of Freundlich adsorption isotherm can be expressed as [34, 35],

$$\ln q_e = \ln K_f + \frac{1}{n}(\ln C_e) \quad (3.8)$$

Where q_e (amount of sorbate adsorbed at equilibrium time), C_e (equilibrium concentration of sorbate in solution), K_f (capacity of the adsorption) and n (intensity of the adsorption) can be determined from the intercept and slope of plot between ln q_e and ln C_e.

3.4.3.2 Langmuir isotherm model

The linearized form of Langmuir can be written as [33],

$$\frac{1}{q_e} = \left(\frac{1}{K_L\, q_m}\right)\frac{1}{C_e} + \frac{1}{q_m} \tag{3.9}$$

The Langmuir constants, q_m (maximum adsorption capacity) and K_L (values for Langmuir) are determined from the plot between $1/q_e$ versus $1/C_e$.

3.4.3.3 Dimensionless separation factor, R_L

The essential characteristics of the Langmuir isotherm can be expressed in terms of a dimensionless separation factor R_L [192];

$$R_L = \frac{1}{1+K_L C_o} \tag{3.10}$$

Where C_0 is the initial concentration of adsorbate (mg/L), and b (L/mg) is Langmuir constant. The value of R_L indicated the type of Langmuir isotherm whether it is linear ($R_L = 1$), favourable ($0 < R_L < 1$) or irreversible ($R_L = 0$).

3.4.3.4 Dubinin-Radushkevich isotherm

The isotherm experimental data further evaluated by Dubinin–Radusckevich equation which is in the linearized can be expressed in the following way [54, 55, 193];

$$\ln q_e = \ln X_m - \beta\varepsilon^2 \tag{3.11}$$

ε is the Polanyi potential which is related to the equilibrium concentration as follows:

$$\varepsilon = RT \ln \frac{1}{C_e} \tag{3.12}$$

Where q_e is the amount of adsorbed MG (mg/g), X_m is defined as maximum adsorption capacity (mg/g), β is a constant related to sorption energy ($mol^2\ kJ^{-2}$), C_e is equilibrium concentration (mol/L), ε is Polanyi sorption potential (the amount of energy required to pull a sorbed molecule from its sorption site to infinity), R is the ideal gas constant

(8.314 J/molK), T is the absolute temperature (k). The mean free energy E (kJ mol^{-1}) of sorption can be estimated by using β values as expressed in the following equation;

$$E = (2\beta)^{-1/2} \tag{3.13}$$

If the E value is between 8 and 16kJ/mol, the adsorption process is followed by a chemical ion-exchange. For E < 8 kJ/mol, the adsorption process is of a physical nature and if E value is higher than 16kJ mol^{-1}, the adsorption process follows particle diffusion [51, 56-60].

3.4.3.5 Thermodynamic equations

Calculation of adsorption equilibrium constant, K_a;

$$K_a = \frac{(q_t)_{250}}{C_e} \tag{3.14}$$

where $(q_t)_{250}$ is the amount adsorbed after 250 min of contact (which is sufficient for attainment of equilibrium as stated before) and C_e is the metal ion concentration (i.e., the equilibrium concentration of the solution) at that time.

Dependence of equilibrium constant on temperature is estimated by applying Van't Hoff equation as follow;

$$\ln K_a = \frac{-\Delta G}{RT} = \frac{\Delta H - T\Delta S}{RT} \tag{3.15}$$

where ΔH is the standard enthalpy change (J/mol), ΔS is the standard entropy change (J/mol.K) and ΔG is the Gibbs free energy change. The ΔH and ΔS can be calculated from a plot of ln K_a vs. 1/T.

3.5 Analytical Procedure

3.5.1 Atomic Adsorption Spectrophotometer (AAS)

Double beam flame Atomic Absorption / Flame Emission Spectrophotometer (AAS) Unit (Model Shimadzu AA-660, Japan) has been used as analytical instrument for measuring the metal ions concentration in the solution before and after adsorption process. The sample solution containing the target metal ions is fed to an autosampler prior to the aspiration into air-acetylene flame. Through the flames, ions within the liquid are reduced to the atomic state, and then these metals in the atomic state can quantitatively absorb light at the wavelengths characteristic of their resonance frequencies (wavelength for Cd^{2+} is 228.8 and Zn^{2+} is 213.9). Light was provided using hollow cathode lamps. The amount of radiation absorbed in the flame is proportional to the concentration of the element present in the flame. Standard solution has to be prepared to obtain a linear calibration curves as instrument reference by following of Beer's Law principle.

3.5.2 UV-VIS Spectrophotometer

UV-VIS spectrophotometer (HACH UV-VIS Spectrophotometer DR 5000, US) has been used for mesuring the concentration of MG dye solution. This instrument generates a beam of monocromatic light from a light source, and then the light transmitted through a solution in cuvet. The compound in the solution adsorbs or reflects the light and the remainder is transmitted through the solution to the detector. The amount of transmitted light through the solution is correlated with the concentration of dye in the solution. Dye concentration has been estimated spectrophotometrically by monitoring the absorbance at 618 nm through the cuvet. Standard solution was prepared to obtain a linear calibration curves or standard curve. By using this slope value and the Beer-Lambert Law, the concentration of dye was

determined by measuring the absorbance. Blank was prepared by using di-ionized water [194].

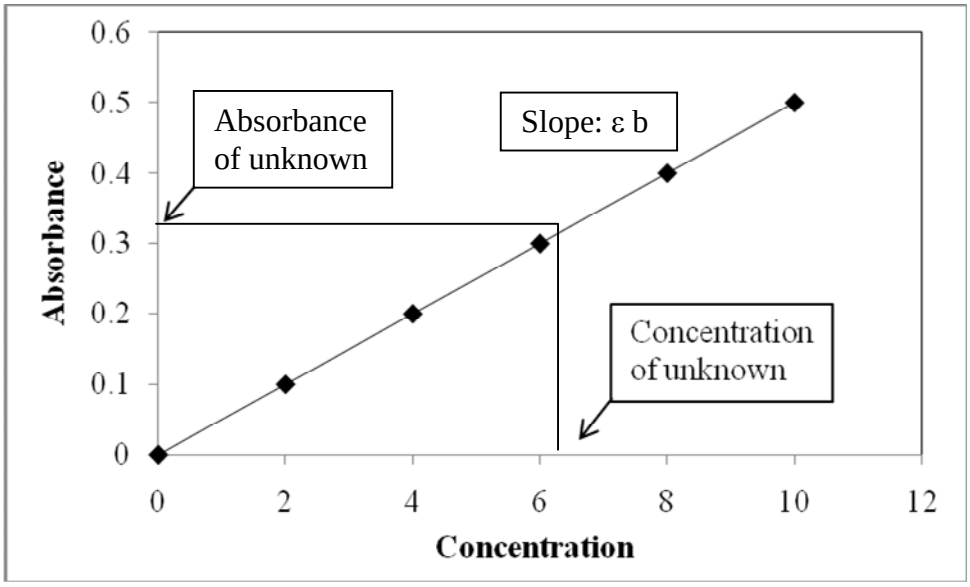

Fig. 3.7: The standard curves. Concentration A: ε b c

5.5.3 pH meter

The pH was measured by Orion pH meter, US. Prior for the analysis, the pH meter has been calibrated with buffer solutions at the following pH values: pH 4.0, pH 7.0 and pH 10.0. The pH probe was rinsed with distilled water and dried with tissue paper. The pH probe was inserted in the test solution and the beaker was gently swirled until the pH reading of the solution become stable and then the pH was recorded. The probe was removed and washed with distilled water for re-use

5.5.4 Laboratory shaker

Laboratory shaker (Thermolyne Big Bill Digital Orbital shaker, M73620-26, US) has been used for all the adsorption experiments. The speed of the shaker was manually controlled at 160 rpm.

5.5.5 Water bath shaker

Poly Science Water bath Dual Action Shaker, US, has been used to agitate the samples for the adsorption study with the effect of temperature especially for temperature above the room temperature.

3.5.6 FTIR Spectroscopy

The PSH was characterized by Fourier transform infra-red (FTIR) Spectroscopy, (Spectrum 2000 Explorer; Perkin Elmer Cetus Instruments, Norwalk, CT) to analyse the organic functional groups present in the adsorbent. The transmission spectrum was acquired at a scan of 47 with 4 cm^{-1} resolution and the spectrum was corrected for a KBr background. The instrument detects the vibration frequency changes for each of the functional groups present in adsorbent samples. Prior to that, the sample has to be in powder state before it is transformed to KBr pellets for analysis. In this case, about 0.1%wt of adsorbent powder was homogenized with the KBr (Potassium bromide), thereafter pressed into a transparent tablet at 9000 psi.

3.5.7 SEM-EDX

The surface morphologies and surface elemental composition of PSH before and after adsorption of metal ions were examined with a field emission Scanning Electron Microscope, SEM-EDX (Leo Supra 50VP, Germany) with gold-coated samples. Samples were gold-coated by a vacuum electric sputter coater to the finest thickness before glue-mounting on it and it was operated at 15 kV. The samples were loaded on

a stub and coated with a gold-palladium film before scanning to avoid charge build-up. SEM images have a characteristic appearance and are useful for judging the surface morphology of the sample. The SEM analyses were recorded using an Oxford Instruments INCA-sight.

3.5.8 CHNS Analyzer

Elemental composition in terms of C-H-N-S was also measured using CHNS Analyser (CHNS 932, LECO, USA).

3.5.9 X-ray fluorescence analyzer

The surface composition of the sorbent was determined by an energy dispersive X-ray fluorescence (XRF Bruker S4 Pioneer, USA) analysis.

3.5.10 Nitrogen adsorption analysis (BET Method)

The specific surface area and pore size of PSH was measured using Brunauer-Emmett-Teller (BET) method by N_2 adsorption isotherm at 77K using a Quantachrome Autosorb Automated Gas Sorption Instrument, UK. Samples were degassed for 20 hours at 100 °C prior to the N_2 adsorption analysis, which was carried out at liquid nitrogen temperature (-196 °C). Surface areas were obtained from a multipoint analysis of the volume of nitrogen adsorbed as a function of the relative pressure. Brunauer–Emmett–Teller (BET) method and Barrett–Joyner–Halenda (BJH) method were used to calculate the surface area and the pore size distribution of PSH. Total volume of pores was calculated at a relative pressure (*P/Po*) of 0.99.

3.5.11 Zeta Potential and pH_{zpc}

The zeta potential of PSH was measured using Malvern Zetasizer Nano ZS potentiometer (Malvern Instruments, UK) to assess the surface charge of PSH. This

technique utilized the measurement of the value of electrophoretic mobility from the rate of migration of dispersed particle under the influence of electric fields. Zeta-potential is calculated from electrophoretic mobility using Smoluchowski equation.

3.5.12 Particle size analyzer

The particle size range was measured using Malvern Particle Size Analyser (Model Master Seizer 2000, UK).

CHAPTER 4

RESULTS AND DISCUSSION

4.1 Characteristic of the adsorbent

4.1.1 Elemental distribution

The characterization of PSH is a crucial element in the adsorption studies of it for the removal of pollutants. The elemental distribution in PSH provides basic information on the element content at the surface of the adsorbent which support the adsorption process. As an example, the elements such as Mg, Ca, S and Na are assumed to enhance the adsorption capacity by their reaction with adsorbate through translocation of metal ions between the adsorbent surface and the adsorbate. Besides that, it confirms the absence of any particulate Cd^{2+}, Zn^{2+} and MG dye attached to the adsorbent particles prior to the adsorption process.

Table 4.1 shows elemental distribution of PSH and GAC. It shows that one gram of PSH contains 0.095% Sulphur, 0.363% Magnesium, 1.020% Potassium, 1.220% Calcium, 1.625% Nitrogen, 5.785% Hydrogen, 36.623% Carbon, 49.501% Oxygen, 3.768% ash and 8.973% moisture. While for GAC, it contains 0.96% Sulphur, 88.11% Carbon, 9.91% Oxygen, 1.02% Silica and 1.02% ash. It indicated that PSH contains Carbon, Oxygen and Hydrogen as the major element content.

Table 4.1

Elemental distribution of PSH and GAC

Parameter	PSH	GAC
Sulphur (%)	0.095	0.96
Magnesium (%)	0.363	-
Potassium (%)	1.020	-
Calcium (%)	1.220	-
Nitrogen (%)	1.625	-
Hydrogen (%)	5.785	-
Carbon (%)	36.623	88.11
Oxygen (%)	49.501	9.91
Silica (%)	-	1.02
Ash (%)	3.768	1.02
Moisture (%)	8.973	-

The commercial granular activated carbon, GAC with extra pure grade form Merck (M: 12.01g/mol) made from wood was utilized in this research as a benchmark adsorbent. However, from CHNS analyzer, it has been observed that PSH contain Carbon (88.9%), Hydrogen (1.848% per gram), Sulphur (0.163% per gram), Nitrogen (0.041% per gram) and ash (3.2959).

The fine particle of PSH after grinding process was then analyzed for their particle size distribution. It has been found that PSH contains 39% of 1.18mm, 24% of 2.0 mm, 23% of 0.6mm, 4% of 0.43mm, 3% of 0.30 mm, 4% of 0.15mm, 3% of less than 0.15 mm (Fig. 4.1). Smaller size particle will have bigger surface area for adsorption which enhances the adsorption capacity. However, the drawback is that of smaller particle it can reduce the flow rate of water through the filtration system [194]. In this case, 0.6 mm has been chosen as the optimum particle size for most of the experiment because it has the smallest available particle size which could maintain the flow rate of solution.

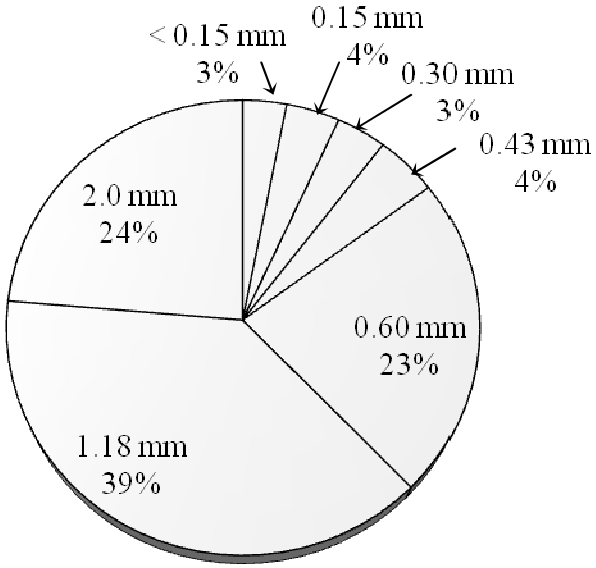

Fig. 4.1: Particle size distribution of PSH

Then the GAC also has been analyzed for their particle size distribution. The sample did not have much size distribution. It contained about 77% of 1.18 mm size and 23% of 2.0 mm size (Fig. 4.2).

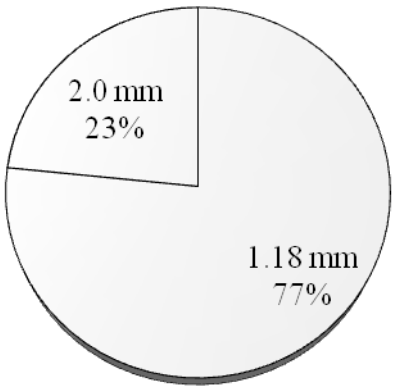

Fig. 4.2: Particle size distribution of GAC

4.1.2 Organic functional group

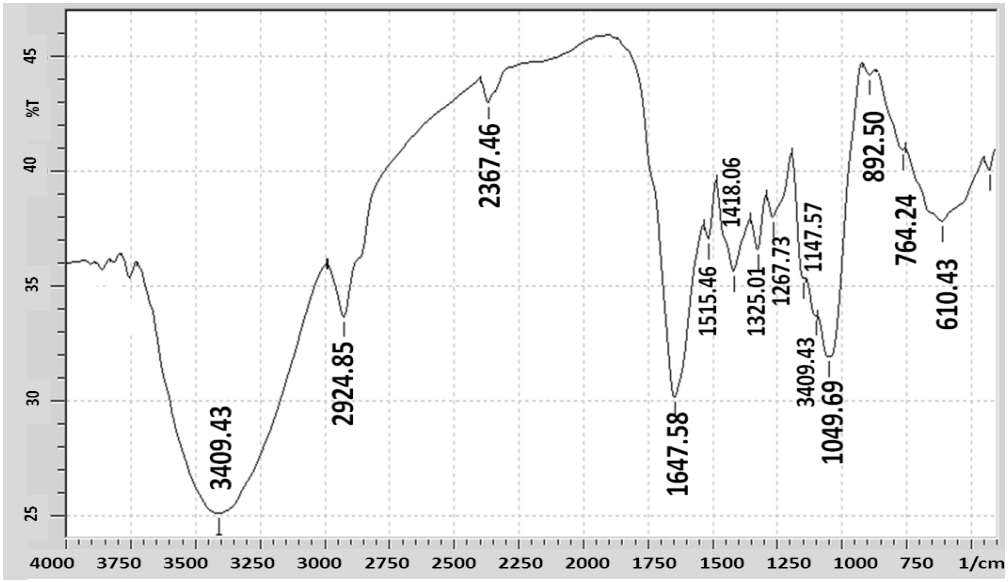

Fig. 4.3: FT-IR spectrum of PSH

Table 4.2

Functional groups of PSH from FTIR spectrum

Band (cm^{-1})	Functional Group
3409	OH (Hydroxyl)
2925	OH (Hydroxyl), C-H (Alkyl)
1648	C=O (Carbonyl) C=ONH2 (Amides) COOH (Carboxyl) C=C
1050 -1648	C-H, S=O (Sulphonyl)
1648 - 3409	N-H (Amine) Aromatic compound

The FTIR spectrum of the PSH is shown in Fig. 4.3. This spectrum is similar to that of some type of biomass or lignocellulosic materials such as pistachio-nut shell and rockrose [195, 196]. Lignin has oxygen functionalities such as phenol, -SO_3H groups which provide sites for metal cation exchange [197]. The broad peak at 3409.43 cm^{-1} can be related to the overlapping of O-H stretching of H-bonded –OH groups with N-H stretching from primary/secondary amines or amides. The bands appearing at 1647.58cm^{-1} were related to the formation of oxygen bearing functional groups like highly conjugated C=O stretching in carboxylic groups, and carboxylate moieties, respectively [198]. The peaks at 1049 - 1647 cm^{-1} indicated the presence of C-H and S=O groups, respectively. The C=O and S=O functional groups generally exhibit very high coordination with heavy metals, hence, enhanced the adsorption capacity. The adsorbent also exhibited typical stretching vibration of N-H bands present in amides and amines and stretching vibration of C=C at 1647.58, 2924.85 and 2367.46 cm^{-1}. The bands between 2924.85 and 1325.01 cm^{-1} indicated the presence of aliphatic species such as $–CH_3$ and $–CH_2–$. Due to the presence of amino groups (stretching at 3409.43 cm^{-1}), the surface of PSH exhibited a basic nature which was apparent from the increase in pH of the solution soaked with PSH [199]. The amino and amide groups provide additional sites for anchoring metal ions through weak complex formation.

Similar to MG dye adsorption, the existence of hydroxyl groups on adsorbent surface shows the availability of negatively charged sites which may develop the attraction between dye and adsorption surface [200, 201]. In this case, the PSH acted as a negative surface that attracted the cationic dye (MG). The quaternary ammonium ion (N^+R^4) as a positive charge in MG may interact with the negative groups on the PSH surface [202]. The C=O and S=O functional groups show strong coordination with cationic metal ions (probably they have similar affinity towards cationic dyes) [198, 203, 204]. Based on the Pearson theory of acid-base reaction, hard acids prefer to interact with hard bases and soft acids with soft bases. In this case, positively charged cationic dye (MG) is soft acids which are likely favors the surface hydroxyl group of soft bases PSH. In addition to hydroxyl group, carboxyl, carbonyl, amine, alkyl group

and sulfonyl groups present in PSH are also responsible for the sorption of cationic substances akin to MG by chemisorption site. In some cases, there is probability of carboxyl, hydroxyl and sulfonyl groups can get dissociated and become negatively charged which may interact with the positive charge of MG dye [202-204].

PSH is a biomass material composed of lignin, cellulose and hemicelluloses. The existence of C=C stretching at 1648cm^{-1} indicated the presence of lignin and the presence of cellulose is indicated by the C-H stretching at 2925cm^{-1}[205].

FTIR spectrum of GAC has been shown in Fig. 4.4. The bands at 1699.65, 1648.54 and 1560.79 cm^{-1}, correspond to the stretching of C=C, C=O and NH_2 functional group. The bands at the range of 1500–1350 cm^{-1} are an indication of the presence of aliphatic species such as $–CH_3$ and $–CH_2–$. On the other hand, the presence of the band in the region of 1699.65 – 1560.79 reveal the existence of aromatic compounds.

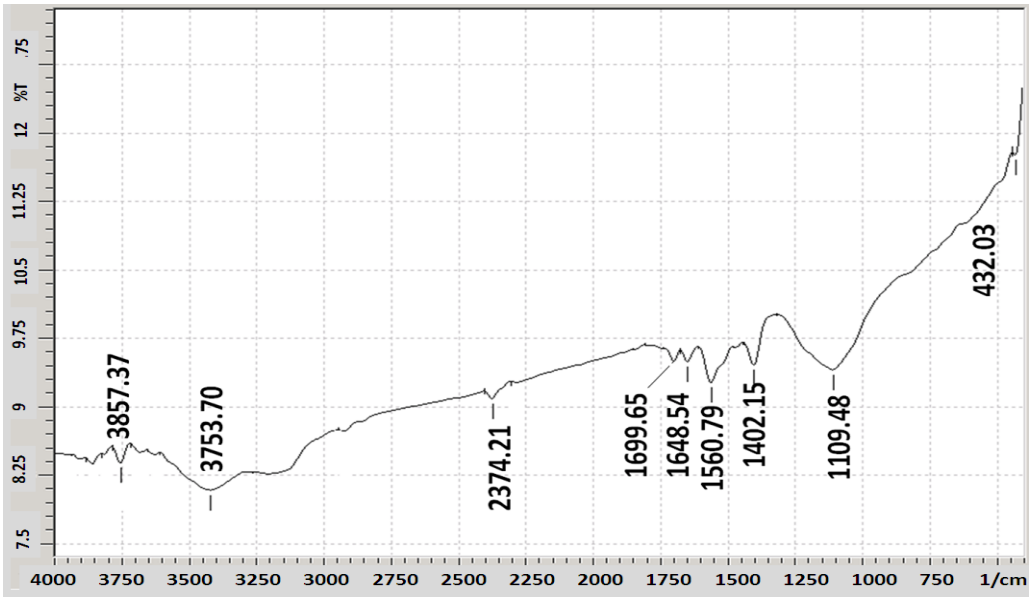

Fig. 4.4: FT-IR spectrum of GAC

Table 4.3

Functional groups of GAC from FTIR spectrum

Band (cm^{-1})	Functional Group
1561-1700	Aromatic compound
1350 -1500	C-H
1561-1699	C=O (Carbonyl) C=C N-H (Amine)

4.1.3 pH, pH_{zpc} and Surface charge

Table 4.4

pH and pH_{zpc} of PSH

Parameter	Value
pH	7.590
pH_{pzc}	2.400

Figure 4.5 shows the variation of zeta potential of PSH as a function of pH. Zeta potential is the manifestation of surface charge density of the adsorbent. Surface charge density has a significant effect on Cd^{2+} and Zn^{2+} metal ions adsorption on PSH. The pH and pH at the point of zero charge, pH_{pzc} of PSH are 7.590 and 2.4. The pH_{pzc} value is the point at which surface functional groups do not contribute to the pH of the solution. Above this pH value, the surface charge became negative and the cation uptake affinity of the adsorbent increases [206].

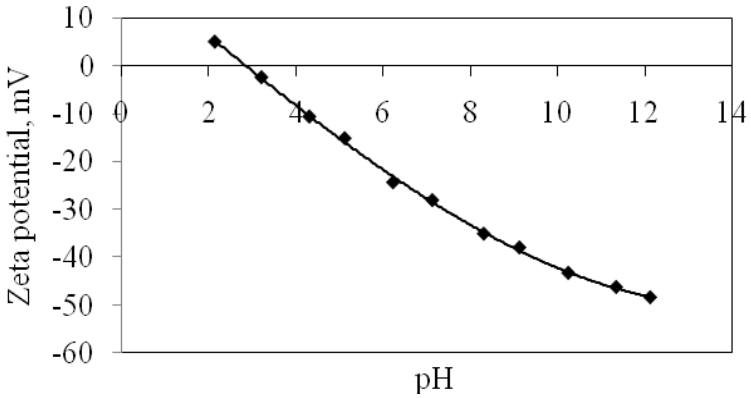

Fig. 4.5: Zeta potential of PSH

4.1.4 Specific surface area, size and pore size distribution

Table 4.5

Specific surface area, size and pore size distribution of PSH and GAC

Parameter	PSH	GAC
Size distribution (mm)	0.15 - 1.18	1.15-2.00
Specific surface area (Multipoint BET-N_2) (m^2/g)	614.01	589.87
External Surface Area (t-method) (m^2/g)	89.11	88.14
Internal surface area (t-method) (m^2/g)	524.9	501.73
Average pore diameter (Å)	30.760	32.50
Total pore volume (cm^3/g)	0.4722	0.1993

The specific surface area, size and pore size distribution of PSH and GAC have been presented in Table 4.5. The surface area of PSH was found to be 614.01m^2/g while GAC is 598.87. The internal surface area was more than the external surface area. The average pore diameter of 30.76 Å and total pore volume was 0.4722cm^3/g.

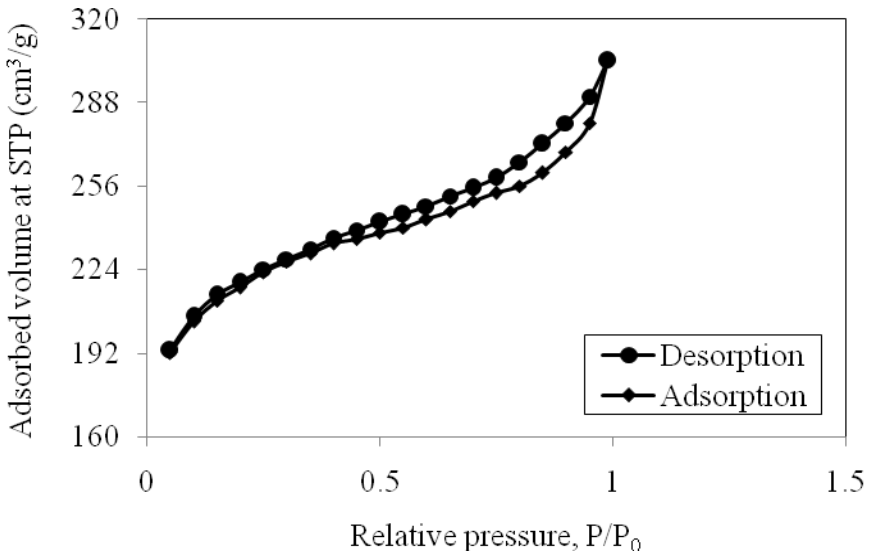

Fig. 4.6: Adsorption desorption Nitrogen

The nitrogen adsorption-desorption curves of PSH is illustrated in Fig. 4.6. The adsorbed volume increased with an increase in P/Po, indicating a wider pore size distribution in the adsorbent PSH. This porous adsorbent exhibited type II isotherm characterized by stronger fluid-solid interactions [199].

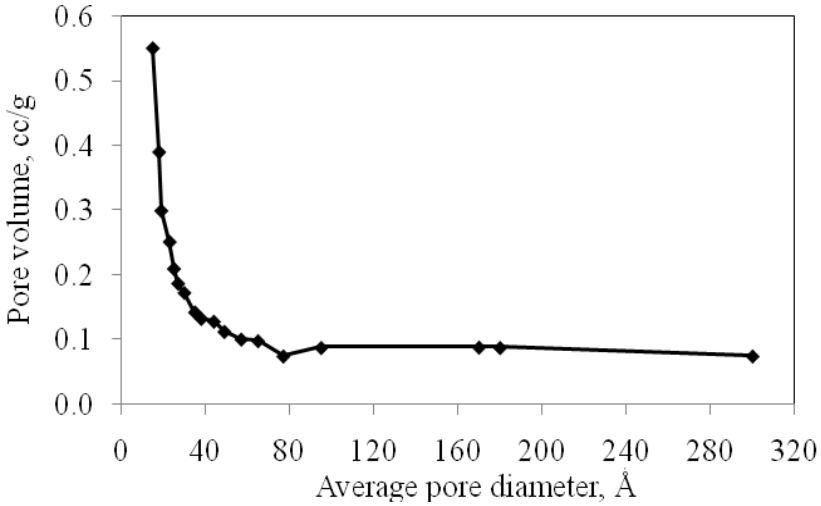

Fig. 4.7: Pore size distribution of PSH

Fig. 4.7 shows the pore size distributions of PSH. It appears that PSH contains both micropores and mesopores. From the nature of porosity the adsorption process can be considered as a mesopore dominated capillary condensation phenomena. The strong interaction between adsorbate molecules and pore walls further controls the filling of micropores during adsorption process [207].

For GAC as comparison, the characteristic evaluation has been done. It has been found that for GAC the specific surface area is 589.87m^2/g, the average pore diameter is 32.5022 Å and total pore volume is 0.1993cm^3/g.

4.1.5 **Surface morphology and elemental distribution by SEM-EDX analysis**

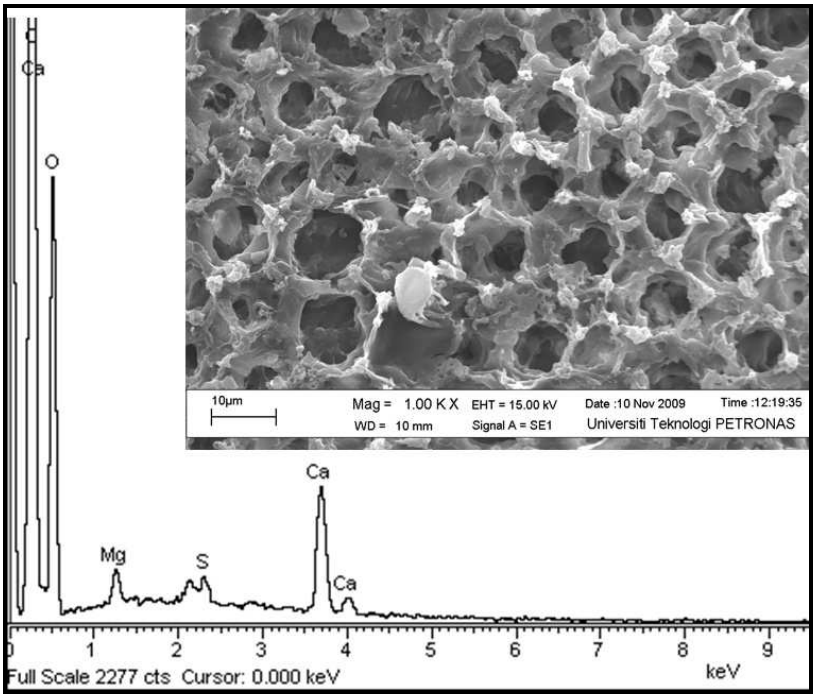

Fig. 4.8: SEM-EDX image of PSH (300mic, ×1000mag)

Scanning electron microscopic photographs of PSH as shown in Fig. 4.8 reveals the surface texture and nature of porosity of the sample. While Figs. 4.9 and 4.10 show pores that have been covered completely by the adsorbed metal ions making PSH surface virtually monolithic in appearance. The availability of pores and internal surface is a requisite for an effective adsorbent. It was observed from Figs. 4.9 and 4.10 that after interaction with Cd^{2+} and Zn^{2+} ions present in solution, peaks corresponding to these ions appeared in the EDX spectra of the PSH sample. It confirmed the attachments of these metal ions on PSH surface during adsorption. Some loses in the intensity of Ca^{2+} and Mg^{2+} ions in PSH after the adsorption can be related to the translocation between alkaline earth metal ion from the adsorbent surface and the transition metal ion from the solution during the adsorption process.

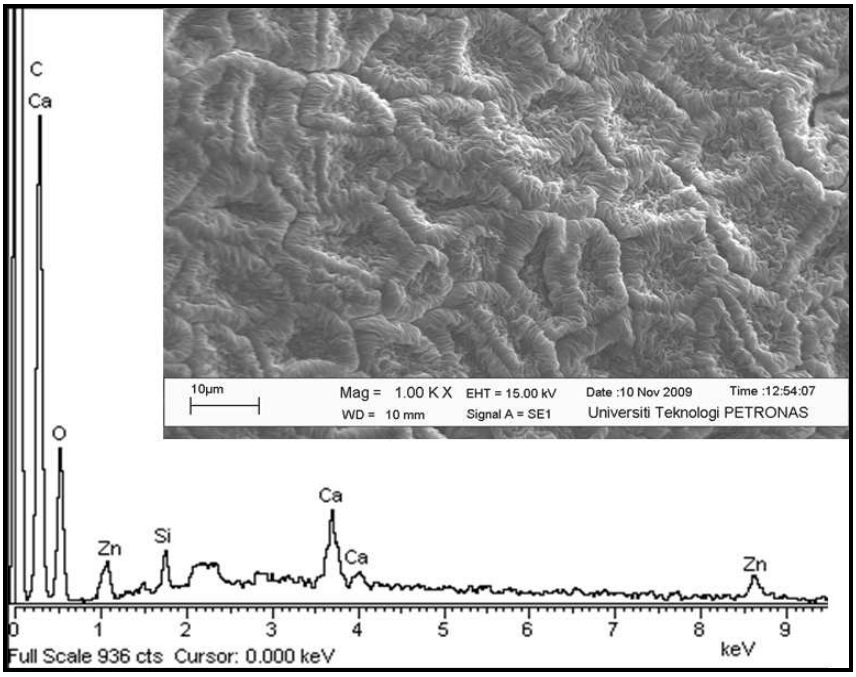

Fig. 4.9: SEM-EDX image of Zn-loaded PSH (300mic, ×1000mag)

Fig. 4.11 shows the scanning photograph of the texture and nature of porosity for GAC. The photograph shows the absence of Mg and Ca from the EDX spectra. The less availability of pores and the texture would be the reason of lesser adsorption

capacity compared to PSH. Possibly GAC sample used required activation with concentrated acid or higher temperature prior to adsorption process for opening the pores. However, by this additional treatment the cost of the product would be increased.

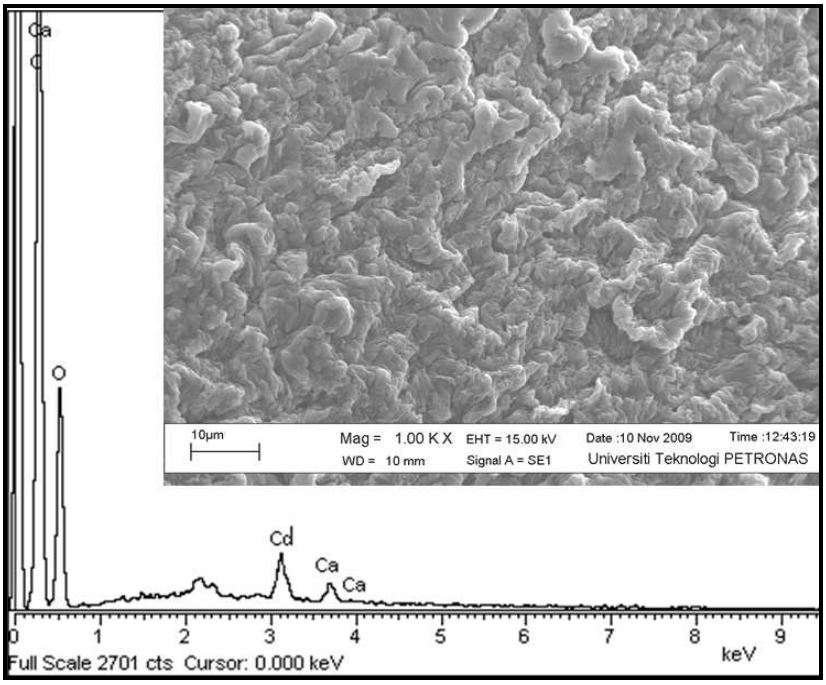

Fig. 4.10: SEM-EDX image of Cd-loaded PSH (300mic, ×1000mag)

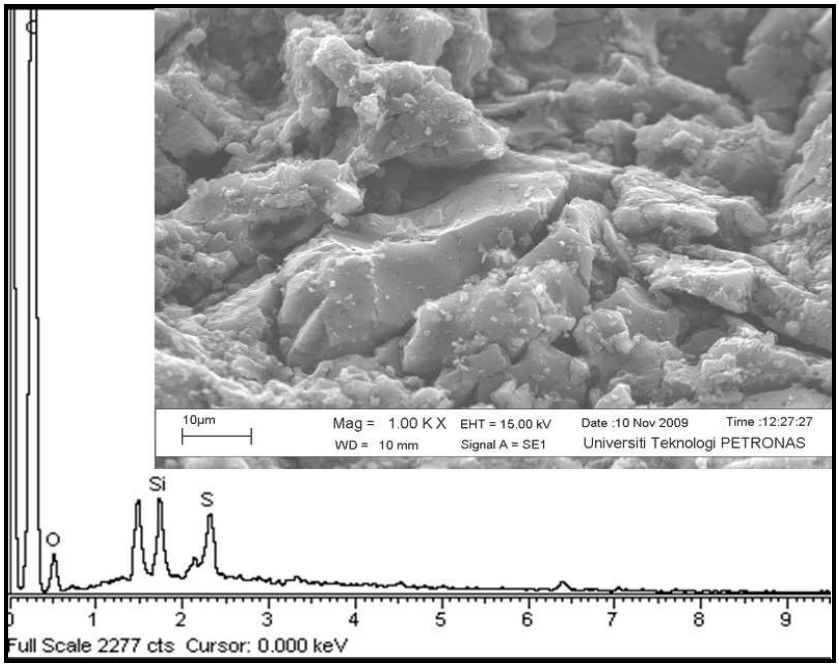

Fig. 4.11: SEM-EDX image of GAC (300mic, ×1000mag)

Fig. 4.12 and 4.13 show the SEM image of PSH and GAC after the MG dye adsorption. The color did not appear here; however the layer of green coloured surface has been covered the adsorbent surface. From the SEM images, the pores were found to be almost absent. It indicated that the empty pores were filled up by the MG dye.

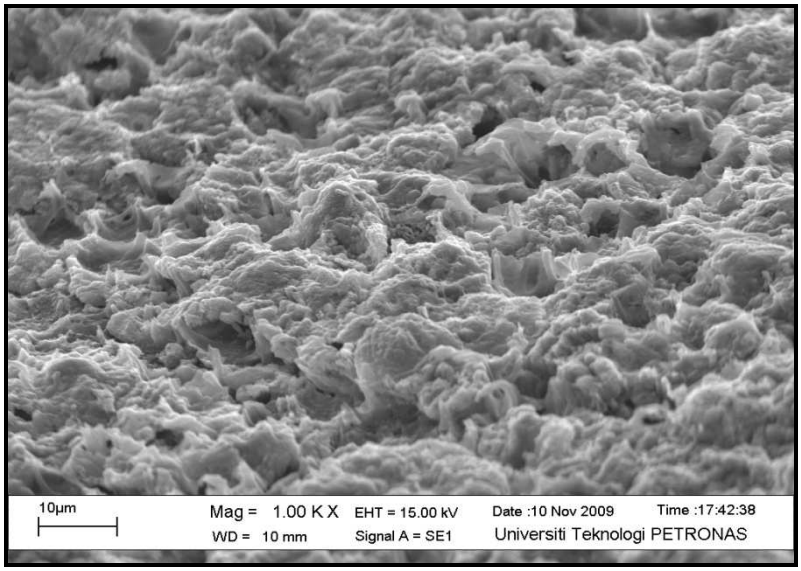

Fig. 4.12: SEM image of PSH after MG dye adsorption (600mic, 1000mag)

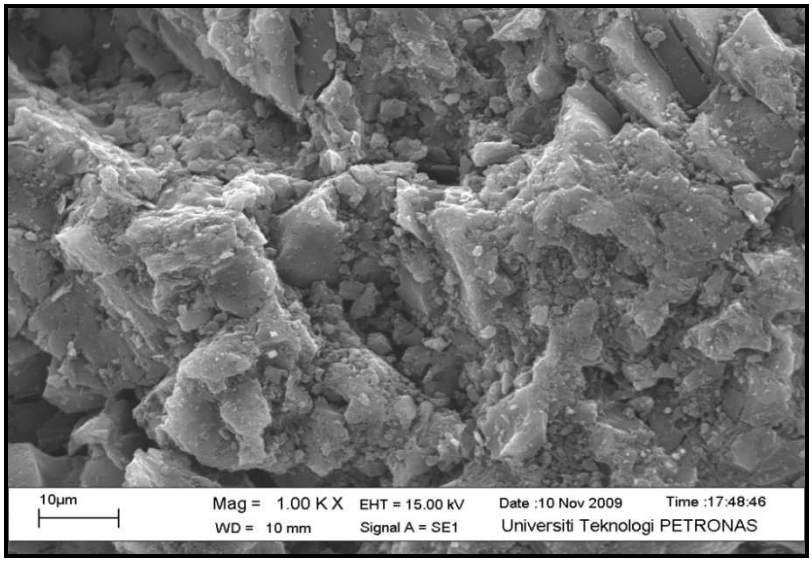

Fig. 4.13: SEM image of GAC after MG dye adsorption (600mic, x1000mag)

4.2 Adsorption of metal ions (Cd^{2+} and Zn^{2+}) and MG dye in aqueous solution by PSH and GAC as comparison, and the influence of anionic surfactant on metal ions removal by PSH

4.2.1 Adsorption kinetics

4.2.1.1 Initial concentration effect for the adsorption of Cd^{2+} and Zn^{2+} metal ions and MG dye onto PSH and GAC, and the influence of anionic surfactant on metal ions removal by GAC

The amount of the adsorption, i.e., mg adsorbate/g of adsorbent increased with increasing contact time at each initial metal ions concentrations and equilibrium was attained within 200-300 minutes for Zn^{2+} and Cd^{2+} systems using PSH and 300-400 minutes for GAC as shown in Figs. 4.14 and 4.15 for PSH and Figs. 4.16 and 4.17 for GAC. Furthermore, it was observed that the amount of metal ions uptake, q_t (mg/g) increased with the increase in the initial metal ions concentration.

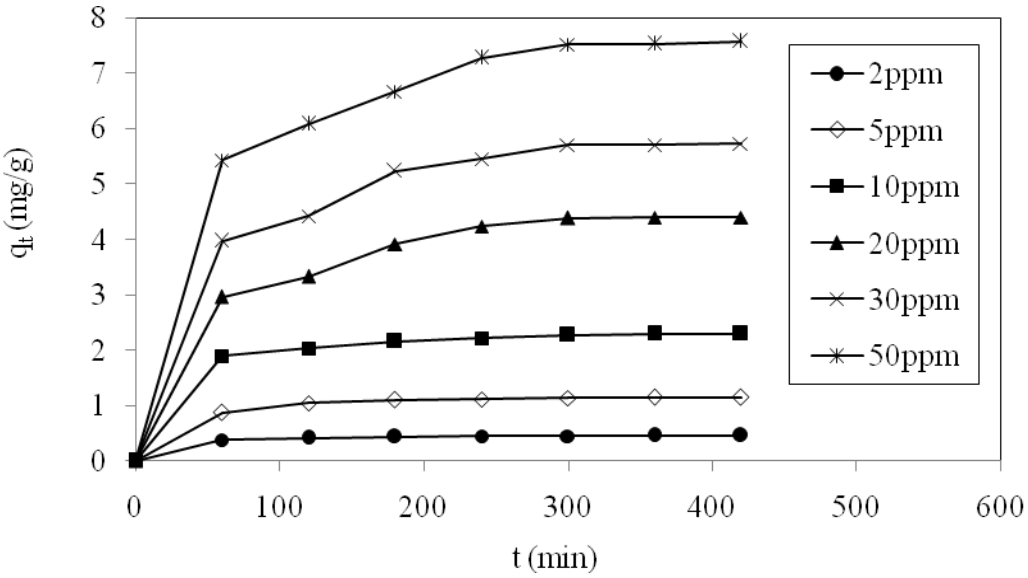

Fig. 4.14: Effect initial concentrations on the adsorption of Zn^{2+} onto PSH (Adsorbent size: 0.6mm, PSH dosage: 0.4g/100ml, pH: 6, Temperature: 24^{o}C)

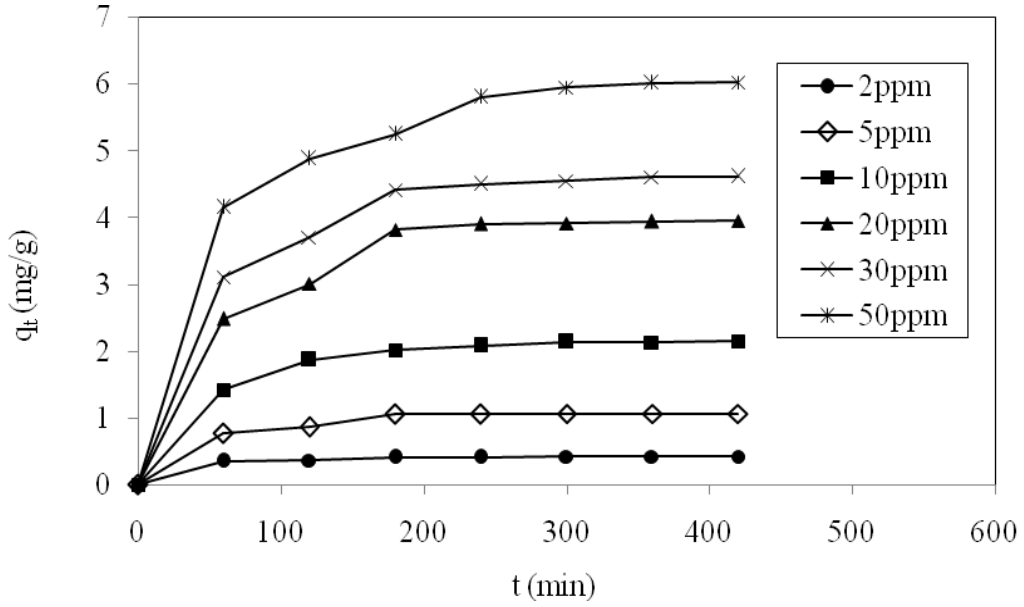

Fig. 4.15: Effect of initial concentrations on the adsorption of Cd^{2+} onto PSH (Adsorbent size: 0.6mm, PSH dosage: 0.4g/100ml, pH: 6, Temperature: 24^{o}C)

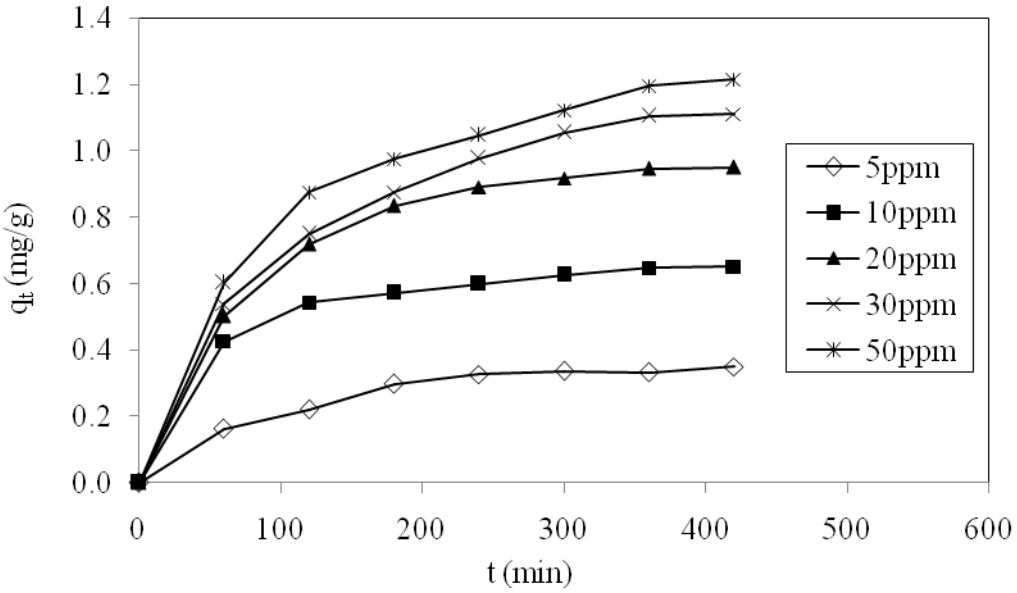

Fig. 4.16: Effect of initial concentrations on the adsorption of Zn^{2+} onto GAC (Adsorbent size: 0.6mm, GAC dosage: 0.4g/100ml, pH: 6, Temperature: 24^{o}C)

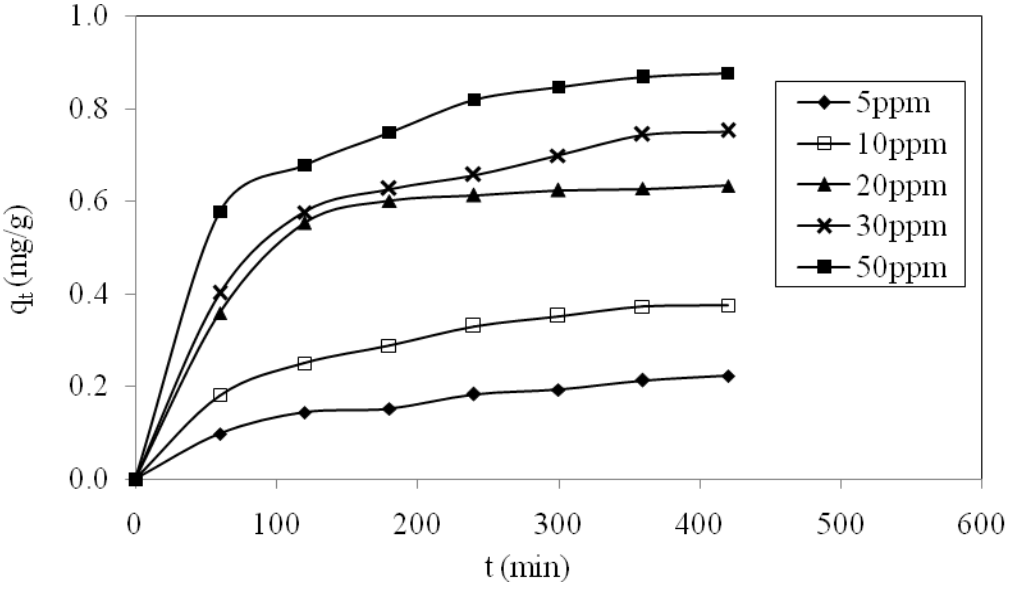

Fig. 4.17: Effect of initial concentrations on the adsorption of Cd^{2+} onto GAC (Adsorbent size: 0.6mm, GAC dosage: 0.4g/100ml, pH: 6, Temperature: 24^{o}C)

Kinetic experiments clearly indicated that adsorption of Zn^{2+} and Cd^{2+} metal ions on PSH followed three-step process, a rapid initial adsorption followed by a period of slower uptake of metal ions and finally no significant uptake [208]. The first step is attributed to the instantaneous utilization of the most readily available active sites on the adsorbent surface (bulk diffusion). Second step, exhibiting additional adsorption, is attributed to the diffusion of the adsorbate from the surface film into the macro-pores of the adsorbent (pore diffusion or intra-particle diffusion) stimulating further movement of metal ions from the liquid phase onto the adsorbent, PSH surface. The last stage is essentially an equilibrium stage.

The effect of initial concentration on the adsorption of MG from the aqueous solutions using PSH and GAC was also studied. The experiments were carried out at a fixed adsorbent dose (0.4g/100ml) in the test solution at a temperature of $24^{o}C$ temperature and pH 6 for different time intervals (2-360min). The adsorption capacity of PSH increased with the increase in initial dye concentration in the solution as shown in Fig. 4.18. This is similar with the adsorption capacity of GAC (Fig. 4.19).

From the results, it was observed that GAC required more time to reach equilibrium with lesser adsorption capacity compared to PSH. Both the time profiles for adsorption of MG on GAC and PSH were single, smooth and continuous curve led to saturation. It suggests the potential monolayer coverage of dye on the surface of the adsorbent [48]. This is also proved by the well fit of the adsorption data with the Langmuir model.

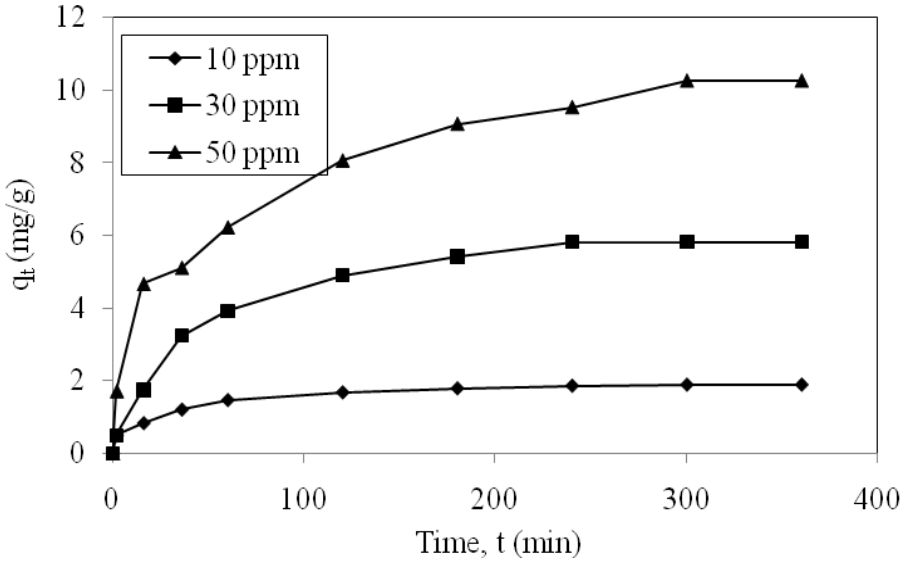

Fig. 4.18: Effect of initial concentrations on MG dye adsorption onto PSH (pH: 6, PSH dosage: 4g/L, Temperature: 24^0C, Agitation speed: 160 rpm, Adsorbent size: 0.6 mm)

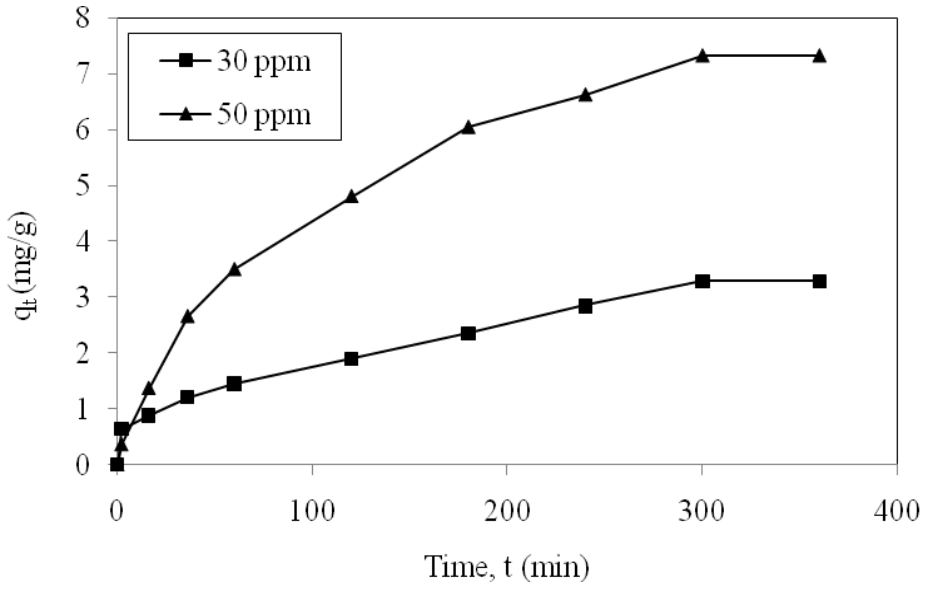

Fig. 4.19: Effect of initial concentrations on MG dye adsorption onto GAC (pH: 6, GAC dosage: 4g/L, Temperature: 24^0C, Agitation speed: 160rpm, Adsorbent size: 0.6mm)

Figs. 4.20 and 4.21 presented the adsorption kinetic of Cd^{2+} and Zn^{2+} on PSH in the presence of Aerosol 22. The adsorption of both Cd^{2+} and Zn^{2+} reached equilibrium within 3 hours as shown in these figures. The adsorption rate of Zn^{2+} decreased from 6.1250 mg/g to 3.9328 mg/g, while the adsorption rate of Cd^{2+} decreased from 3.9770 mg/g to 2.8201 mg/g with the increases of Aerosol 22 in the solution. Aerosol 22 exerted more positive influence on the adsorption of Zn^{2+}. The presence of Aerosol 22 significantly increased the adsorption rate of both the metal ions onto PSH.

Kinetic study from Figs 4.20 and 4.21 revealed that the amount of metal ions adsorbed increased with the decreases in the initial concentration of Aerosol 22 surfactant. The experiments were conducted with four different concentration of surfactant *e.g.* 1, 3, 5 and 7 ppm. The decreasing effect on the adsorption might be related to the formation of micelles by the surfactant when present at higher concentrations. It solubilized the ion molecules and prevented their sorption. Again, the formation of micelles could block the adsorbent pores and could prevent their adsorption capacity [10, 187].

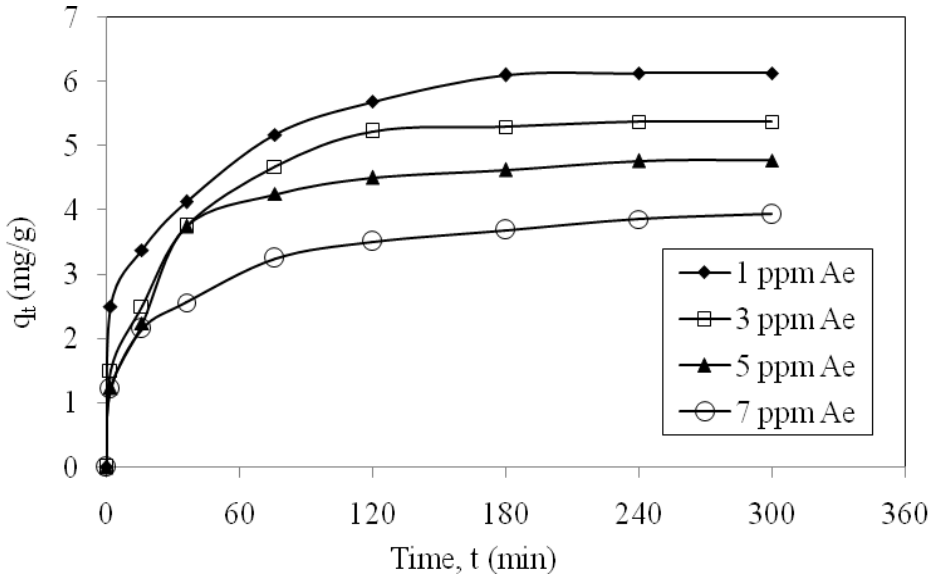

Fig. 4.20: Adsorption kinetic of Zn^{2+} ion on PSH in the presence of different initial concentrations of Aerosol 22 (Zn^{2+}conc.: 30 ppm. PSH dosage: 0.4g/100ml, Adsorbent size: 0.6mm, pH: 6, Temperature: 24^{o}C)

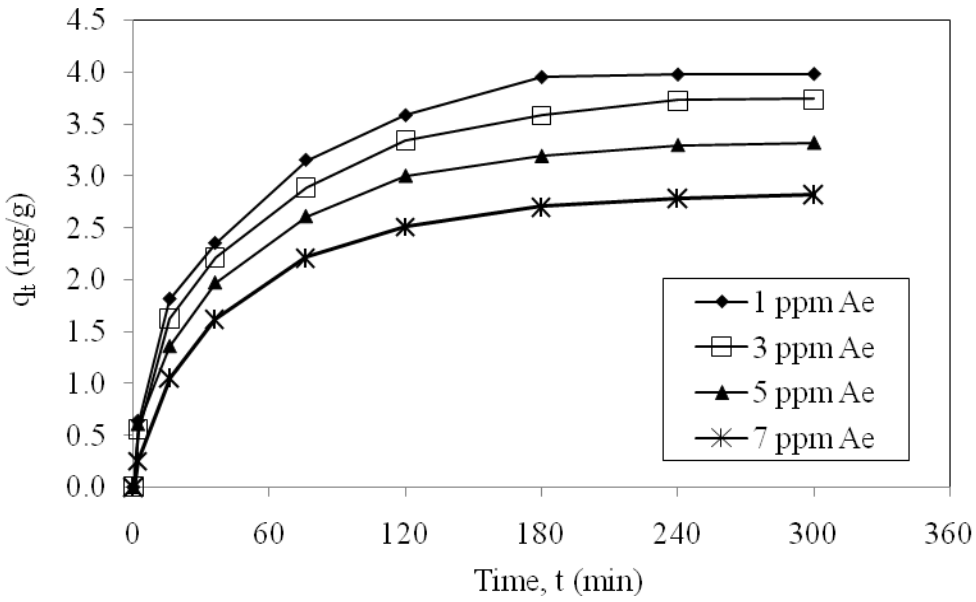

Fig. 4.21: Adsorption kinetic of Cd^{2+} ion on PSH in the presence of different initial concentrations of Aerosol 22 (Cd^{2+}conc.: 30 ppm. PSH dosage: 0.4g/100ml, Adsorbent size: 0.6mm, pH:6, Temperature:24^{o}C)

4.2.1.2 Dosage effect for the adsorption of Cd^{2+} and Zn^{2+} metal ions, and MG dye onto PSH and GAC

It has been found that the amount of metal ions adsorbed varied with the PSH concentration and that the amount adsorbed decreased with an increase in the amount of adsorbent in solution. The experiments were conducted by agitating three different amounts of PSH (200mg, 400mg and 600mg) and two different amount of GAC of (50mg and 100mg) with 100mL of 10ppm metal ion concentration. The resulting effect can be related to the increase in surface area cum active adsorption sites with the increase in adsorbent mass. Similar observations have also been reported by various researchers [5, 31].

The detailed results of the kinetic experiments with varying adsorbent concentrations are presented in Figs. 4.22-4.25. From these plots it is found that the percentage removal increased with the increasing contact time at each adsorbent

dosage and equilibrium is attained within about 200 minutes for both PSH and GAC systems. Further, it was observed that the percentage removal of metal ion for both adsorbent was increased with the increase in the adosrbent dosage.

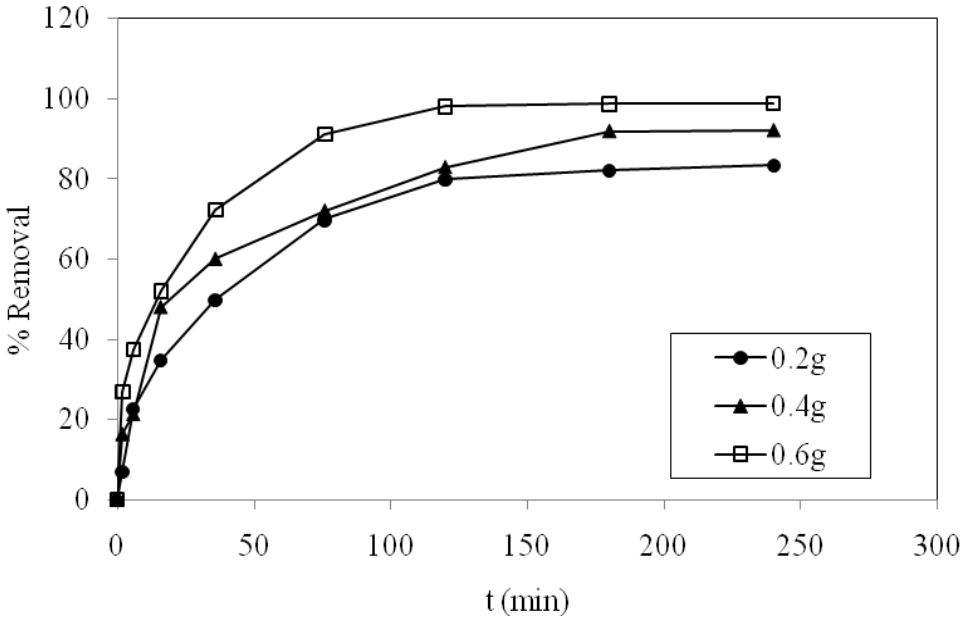

Fig. 4.22: Effect of various PSH dosages on Zn^{2+} ions removal
(Adsorbent size: 0.6mm, C_o: 10ppm, pH: 6, Temperature: 24^oC)

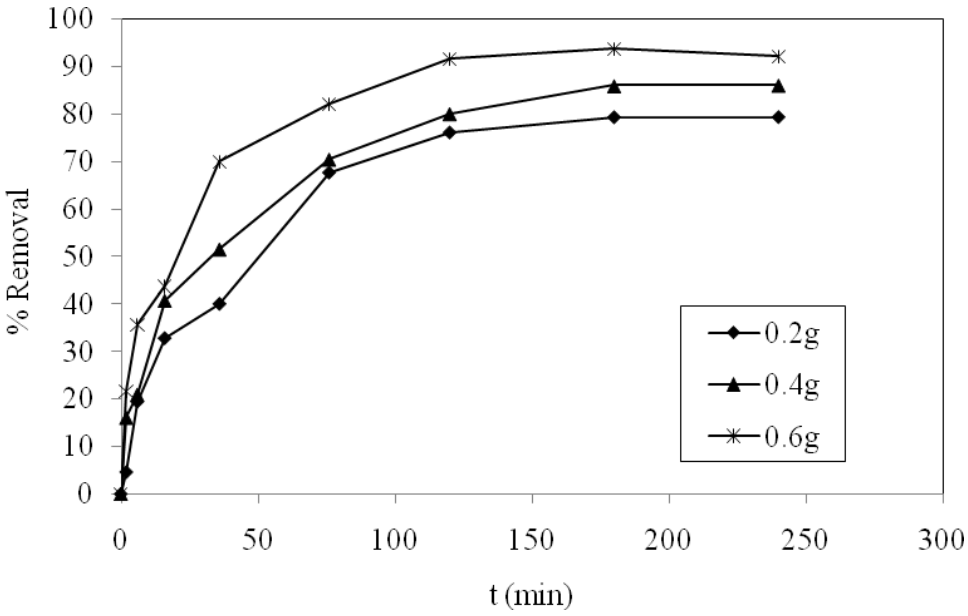

Fig. 4.23: Effect of various PSH dosages on Cd^{2+} ions removal
(Adsorbent size: 0.6mm, C_o: 10ppm, pH: 6, Temperature: 24^oC)

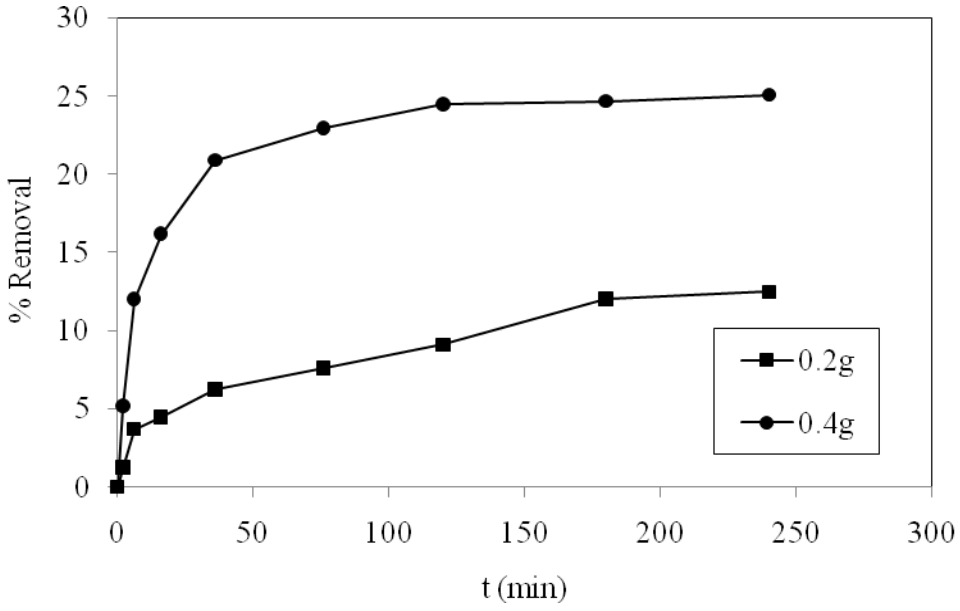

Fig. 4.24: Effect of various GAC dosages on Zn^{2+} ions removal
(Adsorbent size: 1.18mm, C_o: 10ppm, pH: 6, Temperature: 24^oC)

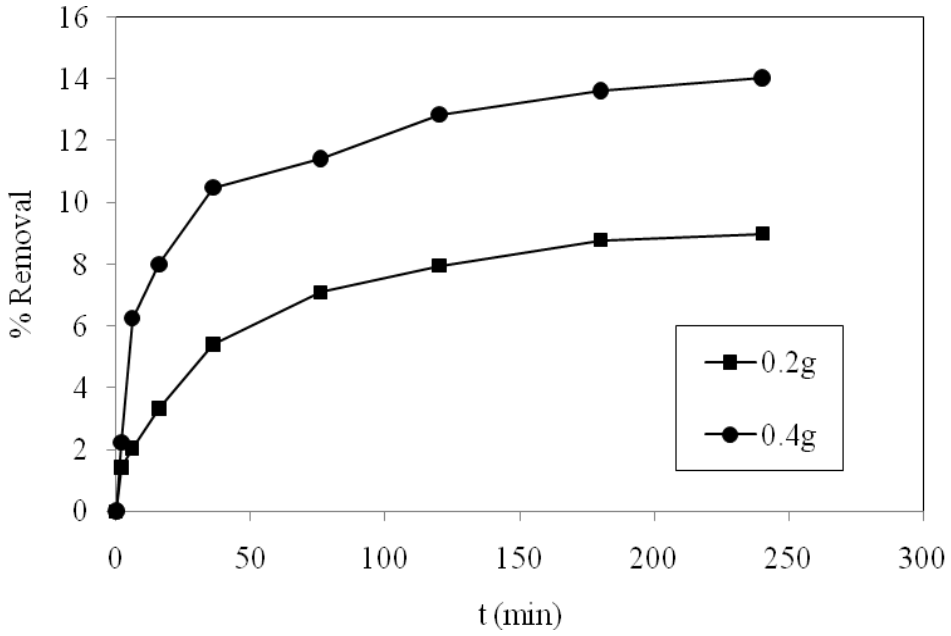

Fig. 4.25: Effect of various GAC dosages on Cd^{2+} ions removal
(Adsorbent size: 1.18mm, C_o: 10ppm, pH: 6, Temperature: 24^oC)

The effect of amount of adsorbent on the removal of MG by PSH at initial concentration of 30 mg/L, particle size of 0.6mm, pH of 6, time length of 6 hours and 24^oC temperature has been shown in Fig. 4.26. It can be seen that the MG removal increased up to a certain limit before it reached equilibrium. Increase in the percentage removal with adsorbent dosage can be attributed to the availability of more adsorption site with the increase of adsorbent surface area [184]. The finding is in agreement with the observations of Mall *et al*. [184] on the biosorption of MG on bagasse fly ash and active carbon.

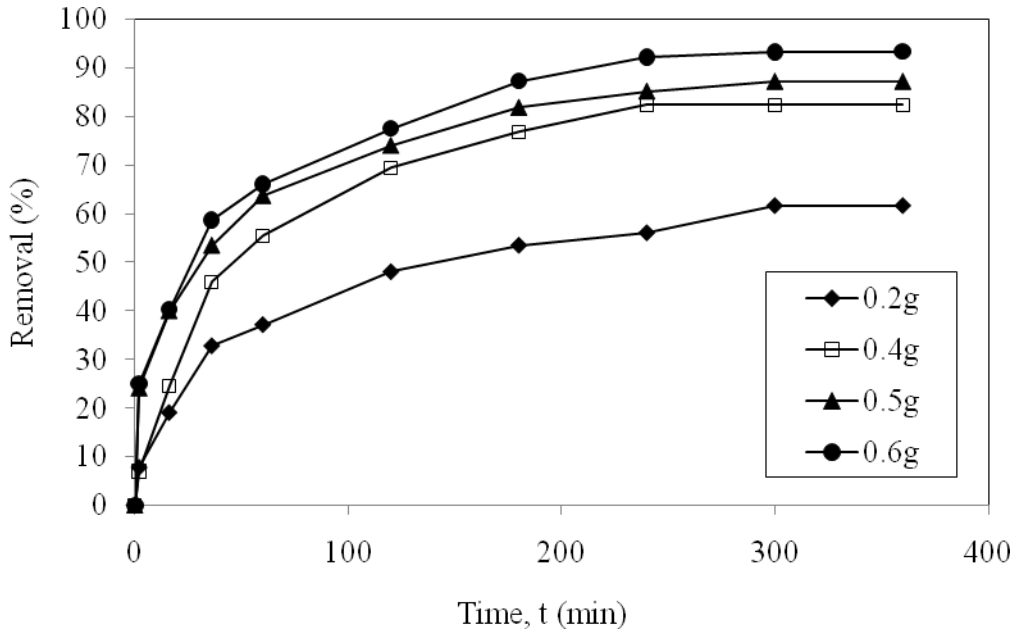

Fig. 4.26: Effect of various PSH dosages on MG dye removal (pH: 6, Dye conc.: 30ppm, Agitation speed: 160 rpm, Adsorbent size: 0.6mm, Temperature: 24^{o}C)

4.2.1.3 Temperature effect for the adsorption of Cd^{2+} and Zn^{2+} ions, and MG dyr onto PSH and GAC

The effect of temperature would significantly speed up the extent of adsorption process. Heating off the treatment environment can optimize the adsorption process and batch method is more applicable for this type of variable. Temperature increase would reduce the time and amount of adsorbent, however it would increase the energy and cost at the same time [209].

The influence of temperature on the metal ions (Cd^{2+} and Zn^{2+}) adsorption onto PSH and GAC was studied in the following way: initial metal ions concentration: 30ppm, particle size 0.6mm, pH 6, shaking time 6 hours and dosage 4g/L respectively. The variation of metal ions adsorption onto PSH and GAC over a temperature range of 24-65^{o}C are shown in Figs. 4.27-4.30. The figures showed that the equilibrium was attained within 200 minutes for all systems. The results revealed

that the adsorption Zn^{2+} and Cd^{2+} onto PSH increased from 5.78 to 7.133 mg/g and 4.610-6.052 mg/g with an increase in the temperature of the solution from 24 to 65^{o}C. It also showed that Zn^{2+} metal ions have more affinity towards PSH with the increase in temperature compared to Cd^{2+} metal ions. The same experimental procedure has been done by using GAC and the similar adsorption patern was observed. The adsorption of Zn^{2+} and Cd^{2+} ions onto GAC increased from 1.055 to 2.320 mg/g and 0.698-1.505 mg/g with an increase in temperature of the solution from 24 to 65^{o}C. The similar observation also was found for the adsorbent derived from chlorella based bio-mass. The increased adsorption capacity might be due to the increase in surface activity and kinetic energy of the solute molecule that enhanced at higher temperatures [210].

Figs. 4.27-4.30 showed the adsorption capacity of PSH was far higher compared to GAC with the increase in temperature. The adsorption of Zn^{2+} ions was higher compared to Cd^{2+} adsorption for both the adsorbents. It shows that, the increament of kinetic energy affected the adsorption capacity with lesser time required to attain equilibrium (less than 200 minute). It is quite obvious from the plot of Zn^{2+} adsorption by PSH (Fig. 4.27).

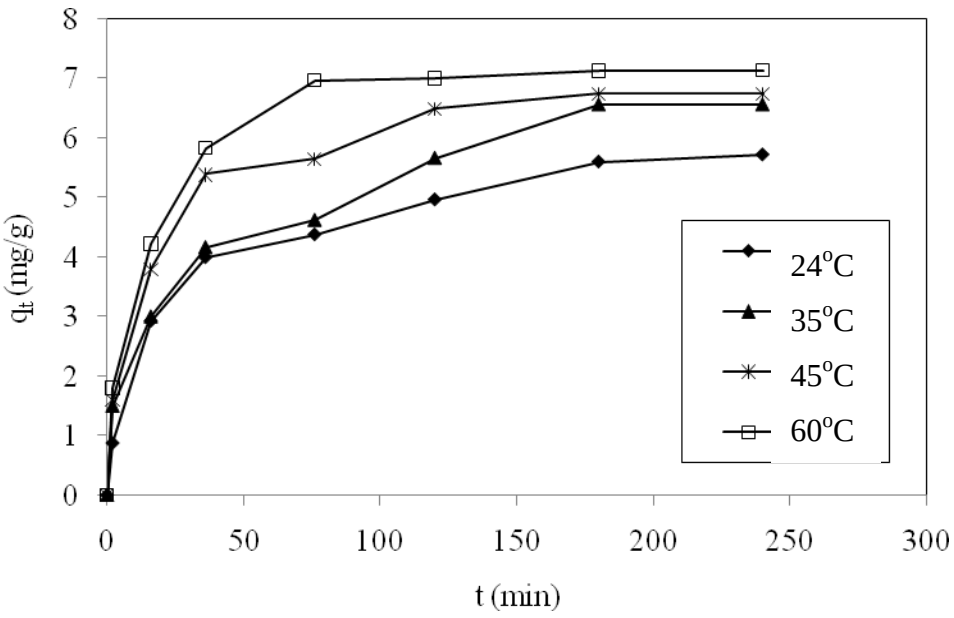

Fig. 4.27: Effect of temperature on Zn^{2+} ions removal by using PSH (Adsorbent size: 0.6mm, C_o: 30ppm, Dosage: 0.4 g/100ml, pH: 6)

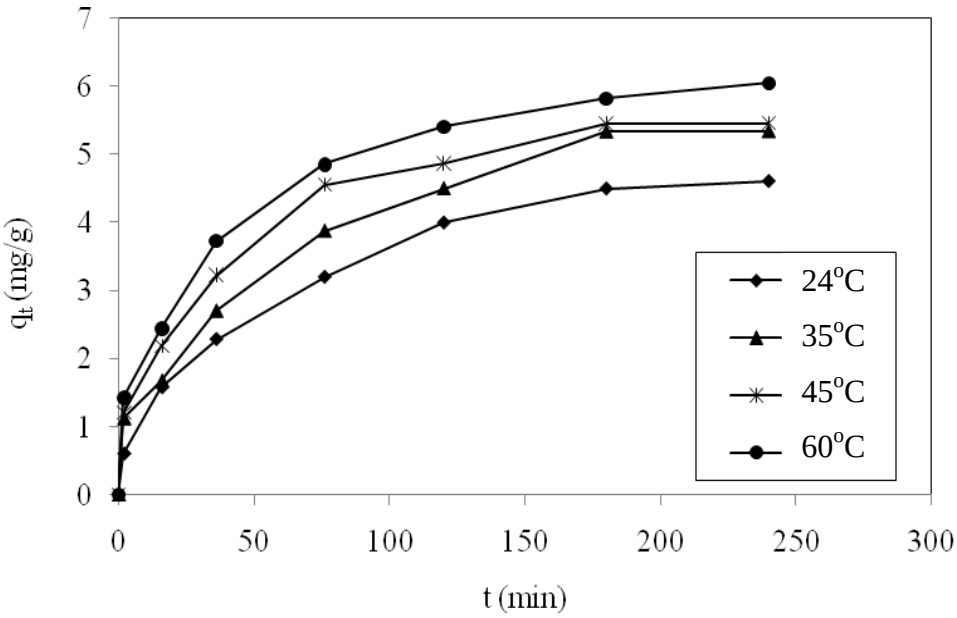

Fig. 4.28: Effect of temperature on Cd^{2+} metal ions removal by using PSH (Adsorbent size: 0.6mm, C_o: 30ppm, Dosage: 0.4 g/100ml, pH: 6)

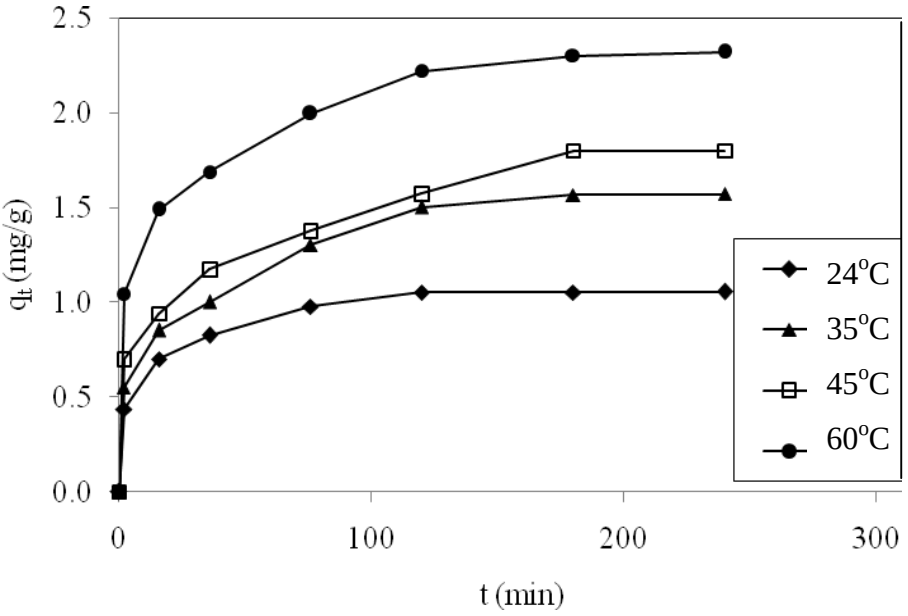

Fig. 4.29: Effect of temperature on Zn^{2+} metal ions removal by using GAC (Adsorbent size: 1.18mm, C_o: 30ppm, Dosage: 0.4 g/100ml, pH: 6)

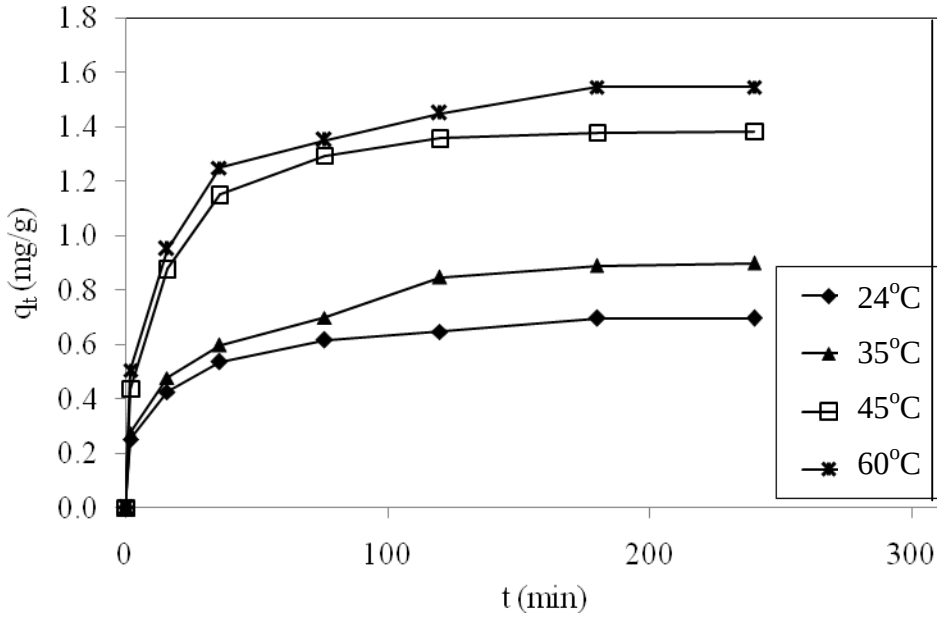

Fig. 4.30: Effect of temperature on Cd^{2+} metal ions removal by using GAC (Adsorbent size: 0.6mm, C_o: 30ppm, Dosage: 0.4 g/100ml, pH: 6)

The influence of temperature on the MG adsorption onto PSH was studied while the MG concentration, particle size, pH, shaking time and dosage were fixed at 30mg/L, 0.6mm, pH 6, 6 h and 4g/L, respectively. The variation of dye adsorption onto PSH over a temperature range of 24-65^{o}C is shown in Fig. 4.31. The result revealed that the adsorption MG increased from 5.8 to 6.7 mg/g with an increase in temperature of the solution from 24 to 65^{o}C. The similar observation also was found from the adsorbent derived from chlorella based bio-mass. The increased of adsorption capacity might be due to the increased of surface activity and kinetic energy of the solute molecule that enhanced by the higher temperature [210]. However, it also has been reported that temperature had negative effect on the MG removal [205].

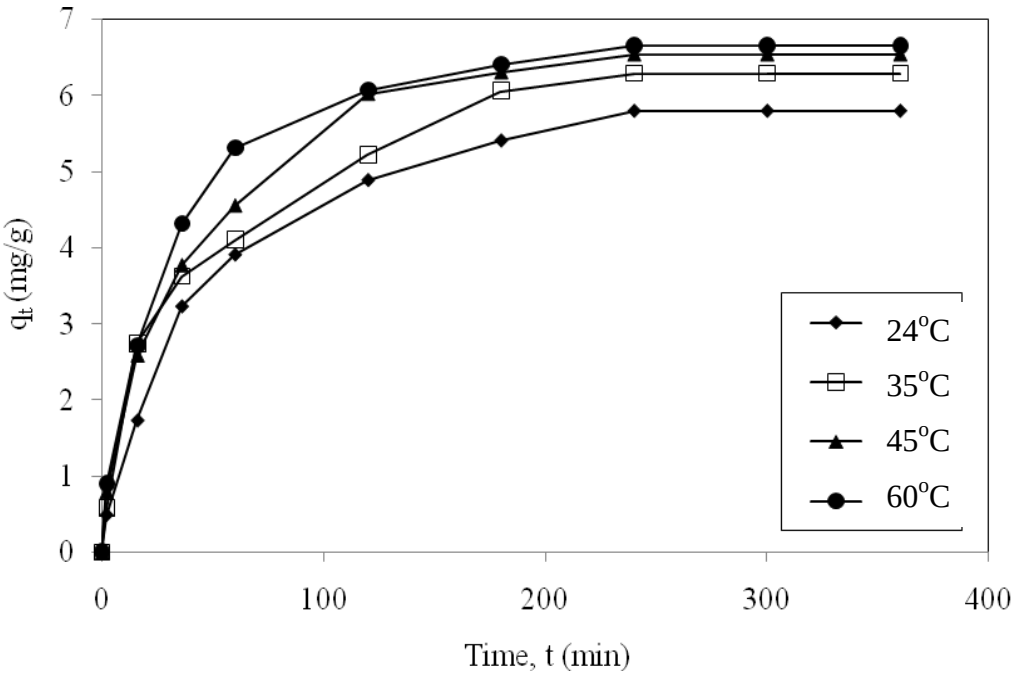

Fig. 4.31: Effect of temperature on MG dye removal by using PSH (pH: 6, PSH dosage: 4g/L, Dye conc.: 30ppm, Agitation speed: 160 rpm, Adsorbent size: 0.6mm,)

4.2.1.4 pH effect for the adsorption of Cd^{2+} and Zn^{2+} ions, and MG dye onto PSH and GAC

The pH of the adsorbate solutions has been identified as the single most important parameter governing adsorption on different adsorbents [3, 5, 6, 8, 9, 211]. It is known that metal species (M (II) = Zn^{2+} and Cd^{2+}) remain present in de-ionized water in the forms of M^{2+}, $M(OH)^{+}$ and $M(OH)_{2(S)}$ [211]. At pH ~ 5.0, the solubility of the $M(OH)_{2(S)}$ is high and therefore, the M^{2+} is the main species in the solution [211]. With the increase in the pH value, the solubility of $M(OH)_{2(S)}$ decreased and at pH ~ 10.0 , the solubility of $M(OH)_{2(s)}$ is very small. At this pH, the main species in the solution is $M(OH)_{2(S)}$. Therefore in the alkaline range, the metal ion precipitation plays the main role in the removal of the M(II) ions which is attributed to the formation of precipitate of $M(OH)_{2(S)}$. To avoid precipitation of the metal ions, all the experiments were carried out at a maximum initial solution pH of 6.0 for both the systems.

The effects of initial solution pH on the amount of adsorption of metal ions by PSH and GAC have been shown in Figs. 4.32-4.35. The removal of metal ions was found to increase when the solution pH was increased from 3.0 to 6.0 for the system. The maximum uptakes of metal ion were obtained at pH 6.0 within this time period. This dependence of metal uptake on pH may be related to the functional groups of the PSH and/or the solution chemistry [9]. Physic seed hull primarily contain weak acidic and basic functional groups. Carboxyl groups (-COOH) are the important groups for metal uptake by physic seed hull or other agricultural based biomaterials. The minimal adsorption at low pH may be due to the higher concentration and high mobility of the H^{+}, which are preferentially adsorbed on PSH surface than metal ions [9]. At higher pH, lowering in the number of H^{+} along with more negative charged ligands gives greater metal ion adsorption. At pH higher than 3-4, carboxylic groups are deprotonated and become negatively charged and therefore exhibit strong attraction with the positively charged metal ions.

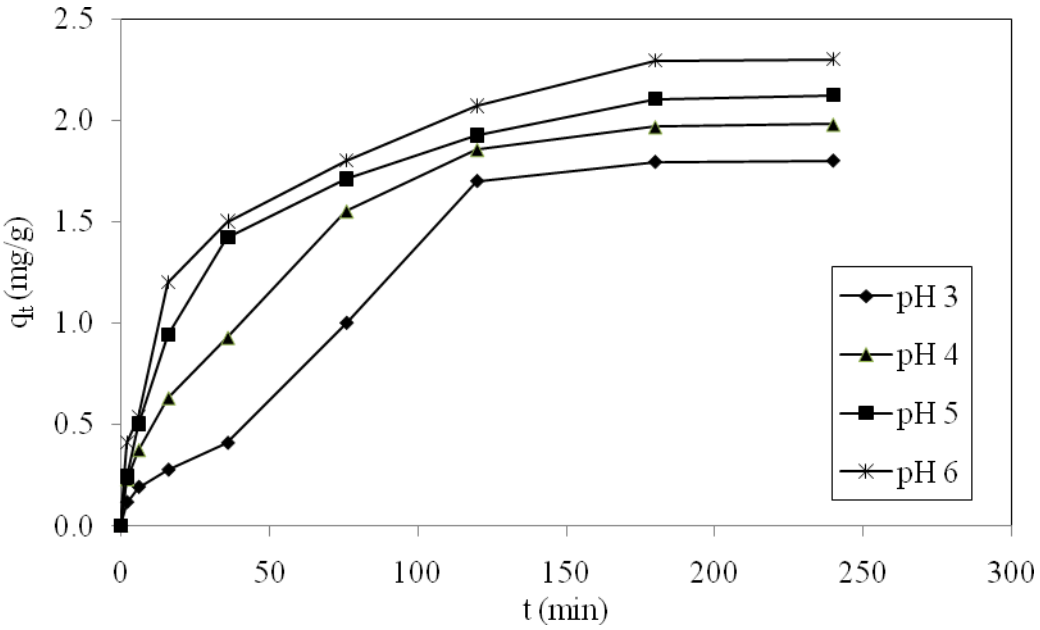

Fig. 4.32: Effect of pH on the adsorption of Zn^{2+} onto PSH (Adsorbent size: 0.6mm, C_o: 10ppm, PSH dosage: 0.4g/100ml, Temperature: 24^oC)

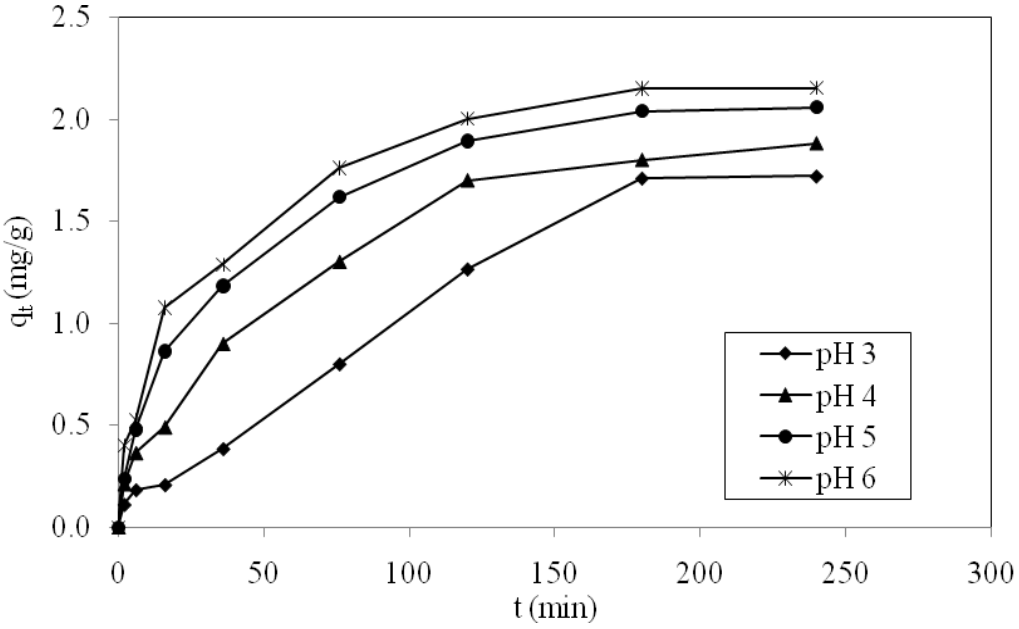

Fig. 4.33: Effect of pH on the adsorption of Cd^{2+} onto PSH (Adsorbent size: 0.6mm, C_o: 10ppm, PSH dosage: 0.4g/100ml, Temperature: 24^oC)

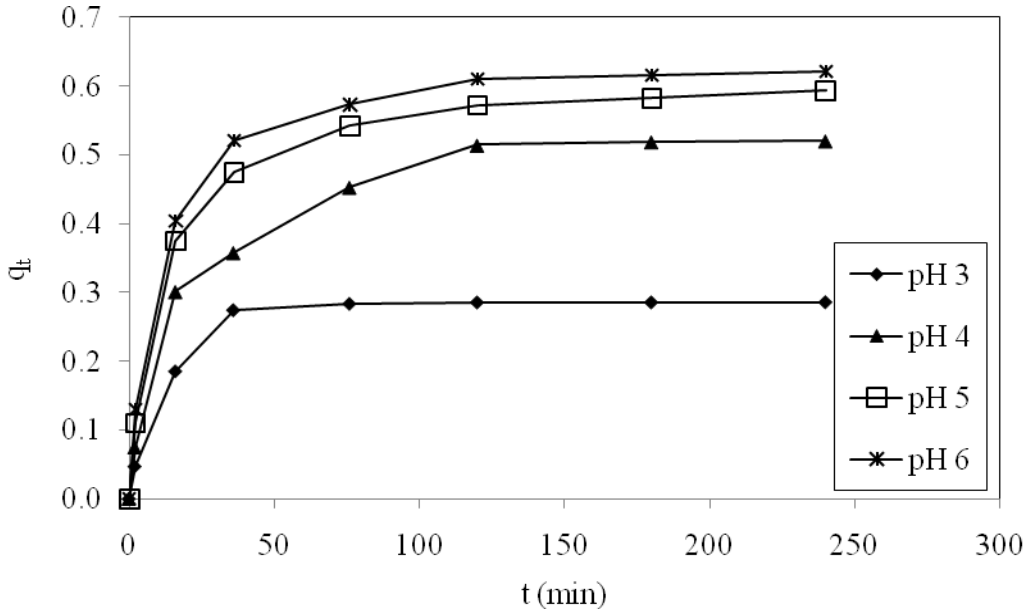

Fig. 4.34: Effect of pH on the adsorption of Zn^{2+} onto GAC (Adsorbent size: 0.6mm, C_o: 10ppm, Dosage: 0.4g/100ml, Temperature: 24^oC)

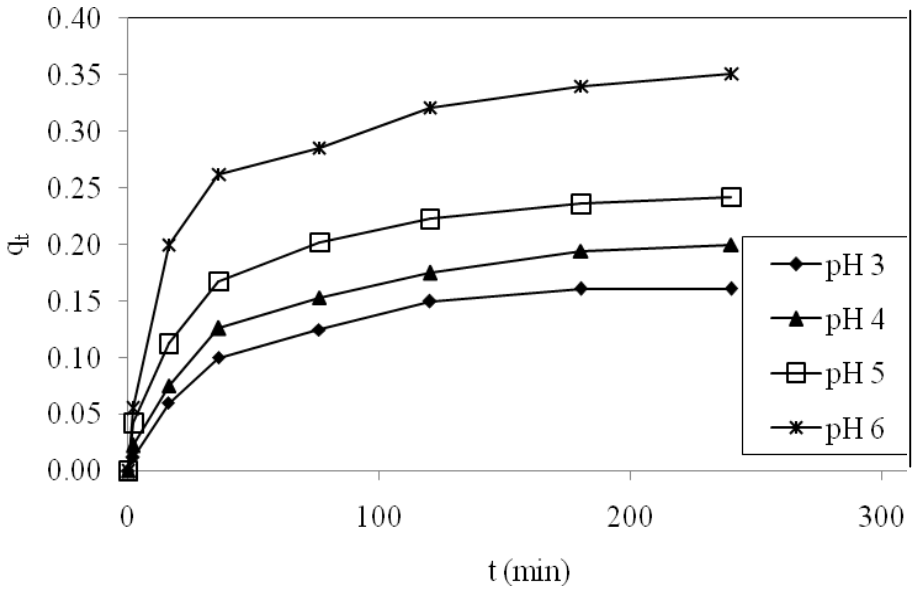

Fig. 4.35: Effect of pH on the adsorption of Cd^{2+} onto GAC (Adsorbent size: 0.6mm, C_o: 10ppm, Dosage: 0.4g/100ml, Temperature: 24^oC)

PSH basically is a lignocellulosic material and developes a negative charged surface in contact with water. MG as a cationic dye would be attracted towards the anionic structure of the adsorbents. However, the nature of the adsorbent surface charge is strongly influenced by the change in pH of the solution and it affects the adsorptive process through dissociation of functional groups on the adsorbate and adsorbent [202]. The effect of pH on the removal of MG has been shown in Figs. 4.36. The experiment was conducted at the pH range of 2-7 as pH is known to affect the stability of MG dye structure and its colour intensity. The colour intensity has not been affected up to pH 7 and the maximum 70% colour reduction was obtained at pH 11 [184]. Fig. 4.36 represents the increase of adsorption capacity with the increase in solution pH. Equilibrium of the process has been attained in 3 hours. From this study, it was observed that PSH had more than 88% MG adsorption at pH 7, and the adsorption was reduced to 82% at pH 6. The minimum adsorption was 58% at pH 2. At a lower pH or acidic medium, the MG (pK_a: 10.3) dye gets protonated consequence to its high positive charge density. The positively charge also increased with the decrease in solution pH. Therefore, the electric repulsion between the positively charged adsorbent surface and the positively charged dye molecule did not favor the adsorption of positively charged dye. The presence of excess H^+ ions could be competitive with dye cations for the adsorption sites of PSH at lower pH [184]. This result was further supported by pseudo-second order model with the assumption that chemisorptions is the rate-controlling mechanism and the data has been tabulated in Table 4.6-4.9.

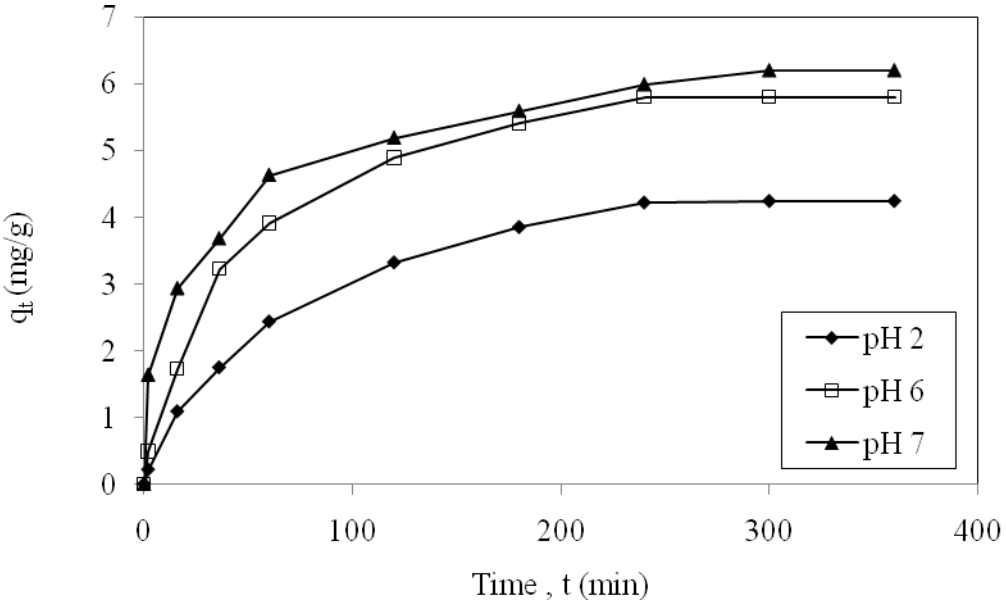

Fig. 4.36: Effect of contact time on MG adsorption by PSH with different pH (PSH dosage: 4g/L, Dye conc.: 30ppm, Agitation speed: 160 rpm, Adsorbent size: 0.6mm, Temperature: 24^{o}C)

4.2.1.5 Particle size effect for the adsorption of Cd^{2+} and Zn^{2+} metal ions, and MG dye onto PSH and GAC

Generally, adsorption is a mass transfer process where the accumulation of material at the interface of two phases takes place [212]. Therefore increased surface area in smaller particles promoted higher degree of adsorption. The time evolution of uptake as a function of the particle size of PSH for adsorption of Zn^{2+} and Cd^{2+} ion has been shown in Figs. 4.37–4.40. From the figures it is apparent that higher the particle size, the lower is the percentage adsorption of metal ions. Similar trends with dose and size for other adsorbents has also been reported by other workers [208, 212-213].

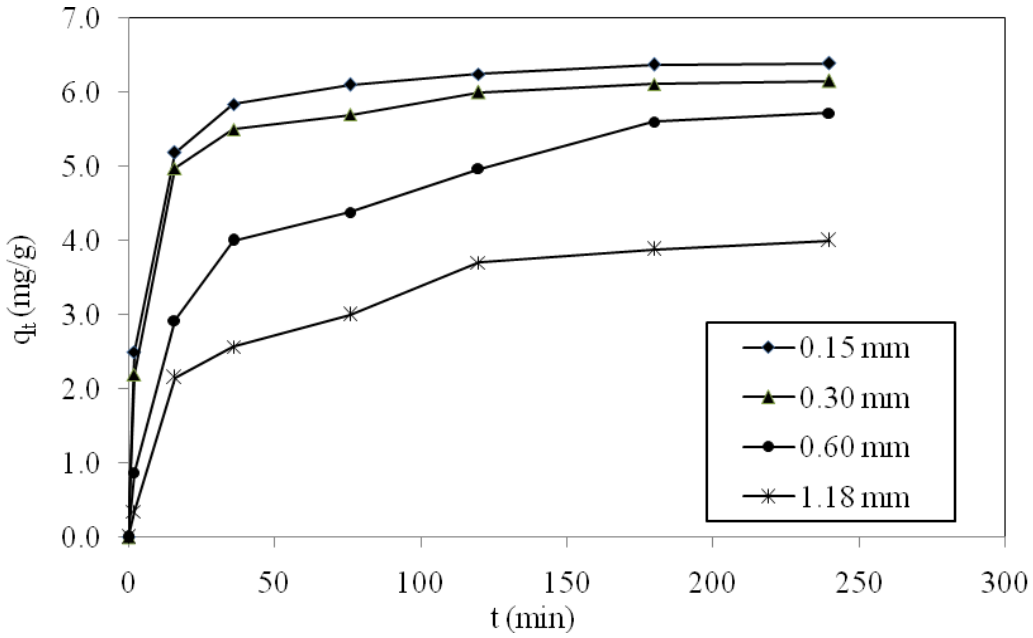

Fig. 4.37: Effect of PSH particle size on the adsorption of Zn^{2+} onto PSH (C_o: 30ppm, PSH dosage: 0.4g/100ml, pH: 6, Temperature: 24^oC)

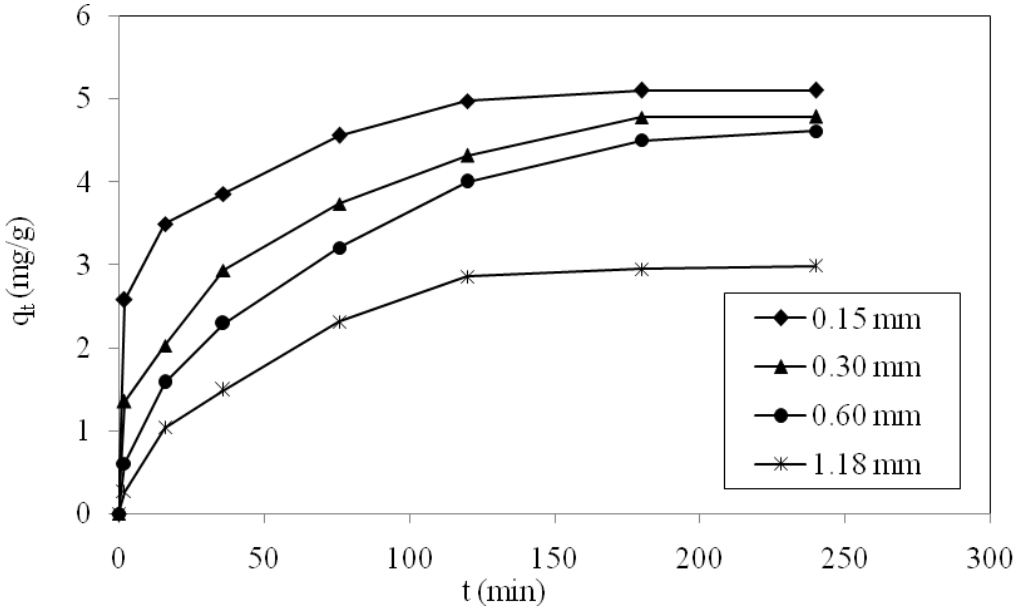

Fig. 4.38: Effect of PSH particle size on the adsorption of Cd^{2+} onto PSH (C_o: 30ppm, PSH dosage: 0.4g/100ml, pH: 6, Temperature: 24^oC)

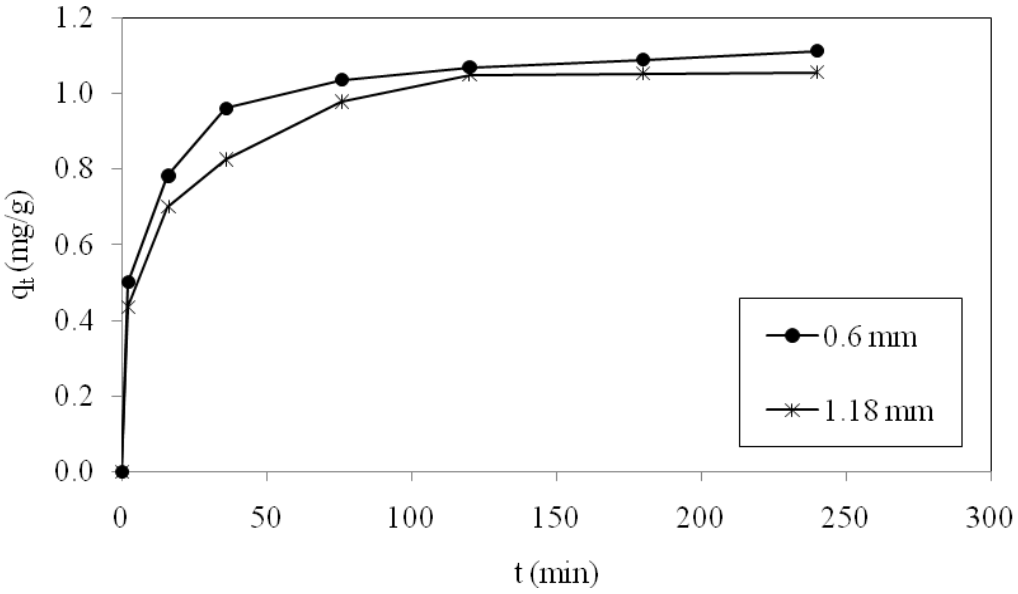

Fig. 4.39: Effect of GAC particle sizes on the adsorption of Zn^{2+} onto GAC (C_o: 30ppm, Dosage: 0.4g/100ml, pH: 6, Temperature: 24^oC)

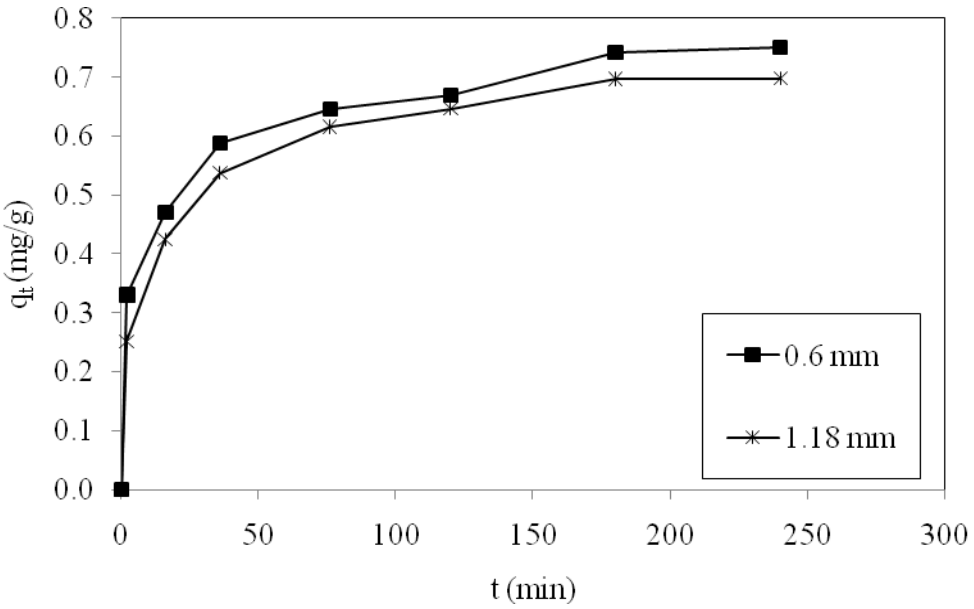

Fig. 4.40: Effect of GAC particle size on the adsorption of Cd^{2+} onto GAC (C_o: 30ppm, Dosage: 0.4g/100ml, pH: 6, Temperature: 24^oC)

Particle size of the adsorbent strongly influences the adsorption capacity. The adsorption capacity increased with the increase in total exposed surface and reduced with the increase of particle diameter for non-porous adsorbents. By this measure, the presence of large number of smaller particles in the adsorption system provides a greater surface area accessible for the dye adsorption [205]. It is evident from Fig. 4.41 that the adsorption of MG is found to increased from 56.46% to 96.49% with a decrease in the particle size of the adsorbent (PSH) from 1.18 to 0.43mm. The data showed an increase in the rate of the dye uptake as the mean diameter of the PSH decreased which contributed to the larger surface area of the adsorbent.

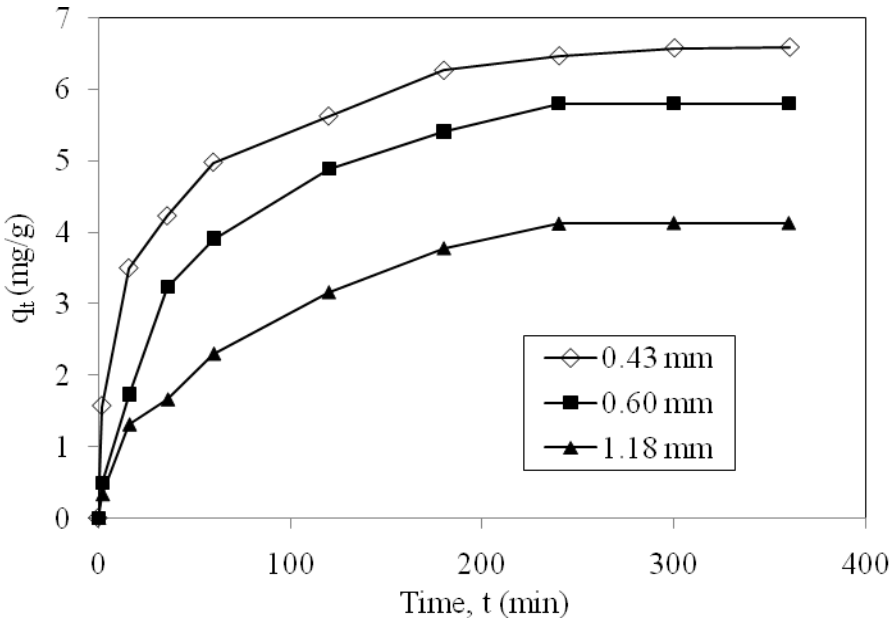

Fig. 4.41: Effect of PSH particle size on MG adsorption onto PSH (pH: 6, PSH dosage: 4g/L, Dye conc.: 30ppm, Agitation speed: 160 rpm, Temperature: 24^{o}C)

4.2.2 Adsorption dynamics

4.2.2.1 Dynamic adsorption for metal ions (Cd^{2+} and Zn^{2+}) removal using PSH and GAC

Adsorption dynamic involves the adsorption mechanisms that control the potential rate and the transient behavior for the adsorption process of metal ions. All these kinetic results under different physico-chemical operating conditions have been fitted with conventional pseudo-first-order, pseudo-second-order, and intraparticle diffusion model following the process described by Naiya et al. [5] and Sen and Meimon [3] respectively. Eq. 3.3 represents the Lagergren pseudo-first-order model, q_t and q_e represent the amount of metal ion adsorbed (mg/g) at any time t and at equilibrium time, respectively, and K_1 represents the first-order adsorption rate constant (min). Plot of log (q_e-q_t) versus t gives a straight line for pseudo-first-order adsorption kinetics, which allows computation of the rate constant K_1.

The adsorption data were then analyzed using the pseudo second-order mechanism (Eqs. 3.4-3.6), where K_2 is the pseudo second-order rate constant (g.mg^{-1} min^{-1}). By integrating and applying boundary conditions to Eq. 3.4, $t=0$ to $t=t$ and $q=0$ to $q=q_t$, Eq. 3.5 was obtained; dq/dt represent the variation in adsorbate uptake with time. The significances of q_t and q_e are similar to that stated before. From a plot of t/q_t versus t the value of the constants K_2 (g.mg^{-1}.min^{-1}) and q_e (mg/g) were calculated. The constant K_2 was used to calculate the initial sorption rate, h (the rate of uptake of adsorbent at vanishingly small time, i.e., $t \rightarrow 0$) as given by Eq. 3.6.

It has been found that the experimental kinetic results are better fitted with pseudo-second-order model since the R^2 value for pseudo-second order model are closer to 1 compared to pseudo-first order model for metal ions adsorption using both the PSH and GAC (Appendix E, Figs. 5.1-5.32). All kinetic parameters have been shown in Tables 4.6-4.9 with the value of linear regression coefficient (R^2).

The significance of pseudo-second-order model for the metal ions uptake was that the adsorption followed basically a multi-step chemisorption process [3, 6]. Moreover, from Tables 4.6 - 4.9 it is apparent that the initial sorption rate (h) and the adsorption (q_e) increased with higher initial metal ions concentration, solution pH and temperature respectively, but decreased with the increase in the particle size of the adsorbents. Similar type model parameters were obtained by various researchers for a few other absorption systems reported in the literature [7, 214].

Table 4.6

Kinetic parameters for the adsorption of Zn^{2+} onto PSH

System parameters	Pseudo-first-order			Pseudo-second-order			
	K_1	q_e	R^2	K_2	q_e	h	R^2
Initial concentration (ppm)							
2	0.0191	0.4776	0.9676	0.2374	0.4684	0.0521	0.9990
5	0.0223	2.0174	0.8456	0.0737	1.1820	0.1030	0.9984
10	0.0205	3.4530	0.8587	0.0388	2.3474	0.2136	0.9985
20	0.0269	18.1970	0.8528	0.0085	4.6533	0.1838	0.9909
30	0.0235	15.5597	0.8435	0.1665	6.0060	0.2683	0.9930
50	0.0223	19.7879	0.7801	0.1266	7.8989	0.3787	0.9941
Initial Solution pH							
3	0.0401	2.3410	0.8468	0.0376	1.8278	0.1255	0.9937
4	0.0435	3.4214	0.8979	0.0256	2.1231	0.1155	0.9905
5	0.0412	2.9957	0.9341	0.0300	2.1659	0.1408	0.9945
6	0.0389	3.3963	0.9144	0.0270	2.4195	0.1580	0.9914
Particle Size (µm)							
150	0.0456	5.8776	0.8901	0.0522	6.4516	2.1716	0.9997
300	0.0438	6.3052	0.8445	0.0443	6.2150	1.7117	0.9995
600	0.0447	12.4681	0.8052	0.0118	5.9453	0.4171	0.9904
1180	0.0419	8.2186	0.7695	0.0138	4.2230	0.2453	0.9899
Temperature (^{o}C)							
24	0.0428	12.2293	0.7613	0.0119	5.9207	0.4186	0.9909
35	0.0557	16.4097	0.8423	0.0089	6.8540	0.4160	0.9821
45	0.0601	13.5301	0.8810	0.0163	6.9686	0.7916	0.9965
60	0.0488	8.8389	0.9297	0.0223	7.3314	1.1989	0.9985

Table 4.7

Kinetic parameters for the adsorption of Cd^{2+} onto PSH

System parameters	Pseudo-first-order			Pseudo-second-order			
	K_1	q_e	R^2	K_2	q_e	h	R^2
Initial concentration (ppm)							
2	0.0207	0.4459	0.9374	0.2459	0.4317	0.0458	0.9985
5	0.0302	2.9758	0.9239	0.0578	1.1071	0.0708	0.9950
10	0.0104	1.3521	0.9525	0.0251	2.2346	0.1256	0.9957
20	0.0228	8.3138	0.9077	0.0101	4.1841	0.1763	0.9902
30	0.0253	13.3444	0.8669	0.2070	4.8309	0.2438	0.9942
50	0.0223	15.4206	0.8521	0.1587	6.3012	0.2836	0.9935
Initial Solution pH							
3	0.0408	0.9224	0.9000	0.0913	1.1788	0.1269	0.9963
4	0.0419	3.4143	0.8589	0.0246	2.0210	0.1006	0.9885
5	0.0431	2.8701	0.9040	0.0332	2.0496	0.1393	0.9943
6	0.0463	3.9428	0.9008	0.0272	2.2665	0.1399	0.9900
Particle Size (µm)							
150	0.0256	3.1857	0.9803	0.0330	5.2083	0.8963	0.9977
300	0.0477	10.1883	0.9034	0.0131	5.0226	0.3293	0.9876
600	0.0451	12.1563	0.8222	0.0079	5.0075	0.1975	0.9724
1180	0.0368	5.1310	0.8887	0.0123	3.2927	0.1334	0.9791
Temperature (^oC)							
24	0.0431	11.8468	0.9374	0.0080	4.9776	0.1980	0.9736
35	0.0444	12.1451	0.8930	0.0072	5.7604	0.2399	0.9701
45	0.0438	11.2279	0.9038	0.0108	5.7604	0.3585	0.9879
60	0.0431	13.4958	0.7387	0.0103	6.2972	0.4089	0.9894

Table 4.8

Kinetic parameters for the adsorption of Zn^{2+} onto GAC

System parameters	Pseudo-first-order			Pseudo-second-order			
	K_1	q_e	R^2	K_2	q_e	h	R^2
Initial concentration (ppm)							
5	0.0193	1.0549	0.6556	0.0521	0.3836	0.0077	0.9662
10	0.0175	1.1495	0.8147	0.0642	0.6761	0.0293	0.9936
20	0.0193	2.2793	0.8464	0.0278	1.0213	0.0290	0.9852
30	0.0177	2.8530	0.8233	0.8202	1.2192	0.0241	0.9709
50	0.0210	4.8228	0.6424	0.7660	1.3055	0.0289	0.9763
Initial Solution pH							
3	0.0348	0.1056	0.8929	0.6823	0.2930	0.0586	0.9984
4	0.0392	0.6249	0.9698	0.1677	0.5448	0.0498	0.9950
5	0.0348	0.6243	0.8690	0.2204	0.6083	0.0816	0.9986
6	0.0398	0.6700	0.8949	0.2448	0.6407	0.1005	0.9989
Particle Size (mm)							
0.6	0.0394	0.8678	0.7930	0.2074	1.1186	0.2595	0.9992
1.18	0.0373	0.8443	0.9761	0.1684	1.0796	0.1963	0.9984
Temperature (^{o}C)							
24	0.0385	0.8790	0.9725	0.1684	1.0796	0.1963	0.9984
35	0.0417	2.3966	0.9247	0.0558	1.6311	0.1484	0.9927
45	0.0357	2.4255	0.9164	0.0423	1.8567	0.1459	0.9880
60	0.0396	2.9943	0.8648	0.0562	2.3714	0.3158	0.9966

Table 4.9

Kinetic parameters for the adsorption of Cd^{2+} onto GAC

System parameters	Pseudo-first-order			Pseudo-second-order			
	K_1	q_e	R^2	K_2	q_e	h	R^2
Initial concentration (ppm)							
5	0.0166	0.6480	0.6284	0.0655	0.2407	0.0038	0.9496
10	0.0207	1.4421	0.7024	0.0459	0.4114	0.0078	0.9679
20	0.0242	1.8463	0.7115	0.0659	0.6658	0.0292	0.9910
30	0.0180	1.8672	0.7415	1.2574	0.7953	0.0213	0.9832
50	0.0187	1.8871	0.7932	1.0908	0.9168	0.0344	0.9913
Initial Solution pH							
3	0.0408	0.2554	0.9077	0.2570	0.1760	0.0080	0.9870
4	0.0316	0.3009	0.8480	0.2422	0.2119	0.0109	0.9881
5	0.0320	3.1754	0.8641	0.3110	0.2513	0.0196	0.9946
6	0.0288	2.5763	0.8693	0.2501	0.3602	0.0325	0.9956
Particle Size (mm)							
0.6	0.0352	0.8774	0.8493	0.1753	0.7598	0.1012	0.9958
1.18	0.1633	1.1773	0.9332	0.1864	0.7133	0.0949	0.9972
Temperature (^oC)							
24	0.0394	0.8494	0.9332	0.1864	0.7133	0.0949	0.9972
35	0.0309	0.9712	0.9393	0.0910	0.9313	0.0789	0.9915
45	0.0484	1.9652	0.8697	0.1261	1.4156	0.2527	0.9989
60	0.0468	2.0119	0.8900	0.0882	1.5798	0.2200	0.9976

The intra-particle diffusion model was applied to the experimental data to ascertain the mechanism of the rate-limiting step. For diffusion controlled adsorption processes, the uptake varies almost linearly with $t^{1/2}$ as shown in Eq. 3.7 [36], where q_t is the amount adsorbed at time t, K_{id} (mg/g.min$^{0.5}$) is the rate constant of intra-particle diffusion and C is value of the intercept (mg/L). The intraparticle diffusion rate constants were determined from the slope of the linear plot of q_t versus $t^{1/2}$ and values of C were determined from the intercept. The process would be controlled by intra-particle diffusion if the plot of q_t versus $t^{1/2}$ gives a straight line. However, if the data gives multilinearity of plots, then the adsorption process takes place by more than one step [215]. The first stage is an external macroporous and mesoporous diffusion or bulk diffusion, followed by linear portion to intra-particle diffusion and finally, the flat plateau to equilibrium when no more adsorption take place [215-216]. The parameter C gives an idea about the thickness (or resistance) of the boundary layer of adsorption [217].

Figs. 4.42 and 4.43 show the multilinear slop of Zn^{2+} and Cd^{2+} adsorption onto PSH. The rate of intra-particle diffusion increased from 0.1074 to 0.2276 mg/g.min$^{0.5}$ for Cd^{2+} and 0.0464 to 0.1934 mg/g.min$^{0.5}$ for Zn^{2+} with the increase in concentrations of both the metal ions from 10 to 30 ppm. From the R^2 values (0.9534–0.9993), it was evident that the adsorption followed the intra-particle diffusion model after 36 minutes of adsorption. The values of C increased from 0.6198 to 1.3022 mg/L for Cd^{2+} and 1.5355 to 2.4136 mg/L for Zn^{2+} with the increase in the initial concentration of Cd^{2+} and Zn^{2+} (10-30 ppm), showing an overall increase in the thickness and the effect of boundary layer.

The following quantitative changes in the three stages are identified from Figs 4.42 and 4.43: the metal ion concentration in the residual solution at equilibrium (C_e) for Cd^{2+} for different initial concentrations dropped to 43-58% at the first stage; at the second stage it reduced to 19-40% and at the third stage it dropped down to 14-38%. For Zn^{2+} with different initial concentrations, the ionic concentrations at equilibrium dropped to 24–47% at the first stage, 11–27% at the second stage and 8–23% at the

third stage of adsorption. This also shows the higher affinity of the adsorbent towards zinc.

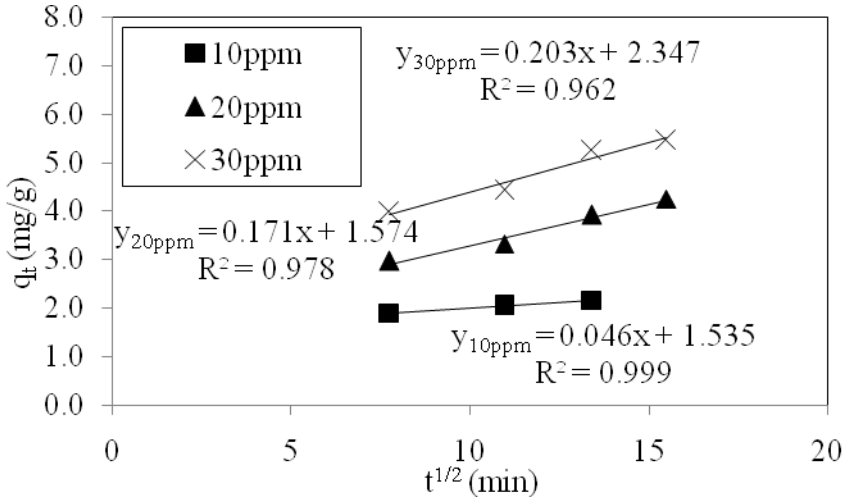

Fig. 4.42: Intraparticle diffusion plots for Zn^{2+} onto PSH at different initial metal ion concentrations (Particle size: 0.6 mm, PSH dosage: 0.4 g/100ml, pH: 6, Temperature: 24°C)

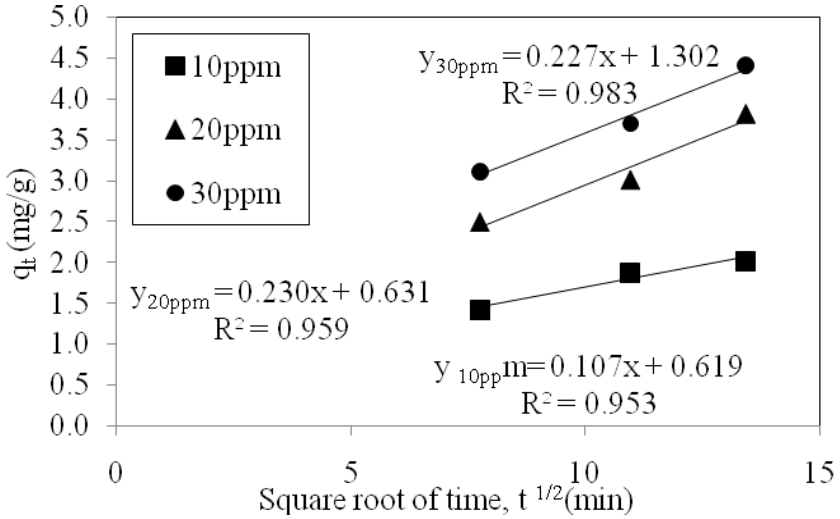

Fig. 4.43: Intraparticle diffusion plots for Cd^{2+} onto PSH at different initial metal ion concentrations (Particle size: 0.6 mm, PSH dosage: 0.4 g/100ml, pH: 5.8, Temperature: 24°C)

Table 4.10

Intra-particle diffusion parameters for the adsorption of metal ions onto PSH

Adsorbate	Initial Conc. (ppm)	K_{id} (mg/g.$min^{0.5}$)	C (mg/L)	R^2
Cd^{2+}	10-30	0.1074 - 0.2276	0.6198 -1.3022	0.9534–0.9993
Zn^{2+}	10-30	0.0464 - 0.1934	1.5355 - 2.4136	0.9534–0.9993

The rate of intra-particle diffusion has been further elucidated for GAC and similar multilayer adsorption process. However, some steps of adsorption only consist of two stepped diffusion controlled process as shown by Fierro *et al.* [215]. The first step is controlled by macroporous and mesoporous diffusion and second step is controlled by microporous diffusion [215]. The intra-particle diffusion increased from 0.0214 to 0.0625 mg/g.$min^{0.5}$ for Zn^{2+} and 0.0189 to 0.0404 mg/g $min^{0.5}$ for Cd^{2+} with the increase in the concentration of both metal ions from 10 to 30 ppm with regression coefficient (R^2) values of 0.9338–0.9961. The values of *C* increase from -0.0029 to 0.0345 mg/L for Zn^{2+} and 0.0373 to 0.1009 mg/L for Cd^{2+} with the increase in the initial concentration of Cd^{2+} and Zn^{2+} (10–30 ppm), showing an increase in the level of thickness and the effect of boundary layer.

For GAC, the two stages of adsorption process can be identified from Figs 4.44 and 4.45. The metal ion concentration in the residual solution at equilibrium (C_e) for Cd^{2+} for different initial concentrations dropped to 86–91% at the first stage and at the second stage it reduced to 85–90%. For Zn^{2+} with different initial concentrations, the ionic concentrations at equilibrium dropped to 76–86% at the first stage and 74–85% at the second stage of adsorption. It shows that zinc has higher affinity towards adsorbent.

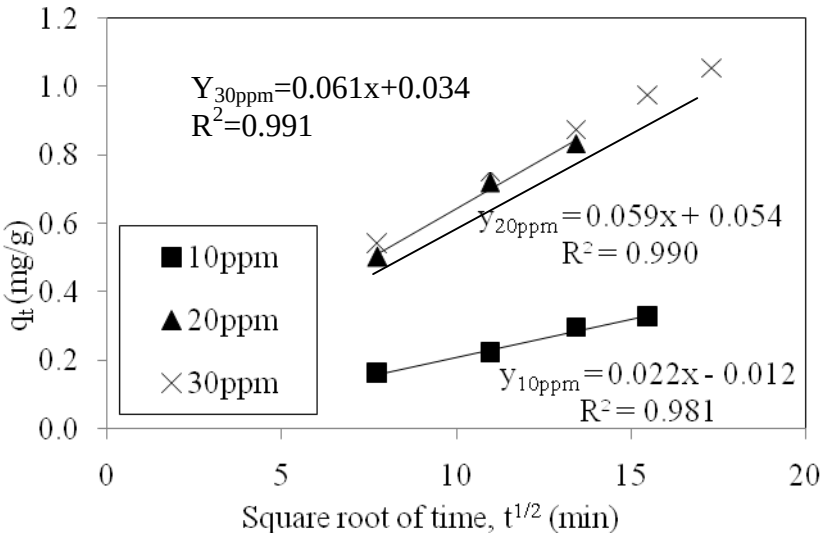

Fig. 4.44: Intraparticle diffusion plots for Zn^{2+} onto GAC at different initial metal ion concentrations (Particle size: 0.6 mm, GAC dosage: 0.4 g/100ml, pH: 6, Temperature: 24°C)

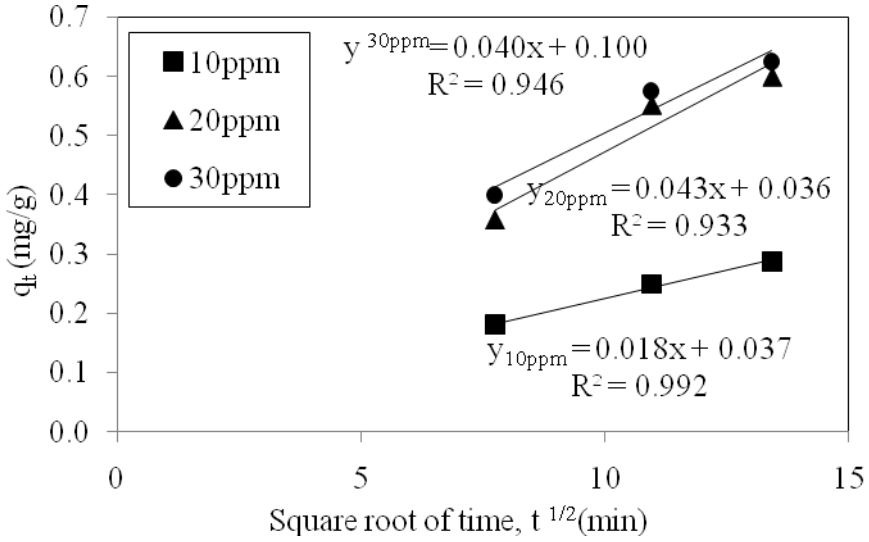

Fig. 4.45: Intraparticle diffusion plots for Cd^{2+} onto GAC at different initial metal ion concentrations (Particle size: 0.6 mm, GAC dosage: 0.4 g/100ml, pH: 6, Temperature: 24°C)

4.2.2.2 Dynamic adsorptions for MG dye removal using PSH and GAC

The R^2 value from the Lagergren pseudo-first order plot has been compared with the R^2 value from pseudo-second order plot for the adsorption of MG on PSH and GAC at different initial concentrations (Refer Appendix E, Figs 5.43-5.46). The R^2 values for both the plots demonstrated that the adsorption fitted well with pseudo second order kinetics model as the regression coefficient is higher or closer to 1. A plot between t/q_t versus t gives the value of the rate constants, K_2 (g/mg.h), equilibrium capacity, q_e (mg/g) and initial sorption rate, h. All the adsorption kinetic parameters were tabulated in Tables 4.11 and 4.12 (Eqs. 3.4-3.6). The validation of pseudo-second-order model indicated that the chemisorption was the rate-controlling step for the process.

The equilibrium capacity for PSH was 1.9384, 6.4103 and 10.7296mg/g when the MG concentration in the test solution was 10, 30 and 50mg/L, respectively. Similarly, adsorption capacity for GAC was increased from 3.5361mg/g to 8.3963mg/g as the dye concentration in the test solution was increased from 30 to 50mg/L, respectively (Tables 4.11 and 4.12) (Appendix E, Figs. 5.43-5.46).

The adsorption dynamic was further studied by varying pH, particle size and temperature to measure the adsorption capacity using the Lagergren pseudo-first order and pseudo-second order models. All the kinetic parameters have been tabulated in Tables 4.11. It shows that the initial sorption rate, h and the adsorption capacity increased with the increase in dye concentration, pH and temperature but reduced with the increases in particle size. The Ho's pseudo-second-order model has been applied extensively for the adsorption of metal ions, dyes, herbicides, oils and organic substances from aqueous systems [233].

The values of the kinetic parameters for adsorption of MG dye onto PSH at different pH, particle size and temperatures were given in Table 4.11. The adsorption process well fits the pseudo-second-order model with high correlation coefficient (>0.99). The table shows that the equilibrium capacity was the lowest at pH 2 for the

pseudo-second order plot. It proves that the high density of positive charge ions at the lower pH affected the MG adsorption on the PSH surfaces. The higher size of particle developed low adsorption capacity and it was proved by the low equilibrium capacity from pseudo-second order plot data. The availability of pores is less for the bigger size particle. It is a fundamental property for choosing a good adsorbent. From the data in Table 4.11, it can be seen that the adsorption uptake values did not vary much for the wide range of temperatures studied. However, increasing temperature usually leads to the increase in the rate of approach to equilibrium and this results is in agreement with Bekci et al.(2009) [202]. (Appendix E, Figs. 5.51-5.52).

Table 4.11
Kinetic parameters for the adsorption of MG onto PSH

System parameters	Pseudo-first-order			Pseudo-second-order			
	K_1	q_e	R^2	K_2	q_e	h	R^2
Initial concentration (ppm)							
10	0.0281	2.6357	0.8761	0.0355	1.9384	0.1333	0.9969
30	0.0373	11.5266	0.8867	0.0059	6.2617	0.2324	0.9923
50	0.0322	25.0496	0.8924	0.0037	10.7296	0.4303	0.9879
pH							
2.2	0.0345	11.4078	0.8729	0.0049	4.7870	0.1118	0.9823
6	0.0373	11.5266	0.8761	0.0059	6.2617	0.2324	0.9923
7.1	0.0345	14.0670	0.7988	0.0094	6.4103	0.3848	0.9947
Particle Size (mm)							
0.43	0.0306	12.2011	0.7821	0.0104	6.8074	0.4823	0.9966
0.6	0.0373	11.5266	0.8761	0.0059	6.2617	0.2324	0.9923
1.18	0.0350	10.8019	0.8915	0.0059	4.5620	0.1219	0.9807
Temperature (^oC)							
24	0.0373	11.5266	0.8761	0.0059	6.2617	0.2324	0.9923
35	0.0378	11.8086	0.8867	0.0066	6.7069	0.2972	0.9936
45	0.0394	11.9261	0.8924	0.0074	6.9348	0.3570	0.9953
60	0.0419	12.3937	0.8838	0.0092	6.9686	0.4470	0.9973

Table 4.12
Kinetic parameters for the adsorption of MG onto GAC

System parameters	Pseudo-first-order			Pseudo-second-order			
	K_1	q_e	R^2	K_2	q_e	h	R^2
Initial concentration (ppm)							
30	0.0302	9.6672	0.7416	0.0055	3.5361	0.0686	0.9304
50	0.0325	24.5358	0.7569	0.0020	8.3963	0.1382	0.9601

PSH and GAC have macro and micro pores and the adsorption mechanism might be governed by intraparticle diffusion. During the adsorption, three distinct steps are observed. Initially the dye molecules encounter the boundary layer effect. Then they diffuse from the boundary layer film onto the adsorbent surface. After a relatively longer contact time they diffuse into the porous structure of the adsorbent and finally, the equilibrium is reached when there is no further adsorption taking place [48, 208]. Intraparticle diffusion model are given in Eq. 3.7 as proposed by Weber and Morris [36] showed that the intraparticle diffusion is the rate-limiting factor for the uptake of adsorbate and it varies with the square root of time.

Figs 4.46 and 4.47 have been presenting the linear plots of the intraparticle diffusion for the adsorption of MG on PSH and GAC. Three different of diffusion stages were noticed at the adsorption profiles of the samples. The intra-particle diffusion increased from 0.065 to 0.745 mg/g.min$^{0.5}$ for PSH and 0.175 to 0.413 mg/g min$^{0.5}$ for GAC with the increasing concentration of MG dye from 10 to 50 ppm for PSH and 30 to 50 ppm for GAC with regression coefficient (R^2) values of 0.936–0.995. The values of C increased from 0.881 to 2.483 mg/L for PSH and 0.106 to 0.268 mg/L for GAC with the increase in initial concentration of MG dye, showing an increase in the level of thickness and the effect of the boundary layer.

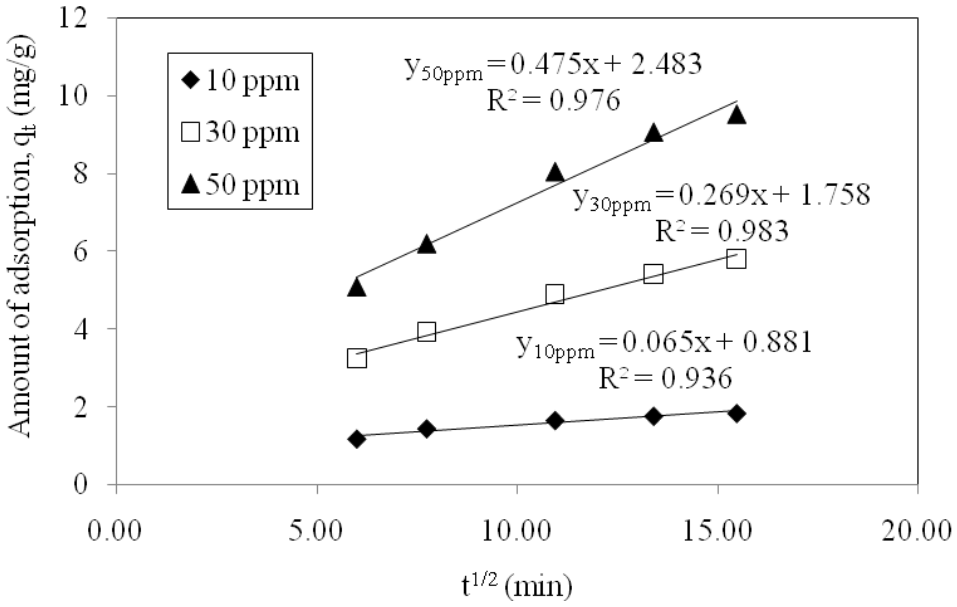

Fig. 4.46: Intraparticle diffusion plot at different initial MG concentrations on PSH (PSH dosage: 4g/L. pH: 6, Shaker speed: 160rpm, Temperature: 24^0C, Adsorbent size: 0.6mm)

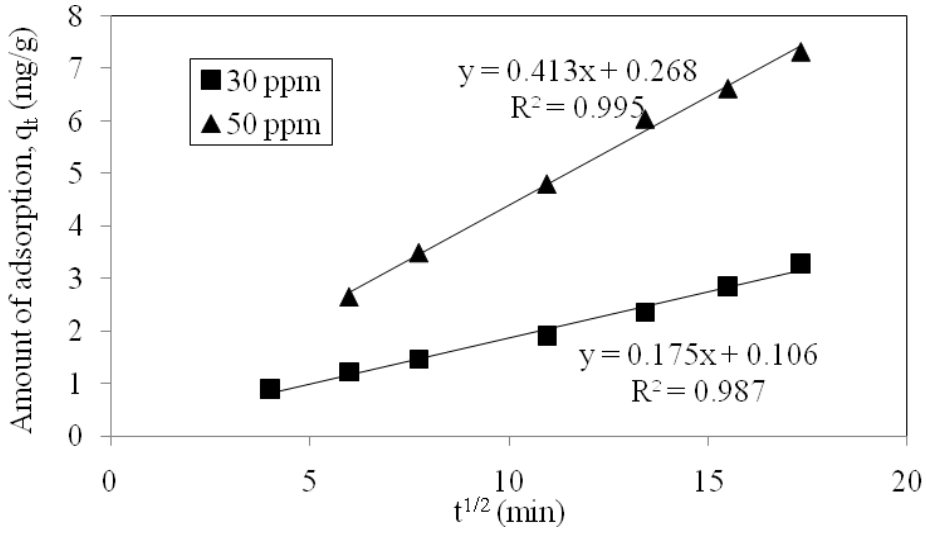

Fig. 4.47: Intraparticle diffusion plot at different initial MG concentrations on GAC (GAC dosage: 4g/L. pH: 6, Shaker speed: 160rpm, Temperature: 24^0C, Adsorbent size: 0.6mm)

Figs. 4.48-4.50 present the intra-particle diffusion for the adsorption of MG onto PSH as a function of temperature, pH and particle size. The data was tabulated in Table 4.13. The results showed that with the increases in temperature from 24-65^{o}C, the intra-particle rate constant and the effect of boundary layer also increased. Similar results was obtained for the effect of pH on the adsorption. However, intra-particle rate constant and the effect of boundary layer or thickness of the boundary layer obtained decreased with the increase in particle size of the adsorbent.

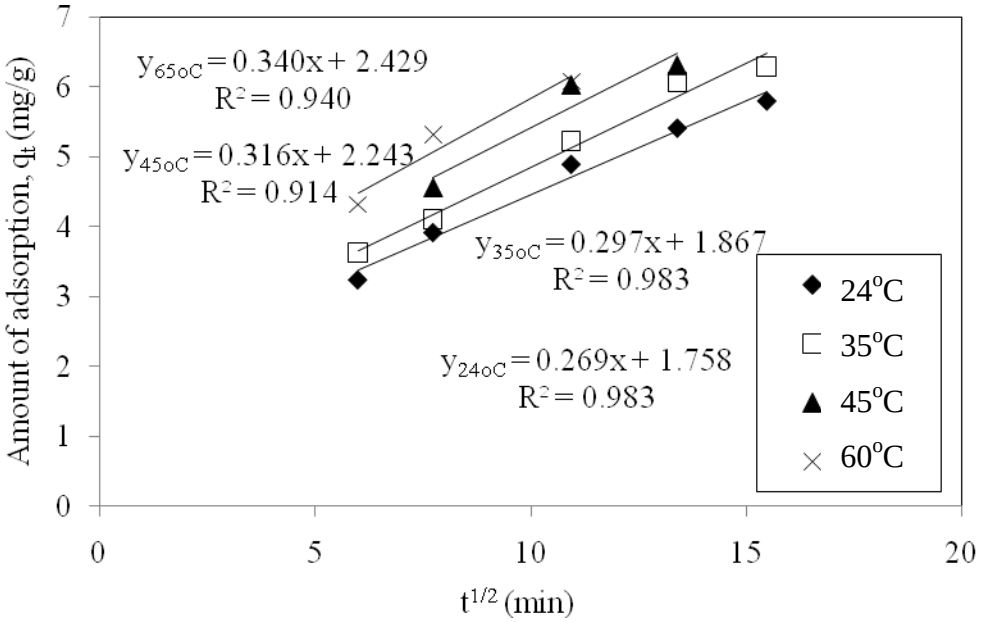

Fig. 4.48: Intraparticle diffusion plot for MG adsorption on PSH at different temperatures (PSH dosage: 4g/L, pH: 6, Agitation speed: 160rpm, Adsorbent size: 0.6mm, Dye conc.:30ppm)

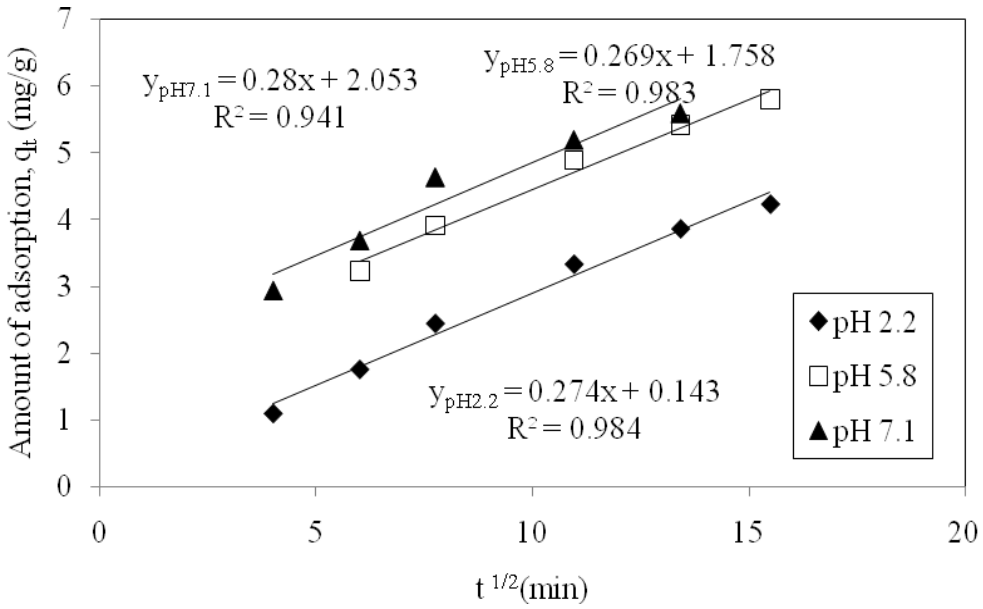

Fig. 4.49: Intraparticle diffusion plot for MG adsorption on PSH at different pH (PSH dosage: 4g/L, Agitation speed: 160rpm, Temperature: 24^{o}C, Adsorbent size: 0.6mm, Dye conc.:30ppm)

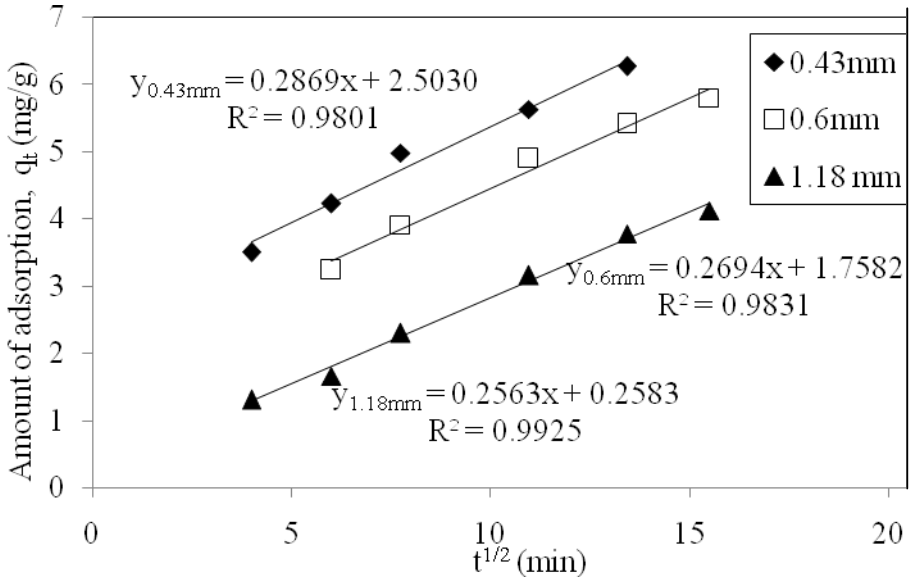

Fig. 4.50: Intraparticle diffusion plot for MG adsorption on PSH at different particle sizes (PSH dosage: 4g/L, pH: 6, Agitation speed: 160rpm, Temperature: 24^{o}C, Dye conc.: 30ppm)

Table 4.13

Intra-particle diffusion parameter for the adsorption of MG onto PSH

Parameter		K_{id} (mg/g.min$^{0.5}$)	C (mg/L)	R^2
Initial conc. (ppm)	10-50	0.6500 - 0.4750	0.8810-2.4830	0.9360 - 0.9760
Particle size (mm)	0.43	0.2869	2.5030	0.9801
	0.6	0.2694	1.7582	0.9831
	1.18	0.2563	0.2583	0.9925
pH	2.2	0.2747	0.1437	0.9849
	6.0	0.2694	1.7582	0.9831
	7.1	0.2800	2.0536	0.9411
Temperature (^{o}C)	24	0.2694	1.7582	0.9831
	35	0.2977	1.8678	0.9837
	45	0.3161	2.2439	0.9140
	65	0.3402	2.4294	0.9405

4.2.2.3 Dynamic adsorption for the effect of anionic surfactant on metal ions removal using PSH

The kinetic plots between t/q_t versus time, *t* for Zn^{2+} and Cd^{2+} adsorption at different concentration of Aerosol 22 produced high regression coefficients for linearity (R^2) which suggest that the adsorption experiment followed pseudo-second-order kinetics (Appendix E, Figs. 5.39-5.40). The initial sorption rate (*h),* the equilibrium adsorption capacity (q_e) and second order rate constant (K_2) have been determined from the slope and intercept of the plot *t/q* versus *t*. All kinetic parameters including the correlation coefficients, R^2 have been calculated and tabulated in Table 4.14. The R^2 values from pseudo-second order kinetic parameters have been compared with Lagergren pseudo-first order parameters and it showed that the data is better fitted with pseudo-second

order model (Appendix E, Figs. 5.41-5.42). The assumption behind the pseudo-second-order model is that the metal ion uptake process is due to chemisorptions [2, 3] and sorption in a multisteped process in this case. Also from Table 4.14 it is clear that the initial sorption rate, *h* and the adsorption capacity increased with the increase in initial surfactant concentration respectively. Similar type model parameters have been obtained by various researchers for different systems [5, 214, 218].

Table 4.14

Kinetic parameters for the adsorption of Cd^{2+} and Zn^{2+} metal ions onto PSH with the effect of anionic surfactant at different concentration

Aerosol 22	Metal ions	Pseudo-first-order			Pseudo-second-order			
Conc.(ppm)	30ppm	K_1	q_e	R^2	K_2	q_e	h	R^2
1	Cd^{2+}	0.0352	6.7889	0.9202	0.0147	4.1911	0.2574	0.9940
3		0.0325	6.6527	0.8482	0.0145	3.9324	0.2244	0.9938
5		0.0343	6.4580	0.7949	0.0171	3.4783	0.2065	0.9937
7		0.0309	5.0015	0.7962	0.0153	3.0084	0.1389	0.9931
1	Zn^{2+}	0.0362	7.6120	0.9437	0.0157	6.3211	0.6289	0.9967
3		0.0362	7.4508	0.9311	0.0171	5.5710	0.5304	0.9970
5		0.0327	6.2302	0.8643	0.0212	4.9140	0.5122	0.9978
7		0.0267	5.0211	0.7804	0.0212	4.0112	0.3416	0.9960

This kinetics experiment proves that adsorption of metal ion on PSH with the effect of anionic surfactant followed three stepped process of intraparticle diffusion mechanism as observed by Jain (2001) [208]. Verifications of these steps were done by fitting the data in diffusion controlled model as shown in Figs. 4.51 and 4.52. The intraparticle diffusion rate constants have been determined from the slope of the linear gradient of the plot q_t versus $t^{1/2}$ as shown in these figures. It showed three separate regions in the plot: initial part of the curve is attributed to rapid adsorption followed by a transition phase or intraparticle diffusion phase and almost flat plateau section due to

intraparticle diffusion resistance. It is clearly evident that adsorption of metal ions on PSH followed three stepped process. Moreover, the adsorption of metal ions on PSH depends on the low concentration of surfactant and the rate of intraparticle diffusion decreased with the increase in the amount of surfactant (1-7ppm). The intra-particle diffusion decreased from 0.3434 to 0.2719 mg/g.min$^{0.5}$ for Zn^{2+} and 0.2142 to 0.1458 mg/g min$^{0.5}$ for Cd^{2+} with the increasing concentration of both metal ions from 10 to 30 ppm having regression coefficient (R^2) values of 0.9502–0.9946. The value of C presented the level of thickness for the effect of boundary layer. It decreased from 2.0368 to 0.9243 mg/L for Zn^{2+} and 1.1635 to 0.8321 mg/L for Cd^{2+} with the increase in the initial concentration of Aerosol 22 (1-7 ppm).

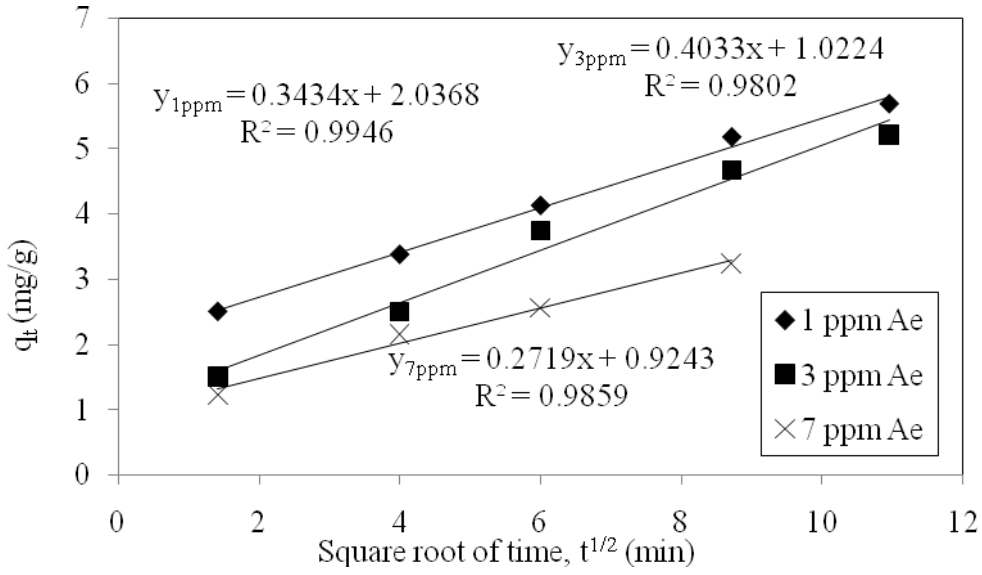

Fig. 4.51: Intraparticle diffusion plot at 1 ppm of Aerosol 22 on the adsorption of Zn^{2+} on PSH (Metal ion conc.: 30 ppm, PSH dosage: 4g/100mL, Adsorbent saiz: 0.6mm, pH: 5.8, Temperature: 24^{0}C, Agitation speed: 160 rpm)

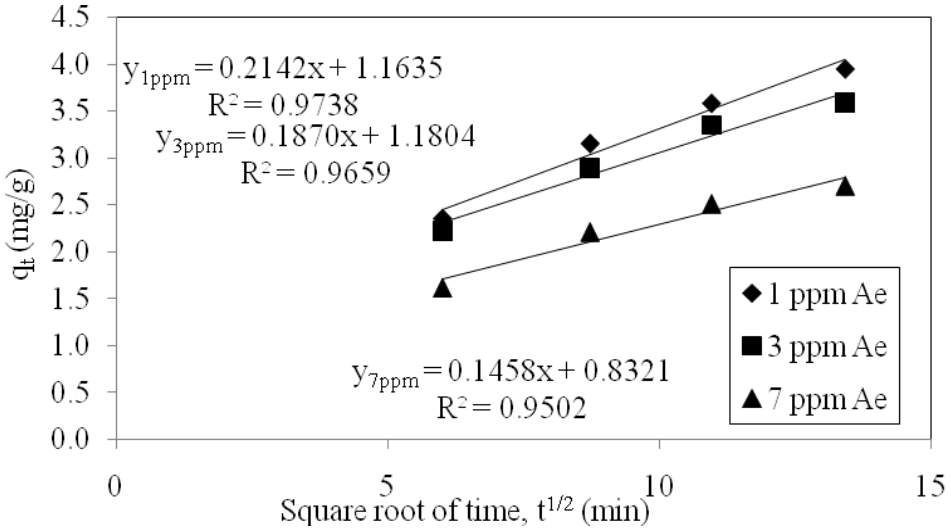

Fig. 4.52: Intraparticle diffusion plot at different initial concentrations of Aerosol 22 on the adsorption of Cd^{2+} on PSH (Metal ion conc.: 30 ppm, PSH dosage: 4g/100mL, Adsorbent size: 0.6mm, pH: 5.8, Temperature: 24^0C, Agitation speed: 160 rpm)

Table 4.15

Intra-particle diffusion parameter for the effect of Aerosol 22 on metal ions adsorption onto PSH

Adsorbate	Initial Conc. (ppm)	K_{id} (mg/g.$min^{0.5}$)	C (mg/L)	R^2
Zn^{2+} + Aer22	30ppm Zn^{2+} + 1-7ppm Aer	0.3434 - 0.2719	2.0368 - 0.9243	0.9502–0.9946
Cd^{2+} + Aer22	30ppm Zn^{2+} + 1-7ppm Aer	0.2142 - 0.1458	1.1635 - 0.8321	0.9502–0.9946

4.2.3 Adsorption isotherm

4.2.3.1 Freundlich isotherm for the adsorption of C^{d2+} and Z^{n2+} metal ions, and MG dye onto PSH and GAC, and the effect of anionic surfactant onto PSH

Adsorption equilibrium data or isotherms are essential for designing an adsorption system. The measured adsorption equilibrium data were fitted with Langmuir, Freundlich and Dubinin–Radushkevich isotherm equations within the metal ions and dye concentrations in the range of 5ppm to 50ppm. The Freundlich adsorption isotherm, which assumes that adsorption takes place on heterogeneous surfaces, can be expressed by Eq. 3.8, where q_e is the amount of metal ion or dye adsorbed at equilibrium time, C_e is equilibrium concentration of metal ions or dye in solution. K_f and n are isotherm parameters which indicate the capacity and the intensity of the adsorption respectively. It can be calculated from the intercept and slope of plot between ln q_e and ln C_e as shown in Figs. 4.53-4.56 [34, 35]. All the calculated parameters were tabulated in Table 4.16 for PSH and GAC. From the regression coefficient value (R^2), it has been observed that GAC data gave better fit with pseudo-first order plot which assumes that the adsorption takes place on heterogeneous surfaces.

The magnitude of the exponent, 1/n, gives an indication of the favorability of adsorption. $n > 1$ represent favorable adsorption condition [219-220]. Fig. 4.57 represents the Freundlich isotherm plot of PSH and GAC for MG dye adsorption, while Figs. 4.58 and 4.59 present the Freundlich isotherm plot for the effect of anionic surfactant onto PSH. All values of K_f, n and the linear regression correlation (R^2) from Freundlich model has been tabulated in Table 4.16.

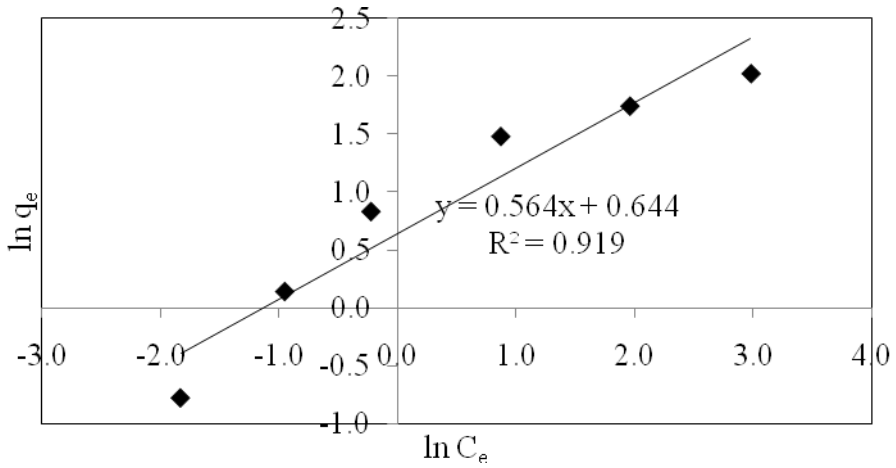

Fig. 4.53: Freundlich isotherm for the adsorption of Zn^{2+} onto PSH (Particle size: 0.6 mm, PSH dosage: 0.4 g/100ml, pH: 6, Temperature: 24^{o}C)

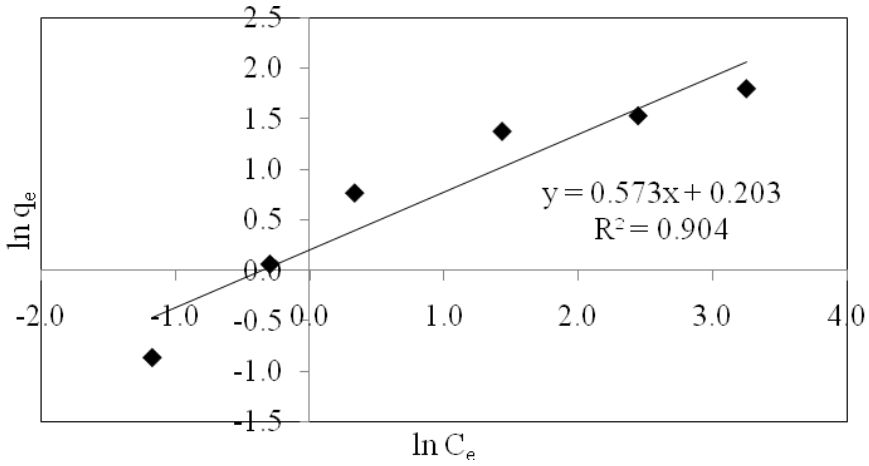

Fig. 4.54: Freundlich isotherm for the adsorption of Cd^{2+} onto PSH (Particle size: 0.6 mm, PSH dosage: 0.4 g/100ml, pH: 6, Temperature: 24^{o}C)

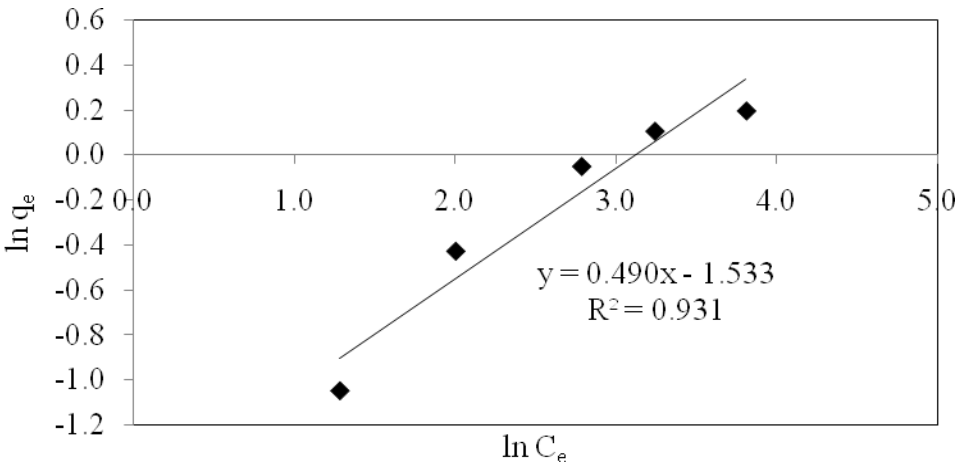

Fig. 4.55: Freundlich isotherm for the adsorption of Zn^{2+} onto GAC (Particle size: 0.6 mm, GAC dosage: 0.4 g/100ml, pH: 6, Temperature: 24^{o}C)

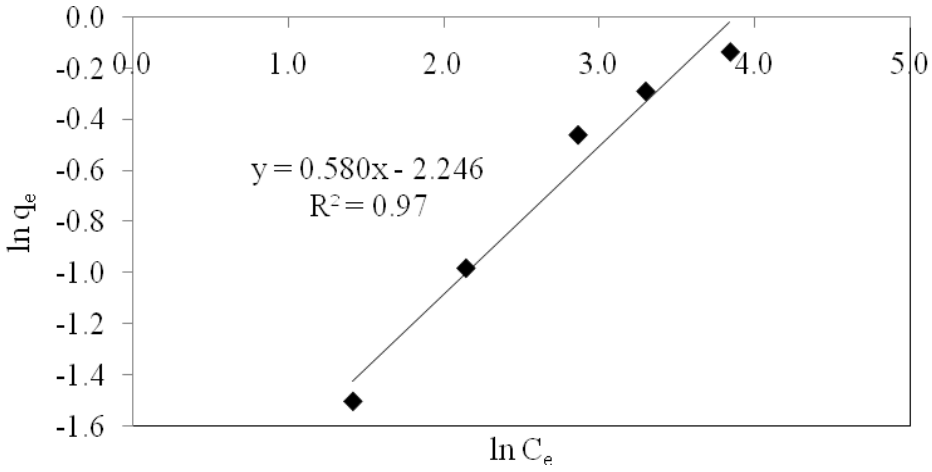

Fig. 4.56: Freundlich isotherm for the adsorption of Cd^{2+} onto GAC (Particle size: 0.6 mm, GAC dosage: 0.4 g/100ml, pH: 6, Temperature: 24^{o}C)

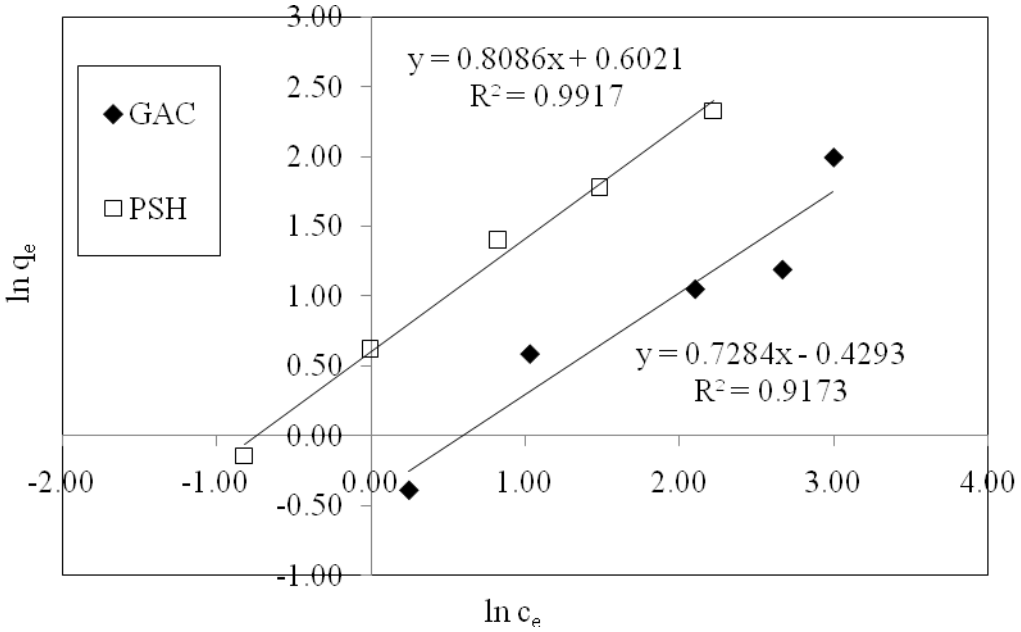

Fig. 4.57: Freundlich plots for MG adsorption on PSH and GAC (pH: 6, Dosage: 4g/L, Temperature: 24^0C, Agitation speed: 160rpm, Adsorbent size: 0.6mm, Dye conc. 30ppm, Time contact: 6 hours)

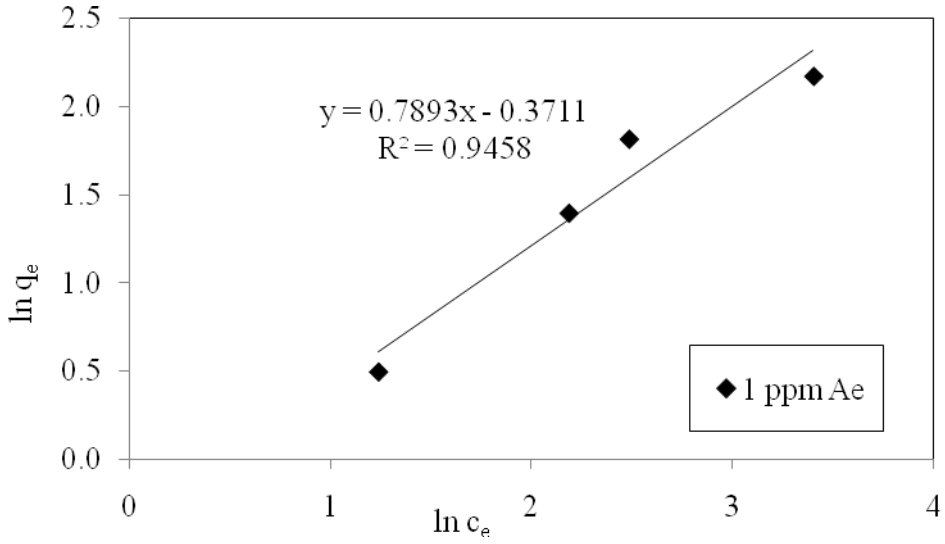

Fig. 4.58: Freundlich isotherm plots for the effect of Aerosol 22 on the adsorption of Zn^{2+} using PSH (Metal ion conc.: 10-65ppm, pH: 6, Dosage: 4g/L, Temperature: 24^oC and Agitation speed: 160rpm, Adsorbent size: 0.6mm)

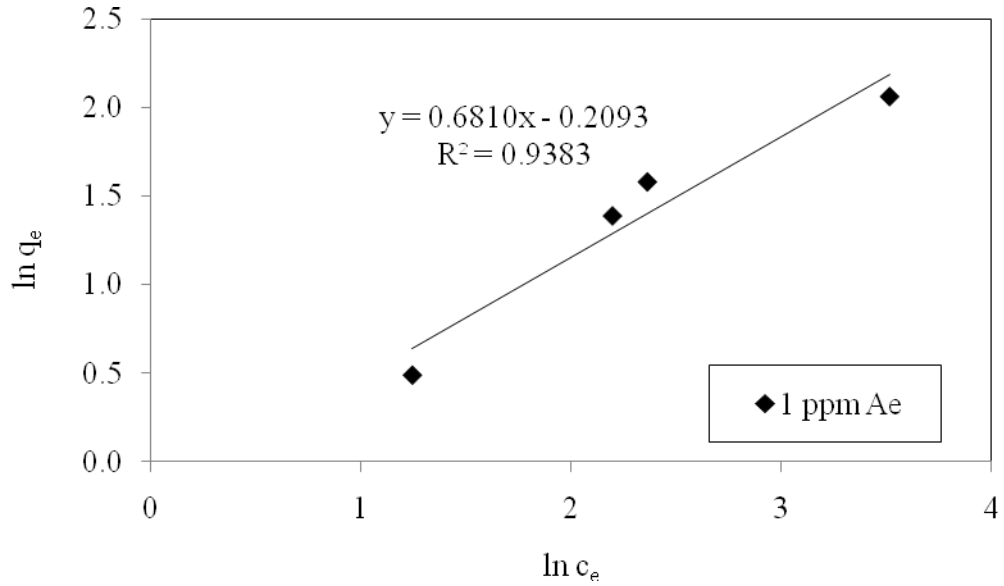

Fig. 4.59: Freundlich isotherm plots for the effect of Aerosol 22 on the adsorption of Cd^{2+} using PSH (Metal ion conc.: 10-65ppm, Surfactant conc.: 1ppm; pH: 6, Dosage: 4g/L, Temperature: 24^{o}C and Agitation speed: 160rpm, Adsorbent size: 0.6mm)

Table 4.16

Freundlich parameters for the adsorption of Cd^{2+} and Zn^{2+} metal ions and dye onto PSH and GAC, and the effect of anionic surfactant on metal ions removal

Adsorbent	Adsorbate	Freundlich		
		k_f	1/n	R^2
PSH	Cd^{2+}	0.8157	0.5730	0.9043
	Zn^{2+}	0.5250	0.5644	0.9190
GAC	Cd^{2+}	9.4499	0.5800	0.9700
	Zn^{2+}	0.2159	0.4910	0.9310
PSH	MG	0.5477	0.8086	0.9917
GAC		1.2367	0.7284	0.9173
PSH	Cd^{2+}+ Aer22	9.1093	0.6810	0.9383
	Zn^{2+}+Aer22	1.4493	0.7893	0.9458

4.2.3.2 Langmuir isotherm for the adsorption of C^{d2+} and Z^{n2+} metal ions and Dye onto PSH and GAC, and the effect of anionic surfactant onto PSH

According to Langmuir model, adsorption occurs uniformly on the active sites of the adsorbent and once an adsorbate occupies a site, no further adsorption can take place at this site. Langmuir isotherm equation was also tested with these same initial metal ion concentrations. The linearized form of Langmuir can be written as Eq. 3.9. The Langmuir constants, q_m (maximum adsorption capacity, mg/g) and K_L (parameter for Langmuir isotherm related to the affinity of the binding sites and energy of adsorption, L/mg) are calculated from the plot of $1/q_e$ versus $1/C_e$.

The Langmuir isotherm appears to give a better fit of the experimental data as evident from the higher values of the correlation coefficients. Table 4.17 presents the fitted Langmuir isotherm parameters for Cd^{2+} and Zn^{2+} adsorption using PSH and GAC systems. Though the uptake of a metal ion depends upon the initial concentration, the Langmuir adsorption capacity given by q_m is independent of solution concentration. The results clearly indicate the affinity and preferential sorption behavior of PSH towards Zn^{2+} as compared to Cd^{2+}. This is an interesting observation that may be explained in the light of a higher ionic potential of Zn^{2+} (5.33) compared to Cd^{2+} (4.2) [221]. Although both the cations have the same charge, Zn^{2+} has a smaller hydration ionic radius (0.072 nm) than Cd^{2+} (0.096 nm) [212], and consequently a higher ionic potential. In spite of having the same hydration number of 6 in aqueous solution, the larger ionic potential and charge density of Zn^{2+} are responsible for the enhanced electrostatic attraction and binding at the active sites of the adsorbent surface. The surface coverage on the basis of ionic size and the Langmuir maximum adsorption capacity (q_m) has also been calculated. The sizes of the hydrated cations, that exist in an aqueous solution, are 0.43 nm for Zn^{2+} and 0.42 nm for Cd^{2+} [223], and the corresponding theoretical surface coverage values are 65.7 m^2/g for Zn^{2+} and 35.3 m^2/g for Cd^{2+}. Since adsorption of the cations occurs at the active sites alone and does not cover the whole surface uniformly, this theoretical

coverage appears reasonable with respect to the BET surface area of the adsorbent. Also the monolayer adsorption capacities for Cd^{2+} and Zn^{2+} metal ions are comparable with other agro based adsorbents [213, 224, 225-232].

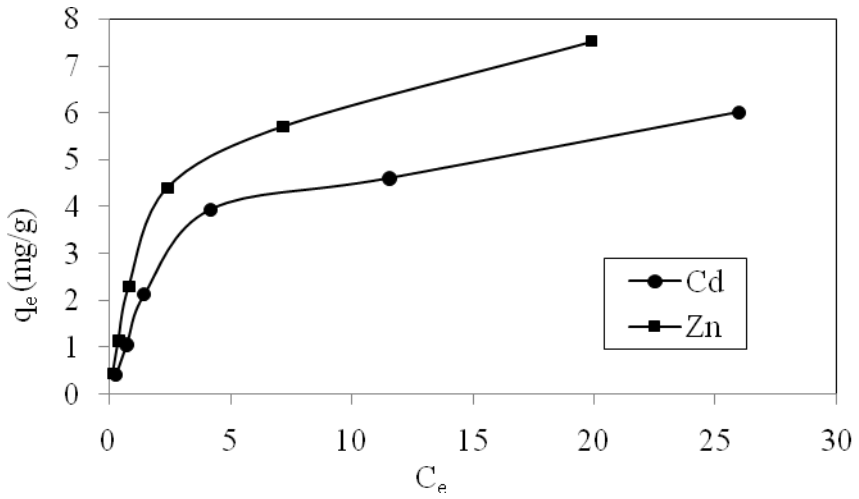

Fig. 4.60: Langmuir isotherm for the adsorption of Cd^{2+} and Zn^{2+} onto PSH (Particle size: 0.6 mm, PSH dosage: 0.4 g/100ml, pH: 6, Temperature: 24^{o}C)

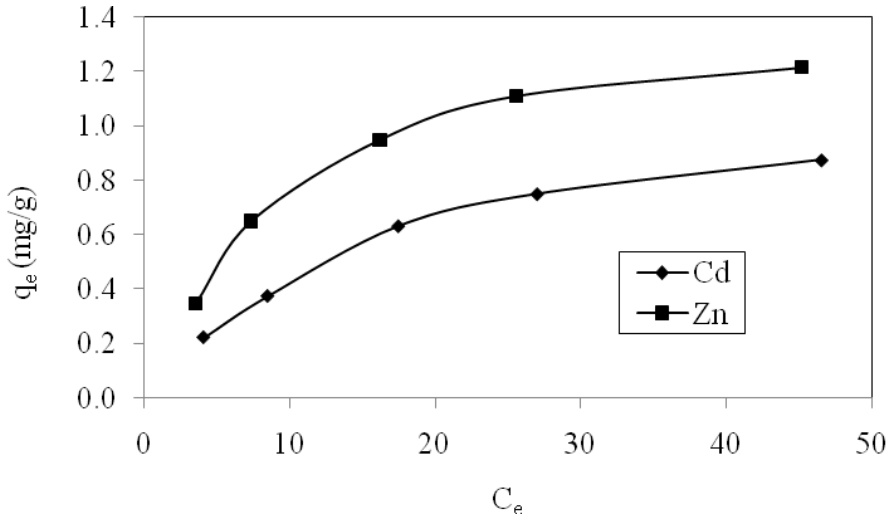

Fig. 4.61: Langmuir isotherm for the adsorption of Cd^{2+} and Zn^{2+} onto GAC (Particle size: 0.6 mm, GAC dosage: 0.4 g/100ml, pH: 6, Temperature: 24^{o}C)

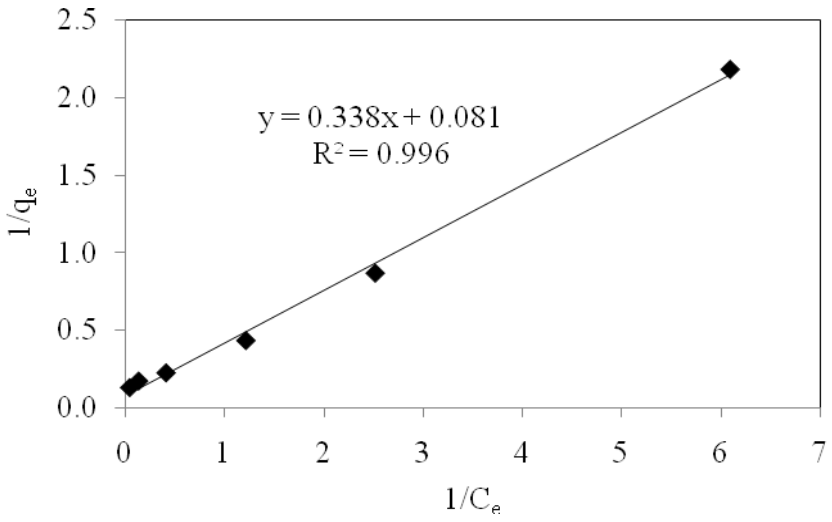

Fig. 4.62: Linear plot of Langmuir isotherm for the adsorption of Zn^{2+} onto PSH (Particle size: 0.6 mm, PSH dosage: 0.4 g/100ml, pH: 6, Temperature: 24^{o}C)

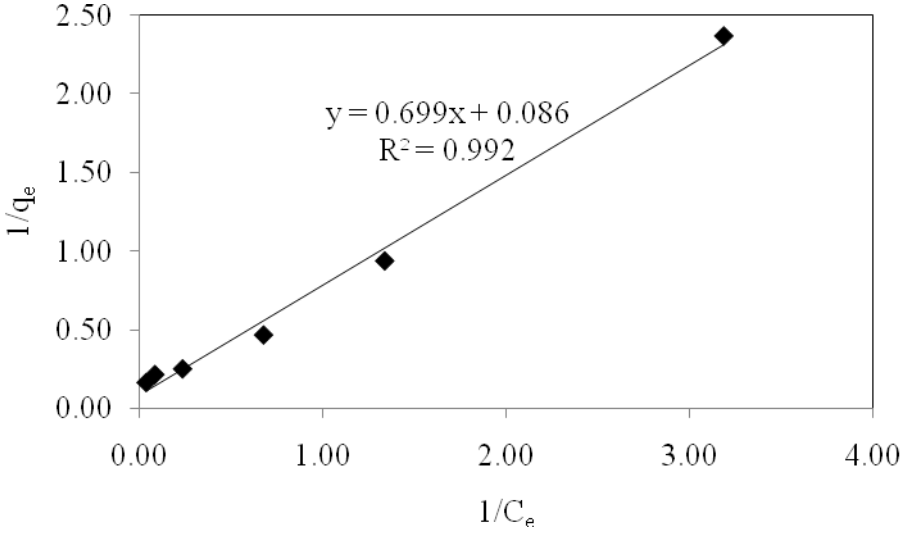

Fig.4.63: Linear plot of Langmuir isotherm for the adsorption of Cd^{2+} onto PSH (Particle size: 0.6 mm, PSH dosage: 0.4 g/100ml, pH: 6, Temperature: 24^{o}C)

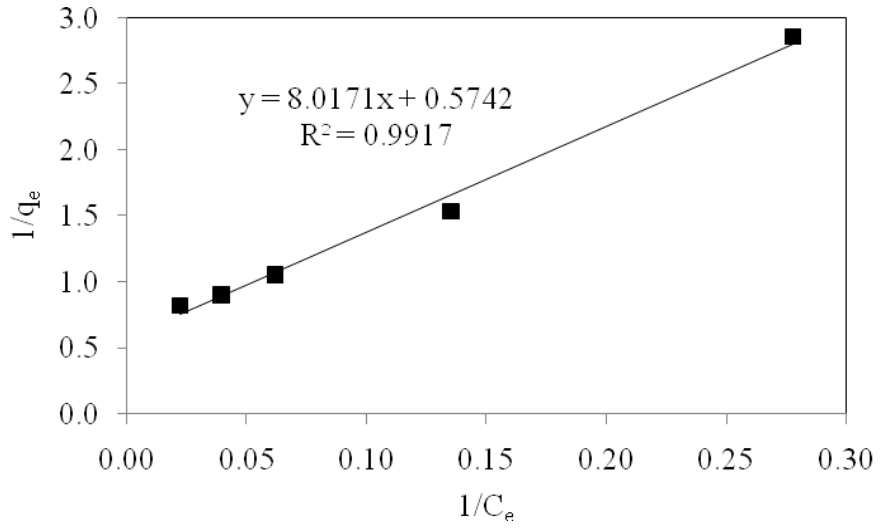

Fig. 4.64: Linear plot of Langmuir isotherm for the adsorption of Zn^{2+} onto GAC (Particle size: 0.6 mm, GAC dosage: 0.4 g/100ml, pH: 6, Temperature: 24^{o}C)

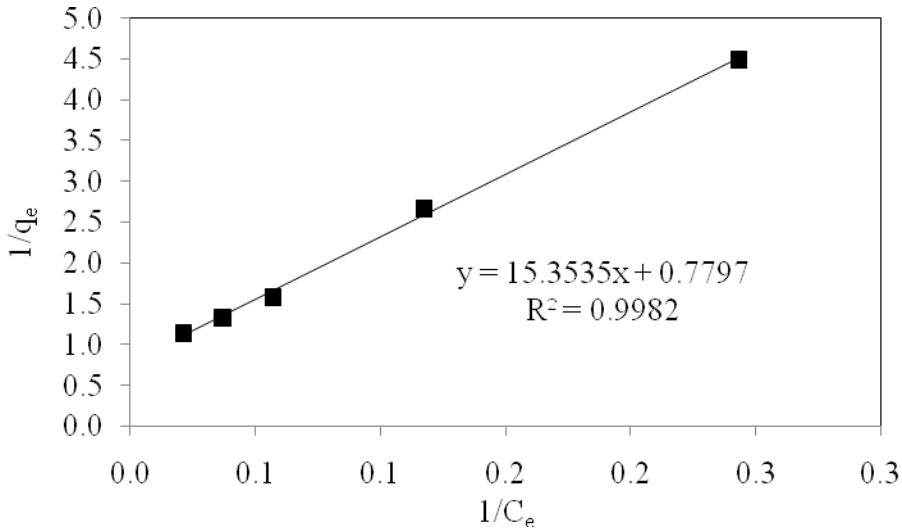

Fig. 4.65: Linear plot of Langmuir isotherm for the adsorption of Cd^{2+} onto GAC (Particle size: 0.6 mm, GAC dosage: 0.4 g/100ml, pH: 6, Temperature: 24^{o}C)

The essential characteristics of the Langmuir isotherm can be expressed in terms of a dimensionless constant known as separation factor R_L that is given by Eq. 3.10. From this equation, C_0 is the initial concentration of adsorbate (mg/L), and K_L (L/mg) is the Langmuir constant. The value of R_L determines whether the adsorption process is favorable or not [192]. The R_L values for the adsorption of Cd^{2+} onto PSH are in the range of 0.1412–0.8043, while for Zn^{2+} onto PSH, the values are in the range of 0.07498–0.6696. The R_L values obtained are found to decrease with the increase in the initial metal ions concentration. This indicated that the adsorption of Cd^{2+} and Zn^{2+} on PSH surface is a favorable process and at high initial metal ions concentration, the adsorption is almost irreversible. The similar pattern are found for GAC, with the R_L values for Zn^{2+} in the range of 0.2183 – 0.7363 and for Cd^{2+} in the range of 0.2826-0.7975. The R_L value for PSH and GAC has been tabulated in Table 4.17 and the plots have been shown in Figs. 4.66 and 4.67.

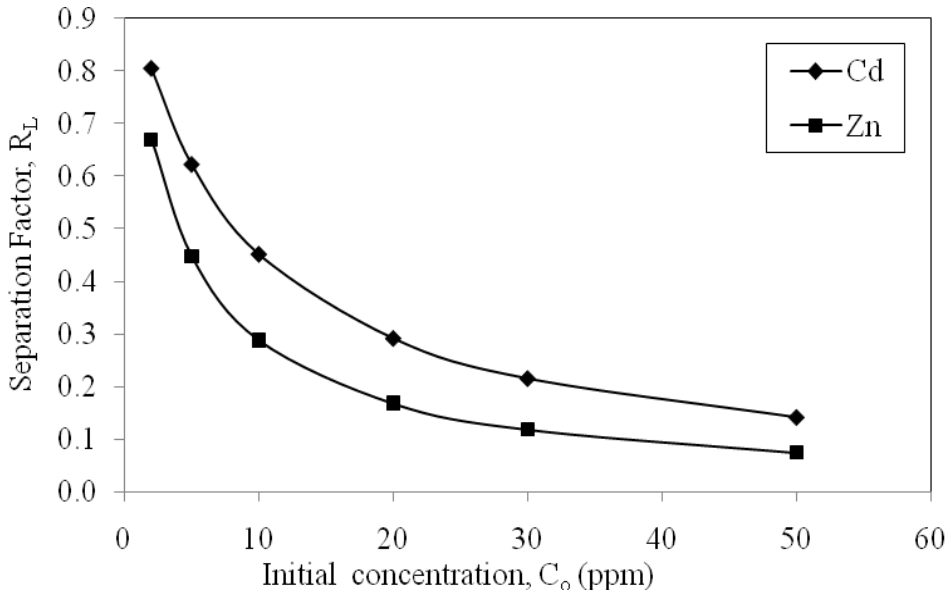

Fig. 4.66: Separation Factor from Langmuir isotherm for Cd^{2+} and Zn^{2+} adsorption onto PSH

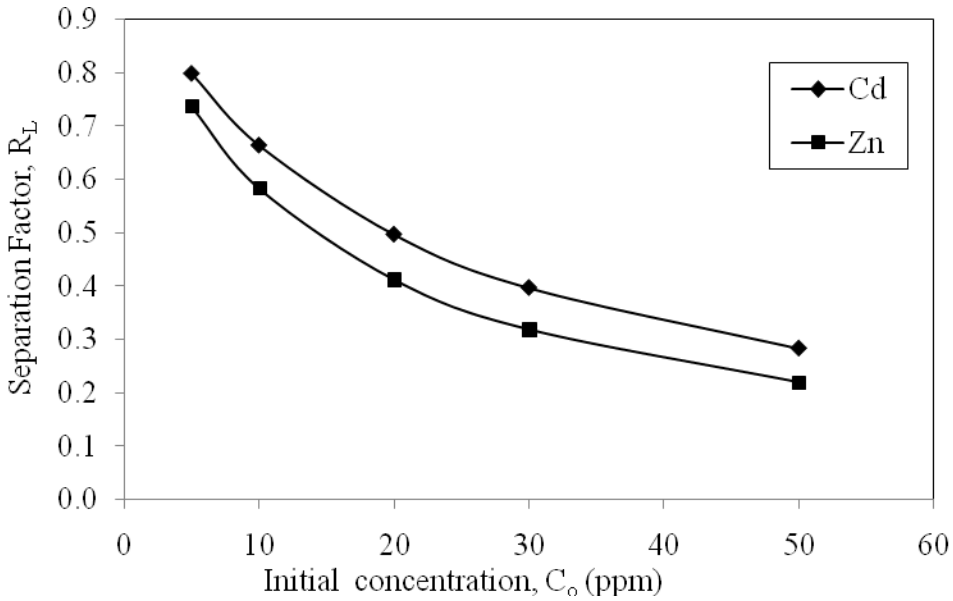

Fig. 4.67: Separation Factor from Langmuir isotherm for Cd^{2+} and Zn^{2+} adsorption onto GAC

Langmuir adsorption capacity for both the metal ions was determined for different pH, particle size of the adsorbents and temperature (Table 4.18). From the table it can be seen that with the change in pH from 3 to 6 the adsorption of Cd^{2+} increased from 2.1805 to 11.9048 mg/g and the adsorption of Zn^{2+} on PSH surface increased from 5.9737 to 15.128 mg/g at 24^{o}C with 0.6 mm particle size of PSH. The variation of q_m with pH are shown in Fig. 5.33 and 5.34. The nature of variation was almost similar for both Cd^{2+} and Zn^{2+}. This can again be explained by the occurrence of an increasing number of negatively charged sites with the increase in pH. However, the adsorption of both Cd^{2+} and Zn^{2+} decreased with the increase in the particle size of PSH. The Langmuir adsorption capacity (q_m) has been plotted against the particle size ratio or relative particle size in Figs. 5.35 and 5.36, which shows a sharp fall on q_m with the increase in size of the adsorbent particles. It can be related to the decrease in the accessibility of the adsorption sites as the particle size increases.

The Langmuir adsorption capacity also has been found to increase with the increases in temperature from 24-60^{o}C (Table 4.18, Figs. 5.37-5.38). However, in order to have a quantitative estimate of the temperature effect and the relevant thermodynamic parameters we have calculated the adsorption equilibrium constant (K_a) at four different temperatures keeping the other parameters unchanged. The equilibrium constant has been calculated using Eq. 3.14. The equilibrium constant is related to the change in free energy and entropy as well as the estimated heat of adsorption applying Van't Hoff Equation (Eq. 3.15). It is reasonable to assume that the thermodynamic quantities remained constant over the range of temperature under consideration. A plot of *ln Ka* against *1/T* is expected to yield a straight line that allows calculation of ΔH and ΔS from the slope and the intercept of such a plot. Figs. 4.68 and 4.69 presented the plots of the adsorption equilibrium constants for both Cd^{2+} and Zn^{2+}. The experimental values of K_a and the calculated values of the thermodynamic quantities have been presented in Table 4.19. The adsorption processes for both the cations were exothermic as evident from the negative values of the heat of adsorption. This is due to the energy released from making new bond between the hydrogen from solvent and the cations from solute exceed the energy required to break the bond. The positive entropy change is an indicative of the orderly arrangement of the species upon adsorption on the surface. The heat of adsorption values and the applicability of the Langmuir model indicate chemisorptions of the metal ions at the active sites.

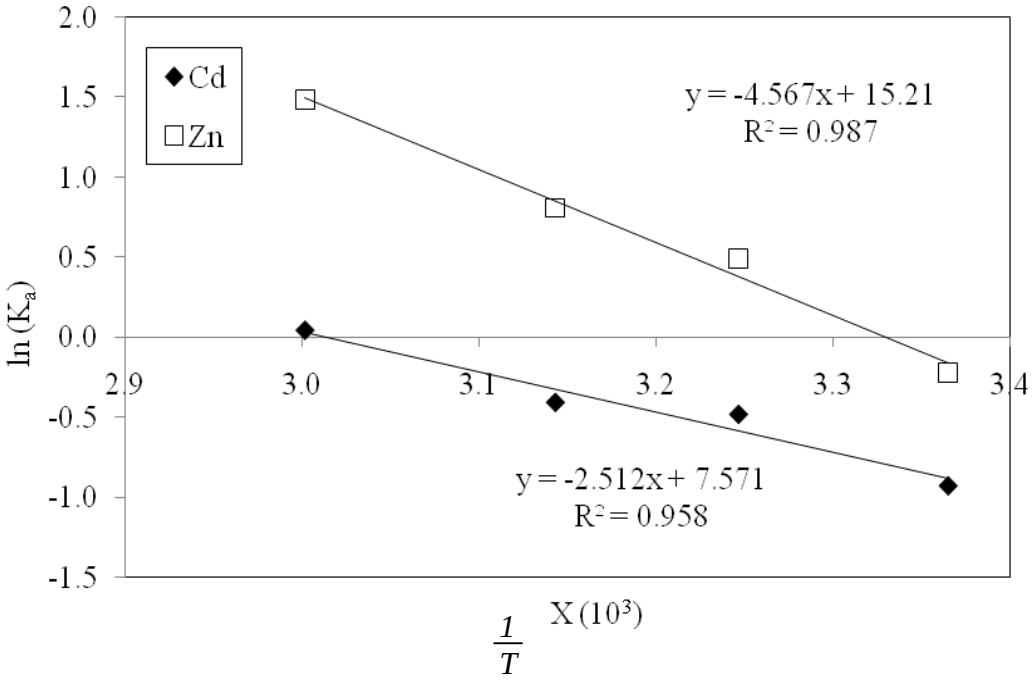

Fig. 4.68: Equilibrium constant plots of Cd^{2+} and Zn^{2+} ions adsorption onto PSH

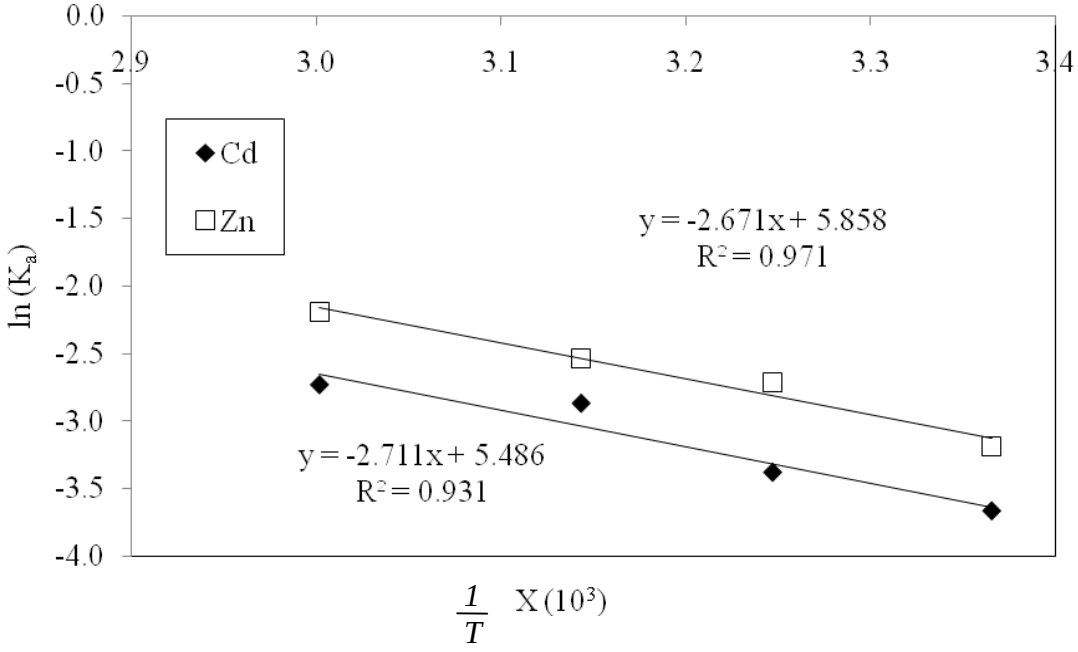

Fig. 4.69: Equilibrium constant plots of Cd^{2+} and Zn^{2+} ions adsorption onto GAC

Many works have been done on the application of the Langmuir adsorption isotherm to explain the adsorption of dyes from aqueous solutions [5, 10, 22, 26, 48, 170, 233]. The equilibrium data for the adsorption of MG dye onto PSH and GAC were fitted better to Langmuir isotherm. The different parameters together with the R^2 value have been listed in Table 4.17 (Refer Eq. 3.9). The dimensionless constant R_L value for the adsorption of MG onto PSH is 0.1747 and GAC is 1.2591. Fig. 4.71 showed that the R_L values obtained decreased with the increase of initial dye concentration. This indicated that the adsorption is a favorable process and at high initial MG concentrations, the adsorption is almost irreversible or more favorable.

The better fitting of the experimental data to Langmuir isotherm compared to Freundlich was also evident from the R^2 value of the plots (Fig. 4.70). The R^2 value was higher in the case of Langmuir (0.9995) as compared to Freundlich (0.9917) for PSH. For GAC also Langmuir (0.9679) value was higher compared to Freundlich (0.9173). It indicates that the adsorption process of MG on PSH and GAC basically followed monolayer adsorption on a homogenous surface. From Table 4.17 it was evident that the computed maximum monolayer adsorption capacity (q_m) of PSH for MG was relatively higher, as it was 21.7865mg/g as compared for GAC 10.3413mg/g. Also from this table presents the fitted Langmuir isotherm parameters for Cd-Aerosol and Zn-Aerosol systems. The R_L value for the adsorption of Zn^{2+} and Cd^{2+} onto PSH with the addition of 1ppm Aerosol 22 surfactant is 0.56403-0.89372 for Zn^{2+} and 0.39001-0.80605 for Cd^{2+}. The R_L values between 0 and 1 indicated that the adsorption has been a favourable process here.

Table 4.20 shows the results of thermodynamic calculation for the adsorption of MG dye onto PSH. The adsorption reaction is exothermic in nature with heat of adsorption value of -16.94 J/mol. Therefore energy of the process indicated that the adsorption is thermodynamically favourable.

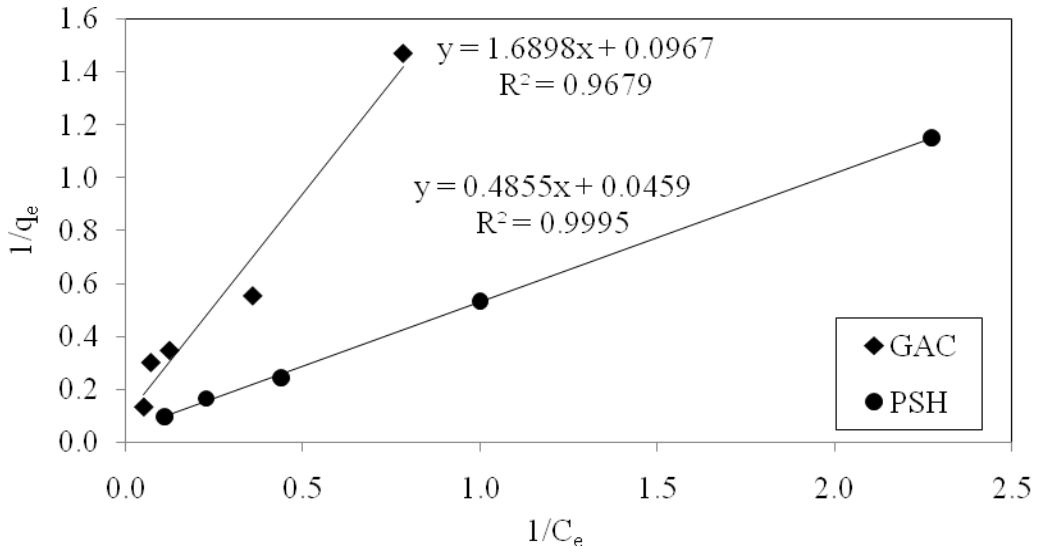

Fig. 4.70: Langmuir plots for MG adsorption on PSH and GAC (pH: 6, Dosage: 4g/L, Temperature: 24^0C, Agitation speed: 160rpm, Adsorbent size: 0.6mm, Dye conc. 30ppm, Time contact: 6 hours)

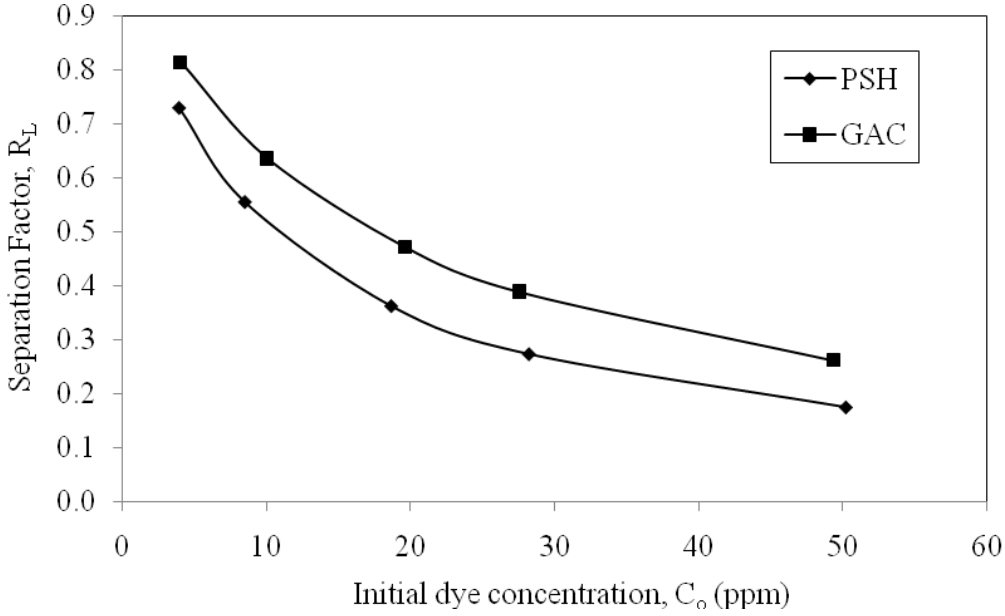

Fig.4.71: Variation of separation Factor (from Langmuir isotherm) with initial dye concentration for MG adsorption onto PSH and GAC

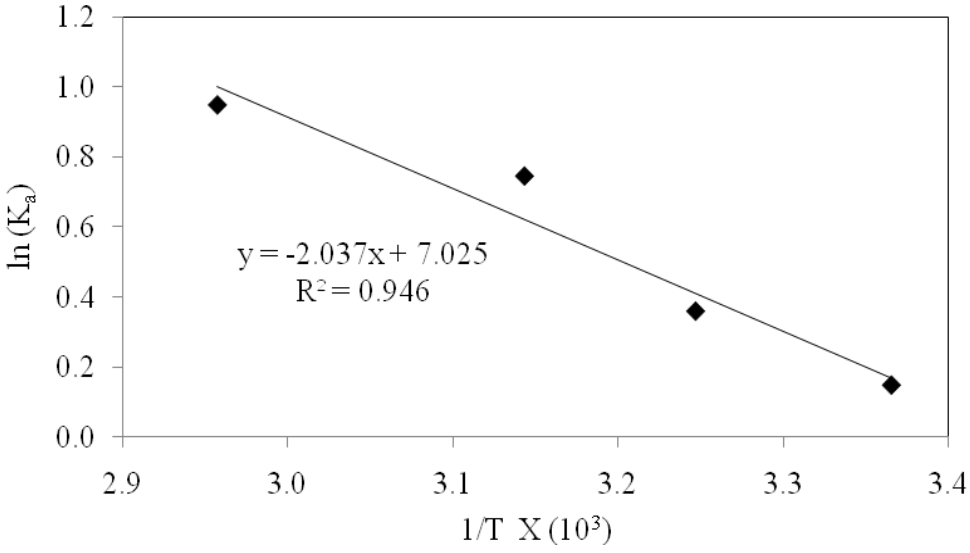

Fig. 4.72: Equilibrium constant plots of MG dye adsorption onto PSH

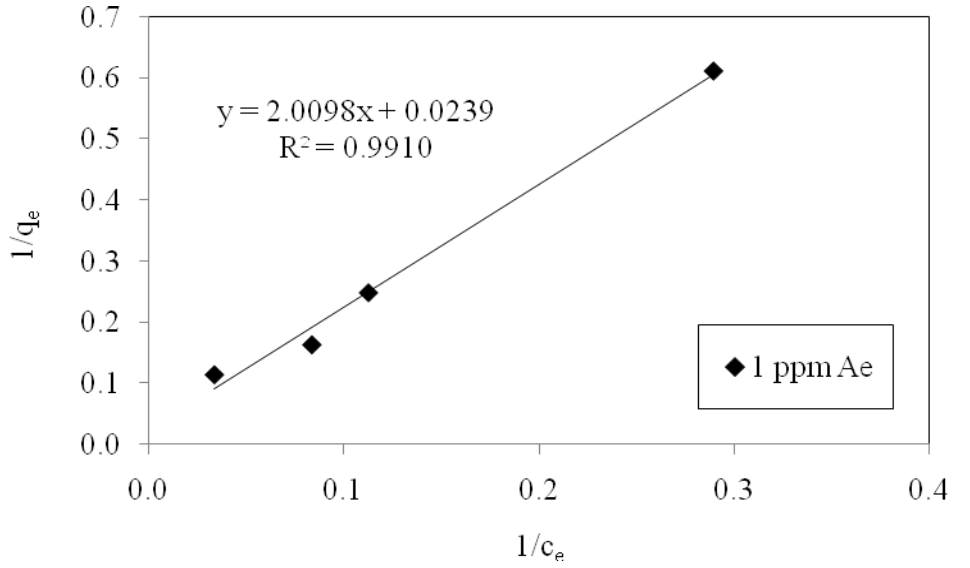

Fig. 4.73: Langmuir isotherm plots for the effect of Aerosol 22 on the adsorption of Zn^{2+} using PSH (Metal ion conc.: 10-65ppm, pH: 6, Dosage: 4g/L, Temperature: 24^{o}C, Agitation speed: 160rpm, Adsorbent size: 0.6mm)

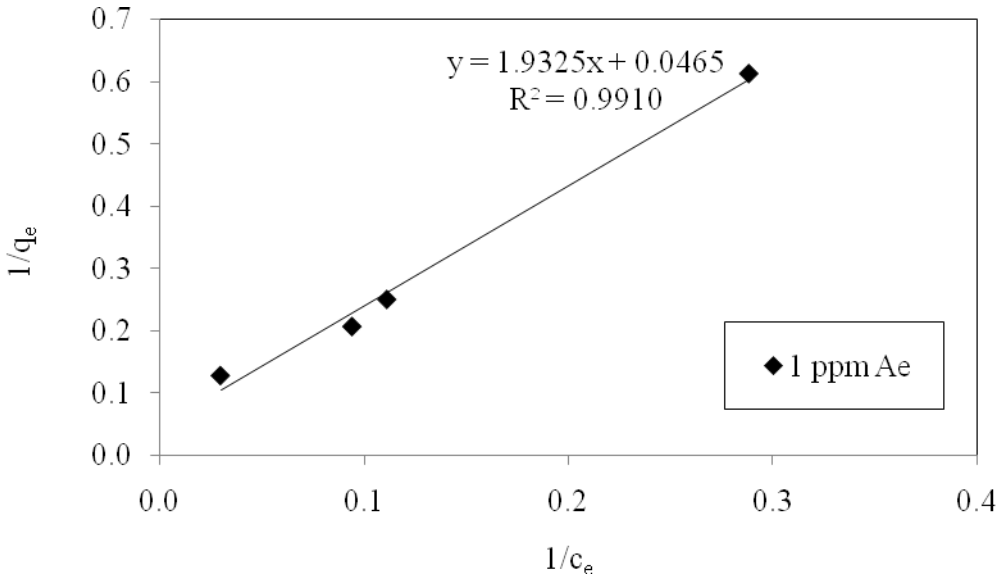

Fig. 4.74: Langmuir isotherm plots for the effect of Aerosol 22 on the adsorption of Cd^{2+} using PSH (Metal ion conc.: 10-65ppm, Surfactant conc.: 1ppm; pH: 6, Dosage: 4g/L, temp.: 24^{o}C, Agitation speed: 160rpm, Adsorbent size: 0.6mm)

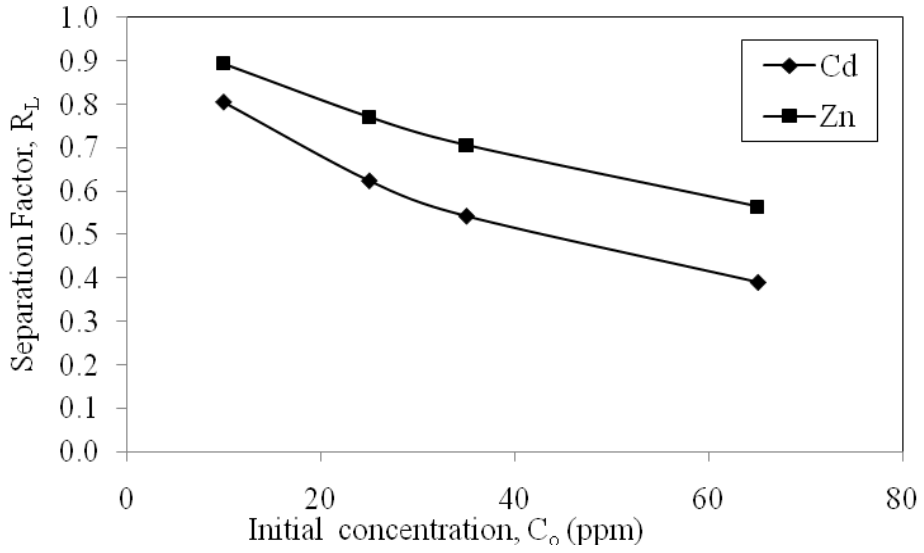

Fig.4.75: Separation Factor from Langmuir isotherm for the effect of metal ions adsorption onto PSH

Table 4.17

Langmuir Isotherm parameters for the adsorption of metal ions (Cd^{2+} and Zn^{2+}) and MG dye onto PSH, and the effect of anionic surfactant on metal ions removal

Adsorbent	Adsorbate	Langmuir parameter			
		q_m	k_L	R_L	R^2
PSH	Cd^{2+}	11.8906	0.1217	0.1412-0.8043	0.9919
	Zn^{2+}	12.2850	0.2467	0.0750-0.6696	0.9958
GAC	Cd^{2+}	1.2825	0.0508	0.2826-0.7975	0.9982
	Zn^{2+}	1.7416	0.0716	0.2183-0.7363	0.9917
PSH	MG	21.7865	0.0945	0.1747-0.6791	0.9995
GAC		10.3413	0.0572	0.2591-0.7776	0.9679
PSH	Cd^{2+}+Aer22	21.5054	0.0241	0.39001-0.80605	0.9910
	Zn^{2+}+Aer22	41.8410	0.0119	0.56403-0.89372	0.9910

Table 4.18

Langmuir isotherm parameters for the adsorption of Cd^{2+} and Zn^{2+} metal ions onto PSH at various conditions

Parameters	Cd^{2+}			Zn^{2+}		
	q_m (mg/g)	k_L (L/g)	R^2	q_m (mg/g)	k_L (L/g)	R^2
Initial Solution pH						
3	2.1805	0.4027	0.9824	5.9737	0.1778	0.9808
4	6.3052	0.1388	0.9931	9.2166	0.1465	0.9953
5	7.8247	0.1367	0.9970	9.3809	0.1566	0.9944
6	11.9048	0.1215	0.9919	15.1286	0.1876	0.9914
Particle Size						
0.15 mm	13.0548	0.1378	0.9969	16.1031	0.2526	0.9987
0.30 mm	12.7714	0.1213	0.9939	15.5280	0.2246	0.9962
0.60 mm	11.9190	0.1213	0.9919	15.1286	0.1876	0.9914
1.18 mm	3.9246	0.2907	0.9969	4.9579	0.4957	0.9957
Temperature						
24^{o}C	11.9048	0.1215	0.9919	15.1057	0.1880	0.9914
35^{o}C	12.1507	0.1393	0.9951	15.2905	0.2650	0.9975
45^{o}C	15.7233	0.1229	0.9933	16.3399	0.3068	0.9942
60^{o}C	24.6305	0.0963	0.9918	27.4725	0.2031	0.9899

*(Constant parameters: C_o: 5, 10, 20, 30 and 50 ppm, Particle size: 0.6 mm, PSH dosage: 0.4 g/100ml, pH: 6, Temperature: 24^{o}C)

Table 4.19

Calculated thermodynamic parameters for metal ions adsorption on PSH and GAC

Adsorbent	Temperature	K_a		ΔG (kJ/mol)		ΔH (J/mol)		ΔS (J/mol)	
	(^{0}C)	Cd^{2+}	Zn^{2+}	Cd^{2+}	Zn^{2+}	Cd^{2+}	Zn^{2+}	Cd^{2+}	Zn^{2+}
PSH	24	0.3960	0.8030						
	35	0.6180	1.6400	-	-	-	-	62.95	126.46
	45	0.6658	2.2500	18.73	37.61	20.88	37.97		
	60	1.0430	4.4400						
GAC	24	0.0256	0.0409						
	35	0.0340	0.0662	-	-	-	-	45.61	48.70
	45	0.0566	0.0789	13.58	14.50	22.54	22.21		
	60	0.0649	0.1120						

Table 4.20

Calculated thermodynamic parameters for MG dye adsorption on PSH

Temperature (^{o}C)	K_a	ΔG (kJ/mol)	ΔH (J/mol)	ΔS (J/mol)
24	1.1600	-17.37	-16.94	58.41
35	1.4326			
45	2.1062			
60	2.5794			

4.2.3.3 Dubinin-Radushkevich isotherm for the adsorption of C^{d2+} and Z^{n2+} metal ions and Dye onto PSH and GAC, and the effect of anionic surfactant onto PSH

The Dubinin–Radushkevich isotherm can be used to describe the adsorption on both homogenous and heterogeneous surfaces [54-55, 193]. The linear form of Dubinin–Radushkevich equation is given by Eqs. 3.11 and 3.12. In these equations, X_m is the Dubinin–Radushkevich monolayer capacity (mg/g), β is a constant related to sorption energy, and ε is the Polanyi potential which is related to the equilibrium concentration. The constant β gives the mean free energy (E) of adsorption per molecule of the adsorbate when it is transferred to the surface of the solid from the

solution and can be computed from Eq. 3.13. The magnitude of *E* is useful to understand whether the adsorption process is chemical ion exchange or physical in nature. For adsorption of both Cd^{2+} and Zn^{2+} onto PSH and GAC, the values of *E* were more than 16kJ/mol (Tables 4.21) implying that the adsorption process was dominated by particle diffusion [234].

For adsorption of MG on both PSH and GAC the values of *E* were 25 and 36 kJ/mol which is more than 16kJ/mol (Table 4.21) indicating that the adsorption process were dominated by particle diffusion [234]. The linear plots of D-R isotherm can be found from Fig. 4.80.

The Dubinin–Radushkevich isotherm also has been utilized in this study of the effect of anionic surfactant. Table 4.21, Figs. 4.81-4.82 show D-R isotherm plots for the effect of Aerosol 22 on the adsorption of Zn^{2+} and Cd^{2+} using PSH. In this study, the *E* value was more than 16kJ/mol indicating that the adsorption process was dominated by particle diffusion [234].

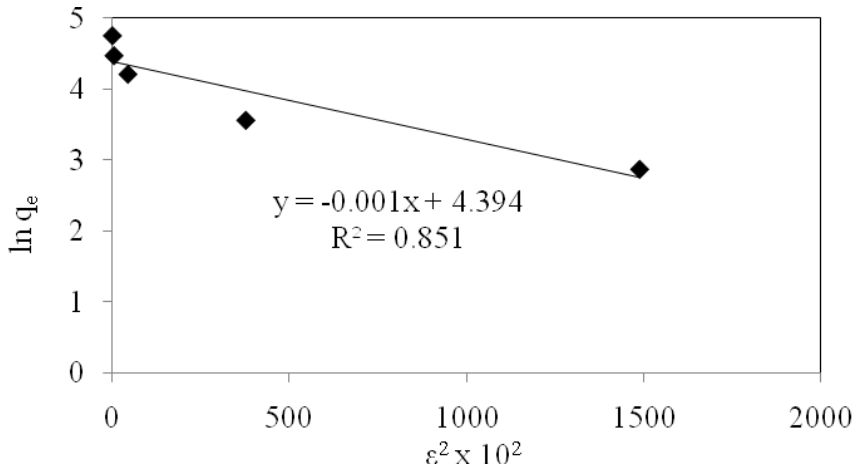

Fig. 4.76: D-R isotherm plot for the adsorption of Zn^{2+} onto PSH (Adsorbent size: 0.6 mm, PSH dosage: 0.4 g/100ml, pH: 6, Temperature: 24^{o}C)

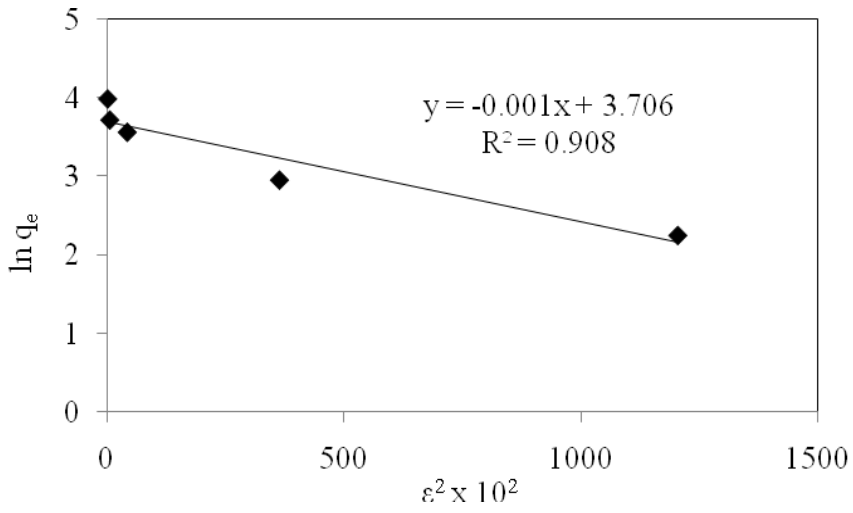

Fig. 4.77: D-R isotherm plot for the adsorption of Cd^{2+} onto PSH (Adsorbent size: 0.6 mm, PSH dosage: 0.4 g/100ml, pH: 6, Temperature: 24^{o}C)

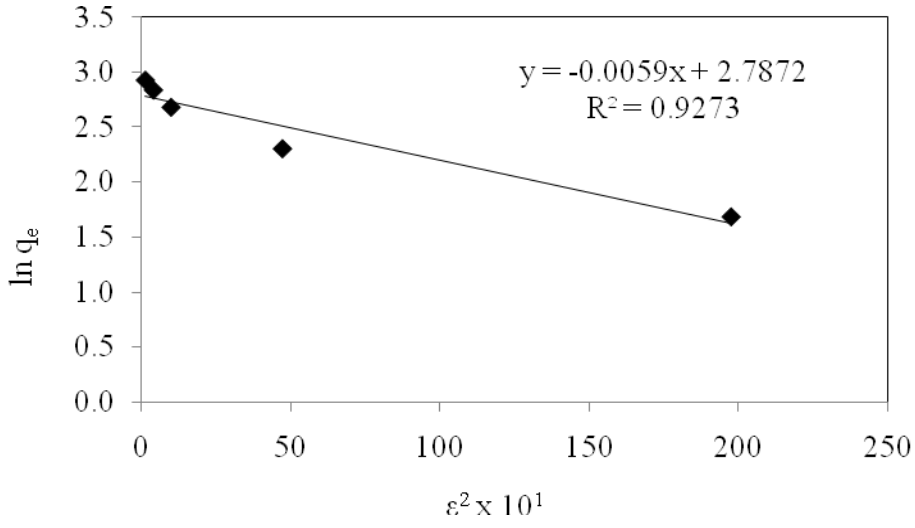

Fig. 4.78: D-R isotherm plot for the adsorption of Zn^{2+} onto GAC (Size: 0.6 mm, GAC dosage: 0.4 g/100ml, pH: 6, Temperature: 24^{o}C)

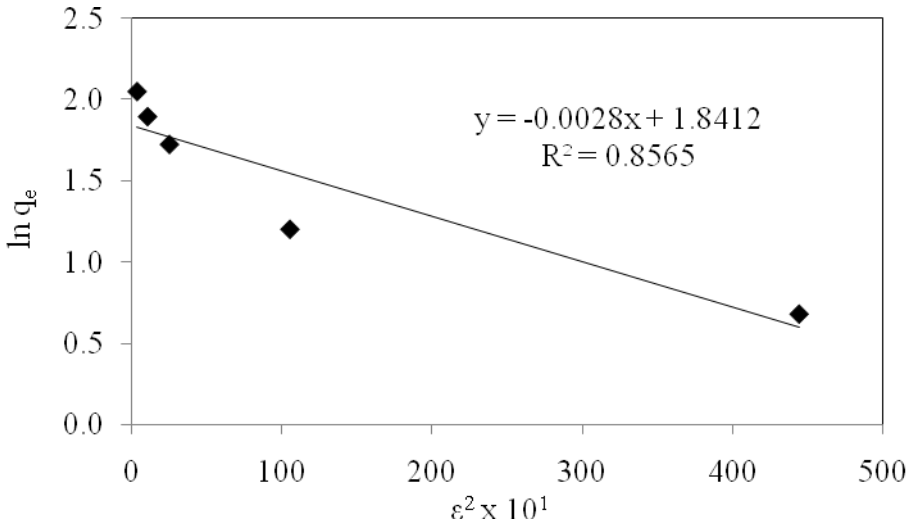

Fig. 4.79: D-R isotherm plot for the adsorption of Cd^{2+} onto GAC (Size: 0.6 mm, GAC dosage: 0.4 g/100ml, pH: 6, Temperature: 24^{o}C)

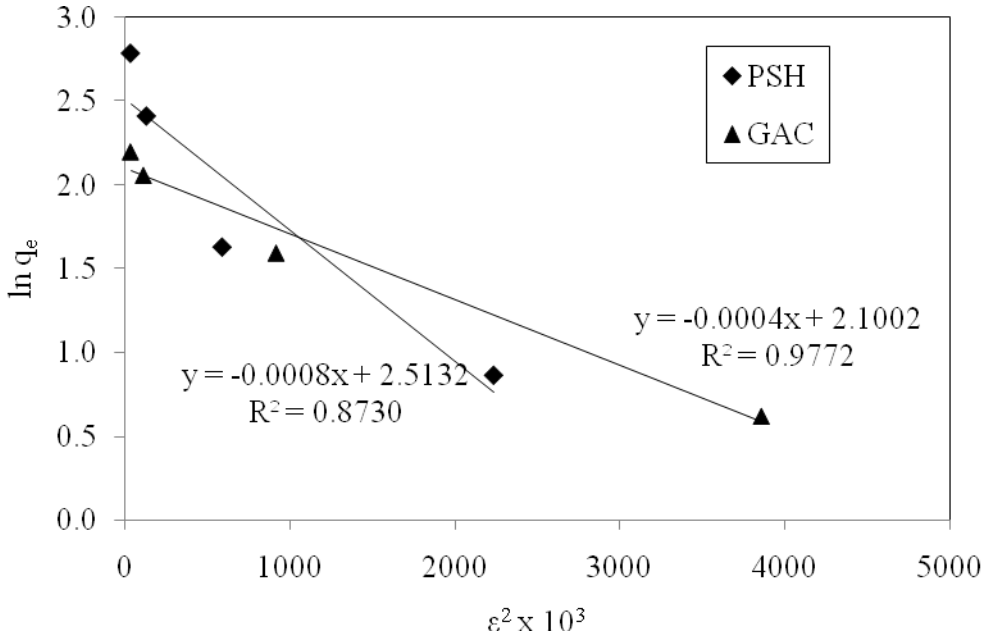

Fig. 4.80: Dubinin–Radushkevich isotherm plots for MG adsorption on PSH and GAC (Initial solution pH: 6, Amount of adsorbent: 4g/L, Temperature: 24^{0}C and Shaker speed: 160rpm, Particle size: 0.6mm)

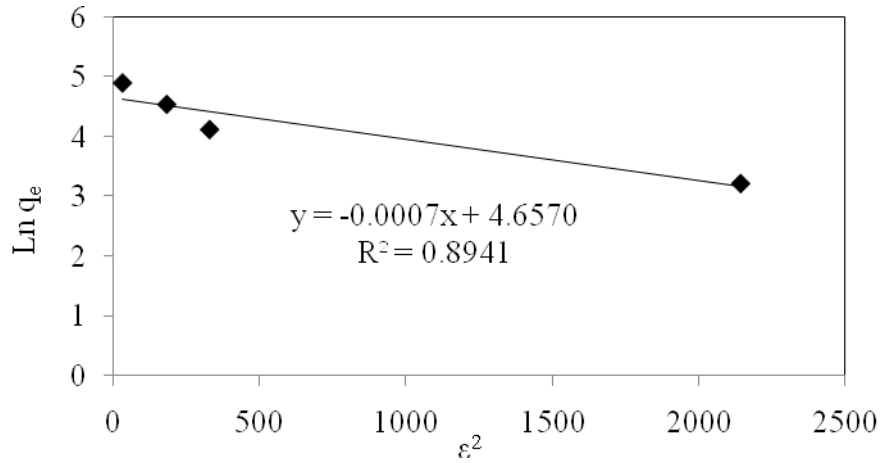

Fig.4.81: D-R isotherm plots for the effect of Aerosol 22 on the adsorption of Zn^{2+} using PSH (Metal ion conc.: 10-65ppm, Surfactant conc.: 1ppm; pH: 6, Dosage: 4g/L, Temperature: 24^{o}C and Speed: 160rpm, Adsorbent size: 0.6mm)

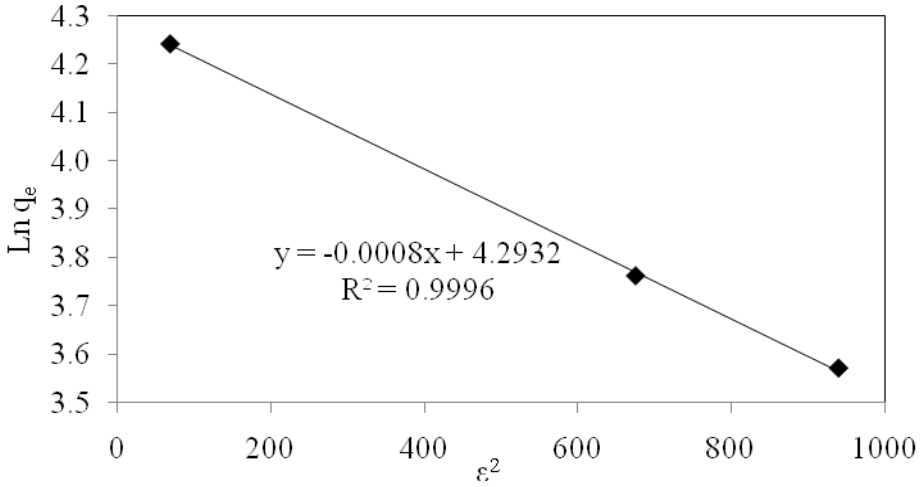

Fig. 4.82: D-R isotherm plots for the effect of Aerosol 22 on the adsorption of Cd^{2+} using PSH (Metal ion conc.: 10-65ppm, Surfactant conc.: 1ppm; pH: 6, Dosage: 4g/L, Temperature: 24^{o}C and Speed: 160rpm, Adsorbent size: 0.6mm)

Table 4.21

D-R Isotherm parameters for the adsorption of metal ions (Cd^{2+} and Zn^{2+}) and MG dye on PSH and GAC, and the effect of anionic surfactant on metal ions removal

Adsorbent	Adsorbate	Dubinin-Radushkevich			
		X_m (ų mol/g)	β (mol^2/kJ^2)	E (kJ/mol)	R^2
PSH	Cd^{2+}	0.0246	0.0013	19.6116	0.9089
	Zn^{2+}	0.0124	0.0011	21.3201	0.8510
GAC	Cd^{2+}	0.1586	0.0028	13.3631	0.8565
	Zn^{2+}	0.0616	0.0059	9.2057	0.9273
PSH	MG	0.0810	0.0078	25.00 0	0.8730
GAC		0.1224	0.0039	35.8060	0.9772
PSH	Cd^{2+}+Aer22	0.0137	0.0008	25.0000	0.9996
	Zn^{2+}+Aer22	0.0095	0.0007	26.7261	0.8941

4.3 Comparison of adsorption capacity (q_m) for metal ions (Cd^{2+} and Zn^{2+}) and MG dye with different adsorbents

The adsorption capacity of PSH towards Cd^{2+} and Zn^{2+} has been compared with other adsorbents as reported in the literature (Tables 4.22 and 4.23). For Zn^{2+} on PSH the comparison has been made with bagasse fly ash [211], rice husk ash [213], chitin [224], peanut hull [225], coffee husk [226], cocoa shell [227], Turkish fly ashes [232] and coir [235]. For Cd^{2+} using PSH the comparison has been made with rice husk ash [213], bagasse fly ash [211], peanut hull [225], coffee husk [226], olive cake [228], chitin [229], juniper bark, juniper wood [230], hazelnut shell and almond shell [231]. The values reported in the form of monolayer adsorption capacity were comparable to the values obtained by other workers under similar conditions.

Table 4.22

Comparison of adsorption capacities of various adsorbents for removal of Zn^{2+}

No.	Adsorbents	pH	Temp. (^oC)	Monolayer adsorption capacity (mg/g)	Ref.
1	Bagasse fly ash	6.0	30	7.03	[211]
2	Rice husk ash	6.0	30	5.88	[213]
3	Turkish fly ashes - Afsin-Elbistan	6.0	22	1.19	[222]
4	Chitin	free	25	5.79	[225]
5	Peanut hull	6.7	25	9.00	[225]
6	Coffee husks	4.0	25	5.60	[226]
7	Cocoa shell	2.0	22	2.90	[227]
8	Turkish fly ashes - Seyitomer	6.0	22	0.36	[232]
9	Coir	5.6	25	8.60	[235]
10	Physic seed hull	6.0	24	12.29	Present work

Table 4.23

Comparison of adsorption capacities of various adsorbents for removal of Cd^{2+}

No	Adsorbents	pH	Temp. (^oC)	Monolayer adsorption capacity (mg/g)	Ref.
1	Bagasse fly ash	6.0	30	6.19	[211]
2	Rice husk ash	6.0	30	3.04	[213]
3	Peanut hull	6.7	25	6.00	[225]
4	Coffee husks	4.0	25	6.90	[226]
5	Olive cake	4.5	35	10.6	[228]
6	Chitin	free	25	14.9	[229]
7	Juniper bark	5.3	25	8.577	[230]
8	Juniper wood	4.8	25	3.181	[230]
9	Hazelnut shell	5.0	25	5.42	[231]
10	Almond shell	5.2	25	3.18	[231]
11	Physic seed hull	6.0	24	11.89	Present work

The adsorption capacity of PSH towards MG dye also has been compared with other adsorbents as reported in the literature (Tables 4.24). The comparison has been made with rattan sawdust [183], granular activated carbon from GSE Company [184], laboratory grade granular activated carbon (GAC, lab grade) [184], neem sawdust [185], algae marine [202], arundo donax root [236], coffee [237] and maize cob [238]. The values reported in the form of monolayer adsorption capacity were comparable to the values obtained by other workers under similar conditions.

Table 4.24

Comparison of adsorption capacities of various adsorbents for removal of MG dye

No.	Adsorbents	pH	Temp. (^{o}C)	Monolayer adsorption capacity (mg/g)	Ref.
1	Algae marine (Caulerpa racemosa)	6.00	25	19.88	[202]
2	GAC (GSE)	7.00	30	8.27	[184]
3	GAC (lab grade)	7.00	30	42.18	[184]
4	Arundo donax root	5.00	30	8.69	[236]
5	Rattan sawdust	4.00	30	62.71	[183]
6	Neem Sawdust	7.00	30	4.35	[205]
7	Coffee	4.00	25	55.30	[237]
8	Maize cob	8.00	27	80.64	[238]
9	PSH	6.00	25	21.79	Present work

CHAPTER 5

CONCLUSIONS AND RECOMMENDATIONS

PSH, an agro waste generated from plant-based oil industry, can be used as a potential low-cost adsorbent for the removal of metal ions (Cd^{2+} and Zn^{2+}) and Malachite green dye from the industrial effluents. The adsorbent PSH does not require any expensive pretreatment. A detailed analysis of the nature of the surface of PSH revealed that surface parameter like functional groups, charge, area and the availability of pores made the material suitable as adsorbent. The commercial granular activated cabon has been used for a comparison study with PSH adsorbent and the results shows that PSH had better potential as an alternative adsorbent due to its capacity.

It has been found that the amount of adsorption for both the metal ions and dye increased with initial metal ion concentration, temperature of adsorption, amount of adsorbent, contact time, pH and smaller particle sizes of the adsorbent respectively. The study also indicated that the adsorption efficiency of PSH is improved in the presence of a small amount of anionic surfactant (Aerosol 22) for the treatment of metal ions-bearing aqueous wastewater. With higher concentrations of the surfactants, the formations of highly ordered aggregates or micelles solubilise the metal ion molecules and prevent their sorption. However, the small amount of surfactant will result on the formation of relatively small and poorly ordered premicellar aggregates that may be sorbed on the sorbent surface and enhanced the Cd^{2+} and Zn^{2+} adsorption. The rate of sorption of metal ions and dye as well as with the addition of surfactant were rapid for the initial 2–10 minutes to take up the major part of the adsorbate from the solution and the adsorption reached equilibrium after 3 hours.

Kinetic experiments indicate that the adsorption of metal ions and dyes on PSH and GAC followed a three-step process comprising of an initial rapid adsorption stage, an intermediate slower and steady adsorption stage and finally almost no adsorption stage. It has also been confirmed by intra-particle diffusion model.

By assuming that both adsorption isotherms take place, D-R isotherm model was utilized. The *E* values for adsorption of metal ions and MG dye on PSH are more than 16kJ/mol, indicating that the adsorption process is dominated by particle diffusion. The experimental results showed that Cd^{2+} and Zn^{2+} ions and MG dye adsorption mechanism followed monolayer chemisorption by fitting well with pseudo-second-order kinetics model and Langmuir isotherm model. Particle size of the adsorbent, solution pH and temperature had significant influence on the adsorption of both the ions by PSH. The monolayer adsorption capacity (q_m) of PSH was comparable with other reported agricultural-based adsorbents. The results showed remarkable capacity of PSH for metal ions and MG adsorption compared to GAC. The data is valuable for designing and fabricating an economical treatment process using batched or stirred-tank flow reactors for the removal of metal ions and MG dye from dilute industrial effluents.

As a recommendation, several criteria have been identified for further research on the utilization of PSH as adsorbent. Instead of using the untreated PSH adsorbent, the activated carbon derived from PSH also could be tested in order to determine the removal efficiency. The adsorption behaviour with other type of metal ions and dyes can be tested as well as multi-component heavy metal ions and dyes. This is because many industrial waste water matrices contain several heavy metal ions and dyes. In order to ensure the system is applicable for industrial use the experiment for column design should be done. Gas adsorption and the adsorption with other organic solution, *e.g.* phenol, benzene, naphthalene as adsorbate also can be tested to expand the uses of PSH adsorbent.

REFERENCES

[1] A. Fraile, S. Penche, F. Gonzalez, M. L. Blazquez, J. A. Munoz, and A. Ballester. (2005). Biosorption of copper, zinc, cadmium and nickel by *Chlorella vulgaris*. *Chem. Ecol*. 21,61

[2] M. Minceva, L. Markovska, and V Meshko. (2007). Removal of Zn^{2+}, Cd^{2+} and Pb^{2+} from binary aqueous solution by natural zeolite and granulated activated carbon. *Maced. J. Chemi. Chem. Engg*. 26 (2), 125

[3] T. K. Sen and M. V. Sarzali. (2008). Removal of cadmium metal ion (Cd^{2+}) from its aqueous solution by aluminium oxide (Al_2O_3): A kinetic and equilibrium study. *Chem. Engg. J*. 142, 256-262

[4] A. K. Bhattacharya, S. N. Mandal, and S. K. Das. (2006). Adsorption of Zn (II) from aqueous solution by using different adsorbents. *Chem. Engg. J*. 123, 43

[5] T. K. Naiya, P. Chowdhury, A. K. Bhattacharya, and S. K. Das. (2008). Saw dust and neem bark as low-cost natural biosorbent for adsorptive removal of Zn(II) and Cd(II) ions from aqueous solutions. *Chem. Engg. J*. 148, 68-79

[6] D. Mohan and K. P. Singh. (2002). Single and multi-component adsorption of cadmium and zinc using activated carbon derived from bagasse-an agricultural waste. *Water Res.* 36, 2304-2318

[7] S. Larous, A. H. Meniai and M. B. Lehocine. (2005). Experimental study of the removal of copper from aqueous solutions by adsorption using sawdust. *Desalination*, 185, 483

[8] C. Zhu, Z. Luan, Y. Wang, and X. Shau. (2007). Removal of cadmium from aqueous solution by adsorption on granular red mud 9GRM). *Sep. Purif. Technol*. 57, 167

[9] A. B. Perez-Marin, V. Meseguer Zapata, J.F. Ortuno, M. Aguilar, J. Saez, and M. Llorens. (2007). Removal of cadmium from aqueous solutions by adsorption onto orange waste. *J. Hazard. Mater*. B139, 122-131.

[10] P. Janoš and V. Šmídová. (2005). Effects of surfactants on the adsorptive removal of basic dyes from water using an organomineral sorbent—iron humate. *J. Colloid Interface Sci*. 291, pp.19-27.

[11] R. T. Daher. (1995). Trace metals. *Anal. Chem*., 67(12), 405

[12] K. Baek, B. K. Kim, and J. W. Yang. (2003). Application of micellar enhanced ultrafiltration for nutrient removal. *Desalination.* 156, 137-144

[13] K. Baek, B. K. Kim, H. J. Cho, and J. W. Yang. (2003). Removal characteristics of anionic metals by micellar-enhanced ultrafiltration, *J. Hazard. Mater*. 99, 303-311

[14] K. Baek, H. H. Lee, and J. W. Yang. (2003). Micellar-enhanced ultrafiltration for simultaneous removal of ferriccyanide and nitrate. *Desalination,* 158, 157-166

[15] K. Baek and J. W. Yang. (2004). Cross-flow micellar-enhanced ultrafiltration for removal of nitrate and chromate: competitive binding, *J. Hazard. Mater*. 108, 119-123

[16] K. Baek and J. W. Yang. (2004). Simultaneous removal of chlorinated aromatic hydrocarbons, nitrate, and chromate using micellar-enhanced ultrafiltration. *Chemosphere*, 57, 1091–1097

[17] M. J. O'Connell, S. M. Bachilo, C. B. Huffman, V. C. Moore, M. S. Strano, E. H. Haroz, K. L. Rialon, P. J. Poul, W. H. Noon, C. Kittrell, J. Ma, R. H. Hauge, B. R. Weisman, and R. E. Smalley. (2000). Band gap fluorescence from individual single-walled carbon nanotubes. *Science*. 297, 593-596

[18] V. K. Garg, R. Kumar, and R. Gupta (2004). Removal of malachite green dye from aqueous solution by adsorption using agroindustries waste: A case study of *Phosopis ceneraria*. *Dyes Pigm*. 62, 1-10

[19] M. N. V. Ravi Kumar, T. R. Sridhari, K. D. Bhavani, and P. K. Dutta. (1998). Trends in color removal from textile mill effluents. *Colorage* 40, 25–34

[20] S. J. Culp. "NTP technical report on the toxicity studies of malachite green chloride and leucomalachite green (CAS Nos. 569-64-2 and 129-73-7)

administered in feed to F344/N rats and B6C3F1 mice". National Center for Toxicological Research, Jefferson, AR 72079, USA: Toxic Rep Ser. (71): 1-F10. 2004

[21] S. J. Culp, F. A. Beland, R. H. Heflich, R. W. Benson, L. R. Blankenship, P. J. Webb, P. W. Mellick, R. W. Trotter, S. D. Shelton, K. J. Greenlees, and M. G. Manjanatha. (2002). Mutagenicity and carcinogenicity in relation to DNA adduct formation in rats fed leucomalachite green. *Mutation Research* 506-507, 55-63

[22] V. K. Garg, R. Gupta, A. B. Vadar, and R. Kumar. (2003). Dye removal from aqueous solution by adsorption on treated sawdust. *Bioresour. Technol*., 89, 121-124

[23] A. G. Liew Abdullah, M. A. Mohd Salleh, M. K. Siti Mazlina, M. J. Megat Mohd Noor, M. R. Osman, R. Wagiran, and S. Sobri. (2005). Azo dye removal by adsorption using waste biomass: sugarcane bagasse. *Int. J. Eng. Tech.* 2(1), 8-13

[24] G. McKay. (1981). Design models for adsorption systems in wastewater treatment. *J. Chem. Technol. and Biotechnol.* 81(31), 717-31.

[25] A. Jumasiah, T. G. Chuah, J. Gimbon, T. S. Y. Choong, and I. Azni. (2005). Adsorption of basic dye onto palm kernel shell activated carbon: sorption equilibrium and kinetics studies. *Desalination*, 186, 57- 64.

[26] A. K. Jain, V. K. Gupta, A. Bhatnagar, and Suhas. (2003). Utilization of industrial waste products as adsorbents for the removal of dyes. *J. Hazard. Mater.* B101, 31-42.

[27] Y. S. Ho, and G. McKay. (2003). Sorption of dyes and copper ions onto biosorbents. *Process Biochemistry*, 38, 1047–1061.

[28] G. McKay. (1996). *Use of adsorbents for the removal of pollutants from wastewaters*. Boca Ratan: CRC Press

[29] D. O. Cooney. (1998) *Adsorption Design for Wastewater Treatment*. Lewis Publishers, Boca Raton.

[30] A. Gurses, C. Dogar, M. Yalcin, M. Ac1ky1ldiz, R. Bayrak, and S. Karaca. (2005). The adsorption kinetics of the cationic dye, methylene blue, onto clay. *J. Hazard. Mater*. 131, 21-228.

[31] U. Kumar (2006). Agricultural products and by-products as low cost adsorbent for heavy metal removal from water and wastewater, a review. *Sci. Res. Essay.* 1(2), 33-37.

[32] S. Lagergren. (1898). About the theory of so-called adsorption of soluble substances. Kungliga Svenska Vetenskapsakademiens, *Handlingar*. 4(24), 1-39.

[33] I. Langmuir. (1918). The adsorption of gases on plane surfaces of glass, mica, and platinum. *J. Am. Chem. Soc*. 40, 1361-1403.

[34] A. W. Adamson (1967). *Physical Chemistry of Surfaces*, 2nd ed. Interscience Publishers Inc., New York.

[35] Freundlich, H. (1926). *Colloid and Capillary Chemistry*. Metheun, London.

[36] W. J. Weber, J. C. Morris. (1963). Kinetics of adsorption on carbon from solution, *J. Sanit. Eng. Div. Am. Soc. Civ. Eng*. 89, 31-60.

[37] I. S. Zekstser. (2000). *Groundwater and the Environment*. Application for the global Community. U.S.A: Lewis Publisher. 175pp

[38] W. McCabe, J. C. Smith, and P. Harriott. (1993). *Unit Operations of Chemical Engineering*, 5th Edition, New York: McGraw-Hill.

[39] V. J. Inglezakis and S. Poulopoulos. (2006). *Adsorption, Ion Exchange, and Catalysis: Design of Operations and Environmental Applications.* Boston: Elsevier

[40] K. V. Ragnarsdottir. (2000). *The Oxford Companion to the Earth*. Ed. Paul Hancock and Brian J. Skinner. *Oxford Reference Online*. Oxford University Press.

[41] J. Daintith. (2000). *A Dictionary of Physics*. Oxford Reference Online. Oxford University Press.

[42] IRIS. (1998). USEPA, *Integrated Risk Information System.* USA

[43] A. Dabrowski, P. Podkoscielny, Z. Hubicki, and M. Barczak. (2005). Adsorption of Phenolic Compounds by Activated Carbon-a Critical Review. *Chemosphere*, 58, 1049

[44] E. Forgacsa, T. Cserhatia, and G. Orosb. (2004). Removal of synthetic dyes fromwastewaters: a review. *Environ. Int.* 30, 953

[45] R. D. Noble and P. A. Terry. (2004). *Principles of Chemical Separations with Environmental Applications,* UK: Cambridge University Press

[46] A. Dabrowski. (2001). Adsorption-from theory to practice. *Adv. Colloid Interface Sci.* 93, 135p.

[47] S. Babel, and T. A. Kurniawan. (2003). Low-cost adsorbents for heavy metals uptake from contaminated water: a review. *J. Hazard. Mater.* B97, 219

[48] K. Conrad and H. C. B. Hansen. (2007). Sorption of zinc and lead on coir, *Bioresour. Technol*. 98, 89-97.

[49] R. H. Perry and D. Green. (1999). *Perry's Chemical Engineer's Handbook,* 7th Edition, McGraw-Hill, International Editions

[50] J. A. Hefne, W. K. Mekhemer, N. M. Alandis, O. A. Aldayel and T. Alajyan. (2008). Kinetic and thermodynamic study of the adsorption of Pb (II) from aqueous solution to the natural and treated Bentonite.*Int. J. Phys. Sci.* 3 (11), 281-288

[51] F. Helfferich. (1962) *Ion Exchange*. New York: Dover Publications

[52] V. J. Inglezakis. (2005). The concept of capacity" in zeolite. Ion–exchange systems. *J. Colloid Interface Sci.* 281**,** 68

[53] M.M. Dubinin, L.V. Radushkevich. (1947). Equation of the characteristic curve of activated charcoal, *Proc. Acad. Sci. USSR* 55, 331–333

[54] Y. S. Ho, C. T. Huang, H. W. Huang. (2002). Equilibrium sorption isotherm for metal ions on tree fern, *Process Biochem.* 37, 1421–1430

[55] M. J. Horsfall, A. I. Spiff. (2005). Equilibrium Sorption Study of Al^{3+}, Co^{2+} and Ag^{+} in Aqueous Solutions by Fluted Pumpkin (Telfairia Occidentalis Hook f.) *Waste Biomass. Acta Chim*. 52, 174–181

[56] S. M. Hasany, M. H. Chaudhary. (1996). Sorption potential of Haro river sand for the removal of antimony fromacidic aqueous solution. *Appl. Radiant. Isot*. 47, 467–471

[57] J. P. Hobson. (1969). Physical adsorption isotherms extending from ultra high vacuum to vapor pressure. *J. Phys. Chem.* 73, 2720–2727

[58] A. Benhammoua, A. Yaacoubi, L. Nibou, B. Tanouti. (2005). Adsorption of metal ions onto Moroccan stevensite: kinetic and isotherm studies. *J. Colloid Interface Sci.* 282, 320–326

[59] J. Romero-Gonzalez, J. R. Peralta-Videa, E. Rodrıguez, S. L. Ramirez, J. L. Gardea-Torresdey. (2005). Determination of thermodynamic parameters of Cr (VI) adsorption from aqueous solution onto *Agave lechuguilla* biomass. *J. Chem. Thermodyn*. 37, 343-347

[60] A. Sari, M. Tuzen, D. Citak, M. Soylak. (2007). Adsorption characteristics of Cu (II) and Pb (II) onto expanded perlite from aqueous solution. *J. Hazard. Mater.* 148, 387–394

[61] A. Tager. (1978). *Physical Chemistry of Polymers,* 2nd Edition, Moscow: MIR Publishers

[62] L. Li, "*Effect of activated carbon surface chemistry and pore structure on the adsorption of trace organic contaminants from aqueous solutio,"* Ph.D Desertation, Dept Civil Eng., North Caroline State Univ., Raleigh. 2002.

[63] M. A. Daley. (1996). Tandon D, Economy J and Hippo EJ. Elucidating the porous structure of activated carbon fibers using direct and indirect methods. *Carbon* 34(10), 1191-1200

[64] K. S. W. Sing, D. H. Everett, R.A.W. Haul, L. Moscou, R. A. Pierotti, J. Rouquerol, and T. Siemieniewska. (1985). Reporting physisorption data for gas solid systems with special reference to the determination of surface-area and porosity (recommendations 1984). *Pure Appl. Chem.* 57(4), 603-619

[65] M. Manes. (1998). *Activated carbon adsorption fundamentals*. In Encyclopedia of environmental analysis and remediation. Editor: Meyers, RA. NY: John Wiley & Sons Inc.

[66] K. Ishizaki. (1998). *Porous materials, process technology and applications*. Boston: Kluwer Academic Publishers.

[67] J. W. Patrick. (1995). *Porosity in carbons*. NY: John Wiley & Sons, Inc.

[68] J. Fraissard. (1997). *Physical adsorption: experiment, theory and applications*. Dordrecht, Boston and London: Kluwer Academic Publishers.

[69] M. Suzuki. (1990). *Adsorption Engineering*. Japan: Elsevier.

[70] M. Ahmedna. "*Granular activated carbon from agricultural by products: Carbon properties and their relationship to sugar decolorization potential*," PhD desertation, Dept. of Food Science. Louisiana State Univ. and Agricultural and Mechanical College.1998

[71] T. J. Fabish and D.E. Schleifer. (1984). Surface-chemistry and the carbon-black work function. *Carbon.* 22(1), 19-38

[72] Y. Leon, C.A. Leon, J.M. Solar, V. Calemma and L.R. Radovic. (1992). Evidence for the protonation of basal plane sites on carbon. *Carbon*. (30) 5, 797-811

[73] S. W. Davis and S. E. Powers. (2000) Alternative sorbents for removing MTBE from gasolinecontaminated ground water. *J. Environ. Eng.* 126(4), 354-360

[74] B. Sirasankar. (2006). *Bioseparations – Principles and Techniques*. New Delhi: Prentice-Hall.

[75] J. Heller. (1996). Physic nut. *Jatropha curcas* L. Promoting the conservation and use of underutilized and neglected crops. 1. Institute of Plant Genetics and Crop Plant Research, Gatersleben/ Int. Plant Genetic Resources Inst., Rome

[76] M. Ye, C. Li, G. Francis and H. R. P. S. Makkar. (2009). Current situation and prospects of *Jatropha curcas* as a multipurpose tree in China. *Springer*

[77] B. Schmook, L. Seralta-Peraza. (1997). J. curcas: distribution and uses in the Yucatan Peninsula of Mexico. In: Biofuels and industrial products from Jatropha curcas (Gu¨ bitz G M; Mittelbach M; Trabi M, eds), pp 53–57. DBV Graz

[78] G. M. Gübitz, M. Mittelbach, and M.Trabi. (1999). Exploitation of the tropical oil seed plant *Jatropha curcas L. Bioresour. Technol.* 67, 73-82.

[79] J. Martı´nez-Herrera, P. Siddhuraju, G. Francis, G. Da´ vila-Ortı´z, and K. Becker. (2006). Chemical composition, toxic/antimetabolic constituents, and effects of different treatments on their levels, in four provenances of Jatropha curcas L. from Mexico. *Food Chemistry*, 96(1), 80–89

[80] N. Kaushik, K. Kumar, S. Kumar, N. Kaushik, and S. Roy. (2007). Genetic variability and divergence studies in seed traits and oil content of Jatropha (*Jatropha curcas* L.) accessions. *Biomass Bioenergy.* 31, 497-502.

[81] P. Sirisomboon, P. Kitchaiya, T. Pholpho, W. Mahuttanyavanitch. (2007). Physical and mechanical properties of *Jatropha curcas* L.fruits, nuts and kernels. Elsevier. *Biosystems Eng.* 97, 201- 207

[82] B. Dehgan and G. L. Webster. (1979). *Morphology and infrageneric relationships of the genus Jatropha (Euphorbiaceae)*. University of California Publications in Botany, Vol. 74

[83] H. Kobilke, "*Untersuchungen zur Bestandesbegründung von Purgiernuß (Jatropha curcas L.),*" Diploma thesis. Univ. Hohenheim, Stuttgart. 1989

[84] J. Heller. (1992). Untersuchungen über genotypische Eigenschaften und Vermehrungsund Anbauverfahren bei der Purgiernuß (*Jatropha curcas* L.). [Studies on genotypic characteristics and propagation and cultivation methods for physic nuts (*Jatropha curcas* L.)]. Dr. Kovac, Hamburg

[85] R.C. Gupta. (1985). Pharmacognostic studies on 'Dravanti'. Part I *Jatropha curcas* Linn. *Proc. Indian Acad. Sci. Plant Sci.* 94(1), 65-82

[86] Y. Solhan, M. S. Affaizza, A. R. Afidah, A. A. Nursila Hanim, and R. Rozieyanie. (2008). Phase Transformation of Rust in the Presence of Various Tannins. *J. Phys. Sci.*19 (1), 31-41

[87] M. Trabi, "*Die Gifstoffe der PurgiernuB (Jatropha curcas L.*" MSc thesis, Graz Univ. of Technology, Graz.1998

[88] M. Wink. "Nutzung pflanzlicher Öle als Kraftstoffe," Forschungsbericht zum Projekt. Consultant's report prepared for GTZ, Germany. 1993

[89] G. M. Gübitz, M. Mittelbach, M. Trabi. (1999). Exploitation of the tropical oil seed plant *Jatropha curcas L. Bioresour Technol.* 67, 73-82

[90] Anonymous. (1978). *The compendium of medical herbs of China*. Editorial Board of the Compendium of Medical Herbs of China (Ed.). Beijing: People's Medical Publishing House.

[91] T. K. Huang. (2001). *Compendium of Materia Medica*. In: Huang TK (Ed.) Compendium of Materia Medica. Beijing: Medicine Science and Technology Press. 232

[92] Anonymous. (2005). *Pharmacopoeia of People's Republic of China*. Committee of Chinese Pharmacopoeia. Beijing: Chemical Industry Press

[93] G. Wang. (2006). *Liquid biofuels for transportation, Chinese potential and implications for sustainable agriculture and energy, in the 21st Century*: assessment study.

[94] H. P. S. Makkar, G. Francis and K. Becker. (2008). Preparation of protein concentrate from Jatropha curcas screw-pressed seed cake and toxic and antinutritional factors in protein concentrate. *J Sci. Food Agric.* 88, 1542-1548

[95] V. N. Gunaseelan. (2009). Biomass estimates, characteristics, biochemical methane potential, kinetics and energy flow from *Jatropha curcus* on dry lands. *Biomass Bioenergy* 33, 589–596

[96] D. K. Sharma, A. K. Pandey, and Lata. (2009). Use of Jatrophacurcas Hull Biomass for Bioactive Compost Production. *Biomass Bioenergy* 33, Elsevier, 159-162

[97] Y. Lin and S. Tanaka. (2006). Ethanol fermentation from biomass resources: current state and prospects. *Appl. Microbiol Biotechnol*. 69, 627–642

[98] R. Anish and M. Rao. (2009). *Bioethanol from Lignocellulosic Biomass, Part III Hydrolysis and Fermentation.* In: Pandey, A. 2009. Handbook of Plant-Based Biofuels. CRC Press

[99] G. Mtui (2009). Recent advances in pretreatment of lignocellulosic wastes and production of value added products. *Afr. J. Biotechnol.* 8 (8), 1398-1415

[100] K. K. Krishnani and S. Ayyappan. (2006). Heavy metals remediation of water using plants and lignocellulosic agrowastes. *Rev. Environ. Contam. Toxicol*. 188, 59-84.

[101] M. Ahmedna, W. E. Marshall, A. A. Husseiny, R. M. Rao, and I. Goktepe. (2004). The use of nutshell carbons in drinking water filters for removal of trace metals. *Water Res*. 38(4), 1062-1068.

[102] M. C. Basso, E. G. Cerrella, and A. L. Cukierman. (2004). Cadmium uptake by lignocellulosic materials: Effect of lignin content. *Sep. Sci. Technol*. 39(5), 1163-1175

[103] L. Dupont, J. Bouanda, J. Dumonceau, and M. Aplincourt. (2005). Biosorption of Cu(II) and Zn(II) onto a lignocellulosic substrate extracted from wheat bran. *J. Environ. Chem. Lett.* 2(4), 165-168

[104] G. Harman, R. Patrick, T. Spittler. (2007). Removal of heavy metals from polluted waters using lignocellulosic agricultural waste products. *Ind. Biotechnol*. 3(4), 366-374

[105] M. Šciban, M. Klašnja, B. Škrbi. (2008). Adsorption of copper ions from water by modified agricultural by-products. *Desalination* 229(1-3), 170-180

[106] W. S. W. Ngah and M. A. K. M. Hanafiah. (2008). Removal of heavy metal ions from wastewater by chemically modified plant wastes as adsorbents: A review. *Bioresour. Technol*. 99(10), 3935-3948

[107] W. T. Tsai, C. Y. Chang, S. Y. Wang, C. F. Chang, S. F. Chien, H. F. Sun. (2001). Utilization of agricultural waste corn cob for the preparation of carbon adsorbent *J. Environ. Sci. Health,* Part B 36(5), 677-686

[108] Q. Gan, S. J. Allen, R. Matthews. (2004). Activation of waste MDF sawdust charcoal and its reactive dye adsorption characteristics. *Waste Manage.* 24(8), 841-848

[109] A. Gürses, Ç. Do_ar, S. Karaca, M. Açikyildiz, and R. Bayrak. (2006). Production of granular activated carbon from waste *Rosa canina* sp. seeds and its adsorption characteristics for dye. *J. Hazard. Mater*. 131(1-3), 254-259

[110] C. Namasivayam and M. V. Sureshkumar. (2006). Anionic dye adsorption characteristics of surfactant-modified coir pith, a waste lignocellulosic polymer. *J. Appl. Poly. Sci.* 100(2), 1538-1546

[111] F. A. Batzias and D. H. Sidiras. (2007). Dye adsorption by prehydrolysed beech sawdust in batch and fixed-bed systems. *Bioresour. Technol.* 98(6), 1208-1217

[112] U. S. Orlando, A. U. Baes, W. Nishijima, and M. Okada. (2002). A new procedure to produce lignocellulosic anion exchangers from agricultural waste materials. *Bioresour. Technol*. 83(3), 195-198

[113] K. K. Kishore, V. Parimala, B. P. Gupta, I. S. Azad, X. Meng, and M. Abraham. (2006). Bagasse-assisted bioremediation of ammonia from shrimp farm wastewater. *Water Environ. Res*. 78(9), 938-950 (13)

[114] L. Yan and T. Shuya. (2006). Ethanol fermentation from biomass resources: Current state and prospects. *Appl. Microbiol. Biotechnol*. 69(6), 627-642

[115] C. Xiao, R. Bolton, and W.L. Pan. (2007). Lignin from rice straw kraft pulping: Effects on soil aggregation and chemical properties. *Bioresour. Technol*. 98(7), 1482-1488

[116] R. M. Rowell. (1990). Opportunities for Lignocellulosic Materials and Composites. *In:* Emerging technologies for materials and chemicals from biomass: Proceedings of symposium; 1990 August 26-31; Washington, DC. Washington, DC. *American Chemical Society*; 1992. Chap. 2. ACS symposium series 476

[117] R. M. Rowell. "*A new generation of composite materials from agro-based fiber*." *In:* Prasad, P. N.; Mark, James E.; Fai, Ting Joo, eds. Polymers and other advanced materials: emerging technologies and business opportunities. Proceedings of the 3d international conference on frontiers of polymers and advanced materials; 1995 January 16-20; Kuata Lumpur, Malaysia. New York, NY: Plenum Press: 659-665

[118] X. Li, "*Toxic metal ion adsorption by base-modified and unmodified biomass of pine sawdust and sunflower seed hulls*," M.Sc. Thesis. Dept. of Chemistry. Faculty of the Graduate School of the Univ. of Texas at El Paso.1997

[119] R. L. Ramos, J. R. Rangel-Mendez, J. Mendozabarron, L. Fuentes-Rubio, and R. M. Guerrerocoronado. (1997). Adsorption of cadmium (II) from aqueous solution onto activated carbon. *Water Sci. Technol.*30, 191-197

[120] J. W. Shim, S. J. Park, and S. K. Ryu. (2001). Effect of modification with HNO3 and NaOH by pitch-based activated carbon fibers. *Carbon*. 39, 11

[121] S. K. Ouki, R.D. Neufeld, and R. Perry. (1997). Use of activated carbon for the recovery of chromium from industrial wastewaters. *J. Chem.Technol.Biotechnol.* 70 (1) 3-8

[122] L. Monser and N. Adhoum. (2002). Modified activated carbon for the removal of copper, zinc, chromium, and cyanide from wastewater. *Sep. Purif. Technol.* 26 (2-3) 137-146

[123] M. N. Saifuddin and P. Kumaran. (2005). Removal of heavy metal from industrial wastewater using chitosan coated oil palm shell charcoal. *Environ. Biotechnol.* 8 (1)

[124] G. McKay. (1995). *Use of Adsorbents for the Removal of Pollutants from Wastewaters*. Boca Raton: CRC Press, Inc.

[125] D. J. Smith, P. Pettit, and T. Schofield. (1996). Activated Carbon in Water Treatment. *Water Supply, the review journal of the International Water Supply Association*, 14(2), 85-98

[126] M. Zappi, K. Graves, A. Aycock, A. Subramani, and S. Tavai, "*Development of Kenaf-based Biosorptive Water Treatment Process*," Technical Interim Report, Project Number 1434-HQ-96-GR-O2679-20, Water Resources Research Institute, Mississippi State University, April 2000

[127] S. E. Bailey, T. J. Olin, R. M. Bricka, and D.D. Adrian. (1999). *A review of potentially low-cost sorbents for Heavy metals*. Department of civil and environmental engineering, Louisiana state university, USA: Elsevier. *Wat. Res.* 33 (11) 2469-2479

[128] J. R. Deans and B.G. Dixon. (1992). Uptake of Pb^{2+} and Cu^{2+} by novel biopolymers. *Water Res.* 26 (4), 469-472

[129] P. A. Brown, S. A. Gill, and S. J. Allen. (2000). Metal Removal from Wastewater Using Peat. *Water Resour.* 34(16), 3907-3916

[130] P. Kumar and S. S. Dara. (1981). Removal of Toxic Heavy Metal Ions From Wastewaters Using Modified Agricultural Waste Materials. *Water Sci. Technol., a Journal of the International Association on Water Pollution Research*, 13(7), 353-361

[131] K. S. Arup. (2002). *Principles of heavy metals separation: An introduction*. In: Arup K.S (ed.). 2002. Environmental Separation of heavy metals – Engineering Processes. Bethlehem. USA: Lewis Publishers.

[132] J.R. Boulding and J. S. Ginn. (2004). *Practical handbook of soil, vadose zone, and groundwater contamination assessment, prevention and remediation, 2nd Ed*. CRC Press. LLC.

[133] A. Kortenkamp. (1996). Casadevall, M.; Faux, S.P.; Jenner, A.; Shayer, R.O.J.; Woodbridge, N. and O'BRIEN, P. A role for molecular oxygen in the formation of DNA damage during the reduction of the carcinogen chromium (VI) by glutathione, *Arch. Biochem. Biophy.* 329(2), 199-208

[134] R. J.E. Martins, R. Pardo, and R. A. R. Boaventura. (2004). Cadmium (II) and zinc (II) adsorption by the aquatic moss Fontinalis antipyretica: effect of temperature, pH and water hardness. *Water Res.* 38, 693-699

[135] G. A. Drash. (1993). Increase of cadmium body burden for this century. *Sci. Total Environ*. 67, 75

[136] G. C. Panda, S. K. Das, S. Chatterjee, P. B. Maity, T. S. Bandopadhyay, and A. K. Guha. (2006). Adsorption of cadmium on husk of *Lathyrus sativus*: Physico-chemical study. *Colloids Surf. B.* 50, 49–54

[137] U. Forstner and G. Wittman. (1979). *Metal Pollution in the Aquatic Environment.* Berlin: Springer-Verlag

[138] D.T. Lide, ed. (2005). *CRC Handbook of Chemistry and Physics*, Internet Version 2005, Available: http://www.hbcpnetbase.com, CRC Press, Boca Raton, FL.

[139] J. Peterson. M. MacDonell, L. Haroun, and F. Monette. (2007). *Radiological and Chemical Fact Sheets to Support Health Risk Analyses for Contaminated Areas*. Argonne National Laboratory Environmental Science Division. U.S. Department of Energy

[140] L. Razak. (1995). T*he effect of cadmium. National Poison Centre*, Universiti Sains Malaysia, Penang. Available: http://www.prn2.usm.my/mainsite/bulletin/sun/1995/sun36.html

[141] B. Simon-Hettich, A. Wibbertmann, D. Wagner, L. Tomaska, and H. Malcolm. (2001). *Environmental Health Criteria 221. Zinc*. United Nations Environment Programme. The International Labour Organization. The World Health Organization, Geneva

[142] R. P. Beliles. (1994). *Zinc*, Zn. In: Clayton GD and Clayton FE ed. Patty's industrial hygiene and toxicology, 4th ed. Part C Toxicology. New York: John Wiley & Sons Inc, 2332–2342

[143] ATSDR. (1999). Toxicological Profiles, U.S. Department of Health and Human Services, *Public Health Service,* Atlanta. Agency for Toxic Substances and Disease Registry

[144] B. Volesky. (1990). *Biosorption of Heavy Metals.* Boca Raton, FL: CRC Press Inc.

[145] E. M. Trujillo, M. Spinti, and H. Zhuang. (1995). *Ion Exchange Technology: Advances in Pollution Control.* In: A.K. SenGupta (Ed.), Technomic Publishing Co., Inc., Lancaster, PA

[146] S. Sukalyan and K. S. Arup. (2002). *Trace Heavy Metal Separation By Chelating Ion Exchangers*. In: Arup K.S (ed.). 2002. Environmental Separation of heavy metals – Engineering Processes. Bethlehem. USA: Lewis Publishers.

[147] U. K. Saha, S. Taniguchi, and K. Sakurai. (2001). Adsorption Behavior of Cadmium, Zinc, and Lead on Hydroxyaluminum– and Hydroxyaluminosilicate–Montmorillonite Complexes. *Soil Sci. Soc. Am. J.* 65, 694–703

[148] W. R. Puls and H. L. Bohn. (1988). Sorption of cadmium, nickel, and zinc by kaolinite and montmorillonite suspensions. *Soil Sci. Soc. Am. J.* 52, 1289-1292

[149] R. G. Pearson. (1963). Hard and soft acids and bases. *J. Am. Chem. Soc*. 85, 3533–3539

[150] M. Misono, E. Ochiai, Y. Saito, and Y. Yoneda. (1967). A new parameter scale for the strength of Lewis acids and bases with the evaluation of their softness. *J. Inorg. Nucl. Chem*. 29, 2685–2691

[151] A. Abd-Elfattah and K. Wada. (1981). Adsorption of lead, copper, zinc, cobalt, and cadmium by soils that differ in cation-exchange materials. *J. Soil Sci.* 32, 271–283

[152] M. B. McBride. (1991). *Processes of heavy and transition metal sorption by soil minerals*. p. 149–175. *In* G.H. Bolt et al. (ed.) Interactions at the soil colloid–soil solution interface. Dordrecht, the Netherlands: Kluwer Academic Publ.

[153] K. Banerjee. (2002). *Case studies for immobilizing toxic metals with iron coprecipitation and adsorption.* In: Arup K.S (Ed.). Environmental Separation of heavy metals – Engineering Processes. Bethlehem. USA. Lewis Publishers.

[154] E. H. F. Stone, "*Treatment of Non-Ferrous Metal Processing Waste of Kynoch Works*." Proceedings of the 25th Industrial Waste Conference, May 1967, Purdue University, West Lafayette, Indiana, 848-865

[155] E. H. F. Stone. (1972). Treatment of Non-Ferrous Metal Processing Waste. *Metal Finish.* 18, 280-290

[156] R. Knapp and E. Paulson. "*Gravity Filtration Reduces Suspended Metals in a Lime Precipitation System*." Proceedings of the 37th Industrial Waste Conference, May 1982, Purdue Univ., West Lafayette, Indiana, 95-104.

[157] R. Osantowski and A. Ruppersberger. "*Upgrading Foundry Wastewater Treatment.*" Proceedings of the 32nd Industrial Waste Conference, May 1977, Purdue University, West Lafayette, Indiana, 102-115

[158] J. McVaugh and W. T. Wall. "*Optimization of Heavy Metals Wastewater Treatment Effluent Quality versus Sludge Treatment.*" Proceedings of the 31st Industrial Waste Conference, May 1976, Purdue University, West Lafayette, Indiana, 17-25

[159] D. Bhattacharyya, A. Jumawan, G. Sun, and K. Schwitzebel. "*Precipitation of Sulfide: Bench Scale and Full Scale Experimental Results*." AIChE Symposium Series 1981, 77(209), 31-32

[160] B. M. Kim and P. A. Amodeo. (1983). Calcium Sulfide Process for Treatment of Metal Containing Wastes. *Environ. Prog.* 2 (3), 175-180

[161] R. W. Peters, Y. Ku, and T. K. Chang. "*Heavy Metals Crystallization Kinetics in an MSMPR Crystallizer Employing Sulfide Precipitation*." AIChE Symposium Series 1984, 80 (240), 55-75

[162] R. W. Peters, and Y. Ku. (1984). *Removal of Heavy Metals from Industry Plating Wastewaters by Sulfide Precipitation*. Proceedings of the Industrial Wastes Symposia, 57th Water Poll. Control Fed. Annual Conference, 279-311

[163] D. Bhattacharyya, A. B. Jumawan, and R. B. Grieves. (1979). Separation of Toxic Heavy Metals by Sulfide Precipitation. *Sep. Sc. Tech.* 14, 441-452

[164] B. E. Reed. (2002). *Removal of heavy metals by activated carbon*. In: Arup K.S (Ed.). 2002. Environmental Separation of heavy metals – Engineering Processes. Bethlehem. USA: Lewis Publishers.

[165] E. A. Sigworth and S. B. Smith. (1972). Adsorption of Inorganics by Activated Charcoal. *J. AWWA.* 64, 386-391

[166] A. Netzer and D. E. Hughes. (1984). Adsorption of Copper, Lead, and Cobalt by Activated Carbon. *Water Res.* 18 (8), 927

[167] R. M. Smith and A. E. Martell. (1976). *Critical Stability Constants*, Plenum Press, New York

[168] M. O. Corapcioglu and C.P. Huang. (1987). The Adsorption of Heavy Metals onto Hydrous Activated Carbon. *Water Res.* 9(9), 1031

[169] C. P. Huang and D. W. Blankenship (1984). The Removal of Mercury (II) from Dilute Aqueous Solution by Activated Carbon. *Water Res.* 18 (1), 37.

[170] Q. Sun and L. Yang. (2003). The adsorption of basic dyes from aqueous solution on modified peat-resin particle. *Water Res*. 37, 1535–1544

[171] N. Daneshvar, M. Ayazloo, A. R. Khata and M. Pourhassan. (2007). Biological decolorization of dye solution containing malachite green by microalgae *Cosmarium* sp. *Bioresour. Technol*. 98, 1-7

[172] V. K. Gupta, A. Mittal, L. Krishnan and V. Gajbe. (2004). Adsorption kinetics and column operations for the removal and recovery of malachite green from wastewater using ash. *Sep. Purif. Technol*. 40, 87-96

[173] K. V. K. Rao. (1995). Inhibition of DNA synthesis in primary rat hepatocyte cultures by malachite green: A new liver tumor promoter. *Toxicol. Lett*. 81, 107-113

[174] K. V. Kumar, S. Sivanesan, and V. Ramamurthi. (2005). Adsorption of malachite green onto Pithophora sp., a fresh water alga: Equilibrium and kinetic modeling. *Process Biochem*. 40, 2865–2872

[175] S. Srivastava, R. Sinha, and D. Roy. (2004). Toxicological effects of malachite green, *Aquat. Toxicol*. 66, 319–329

[176] B. P. Cho, T. Yang, L. R. Blankenship, J. D. Moody, M. Churchwell, F. A. Beland andS. J. Culp. (2003). Synthesis and Characterization of N-Demethylated Metabolites of Malachite Green and Leucomalachite Green. *Chem. Res. Toxicol.* 16 (3), 285-294

[177] R. M. Christie. (2001). *Colour Chemistry*. The Royal Society of Chemistry. U.K. 205

[178] F. J. Green. (1990). *The Sigma-Aldrich Handbook of Stains, Dyes and Indicators.* Aldrich Chem. Comp.

[179] H. Du, R. A. H. Fuh, J. Li, A. Corkan, and J. S. Lindsey. (1998). PhotochemCAD: A computer-aided design and research tool in photochemistry. *Photochem. Photobiol.* 68, 141-142

[180] C. Akmil-Basar, Y. Onal, T. Kılıcer, and D. Eren. (2005). Adsorptions of high concentration malachite green by two activated carbons having different porous structures. *J. Hazard. Mater*. B127, 73-80

[181] S. S. Tahir and N. Rauf. (2006). Removal of a cationic dye from aqueous solutions by adsorption onto bentonite clay. *Chemosphere*, 63, 1842-1848

[182] Y. Guo, S. Yang, W. Fu, J. Qi, R. Li, Z. Wang, and H. Xu. (2003) Adsorption of malachite green on micro- and mesoporous rice husk-based active carbon. *Dyes Pigm.* 56, 219-229

[183] B. H. Hameed and M. I. El-Khaiary. (2008). Kinetics and equilibrium studies of malachite green adsorption on rice straw-derived char. *J. Hazard. Mater*. 153, 701–708

[184] I. D. Mall, V. C. Srivastava, N. K. Agarwal, and I. M. Mishra. (2005). Adsorptive removal of malachite green dye from aqueous solution by bagasse fly ash and activated carbon-kinetic study and equilibrium isotherm analyses, Colloids Surf. A: Physicochem. *Eng. Aspects*, 264, 17–28

[185] C. A. Miller and P. Neogi. (1985). *Interfacial Phenomena – Equilibrium and Dynamic Effects.* New York: Marcel Dekker

[186] C. Treiner. (2002). *Surfactant adsorption and adsorption induced by surfactants at solid-water interfaces*. In: P. Somasundaran, A. Hubbard (Eds.), Encyclopedia of Surface and Colloid Science, Marcel Dekker Inc., New York, 5154–516

[187] H. D. Choi, J. M. Cho, K. Baek, J. S. Yang, and J. Y. Lee. (2008). Influence of cationic surfactant on adsorption of Cr (VI) onto activated carbon. *J. Hazard. Mater*. 161, 2-3, 1565-1568

[188] D. Myers. (1999). *Surfaces, Interfaces, and Colloids: Principles and Applications*, New York: Wiley-VCH, 400–401.

[189] J. Goodwin. (2004). *Colloids and Interfaces with Surfactants and Polymers - An Introduction.* England: John Wiley & Sons.

[190] J. Medham, R.C. Denny, J.D. Barnes, M. Thomas, *Vogel's textbook of quantitative chemical analysis* (5th. Ed. ed.). Harlow, Pearson Education. 2000. ISBN 0 582 22628 7. Appendix 5

[191] Y. S. Ho, G. Mckay. (1998). Kinetic models for the sorption of dye from aqueous solution by wood, *Trans IchemE*; 76B, 313-318

[192] K. R. Hall, L. C. Eagleton, A. Acrivos, T. Vermeulen. (1966). Pore-and solid-diffusion kinetics in fixed-bed adsorption under constant-pattern conditions. *I & EC Fundam*, 5, 212-223

[193] M.M. Dubinin, L.V. Radushkevich. (1947). Equation of the characteristic curve of activated charcoal, *Proc. Acad. Sci. USSR* 55, 331–333

[194] S. E. Kegley, D. Landfear, D. Jenkins, B. Gross, K. Shomglin. Water Treatment, How we can purify our water? Beta Version, Chem Connections. John Wiley and Sons, Inc. US. 2000

[195] A. C. Lua, T. Yang. (2005). Characteristics of activated carbon prepared from pistachio-nut shell by zinc chloride activation under nitrogen and vacuum conditions. *J. Colloid Interface Sci.* 290, 505–513

[196] V. Gomez-Serrano, J. Pastor-Villegas, A. Perez-Florindo, C. Duran-Valle, C. Valenzuela- Calahorro. (1996). FT-IR study of rockrose and of char and activated carbon. *J. Anal. Appl. Pyrolysis* 36, 71-80

[197] S. B. Lalvani, A. Hubner, T. S. Wiltowski. (1997). Metal removal from process water by lignin, *Environ. Technol.* 18, 1663–1668

[198] M.M. Rao, A. Ramesh, G.P.C. Rao, K. Seshaiah. (2006). Removal of copper and cadmium from the aqueous solutions by activated carbon derived from Ceiba pentandra hull, *J. Hazard. Mater.* B129, 123-129

[199] T. J. Barton, L. M. Bull, W. G. Klemperer, D. A. Loy, B. McEnaney, M. Misono, P.A. Monson, G. Pez, G. W. Scherer, J. C. Vartuli, and O. M. Yaghir. (1999). Tailored Porous Materials, *Chem. Mater*. 11. 2633-2656

[200] J. L. Schnoor. *Environmental Modeling: fate and transport of pollutants in water, Air and soil*. Wiley and Sons INC., New York. 1996

[201] M. Husseien, A. A. Amer, A. El-Maghraby, and N. A. Taha. (2007). Utilization of barley straw as a source of a activated carbon for removal of methylene blue from aqueous solution. *J. Appl. Sci. Res*., 3 (11), 1352-1358

[202] Z. Bekci¸ Y. Seki, L. Cavas. (2009). Removal of malachite green by using an invasive marine alga *Caulerpa racemosa* var. *cylindracea, J. Hazard. Mater.* 161, 1454–1460

[203] K. A. Krishnan, T. S. Anirudhan. (2003). Removal of Cadmium (II) from aqueous solutions by steam activated sulphurised carbon prepared from sugar-cane bagasse pith: Kinetics and equilibrium studies. *Water SA* 29(2). 147-156

[204] R. G. Pearson. (1988). Absolute electronegativity and hardness: Application. *Inorg. Chem*. 27, 734-738

[205] S. D. Khattri, M. K. Singh. (2009). Removal of malachite green from dye wastewater using neem sawdust by adsorption. *J. Hazard. Mater*. 167, 1089–1094

[206] A. Marcilla, M. I. Beltrán, R. Navarro. (2007). Application of TG/FTIR to the study of the regeneration process of HUSY and HZSM5 zeolites, *J. Therm. Anal. Cal.* 87, 325-330

[207] A. A. Abia, E. D. Asuquo. (2006). Lead (II) and nickel (II) adsorption kinetics from aqueous metal solutions using chemically modified and unmodified agricultural adsorbents, *Afr. J. Biotechnol*. 5 (16), 1475–1482

[208] C. K. Jain. (2001). Adsorption of zinc onto bed sediments of the river Ganga: adsorption models and kinetics. *Hydrol. Sci. J. des Sci. Hydrologiques*. 46 (3), 419

[209] S. E. Kegley, D. Landfear, D. Jenkins, B. Gross, K. Shomglin. Water Treatment, How we can purify our water? Beta Version, Chem Connections. John Wiley and Sons, Inc. US. 2000

[210] W. T. Tsai, H. R. Chen. (2010). Removal of malachite green from aqueous solution using low-cost chlorella-based biomass. *J. Hazard. Mater.* 175, 844–849

[211] V. C. Srivastava, I. D. Mall, I. M. Mishra. (2006). Modelling individual and competitive adsorption of cadmium (II) and zinc (II) metal ions from aqueous solution onto bagasse fly ash, *Sep. Sci. Technol*. 41, 2685

[212] E. R. Alley, *Water Quality Control Handbook*, vol. 8, McGraw Hill, 125–141. 2000

[213] V. C. Srivastava, I. D Mall, I. M. Mishra. (2008). Removal of Cadmium (II) and Zinc (II) Metal Ions from Binary Aqueous Solution by Rice Husk Ash. *Colloids Surf. A.* 312, 172–184

[214] T. Karthikeyan, S. Rajgopal, L. R. Miranda. (2005). Chromium (VI) adsorption from aqueous solution by Hevea brasilinesis saw dust activated carbon. *J. Hazard. Mater.* B124, 192-199.

[215] V. Fierro, V. Torné-Fernández, D. Montané, A. Celzard. (2008). Adsorption of phenol onto activated carbons having different textural and surface properties. *Microporous Mesoporous Mater.* 111, 276–284

[216] C.K. Jain, D.C. Singhal, M.K. Sharma. (2004). Adsorption of zinc on bed sediment of River Hindon: adsorption models and kinetics. *J. Hazard. Mater*. B114, 231-239

[217] Y. Önal, C. Akmil-Basar, D. Eren, C. Sarýcý-Ozdemir, T. Depci. (2006). Adsorption kinetics of malachite green onto activated carbon prepared from TunC, bilek lignite, *J. Hazard. Mater*. 128, 150–157

[218] N. K. Hamadi, X. D. Chen, M. M. Farid, M. G. Q. Lu. (2001). Adsorption kinetics for the removal of chromium (VI) from aqueous solution by adsorbents derived from used tires and sawdust. *Chem. Engg. J*. 84, 95-105

[219] Y. S. Ho, G. McKay. (1978). Sorption of dye from aqueous solution by peat. *Chem. Eng. J*. 70, 115–124

[220] R. E. Treybal. Mass Transfer Operations. Second ed., McGraw Hill, New York. 1968

[221] U.K. Saha, S. Taniguchi, K. Sakurai. (2002). Simultaneous adsorption of cadmium, zinc and lead on hydroxyaluminum and hydroxyaluminosilicate-montmorillonite complexes. *Soil Sci. Soc. Am.* J. 66, 117–128

[222] S. Mayhew. (2004). *A Dictionary of Geography*. Oxford Reference Online. Oxford University Press.

[223] E. Demirbas, N. Dizge, M.T. Sulak, M. Kobya. (2009). Adsorption kinetics and equilibrium of copper from aqueous solutions using hazelnut shell activated carbon, *Chem. Eng. J.* 148, 480-487

[224] B. Benguella and H. Benaissa. (2002). Effects of competing cations on cadmium biosorption by chitin. Colloids and Surfaces A: *Physicochemical and Engineering Aspects* 201, 143–150

[225] P. Brown, I. A. Jefcoat, D. Parrish, S. Gill, E. Graham. (2000). Evaluation of the adsorptive capacity of peanut hull pellets for heavy metals in solution, *Adv. Environ*. Res. 4, 19-29

[226] W. E. Oliveira, A. S. Franca, L. S. Oliveira, S. D. Rocha. (2008). Untreated coffee husks as biosorbents for the removal of heavy metals from aqueous solutions, *J. Hazard. Mater*. 152, 1073-1081

[227] N. Meunier, J. Laroulandie, V. F. Blais, R. D. Tyagi. (2003). Cocoa shells for heavy metal removal from acidic solutions, *Bioresour. Technol*. 90, 255-263

[228] S. Doyurum and A. Çelik. (2006). Pb (II) and Cd (II) removal from aqueous solutions by olive cake, *J. Hazard. Mater*. B138, 22-28

[229] B. Benguella and H. Benaissa. (2002). Cadmium removal from aqueous solutions by chitin: kinetic and equilibrium studies, *Water Res*. 36, 2463-2474

[230] E. W. Shin, K. G. Karthikeyan, M. A. Tshabalala. (2007). Adsorption mechanism of cadmium on juniper bark and wood. *Bioresour. Technol.* 98, 588-594

[231] Y. Bulut, Z. Tez. (2007). Adsorption studies on ground shells of hazelnut and almond. *J. Hazard. Mater.* 149, 35-41

[232] B. Bayat. (2002). Comparative study of adsorption properties of Turkish fly ashes. I. The case of nickel(II), copper(II) and zinc(II). *J. Hazard. Mater.* B95, 251-273

[233] Y. S. Ho, D. A. J. Wase, C. F. Forster. (1996). Kinetic studies of competitive heavy metal adsorption by sphagnum moss peat. *Environ. Technol*. 17, 71-77

[234] D. J. Shaw. Introduction to Colloid and Surfaces Chemistry, Butterworth-Heinemann, Oxford. Chap. 6. 1992

[235] K. Conrad and H. C. B. Hansen. (2007). Sorption of zinc and lead on coir, *Bioresour. Technol*. 98, 89-97.

[236] J. Zhang, Y. Li, C. Zhang, Y. Jing. (2008). Adsorption of malachite green from aqueous solution onto carbon prepared from Arundo donax root. *J. Hazard. Mater*. 150, 774–782

[237] M. Baek, C. O. Ijagbemi, S. O, D. Kim. (2010). Removal of Malachite Green from aqueous solution using degreased coffee bean. *J. Hazard. Mater.* 176, 820-828

[238] G. H. Sonawane and V. S. Shrivastava. (2009). Kinetics of decolourization of malachite green from aqueous medium by maize cob (Zea maize): An agricultural solid waste. *Desalination* 247, 430-441

APPENDICES

APPENDIX A

RESEARCH PLAN FLOW CHART

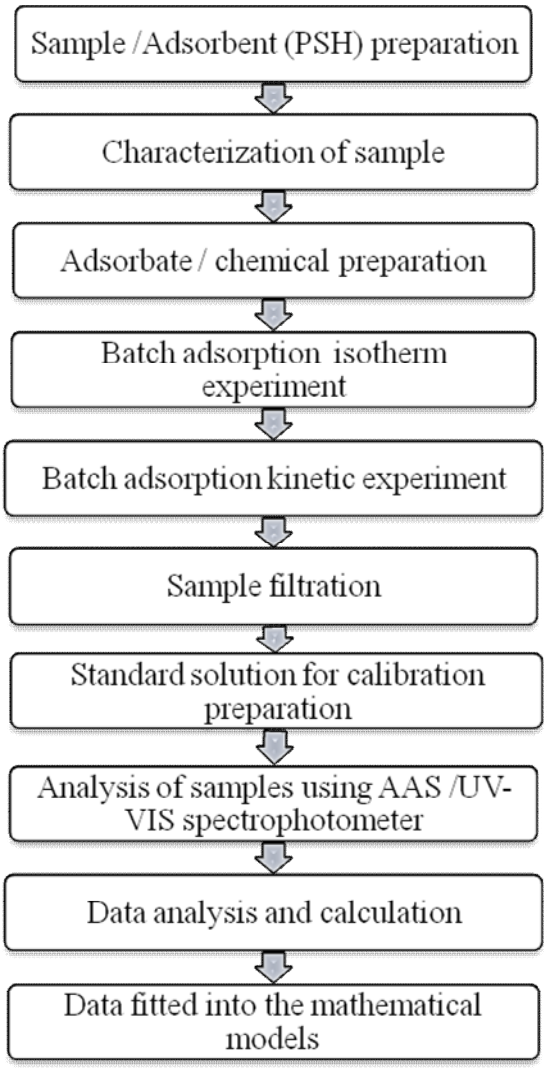

APPENDIX B

CHEMICAL PREPARATION PROCEDURE

a. Cd^{2+} stock solution (1000 ppm)

2.74 g oven dried (105^{o}C) $Cd(NO_3)_2$ placed into 1000 mL volumetric flask and the volume was made up to 1L with di-ionized water.

b. Zn^{2+} stock solution (1000 ppm)

4.55 g oven dried (105^{o}C) $Zn(NO_3)_2$ placed into 1000 mL volumetric flask and the volume was made up to 1L with di-ionized water.

c. Malachite green stock solution (1000 ppm)

1 g oven dried (105^{o}C) Malachite green placed into 1000 mL volumetric flask and the volume was made up to 1L with di-ionized water.

d. Aerosol 22 stock solution preparation (1000 ppm)

1 g of Aerosol 22 placed into 1000 mL volumetric flask and the volume was made up to 1L with di-ionized water.

e. Calculation for preparing metal ion stock solutions

Calculation of amount of $Zn(NO_3)_2$ needs to obtain 1000ppm of Zn^{2+} metal ions concentration or 1g of Zn^{2+} ion.

Concentration = mass of solute (mg) / volume of solution (L)

= mg/L or ppm

1000ppm = 1g pure metal ion in 1 L DI water

Calculation;

e.g: 1 g of Zn^{2+} metal ion from $Zn(NO_3)_2$ salt powder:

$$\text{Amount of } Zn(NO_3)_2 = \text{Amount of } Zn^{2+} \text{ X } \frac{\text{Molecular Weighty of } Zn(NO_3)_2}{\text{Molecular Weight of Zn}}$$

$$= 1\text{g X } \frac{297.47 \text{ g/mol}}{65.409 \text{ g/mol}}$$

$$= 4.548\text{g}$$

4.548 g of $Zn(NO_3)_2$ salt is dissolved and bring to 1 L volume to give a concentration of 1000 ppm of element.

f. Preparation of 5, 10, 30 and 50 ppm stock solution from 1000 ppm stock solution

The calculation for diluting the cadmium stock solution is as follows:

$c_1V_1 = c_2V_2$

Where, C_1 = stock solution concentration

V_1 = stock solution volume needed

C_2 = desired solution concentration

V_2 = new concentration solution volume after the addition of di-ionized water to V1

e.g., Preparation of 50 ppm of $Cd(NO_3)_2$ solution from 1000 mL stock solution

$C_1V_1 = C_2V_2$

(1000 ppm) (V_1) = (50 ppm) (250 mL)

V_1 = 12.5 mL

As a result, 12.5 mL of the stock solution will be added into the 250 mL volumetric flask and the volume was made up to 250 mL with di-ionized water.

g. Universal Buffer mixer preparation

Preparation of 0.2 M sodium hydrogen phosphate (Na_2HPO_4)

28.39g oven dried (105^oC) Na_2HPO_4 placed into 1000 mL volumetric flask and the volume was made up to 1L with di-ionized water.

Preparation of 0.1 M of citric acid ($C_6H_8O_7$)

19.2 g oven dried (105^oC) citric acid placed into 1000 mL volumetric flask and the volume was made up to 1L with di-ionized water.

h. Calculation data from spectrometer (AAS and UV-VIS)

Calculation for Cd^{2+}, Zn^{2+} and dye;
ppm χ = gf X df X abs
gf = Σstrd / Σabs
ppm χ = gf X (100mL/1g) X 10 X abs
*gf= graph factor
*df = dilution factor
* abs = absorbance

APPENDIX C

EXPERIMENTAL PROCEDURES

a. Adsorption kinetic and isotherm experiment

1. 30 ppm of metal ion/dye solution was prepared and 10 mL of solution is taken into sample bottle as initial concentration.
2. 0.4 g of adsorbent was added into polyethylene bottle contains 100 mL of 30ppm metal ions solution and agitated on Laboratory shaker at 160 rpm.
3. After two minutes, the sample bottles was taken out from the shaker and immediately suck 10mL of the solution using Watman No. 0.45 syringe filter for filtration.
4. The filtrate was added into sample bottles and then diluted 10 times before analyzed in Atomic Adsorption Spectrophotometer (AAS).
5. The standard solutions of metal ions and dye for calibration curves were prepared prior to AAS analysis and UV-VIS spectrophotometer analysis.
6. After dilution, the diluted sample of metal ion was added into 10 mL test tube and arranged in autosampler for AAS analysis. For dye analysis, the diluted dye sample was added into 10 mL cuvet for UV-VIS analysis.
7. The similar method was repeated for different time interval (5, 10, 20, 30, 60, 120, 240, 300, 360).
8. The process was repeated until the concentration reaches equilibrium.
9. Steps 1 – 8 were repeated for other metal ions concentrations (2, 5, 10, 30, 50 ppm)
10. The data in concentration (ppm) was multiplied by dilution factor (10).

11. The analysis was then repeated for different temperature, pH, dosage and particle size for study the different effect on metal ion /dye adsorption.
12. For isotherm experiment, the similar procedure from 1 to 10 were repeated; however the time scale was taken longer as it reached equilibrium (6 hours approximately).

APPENDIX D

DATA ANALYSIS

METAL ION ADSORPTION ON PSH AND GAC

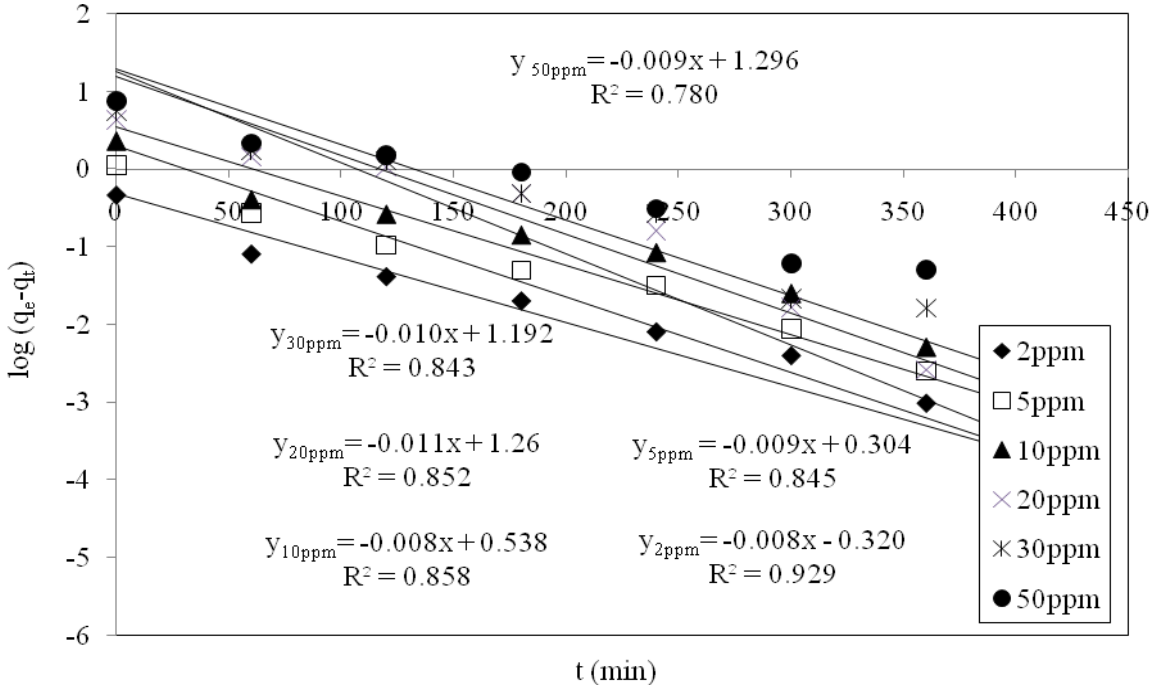

Fig. 5.1: Pseudo-first-order kinetic plots for Zn^{2+} removal at different initial concentrations using PSH (Size: 0.6 mm, PSH dosage: 0.4 g/100mL, pH: 6, Temperature: 24^{o}C, Agitation speed: 160 rpm)

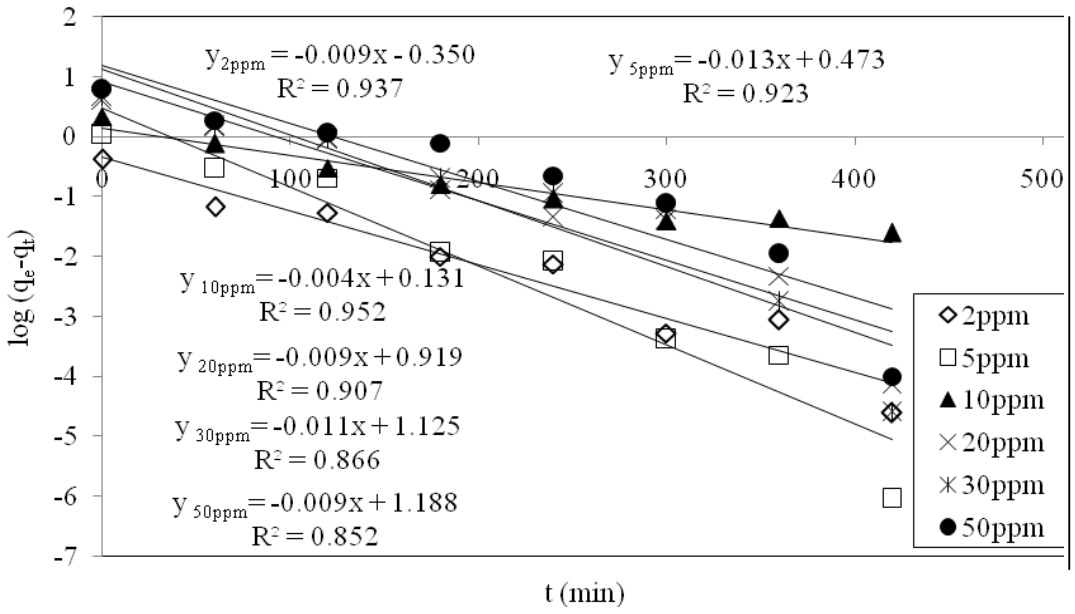

Fig. 5.2: Pseudo-first-order kinetic plots for Cd^{2+} removal at different initial concentrations using PSH (Size: 0.6 mm, PSH dosage: 0.4 g/100mL, pH: 6, Temperature: 24°C, Agitation speed: 160 rpm)

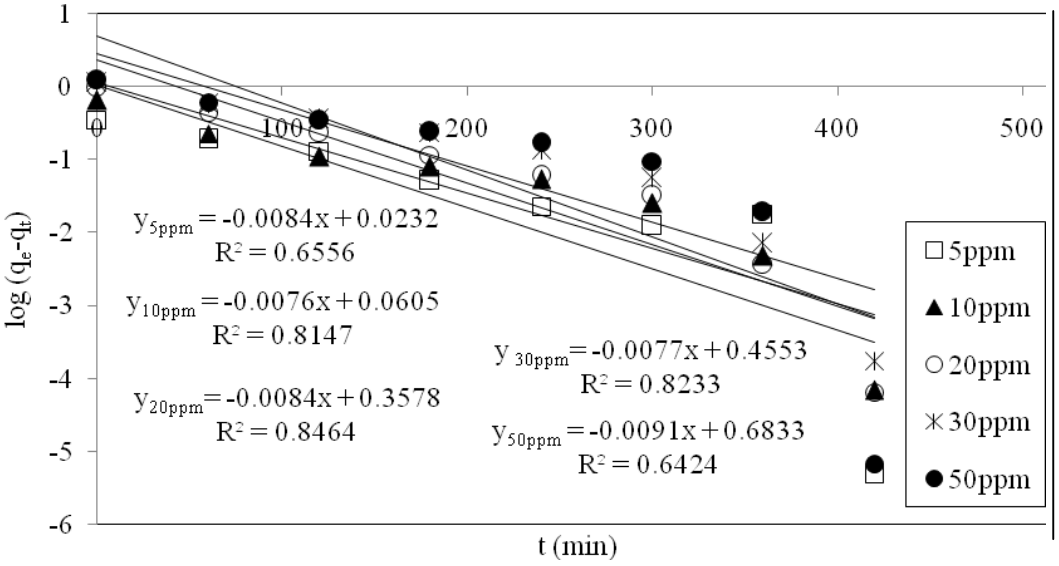

Fig. 5.3: Pseudo-first-order kinetic plots for Zn^{2+} removal at different initial concentrations using GAC (Size: 0.6 mm, GAC dosage: 0.4 g/100mL, pH: 6, Temperature: 24°C, Agitation speed: 160 rpm)

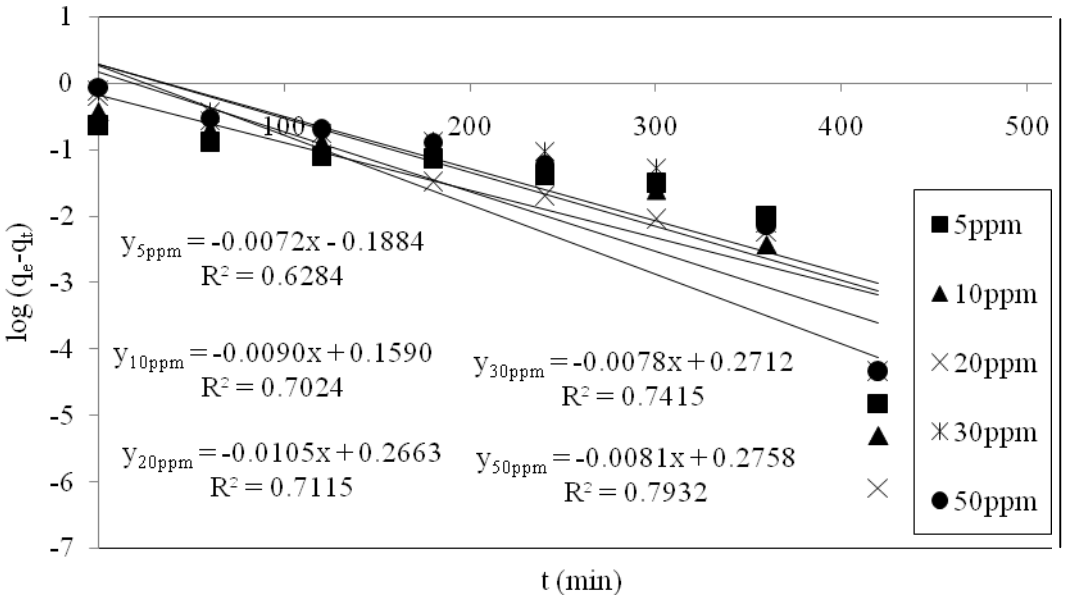

Fig. 5.4: Pseudo-first-order kinetic plots for Cd^{2+} removal at different initial concentrations using GAC (Size: 0.6 mm, GAC dosage: 0.4 g/100mL, pH: 6, Temperature: 24°C, Agitation speed: 160 rpm)

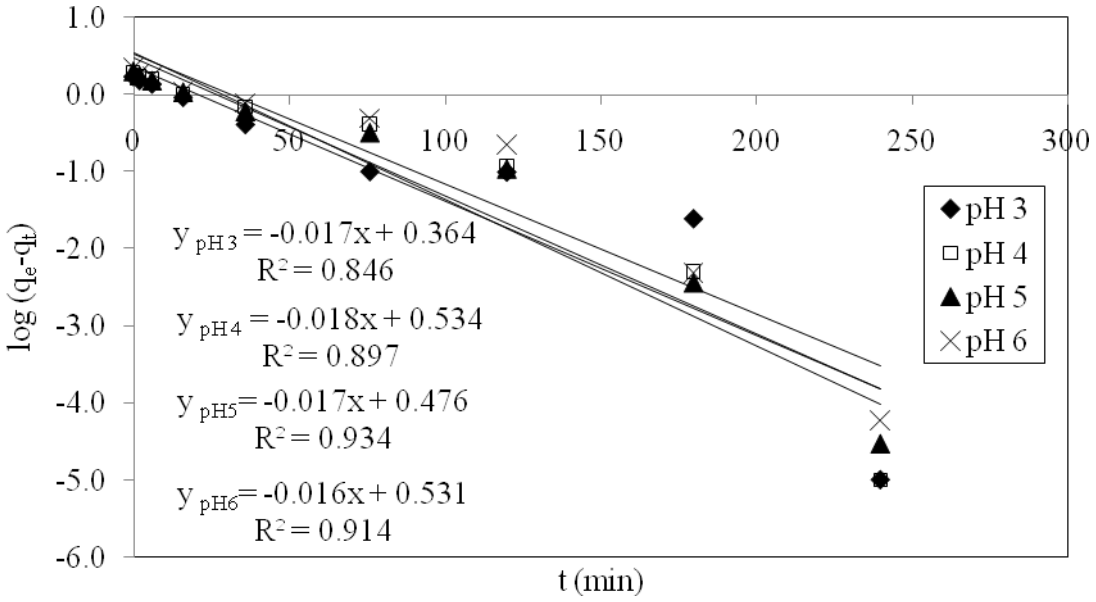

Fig. 5.5: Pseudo-first-order kinetic plots for Zn^{2+} removal at different pH of solution using PSH (Size: 0.6 mm, C_o: 10 ppm, PSH dosage: 0.4 g/100mL, Temperature: 24°C, Agitation speed: 160 rpm)

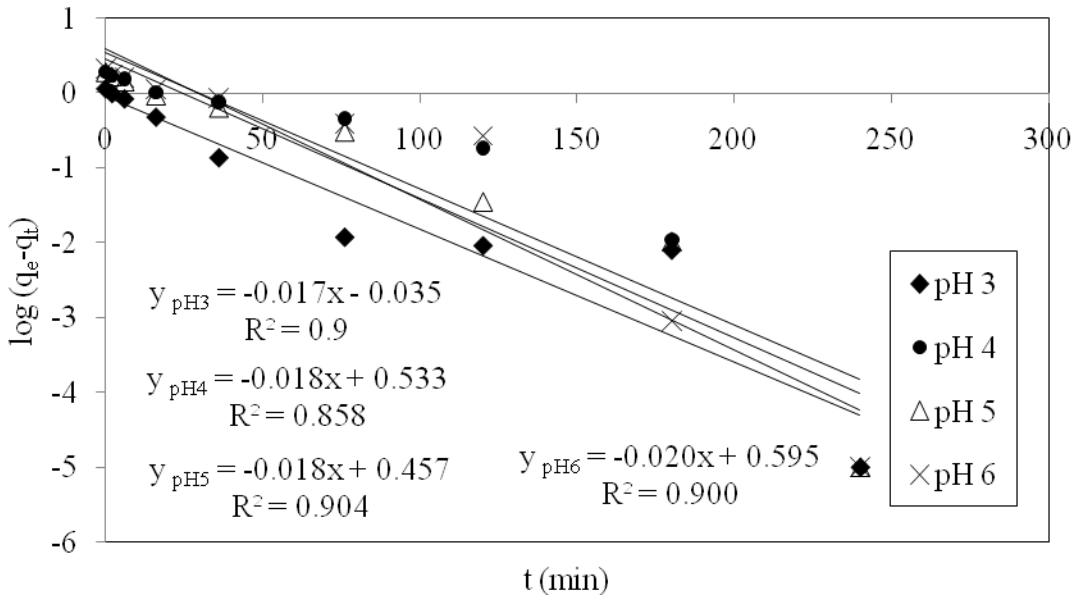

Fig. 5.6: Pseudo-first-order kinetic plots for Cd^{2+} removal at different pH of solution using PSH (Size: 0.6 mm, C_o: 10 ppm, PSH dosage: 0.4 g/100mL, Temperature: 24°C, Agitation speed: 160 rpm)

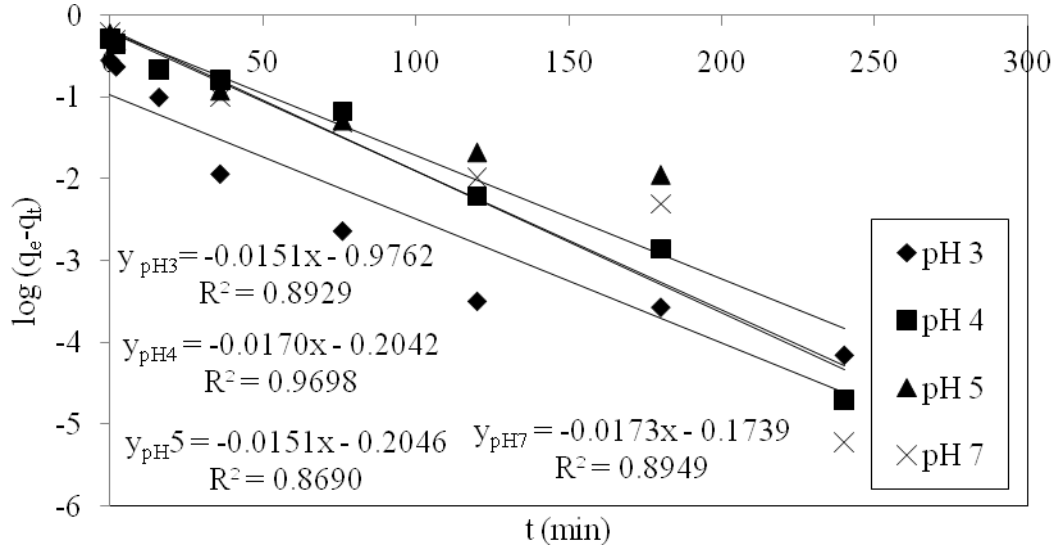

Fig. 5.7: Pseudo-first-order kinetic plots for Zn^{2+} removal at different pH of solution using GAC (Size: 0.6 mm, C_o: 10 ppm, GAC dosage: 0.4 g/100mL, Temperature: 24°C, Agitation speed: 160 rpm)

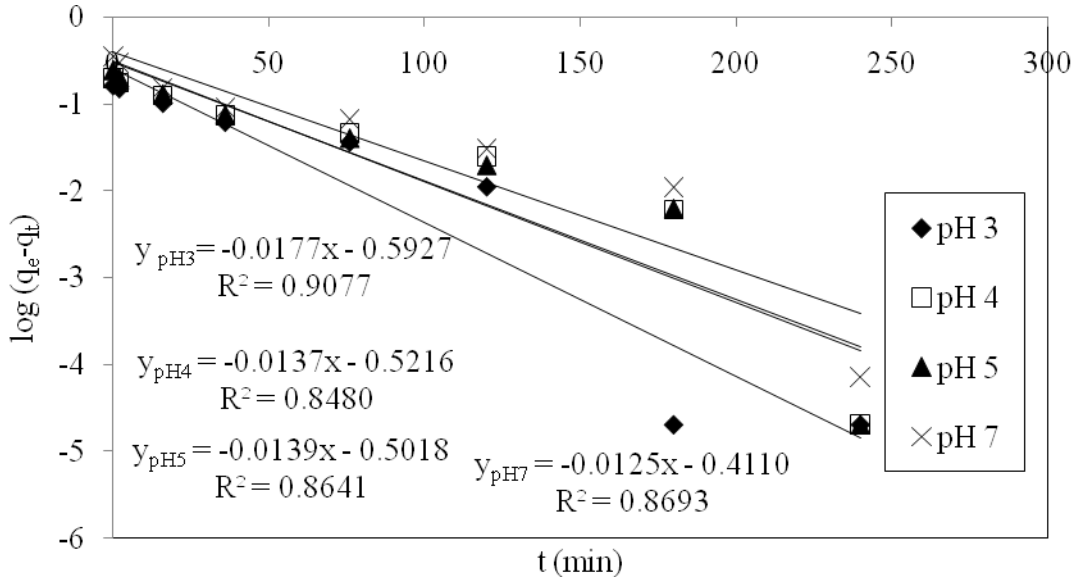

Fig. 5.8: Pseudo-first-order kinetic plots for Cd^{2+} removal at different pH of solution using GAC (Size: 0.6 mm, C_o: 10 ppm, GAC dosage: 0.4 g/100 mL, Temperature: 24°C, Agitation speed: 160 rpm)

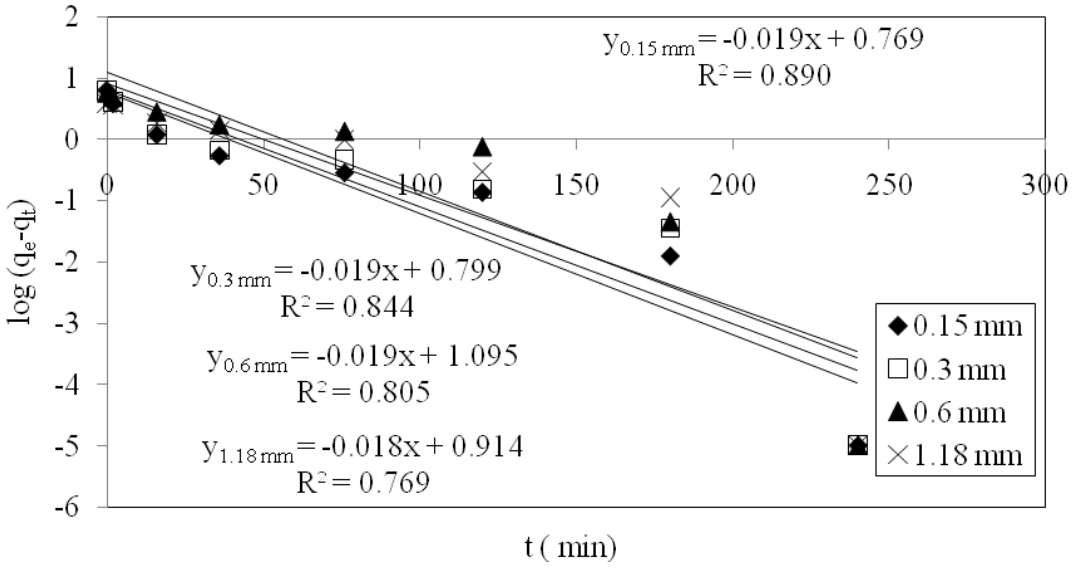

Fig. 5.9: Pseudo-first-order kinetic plots for Zn^{2+} removal at different particle size of PSH (C_o: 30 ppm, PSH dosage: 0.4 g/100mL, pH: 6, Temperature: 24°C, Agitation speed: 160 rpm)

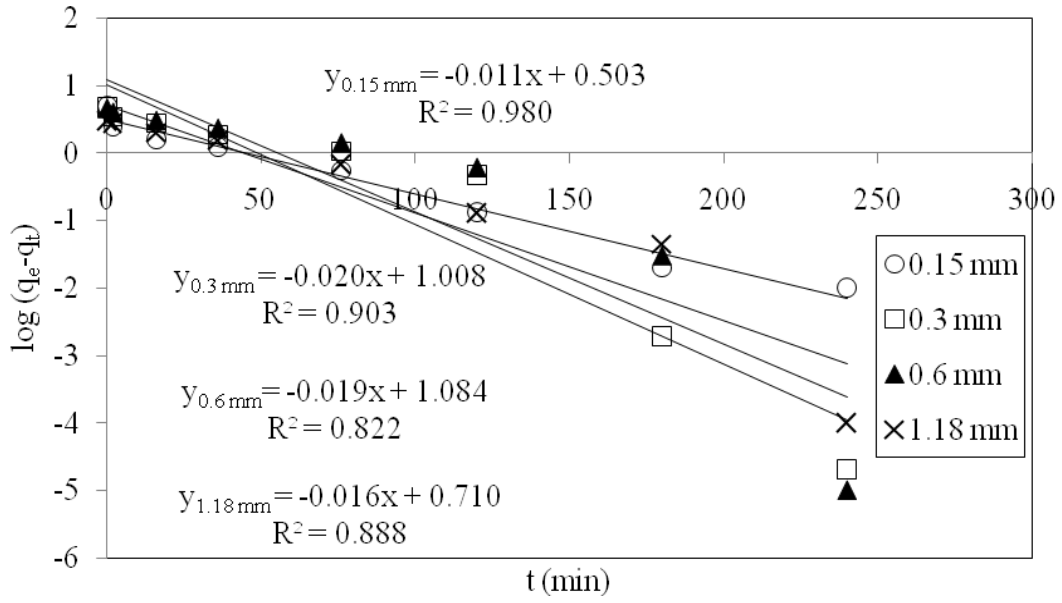

Fig.5.10: Pseudo-first-order kinetic plots for Cd^{2+} removal at different particle size of PSH (C_o: 30 ppm, PSH dosage: 0.4 g/100mL, pH: 6, Temperature: 24^oC, Agitation speed: 160 rpm)

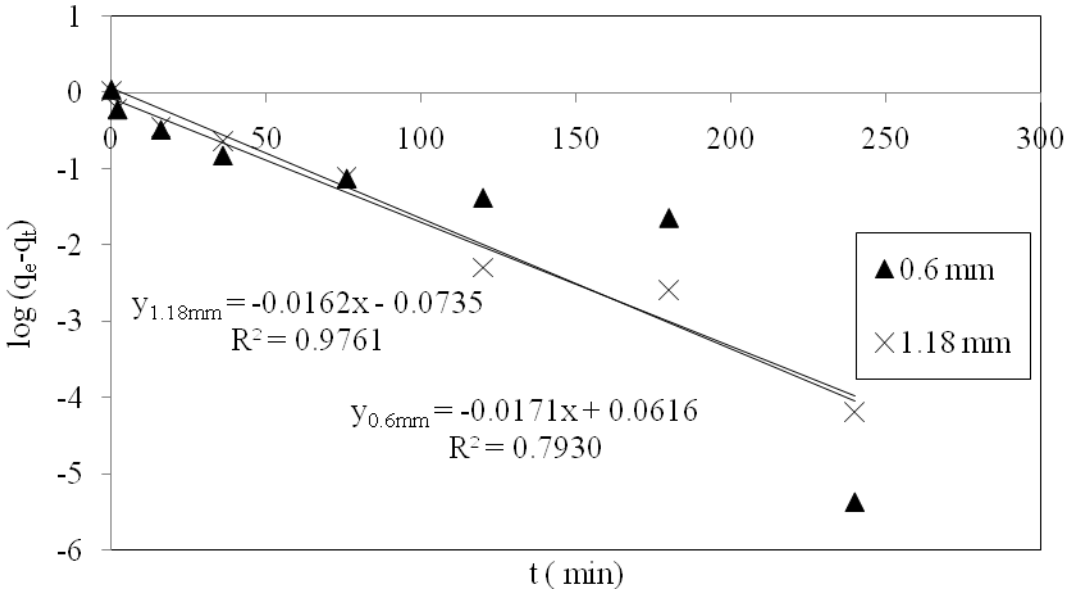

Fig. 5.11: Pseudo-first-order kinetic plots for Zn^{2+} removal at different particle size of GAC (C_o: 30 ppm, GAC dosage: 0.4 g/100mL, pH: 6, Temperature: 24^oC, Agitation speed: 160 rpm)

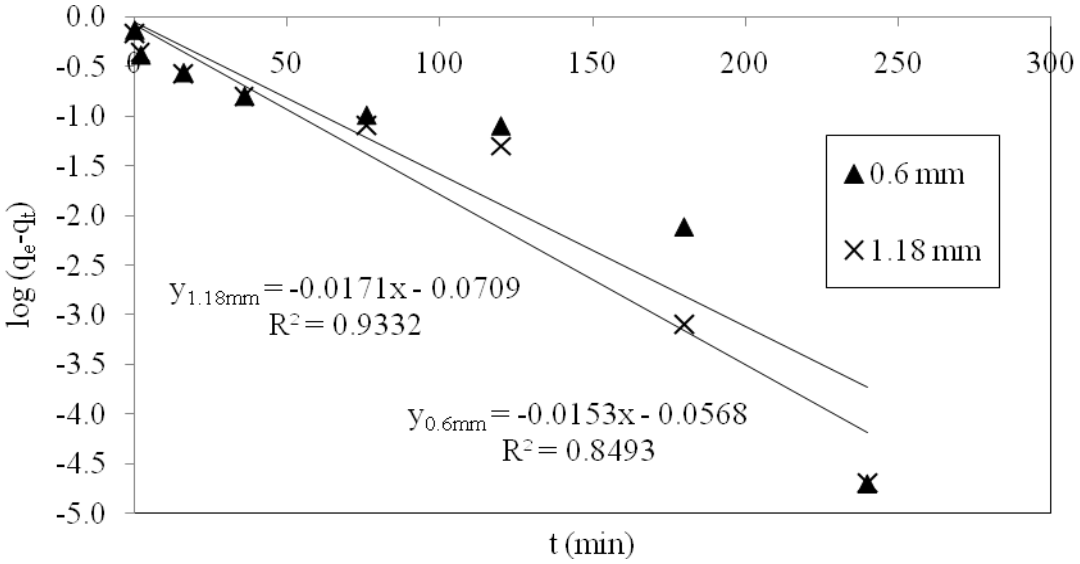

Fig.5.12: Pseudo-first-order kinetic plots for Cd^{2+} removal at different particle size of GAC (C_o: 30 ppm, GAC dosage: 0.4 g/100mL, pH: 6, Temperature: 24°C, Agitation speed: 160 rpm)

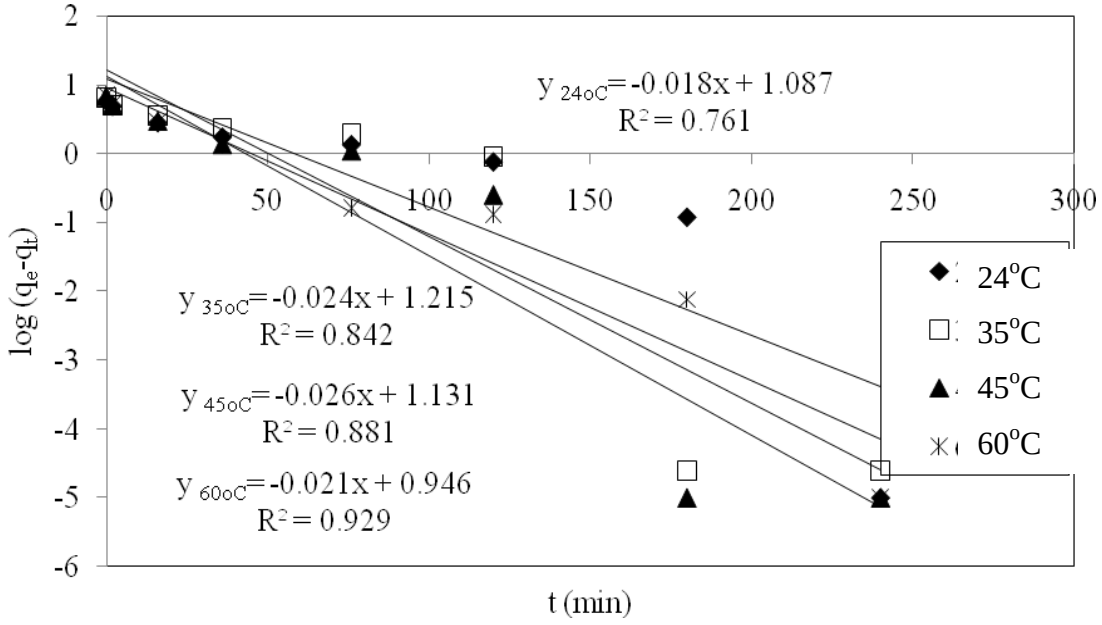

Fig. 5.13: Pseudo-first-order kinetic plots for Zn^{2+} removal at different temperature of solution using PSH (Size: 0.6 mm, C_o: 30 ppm, PSH dosage: 0.4 g/100mL, pH: 6, Agitation speed: 160 rpm)

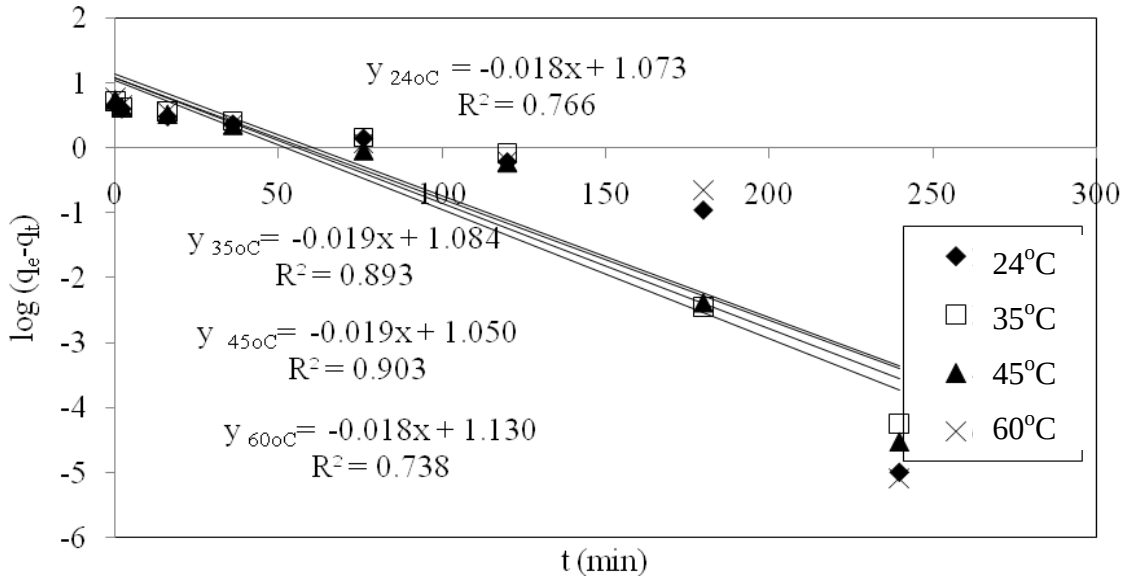

Fig. 5.14: Pseudo-first-order kinetic plots for Cd^{2+} removal at different temperature of solution using PSH (Size: 0.6 mm, C_o: 30 ppm, PSH dosage: 0.4 g/100mL, pH: 6, Agitation speed: 160 rpm)

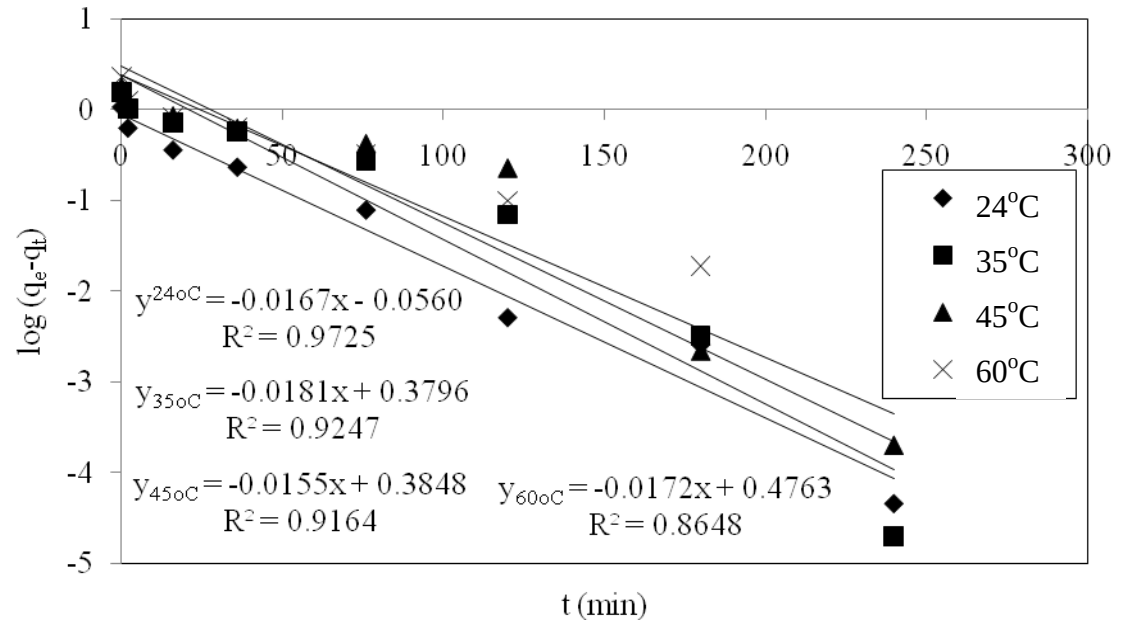

Fig. 5.15: Pseudo-first-order kinetic plots for Zn^{2+} removal at different temperature of solution using GAC (Size: 0.6 mm, C_o: 30 ppm, GAC dosage: 0.4 g/100mL, pH: 6, Agitation speed: 160 rpm)

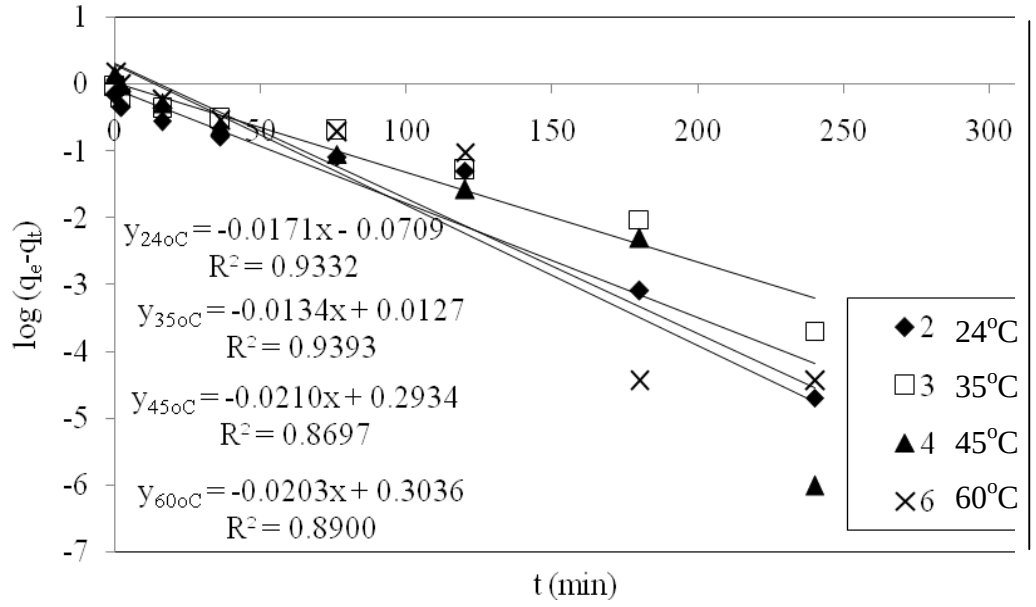

Fig. 5.16: Pseudo-first-order kinetic plots for Cd^{2+} removal at different temperature of solution using GAC (Size: 0.6 mm, C_o: 30 ppm, GAC dosage: 0.4 g/100mL, pH: 6)

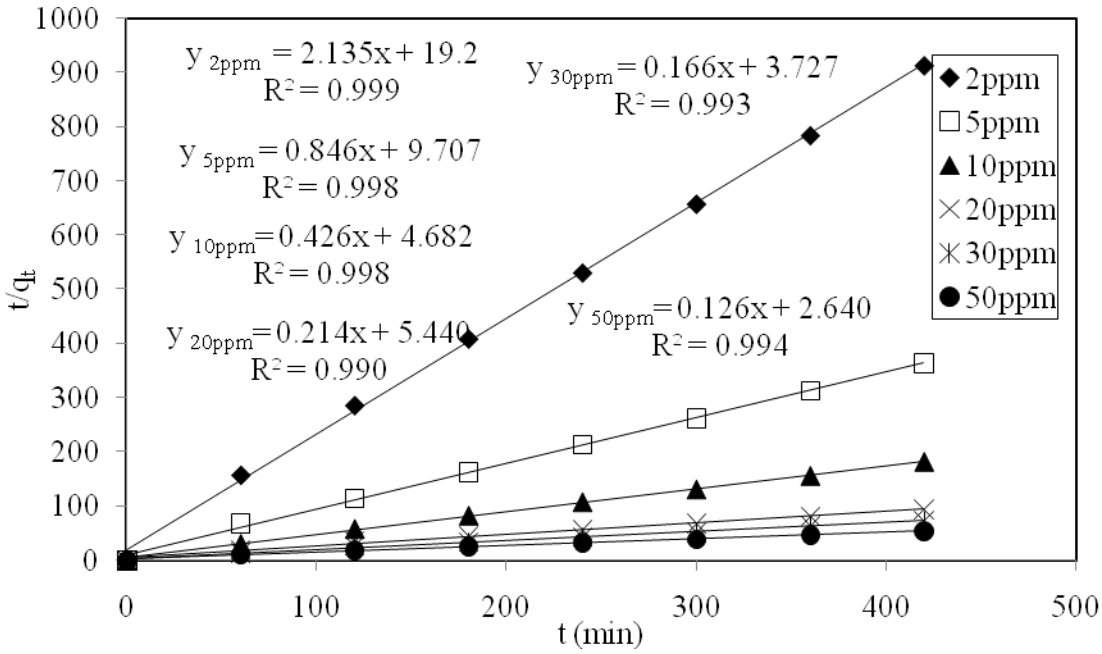

Fig. 5.17: Pseudo-second-order kinetic plots for Zn^{2+} removal at different initial concentrations of solution using PSH (Size: 0.6 mm, PSH dosage: 0.4 g/100mL, pH: 6, Temperature: 24°C, Agitation speed: 160 rpm)

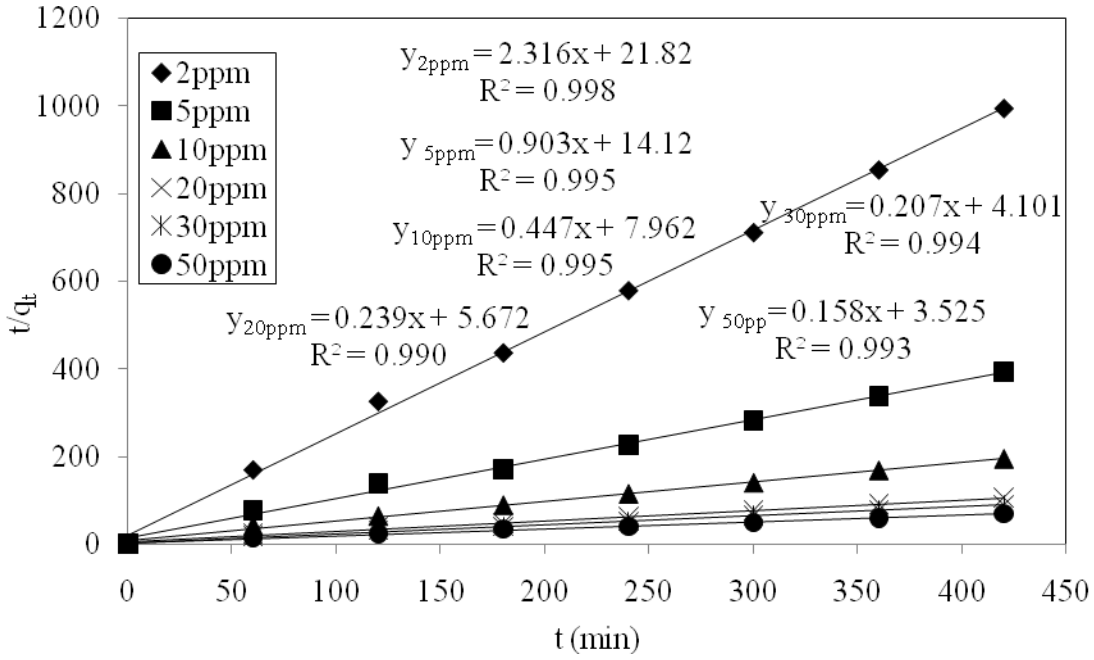

Fig. 5.18: Pseudo-second-order kinetic plots for Cd^{2+} removal at different initial concentrations of solution using PSH (Size: 0.6 mm, PSH dosage: 0.4 g/100mL, pH: 6, Temperature: 24°C, Agitation speed: 160 rpm)

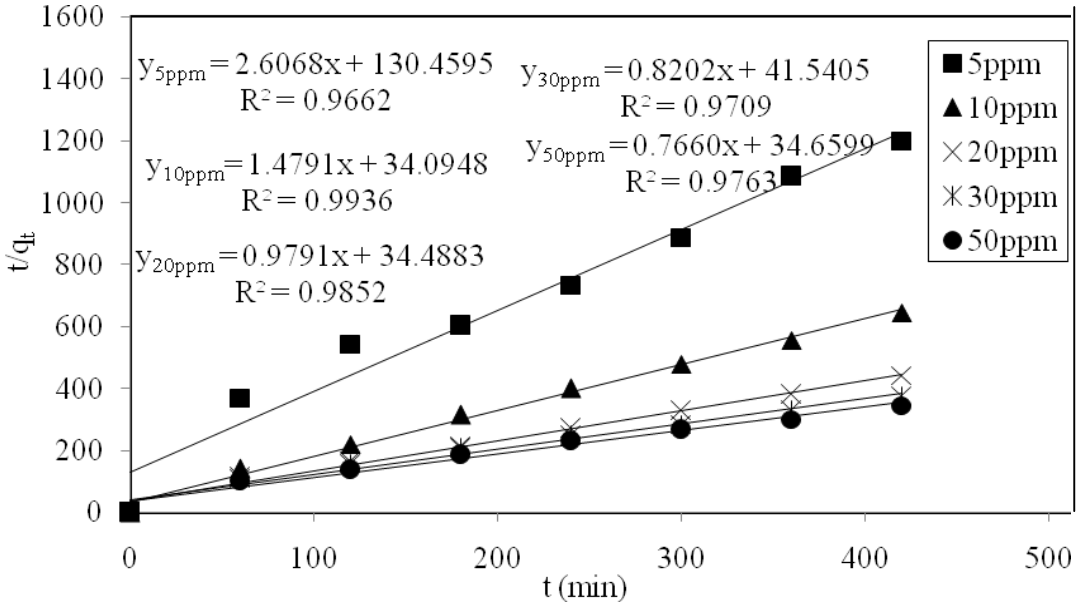

Fig. 5.19: Pseudo-second-order kinetic plots for Zn^{2+} removal at different initial concentrations of solution using GAC (Size: 0.6 mm, GAC dosage: 0.4 g/100mL, pH: 6, Temperature: 24°C, Agitation speed: 160 rpm)

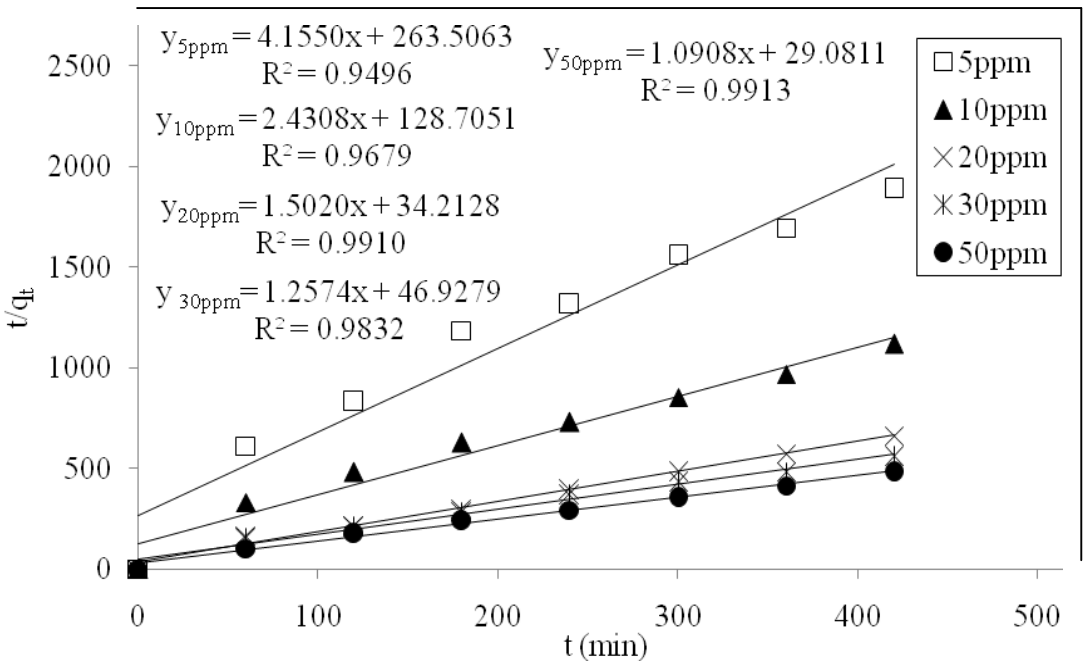

Fig. 5.20: Pseudo-second-order kinetic plots for Cd^{2+} removal at different initial concentrations of solution using GAC (Size: 0.6 mm, GAC dosage: 0.4 g/100mL, pH: 6, Temperature: 24^{o}C, Agitation speed: 160 rpm)

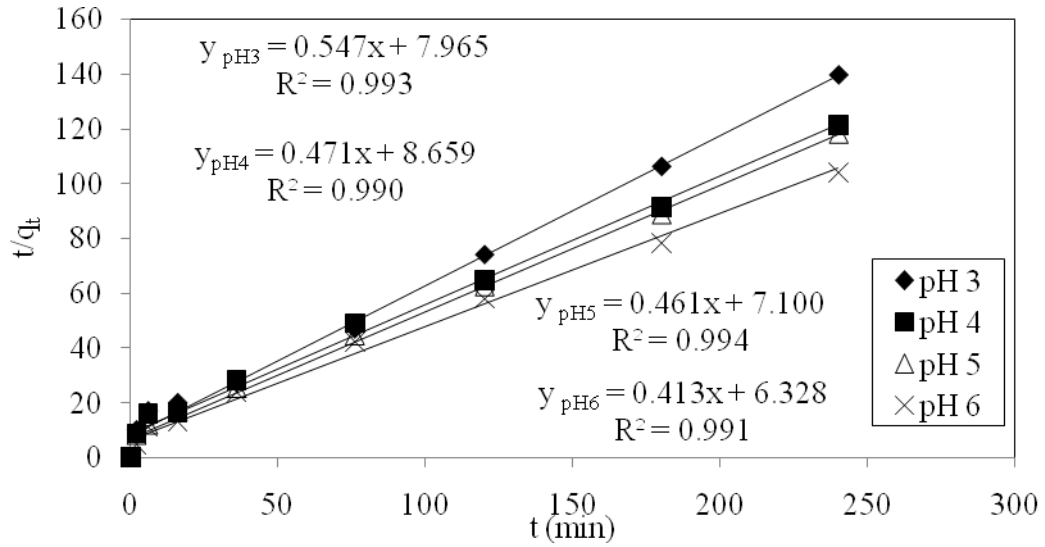

Fig. 5.21: Pseudo-second-order kinetic plots for Zn^{2+} removal at different pH of solution using PSH (Size: 0.6 mm, C_o: 10 ppm, PSH dosage: 0.4 g/100mL, Temperature: 24^{o}C, Agitation speed: 160 rpm)

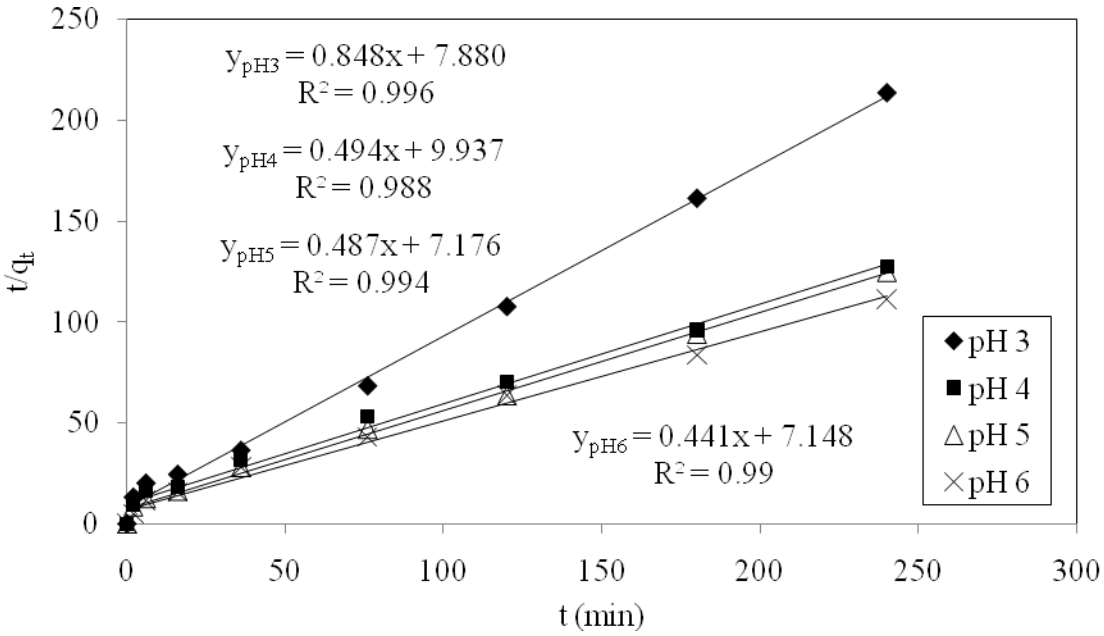

Fig. 5.22: Pseudo-second-order kinetic plots for Cd^{2+} removal at different pH of solution using PSH (Size: 0.6 mm, C_o: 10 ppm, PSH dosage: 0.4 g/100mL, Temperature: 24°C, Agitation speed: 160 rpm)

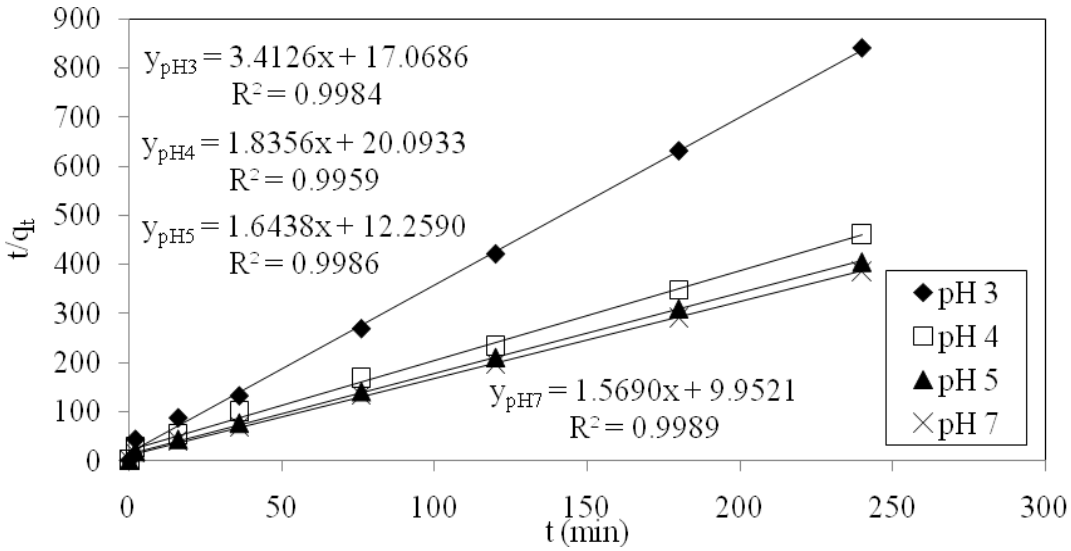

Fig. 5.23: Pseudo-second-order kinetic plots for Zn^{2+} removal at different pH of solution using GAC (Size: 0.6 mm, C_o: 10 ppm, GAC dosage: 0.4 g/100mL, Temperature: 24°C, Agitation speed: 160 rpm)

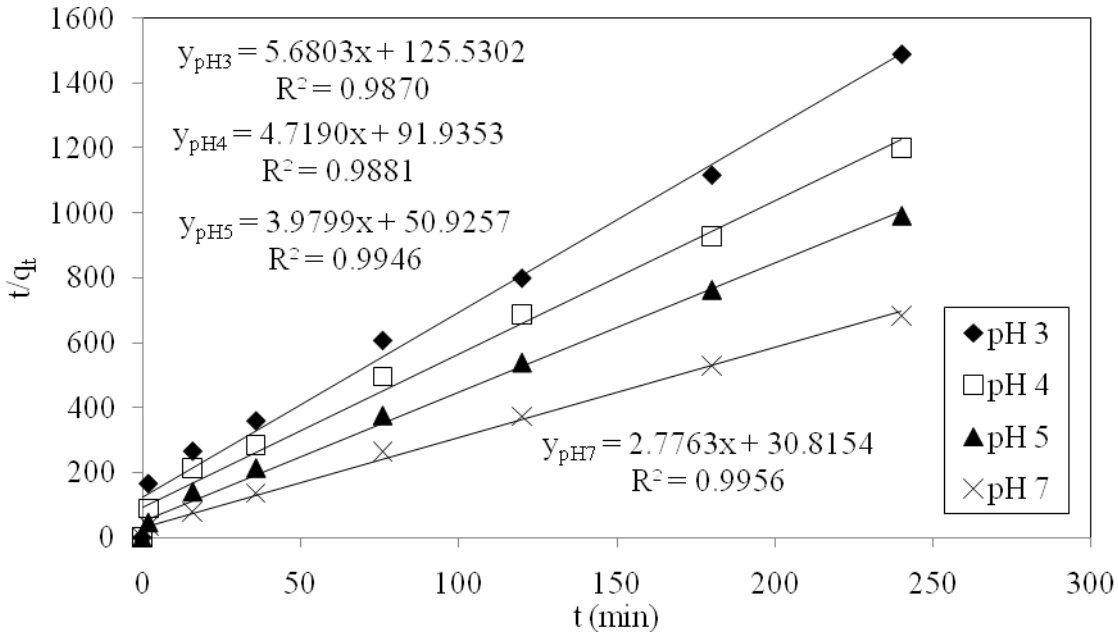

Fig. 5.24: Pseudo-second-order kinetic plots for Cd^{2+} removal at different pH of solution using GAC (Size: 0.6 mm, C_o: 10 ppm, GAC dosage: 0.4 g/100mL, Temperature: 24°C, Agitation speed: 160 rpm)

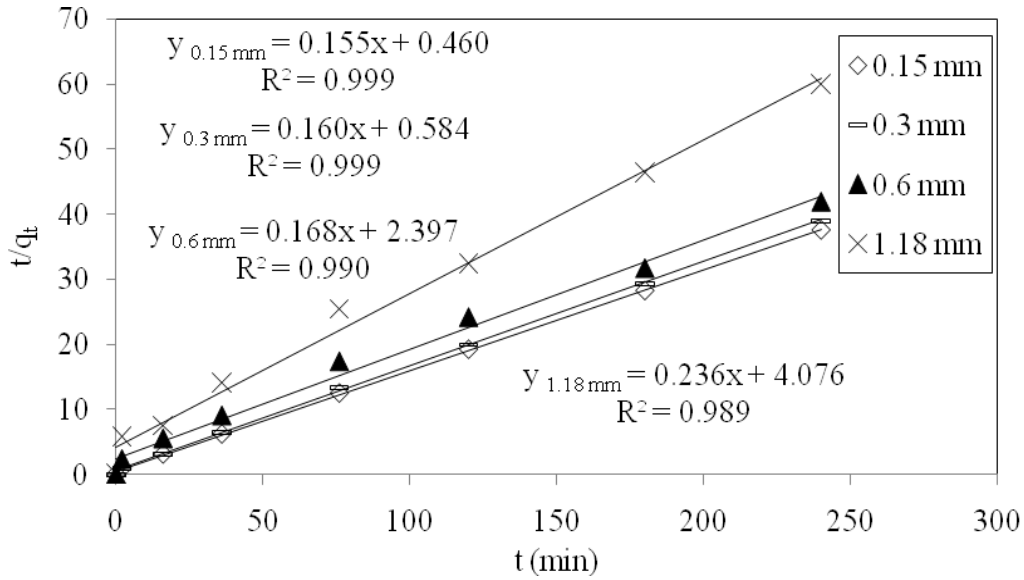

Fig. 5.25: Pseudo-second-order kinetic plots for Zn^{2+} removal at different particle size of PSH (C_o: 30 ppm, PSH dosage: 0.4 g/100mL, pH: 6, Temperature: 24°C, Agitation speed: 160 rpm)

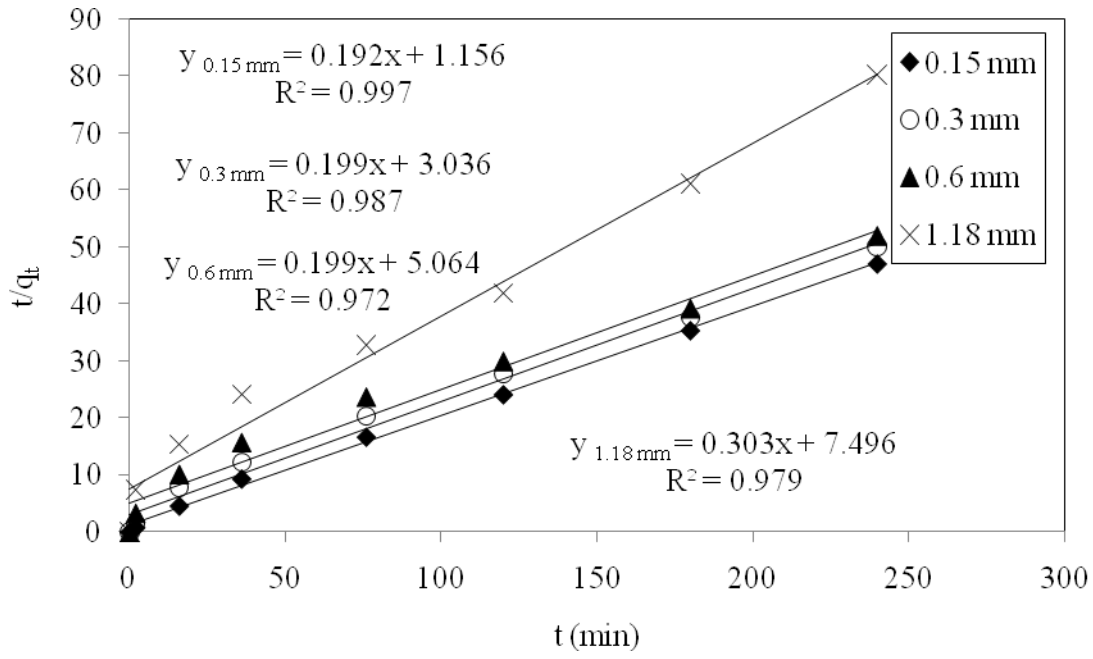

Fig. 5.26: Pseudo-second-order kinetic plots for Cd^{2+} removal at different particle size of PSH (C_o: 30 ppm, PSH dosage: 0.4 g/100mL, pH: 6, Temperature: 24^oC, Agitation speed: 160 rpm)

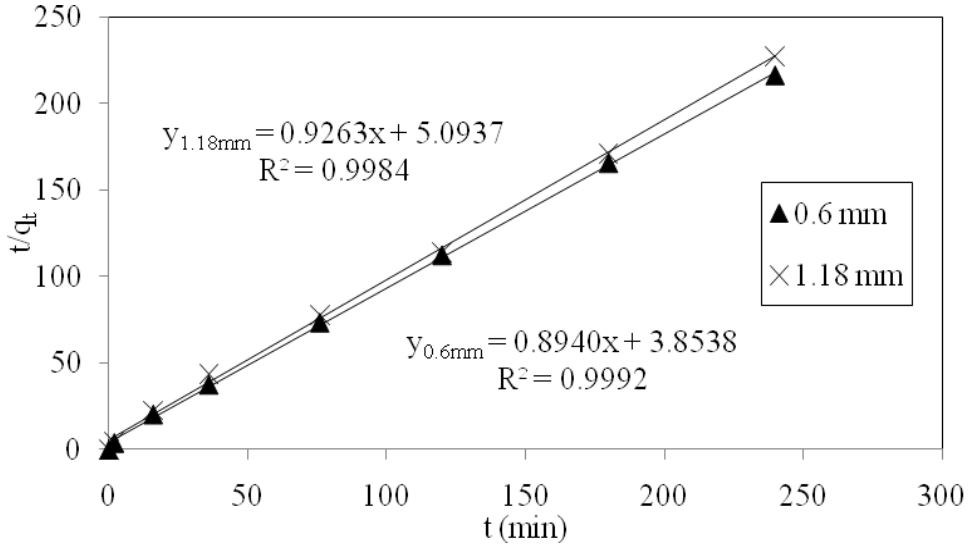

Fig. 5.27: Pseudo-second-order kinetic plots for Zn^{2+} removal at different particle size of GAC (C_o: 30 ppm, GAC dosage: 0.4 g/100mL, pH: 6, Temperature: 24^oC, Agitation speed: 160 rpm)

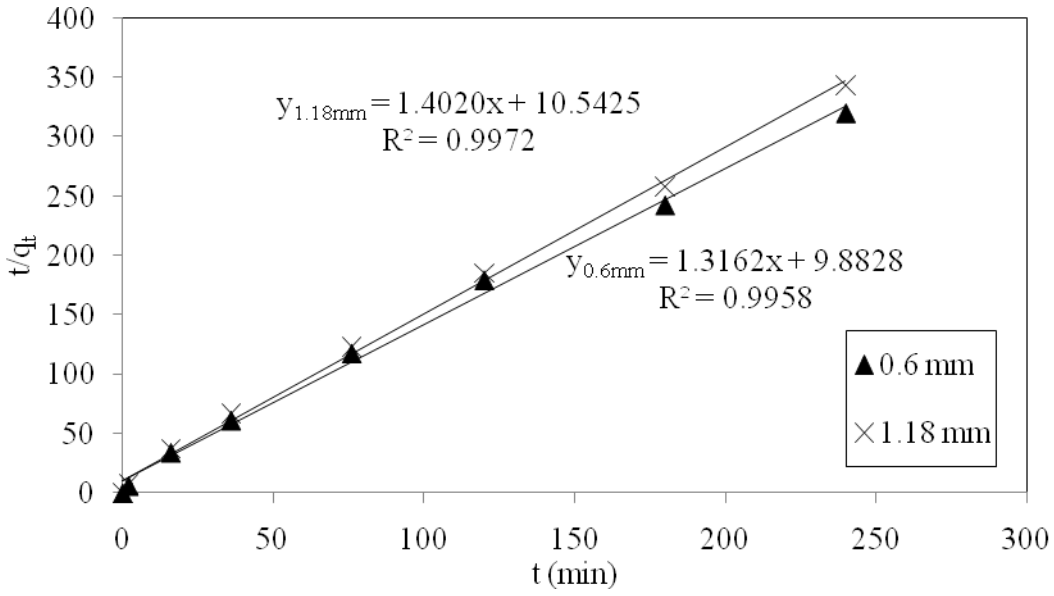

Fig. 5.28: Pseudo-second-order kinetic plots for Cd^{2+} removal at different particle size of GAC (C_o: 30 ppm, GAC dosage: 0.4 g/100mL, pH: 6, Temperature: 24°C, Agitation speed: 160 rpm)

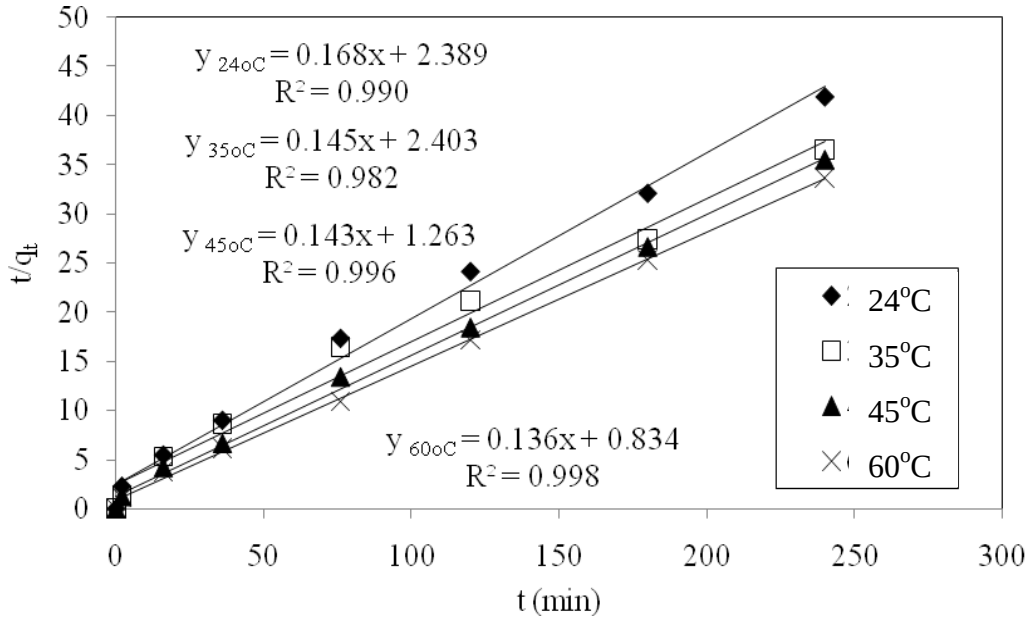

Fig. 5.29: Pseudo-second-order kinetic plots for Zn^{2+} removal at different temperature of solution using PSH (Size: 0.6 mm, C_o: 30 ppm, PSH dosage: 0.4 g/100mL, pH: 6, Agitation speed: 160 rpm)

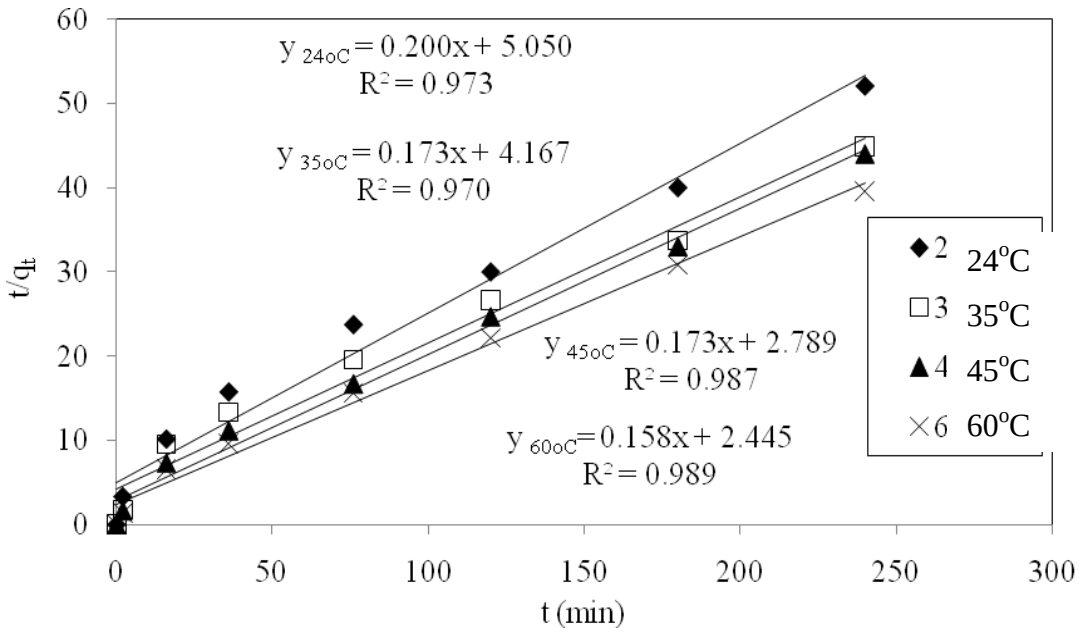

Fig. 5.30: Pseudo-second-order kinetic plots for Cd^{2+} removal at different temperature of solution using PSH (Size: 0.6 mm, C_o: 30 ppm, PSH dosage: 0.4 g/100mL, pH: 6, Agitation speed: 160 rpm)

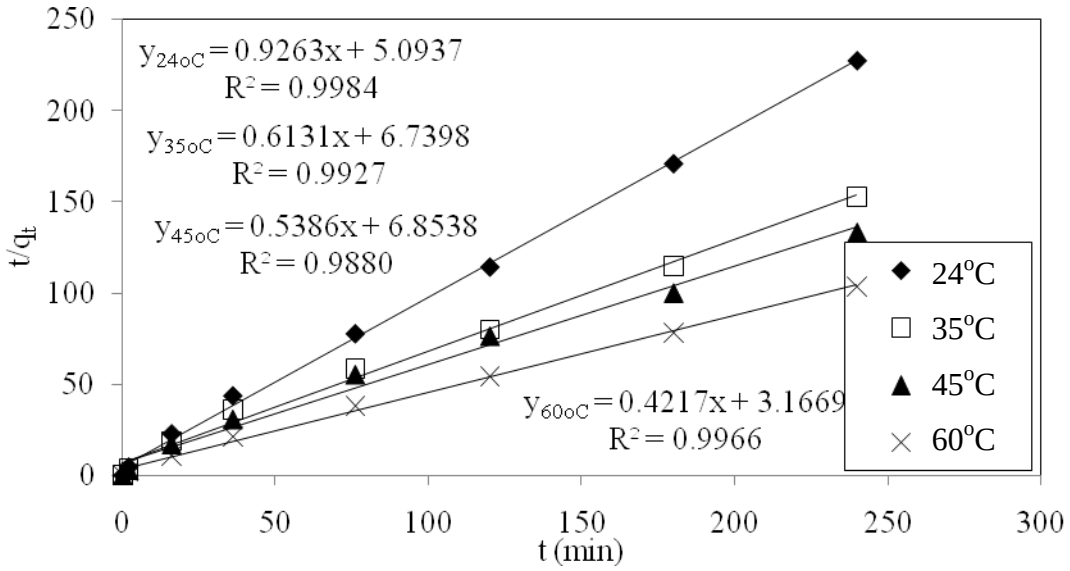

Fig. 5.31: Pseudo-second-order kinetic plots for Zn^{2+} removal at different temperature of solution using GAC (Size: 0.6 mm, C_o: 30 ppm, GAC dosage: 0.4 g/100mL, pH: 6, Agitation speed: 160 rpm)

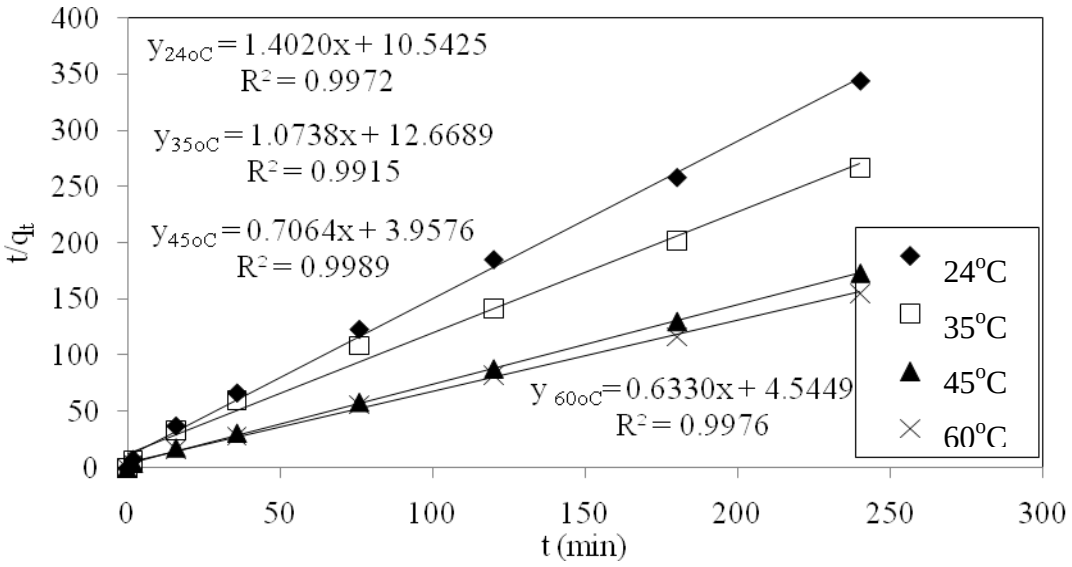

Fig. 5.32: Pseudo-second-order kinetic plots for Cd^{2+} removal at different temperature of solution using GAC (Size: 0.6 mm, C_o: 30 ppm, GAC dosage: 0.4 g/100mL, pH: 6, Agitation speed: 160 rpm)

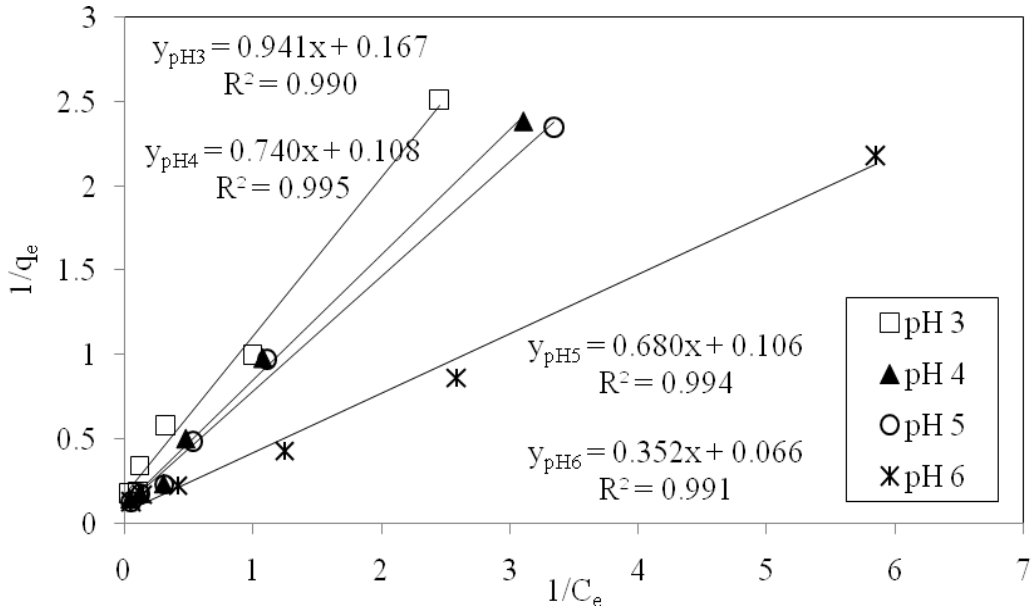

Fig. 5.33: Langmuir isotherm for the adsorption of Zn^{2+} onto PSH at different pH of solution (Size: 0.6 mm, PSH dosage: 0.4 g/100mL, C_o: 30 ppm, Temperature: 24°C, Agitation speed: 160 rpm)

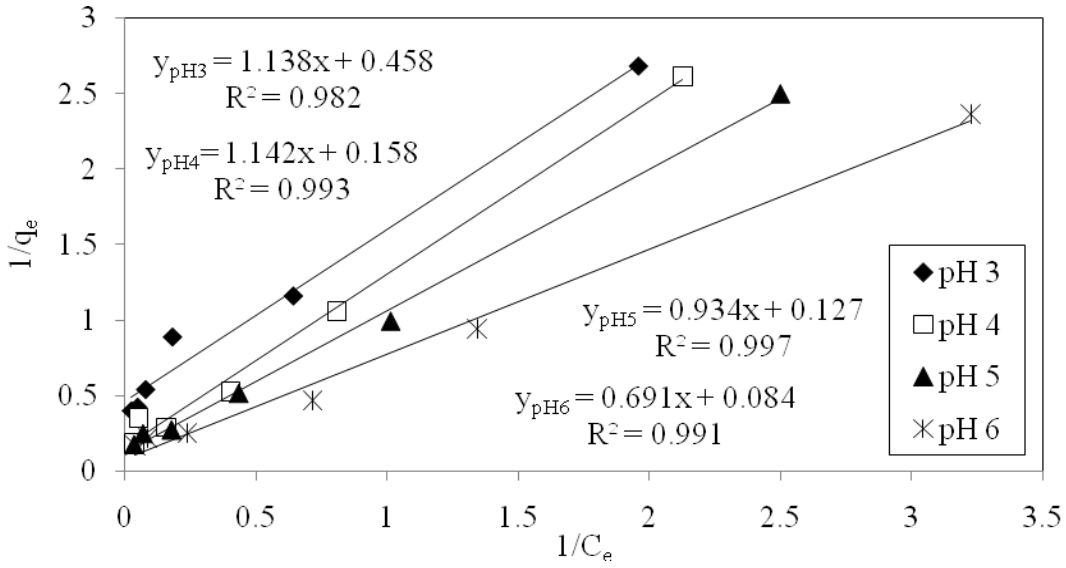

Fig. 5.34: Langmuir isotherm for the adsorption of Cd^{2+} onto PSH at different pH of solution (Size: 0.6 mm, PSH dosage: 0.4 g/100mL, Temperature: 24°C, C_o: 30 ppm, Agitation speed: 160 rpm)

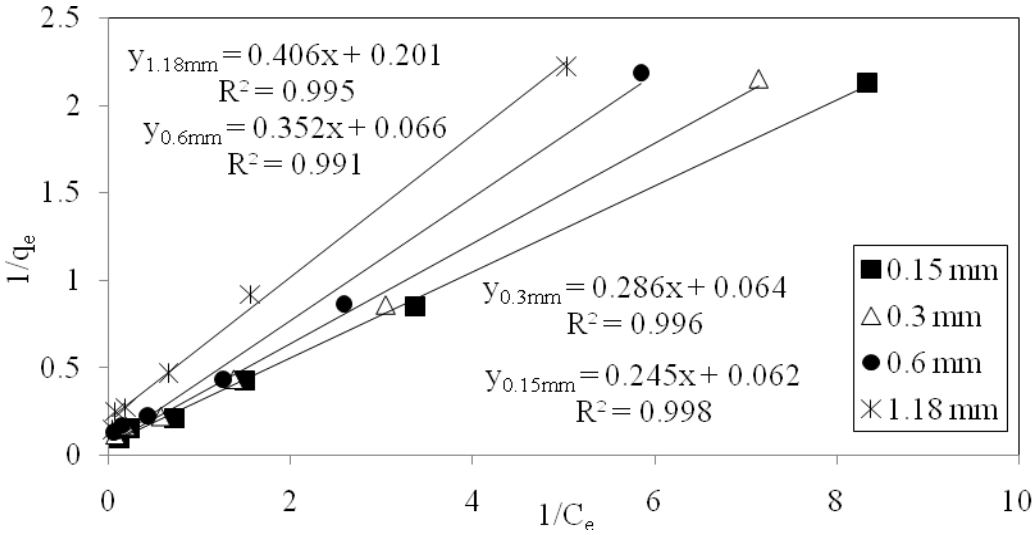

Fig. 5.35: Langmuir isotherm for the adsorption of Zn^{2+} onto PSH at different particle size area (PSH dosage: 0.4 g/100mL, pH: 6, Temperature: 24°C, C_o: 30 ppm, Agitation speed: 160 rpm)

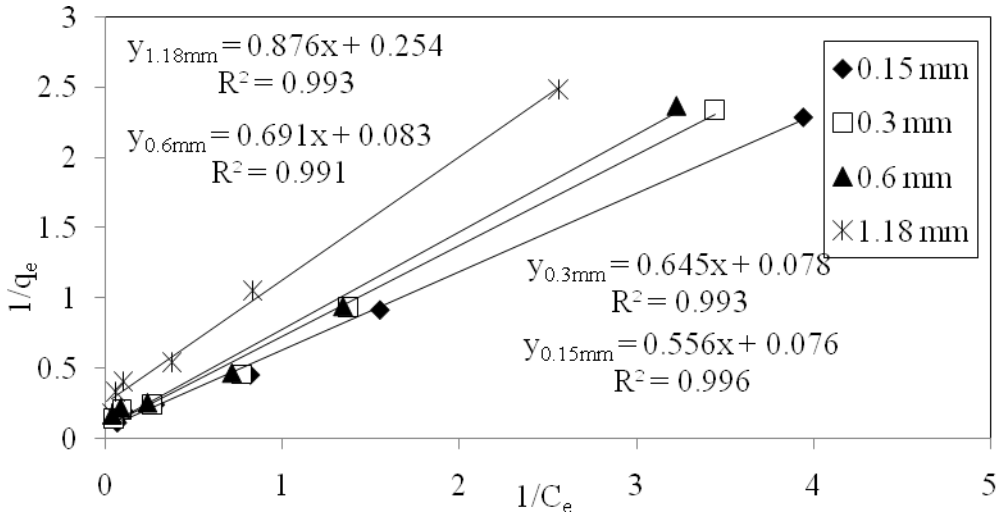

Fig. 5.36: Langmuir isotherm for the adsorption of Cd^{2+} onto PSH at different particle size area (PSH dosage: 0.4 g/100mL, pH: 6, Temperature: 24°C, C_o: 30 ppm, Agitation speed: 160 rpm)

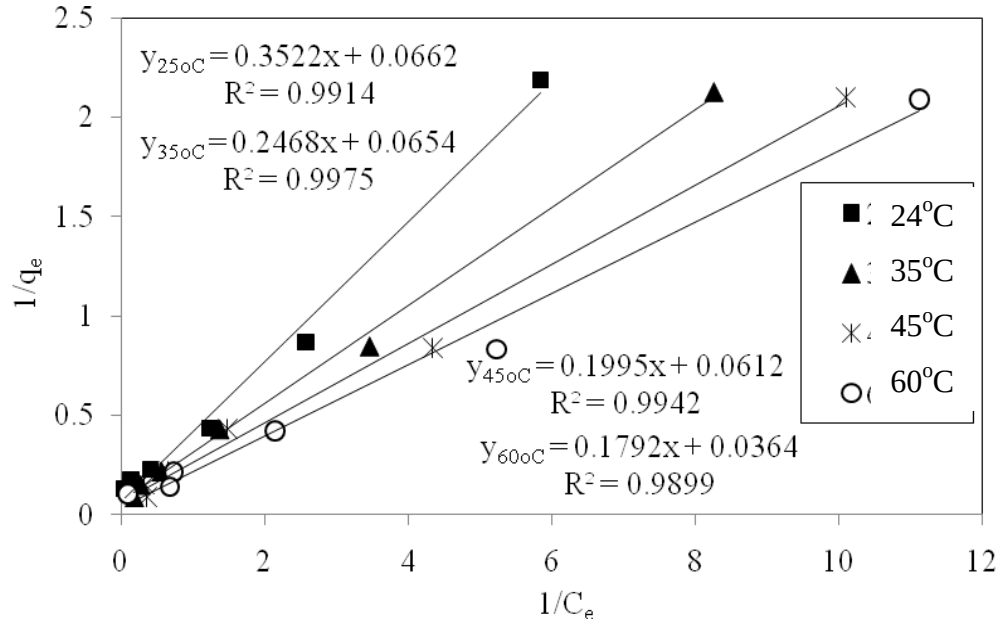

Fig. 5.37: Langmuir isotherm for the adsorption of Zn^{2+} onto PSH at different temperature of solution (Size: 0.6 mm, PSH dosage: 0.4 g/100mL, pH: 6, C_o: 30 ppm, Agitation speed: 160 rpm)

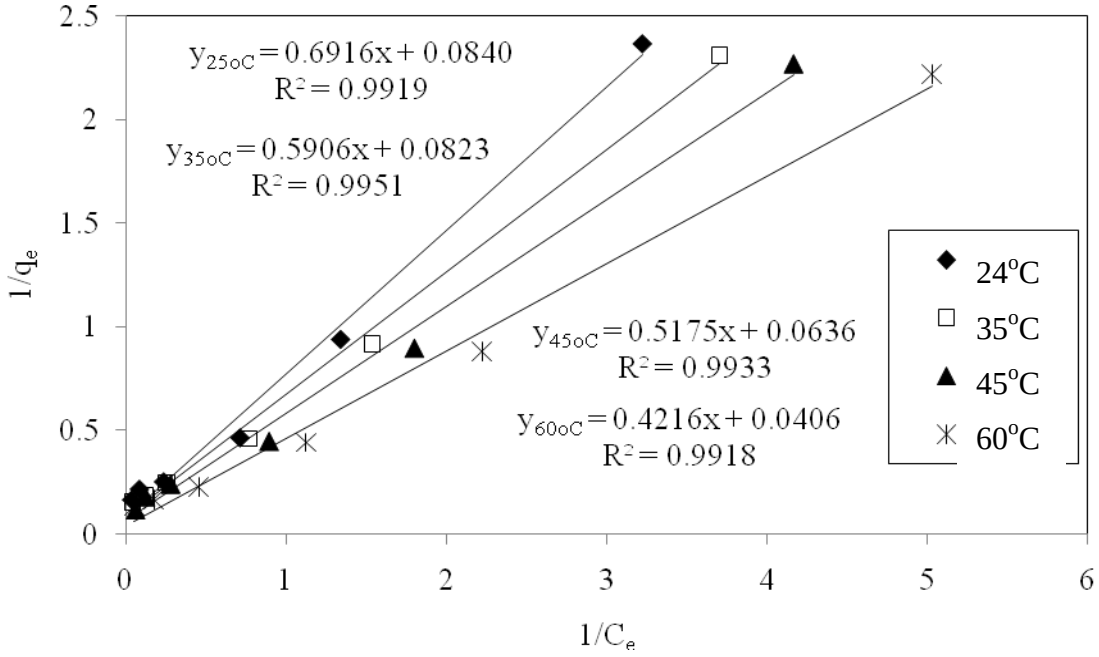

Fig 5.38: Langmuir isotherm for the adsorption of Cd^{2+} onto PSH at different temperature of solution (Size: 0.6 mm, PSH dosage: 0.4 g/100mL, pH: 6, C_o: 30 ppm, Agitation speed: 160 rpm)

METAL ION ADSORPTION ON PSH AND GAC WITH THE EFFECT OF AEROSOL 22

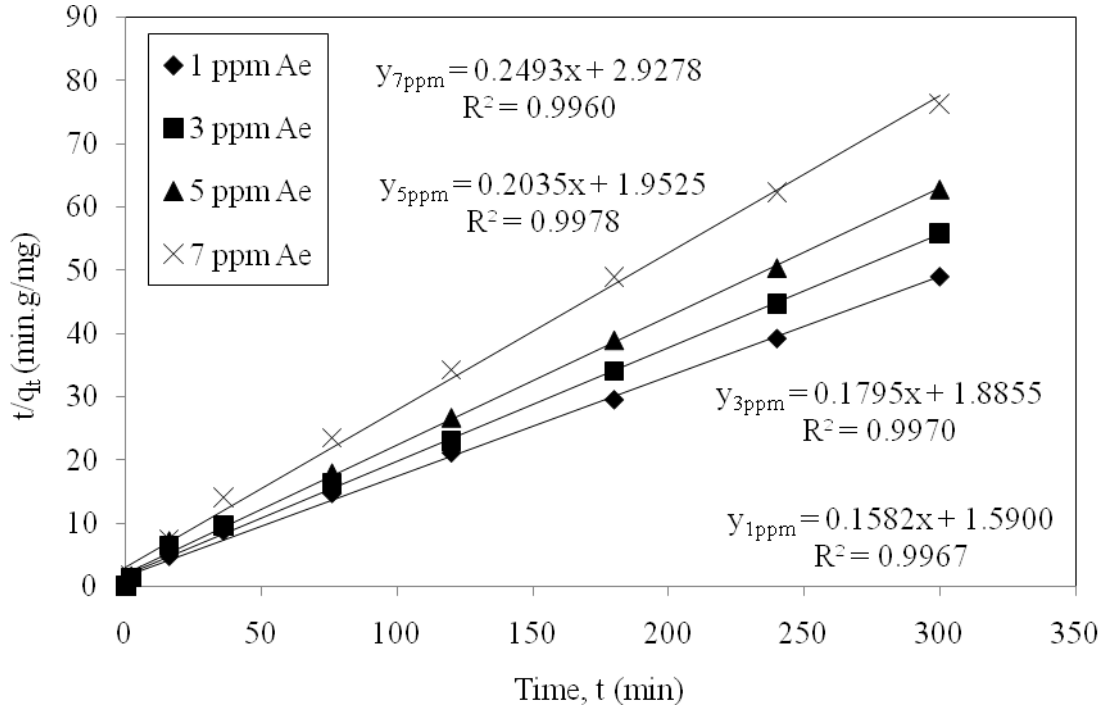

Fig. 5.39: Pseudo-second-order kinetic model for Zn^{2+} adsorption by PSH at different concentration of Aerosol 22 (Metal ion conc.: 30 ppm, PSH dosage: 4g/100mL, Saiz: 0.6 mm, pH: 6, Temperature: 24^0C, Agitation speed: 160 rpm)

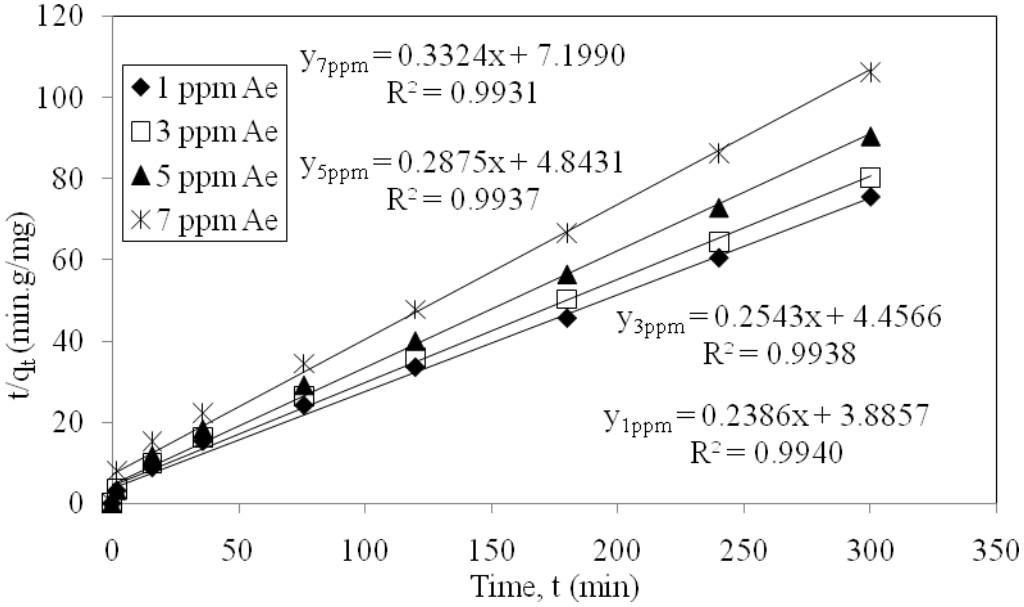

Fig. 5.40: Pseudo-second-order kinetic model for Cd^{2+} adsorption by PSH at different concentration of Aerosol 22 (Metal ion conc.: 30 ppm, PSH dosage: 4g/100mL, Saiz: 0.6mm, pH: 6, Temperature: 24^0C, Agitation speed: 160 rpm)

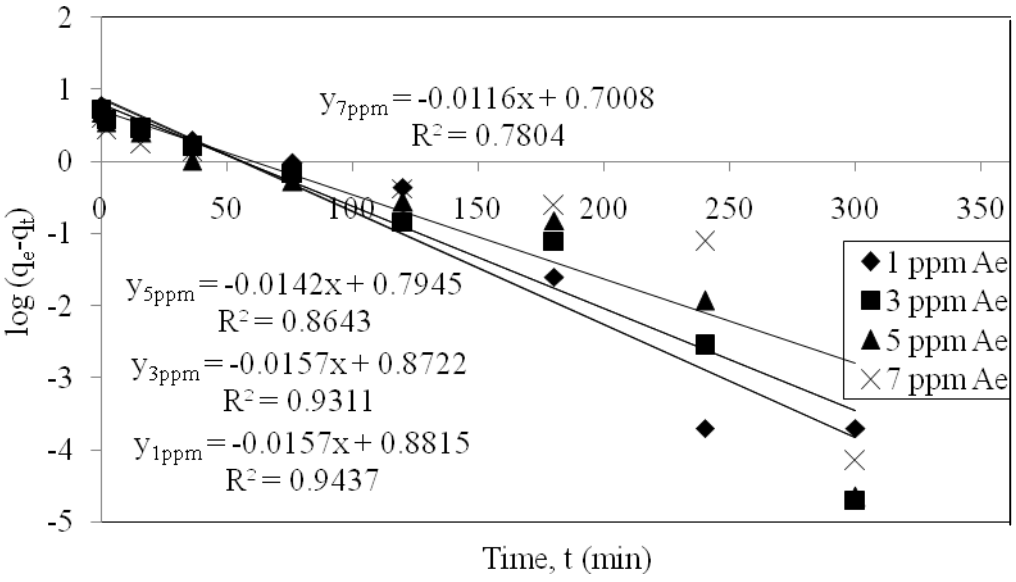

Fig. 5.41: Pseudo-first-order kinetic model for Zn^{2+} adsorption by PSH at different concentration of Aerosol 22 (Metal ion conc.: 30 ppm, PSH dosage: 4g/100mL, Saiz: 0.6mm, pH: 6, Temperature: 24^0C, Agitation speed: 160 rpm)

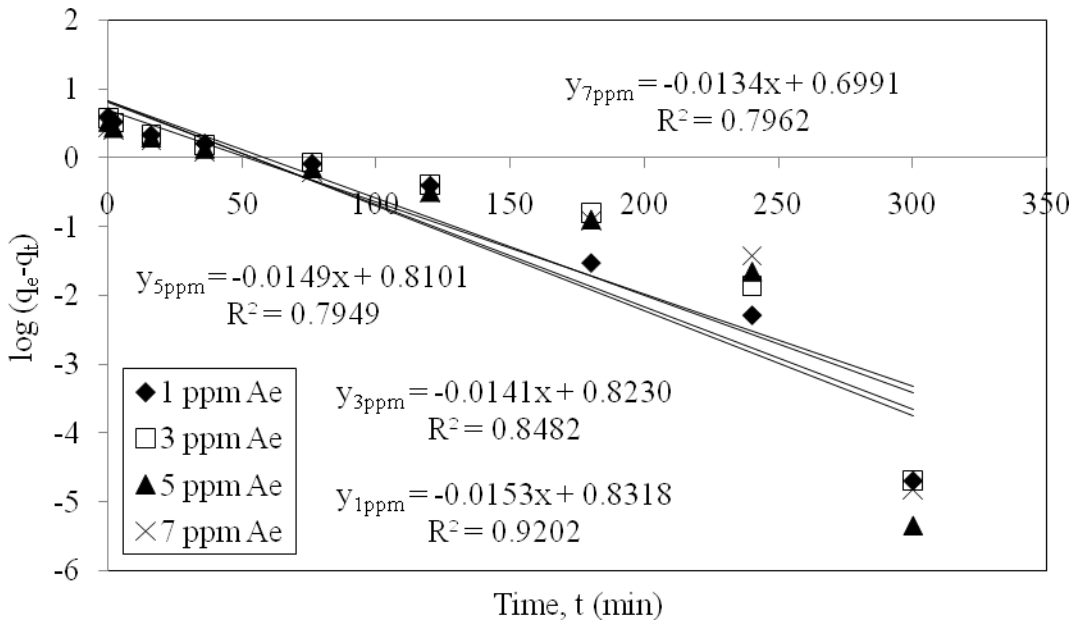

Fig. 5.42: Pseudo-first-order kinetic model for Cd^{2+} adsorption by PSH at different concentration of Aerosol 22 (Metal ion conc.: 30 ppm, PSH dosage: 4g/100mL, Saiz: 0.6mm, pH: 6, Temperature: 24^0C, Agitation speed: 160 rpm)

MG DYE ADSORPTION ON PSH AND GAC

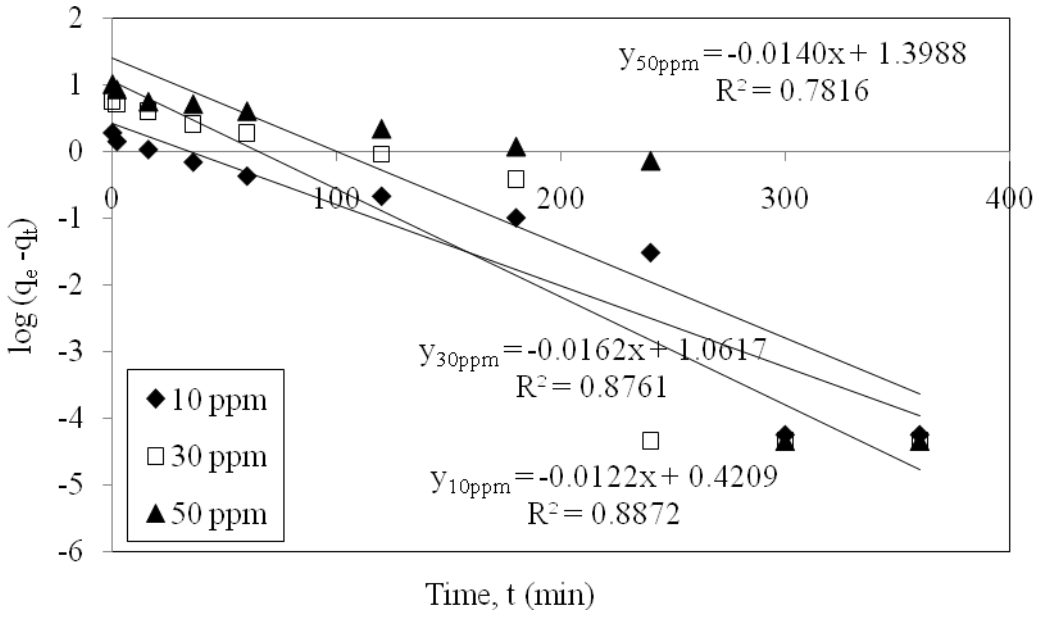

Fig. 5.43: Pseudo-first-order kinetic model for MG adsorption by PSH at different initial dye concentration (PSH dosage: 4 g/L, pH: 6, Agitation speed: 160rpm, Temperature: 24^0C, Size: 0.6mm)

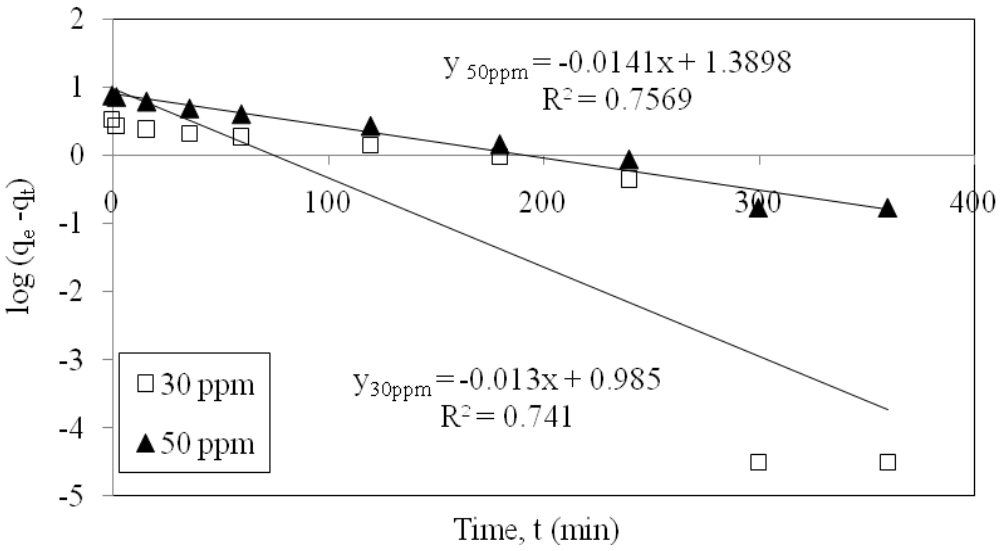

Fig. 5.44: Pseudo-first-order kinetic model for MG adsorption by GAC at different initial dye concentrations (GAC dosage: 4g/L, pH: 6, Agitation speed: 160rpm, Temperature: 24^0C, Size: 0.6mm)

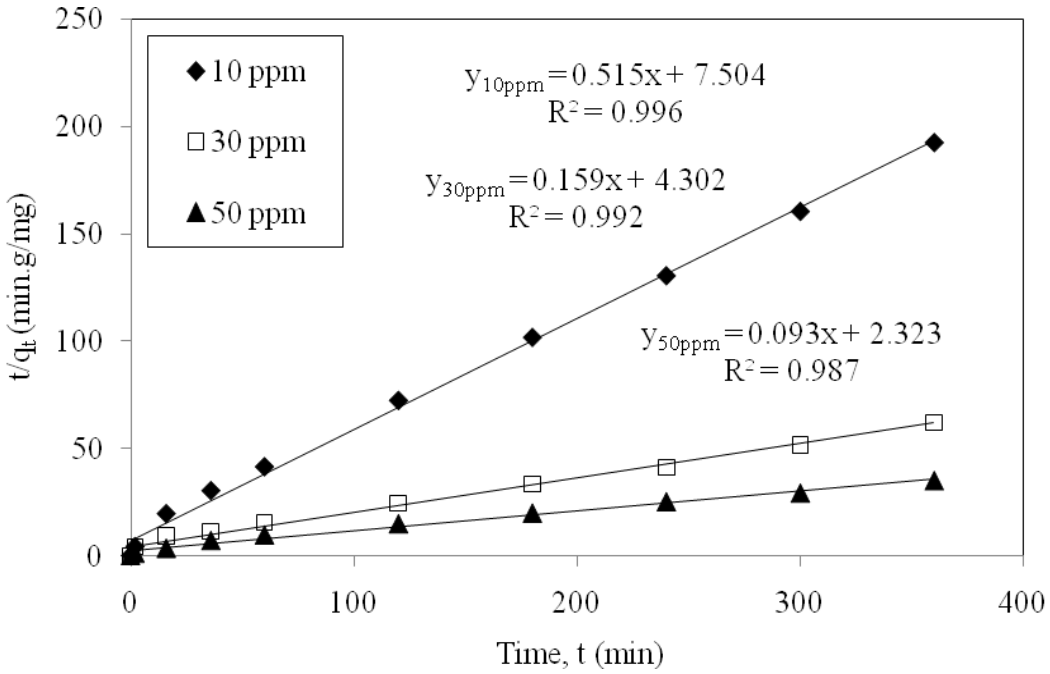

Fig. 5.45: Pseudo-second-order kinetic model for MG adsorption by PSH at different initial dye concentrations (PSH dosage: 4g/L. pH: 6, Agitation speed: 160rpm, Temperature: 24^0C, Size: 0.6mm)

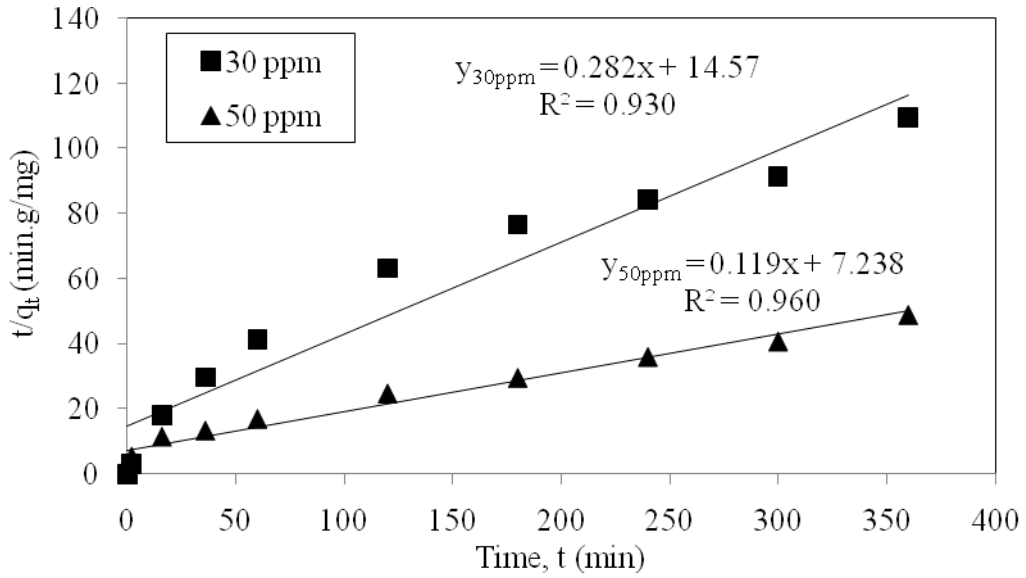

Fig. 5.46: Pseudo-second-order kinetic model for MG adsorption by GAC at different initial dye concentrations (GAC dosage: 4g/L, pH: 6, Agitation speed: 160rpm, Temperature: 24^0C, Size: 0.6mm)

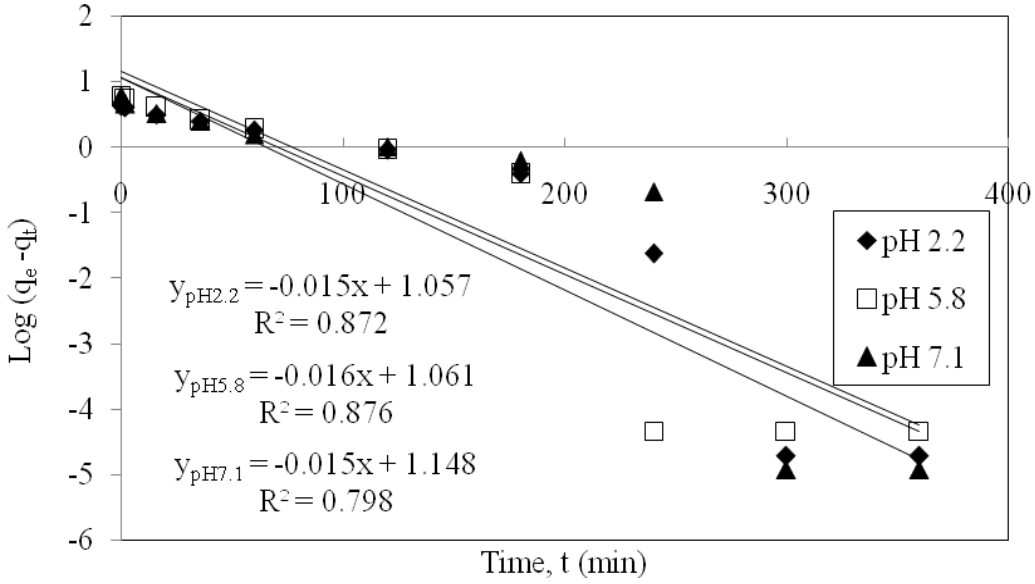

Fig. 5.47: Pseudo-first-order kinetic model for MG adsorption by PSH at different pH of solution (PSH dosage: 4g/L, Agitation speed: 160rpm, Temperature: 24^0C, Size: 0.6mm, C_0: 30ppm)

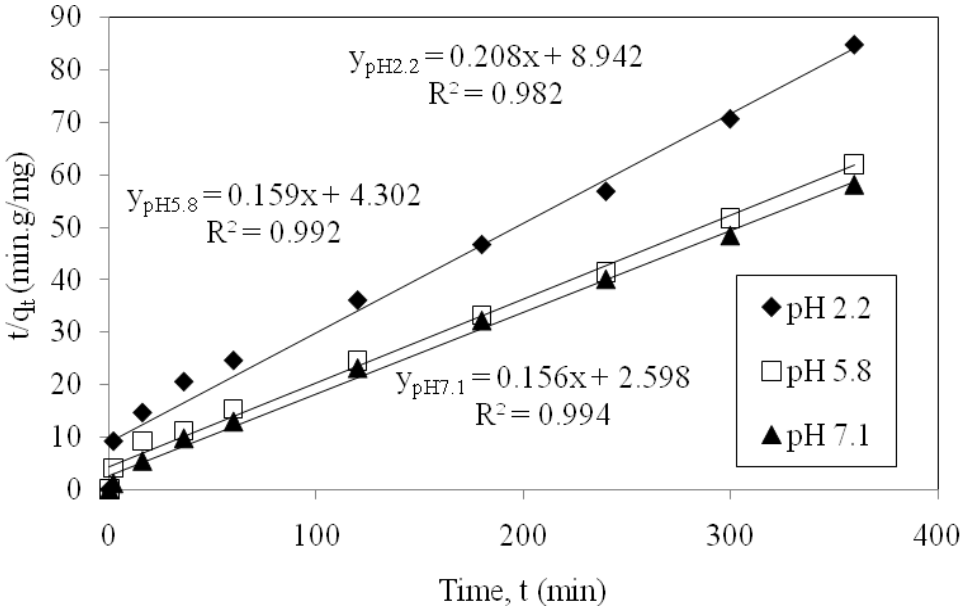

Fig. 5.48: Pseudo-second-order kinetic model for MG adsorption by PSH at different pH of solution (PSH dosage: 4g/L, Agitation speed: 160rpm, Temperature: 24^0C, Size: 0.6mm, C_0: 30ppm)

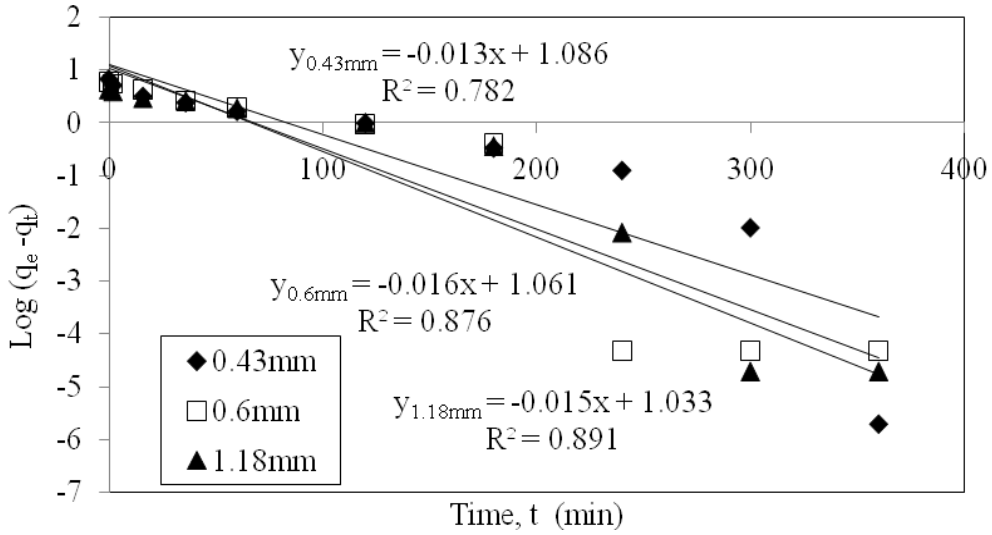

Fig. 5.49: Pseudo-first-order kinetic model for MG adsorption by PSH at different particle size of adsorbent (PSH dosage: 4g/L, pH: 6, Agitation speed: 160rpm, Temperature: 24^0C, C_0: 30ppm)

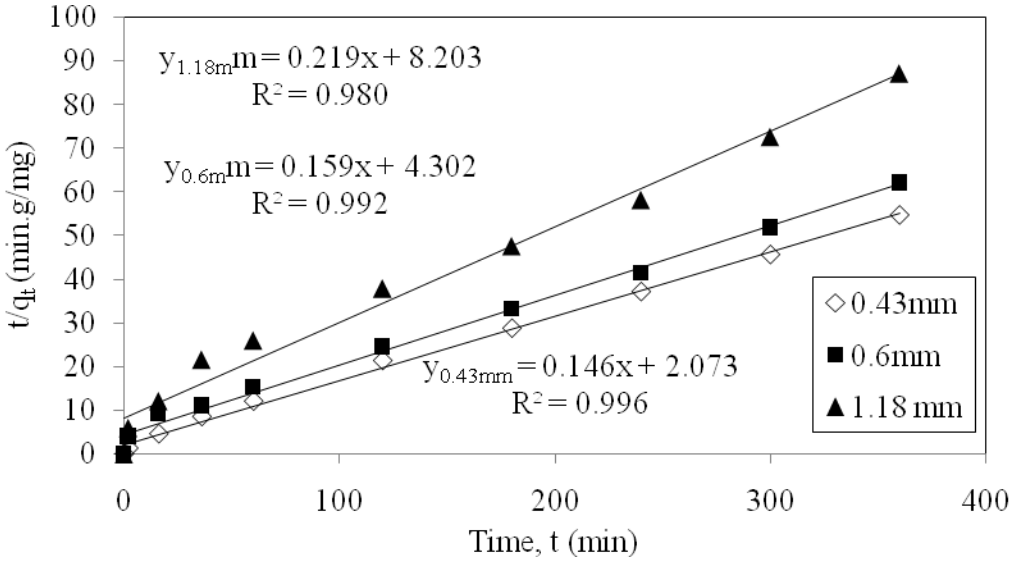

Fig. 5.50: Pseudo-second-order kinetic model for MG adsorption by PSH at different particle size of adsorbent (PSH dosage: 4g/L, pH: 6, Agitation speed: 160rpm, Temperature: 24^0C, C_0: 30ppm)

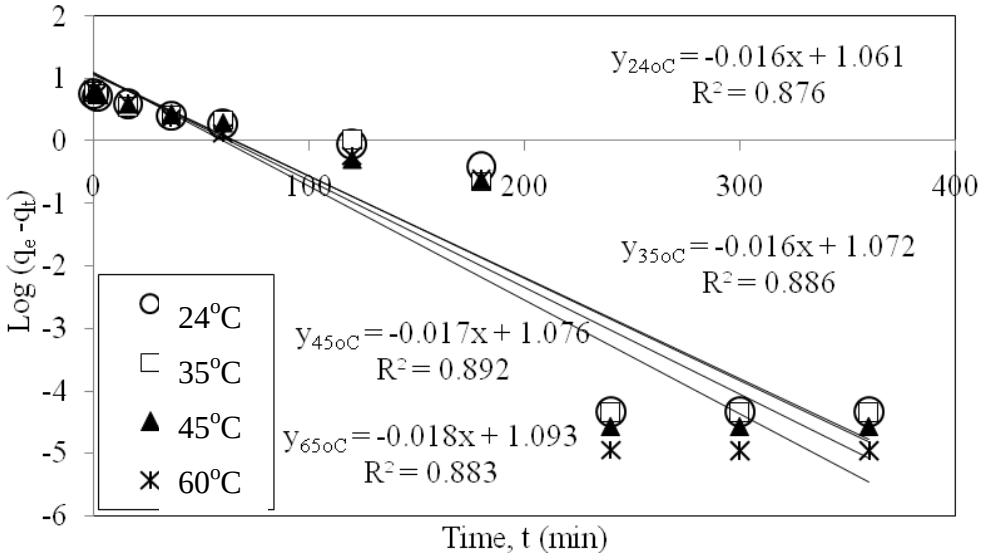

Fig. 5.51: Pseudo-first-order kinetic model for MG adsorption by PSH at different temperature of solution (PSH dosage: 4g/L, pH: 6, Agitation speed: 160rpm, Size: 0.6mm, C_0: 30ppm)

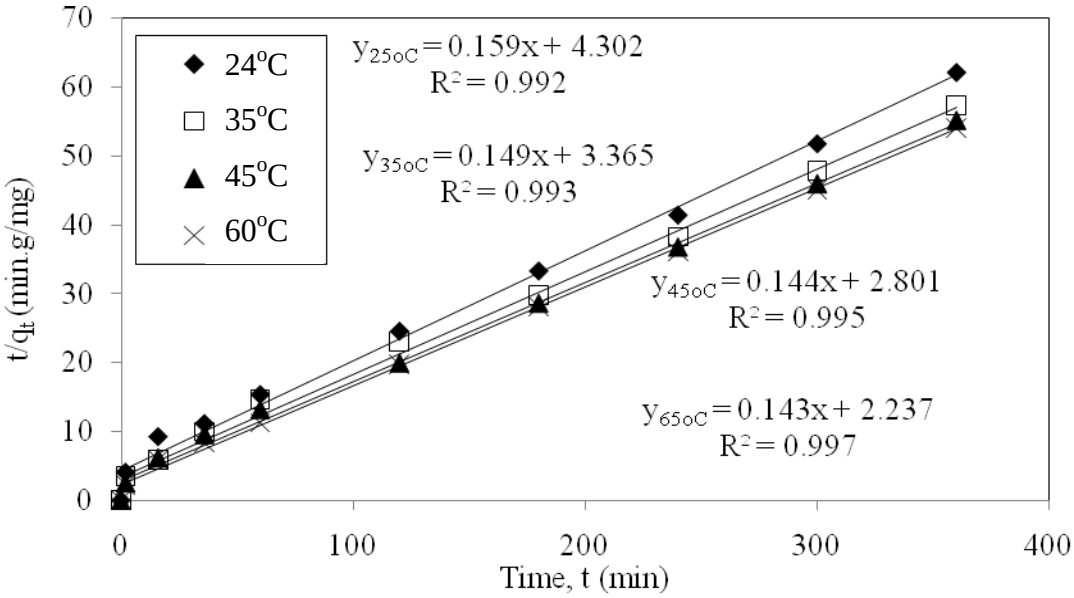

Fig. 5.52: Pseudo-second-order kinetic model for MG adsorption by PSH at different temperature of solution (PSH dosage: 4g/L. pH: 6, Agitation speed: 160rpm, Size: 0.6mm, C_0: 30ppm)